PROBING THE CARDIAC ARM OF THE BAROREFLEX AND COMPLEMENTARY BRANCHES

EDITED BY: Alberto Porta and Maja Elstad
PUBLISHED IN: Frontiers in Neuroscience and Frontiers in Physiology

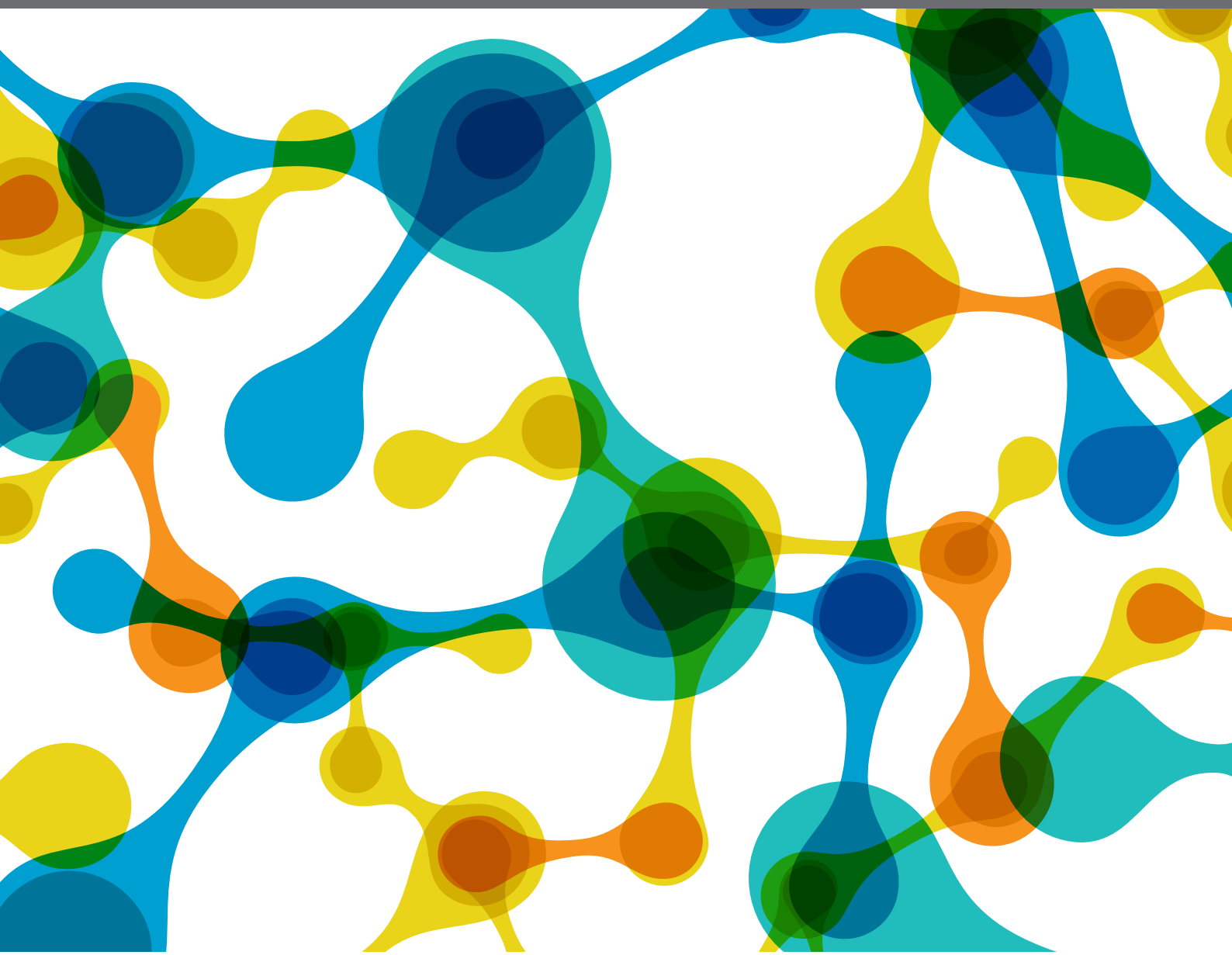

frontiers Research Topics

frontiers

ISSN 1664-8714
ISBN 978-2-88963-478-1
DOI 10.3389/978-2-88963-478-1

About Frontiers

Frontiers is more than just an open-access publisher of scholarly articles: it is a pioneering approach to the world of academia, radically improving the way scholarly research is managed. The grand vision of Frontiers is a world where all people have an equal opportunity to seek, share and generate knowledge. Frontiers provides immediate and permanent online open access to all its publications, but this alone is not enough to realize our grand goals.

Frontiers Journal Series

The Frontiers Journal Series is a multi-tier and interdisciplinary set of open-access, online journals, promising a paradigm shift from the current review, selection and dissemination processes in academic publishing. All Frontiers journals are driven by researchers for researchers; therefore, they constitute a service to the scholarly community. At the same time, the Frontiers Journal Series operates on a revolutionary invention, the tiered publishing system, initially addressing specific communities of scholars, and gradually climbing up to broader public understanding, thus serving the interests of the lay society, too.

Dedication to Quality

Each Frontiers article is a landmark of the highest quality, thanks to genuinely collaborative interactions between authors and review editors, who include some of the world's best academicians. Research must be certified by peers before entering a stream of knowledge that may eventually reach the public - and shape society; therefore, Frontiers only applies the most rigorous and unbiased reviews.
Frontiers revolutionizes research publishing by freely delivering the most outstanding research, evaluated with no bias from both the academic and social point of view. By applying the most advanced information technologies, Frontiers is catapulting scholarly publishing into a new generation.

What are Frontiers Research Topics?

Frontiers Research Topics are very popular trademarks of the Frontiers Journals Series: they are collections of at least ten articles, all centered on a particular subject. With their unique mix of varied contributions from Original Research to Review Articles, Frontiers Research Topics unify the most influential researchers, the latest key findings and historical advances in a hot research area! Find out more on how to host your own Frontiers Research Topic or contribute to one as an author by contacting the Frontiers Editorial Office: researchtopics@frontiersin.org

PROBING THE CARDIAC ARM OF THE BAROREFLEX AND COMPLEMENTARY BRANCHES

Topic Editors:
Alberto Porta, University of Milan, Italy
Maja Elstad, University of Oslo, Norway

Citation: Porta, A., Elstad, M., eds. (2020). Probing the Cardiac Arm of the Baroreflex and Complementary Branches. Lausanne: Frontiers Media SA.
doi: 10.3389/978-2-88963-478-1

Table of Contents

frontiers in Neuroscience

EDITORIAL
published: 10 January 2020
doi: 10.3389/fnins.2019.01422

Editorial: Probing the Cardiac Arm of the Baroreflex and Complementary Branches

Alberto Porta[1,2]* *and Maja Elstad*[3]

[1] Department of Biomedical Sciences for Health, University of Milan, Milan, Italy, [2] Department of Cardiothoracic, Vascular Anesthesia and Intensive Care, IRCCS Policlinico San Donato, Milan, Italy, [3] Division of Physiology, Institute of Basic Medical Sciences, University of Oslo, Oslo, Norway

Keywords: heart rate variability, arterial blood pressure, sympathetic neural activity, cardiovascular control, peripheral resistances, autonomic nervous system, baroreflex sensitivity

Editorial on the Research Topic

Probing the Cardiac Arm of the Baroreflex and Complementary Branches

Baroreflex (BR) is one of the most important mechanisms in short-term regulation of arterial pressure (AP) (Robertson et al., 2012). The BR has a key role in limiting excessive AP rises via the activation of a vagal reflex (Robertson et al., 2012) producing several consequences on physiological variables. The most frequently evaluated consequence is the lengthening of heart period (HP) (Pickering et al., 1972). Baroreflex is crucial in bipedal animals like humans to prevent AP drops while standing via a sympathetic activation eliciting the HP shortening (Montano et al., 1994; Cooke et al., 1999; Marchi et al., 2016; De Maria et al., 2018) and the increase of burst rate of integrated postganglionic efferent sympathetic nerve activity directed to muscles (Sundlof and Wallin, 1978; Cooke et al., 1999; Furlan et al., 2000; Marchi et al., 2016). The BR engagement limits excessive AP variability in both humans and animals (Bertinieri et al., 1988; Parati et al., 1988; Frankel et al., 1993; Porta et al., 2000; Fazan et al., 2005).

The clinical evaluation of the BR control started with Smyth et al. (1969) who provided a practical, even though invasive, way to characterize BR via the estimate of the baroreflex sensitivity (BRS), namely the magnitude of HP changes observed in response to a pharmacologically induced unit variation of systolic AP (SAP). This interventional method is predictive for clinical outcomes (La Rovere et al., 1998) but, as it is inherently both non-physiological and invasive, researchers proposed noninvasive, non-interventional, and non-pharmacological surrogate techniques based on spontaneous fluctuations of HP and SAP with the aim at enlarging and favoring clinical applications (Laude et al., 2004). Both interventional and non-interventional techniques made the BR assessment popular but they contributed to form the common belief that BR is coincident with its cardiac arm operating to keep AP constant via HP adjustments. However, cardiac BR (cBR) is neither the unique arm of the BR nor the most important one, given that recent heart transplanted patients can stand up (Smith et al., 1989; Karemaker and Wesseling, 2008) and technologies for baroreflex failure target directly vasomotor sympathetic nerves (Hosokawa and Sunagawa, 2016). One of the consequences of the view identifying the BR with cBR is the tendency of interpreting modifications of the mean AP experienced during everyday life in spite of homeostatic characteristic of the BR as a result of its noisy nature (Karemaker and Wesseling, 2008). Conversely, the stochastic nature of the BR might be the simple consequence of its complex and composite nature: indeed, since the BR can target several physiological variables including heart rate, sympathetic activity, peripheral resistances, cardiac contractility, and stroke volume just to mention a few

OPEN ACCESS

Edited and reviewed by:
Vaughan G. Macefield, Baker Heart and Diabetes Institute, Australia

***Correspondence:**
Alberto Porta
alberto.porta@unimi.it

Specialty section:
This article was submitted to Autonomic Neuroscience, a section of the journal Frontiers in Neuroscience

Received: *05 December 2019*
Accepted: *16 December 2019*
Published: *10 January 2020*

Citation:
Porta A and Elstad M (2020) Editorial: Probing the Cardiac Arm of the Baroreflex and Complementary Branches. Front. Neurosci. 13:1422. doi: 10.3389/fnins.2019.01422

(Smyth et al., 1969; Sundlof and Wallin, 1978; Casadei et al., 1992; Kienbaum et al., 2001; Yasumasu et al., 2005; Vaschillo et al., 2012; Borgers et al., 2014; Barbic et al., 2015; Elstad et al., 2015; Hosokawa and Sunagawa, 2016; Reyes del Paso et al., 2017; Porta et al., 2018) and since the functioning of all these branches is weakly correlated as it appears from the weak correlation among BRSs (Rudas et al., 1999; O'Leary et al., 2003; Dutoit et al., 2010; Taylor et al., 2015; Marchi et al., 2016), it is not surprising to observe that mean AP does not always obey to the homeostatic principle. The composite nature of the BR is compatible with the observation that short-term fluctuations of HP are not intimately and always linked to those of SAP (Diaz and Taylor, 2006).

The aim of this Research Topic is, on the one hand, to stress the composite nature of the BR and the need of overcome a description solely based on the assessment of the cBR and, on the other hand, the possibility to provide a more complete, and faithful, description of the BR based on the use of a multivariate integrated approach exploiting simultaneous recordings of several physiological variables and state-of-the-art signal processing techniques applied to their spontaneous fluctuations. Among the most relevant challenges that need to be faced to make this approach successful we recall the inherent difficulty posed by the small amplitude of the spontaneous SAP fluctuations in assuring a BR description uncorrupted by confounding mechanisms operating in causal directions incompatible with a BR engagement (Porta et al., 2000, 2013; Diaz and Taylor, 2006).

In this Research Topic the complexity and composite nature of the BR and its assessment is illustrated by the diversity in the contributions. They stress the relevance of the simultaneous assessment of cardiac and sympathetic arms of the BR in healthy subjects (Barbic et al.) and patients (Brunetta et al.), the different characteristics of the BR arms likely to contribute to their weakly correlated behaviors (De Maria et al.), the importance of the clinical information that can be derived from BR markers estimated from spontaneous variability (Bari et al. and Solaro et al.), the chance of elucidating the brainstem nuclei functioning involved in the modulation of the activity of all BR branches (Gerlach et al.), the importance of modeling the dynamical interactions among variables via modeling approaches accounting for directionality (Chalacheva et al.) and feedforward influences (Parati et al.), the possibility given by advanced signal processing tools to provide a more insightful description of the complex behavior of the cBR arm (de Boer and Karemaker) and to limit the effects of confounding factors (Silva et al.), and the opportunity of exploiting smart technologies to broaden the range of applications of BR monitoring (Lázaro et al.). We hope this Research Topic contributes to understanding the complex nature of the BR and its assessment.

AUTHOR CONTRIBUTIONS

AP and ME conceived the contribution, drafted the manuscript, edited and revised the manuscript, and approved the final version of the manuscript.

REFERENCES

Barbic, F., Heusser, K., Marchi, A., Zamunér, A. R., Gauger, P., Tank, J., et al. (2015). Cardiovascular parameters and neural sympathetic discharge variability before orthostatic syncope: role of sympathetic baroreflex control to the vessels. *Physiol. Meas.* 36, 633–641. doi: 10.1088/0967-3334/36/4/633

Bertinieri, G., Di Rienzo, M., Cavallazzi, A., Ferrari, A. U., Pedotti, A., and Mancia, G. (1988). Evaluation of baroreceptor reflex by blood pressure monitoring in unanesthetized cats. *Am. J. Physiol.* 254, H377–H383. doi: 10.1152/ajpheart.1988.254.2.H377

Borgers, A. J., van den Born, B.-J., Alkemade, A., Eeftinck Schattenkerk, D. W., van Lieshout, J. J., Wesseling, K. H., et al. (2014). Determinants of vascular and cardiac baroreflex sensitivity values in a random population sample. *Med. Biol. Eng. Comput.* 52, 65–73. doi: 10.1007/s11517-013-1111-0

Casadei, B., Meyer, T. E., Coats, A. J., Conway, J., and Sleight, P. (1992). Baroreflex control of stroke volume in man: an effect mediated by the vagus. *J. Physiol.* 448, 539–550. doi: 10.1113/jphysiol.1992.sp019056

Cooke, W. H., Hoag, J. B., Crossman, A. A., Kuusela, T. A., Tahvanainen, K. U. O., and Eckberg, D. L. (1999). Human responses to upright tilt: a window on central autonomic integration. *J. Physiol.* 517, 617–628. doi: 10.1111/j.1469-7793.1999.0617t.x

De Maria, B., Bari, V., Ranucci, M., Pistuddi, V., Ranuzzi, G., Takahashi, A. C. M., et al. (2018). Separating arterial pressure increases and decreases in assessing cardiac baroreflex sensitivity via sequence and bivariate phase-rectified signal averaging techniques. *Med. Biol. Eng. Comput.* 56, 1241–1252. doi: 10.1007/s11517-017-1765-0

Diaz, T., and Taylor, J. A. (2006). Probing the arterial baroreflex: is there a 'spontaneous' baroreflex? *Clin. Auton. Res.* 16, 256–261. doi: 10.1007/s10286-006-0352-5

Dutoit, A. P., Hart, E. C., Charkoudian, N., Wallin, B. G., Curry, T. B., and Joyner, M. J. (2010). Cardiac baroreflex sensitivity is not correlated to sympathetic baroreflex sensitivity within healthy young humans. *Hypertension* 56, 1118–1123. doi: 10.1161/HYPERTENSIONAHA.110.158329

Elstad, M., Walløe, L., Holme, N. L., Maes, E., and Thoresen, M. (2015). Respiratory sinus arrhythmia stabilizes mean arterial blood pressure at high-frequency interval in healthy humans. *Eur. J. Appl. Physiol.* 115, 521–530. doi: 10.1007/s00421-014-3042-3

Fazan, R. Jr., de Oliveira, M., da Silva, V. J., Joaquim, L. F., Montano, N., Porta, A., et al. (2005). Frequency-dependent baroreflex modulation of blood pressure and heart rate variability in conscious mice. *Am. J. Physiol.* 289, H1968–H1975. doi: 10.1152/ajpheart.01224.2004

Frankel, R. A., Metting, P. J., and Britton, S. L. (1993). Evaluation of spontaneous baroreflex sensitivity in conscious dogs. *J. Physiol.* 462, 31–45. doi: 10.1113/jphysiol.1993.sp019541

Furlan, R., Porta, A., Costa, F., Tank, J., Baker, L., Schiavi, R., et al. (2000). Oscillatory patterns in sympathetic neural discharge and cardiovascular variables during orthostatic stimulus. *Circulation* 101, 886–892. doi: 10.1161/01.CIR.101.8.886

Hosokawa, K., and Sunagawa, K. (2016). Closed-Loop neuromodulation technology for baroreflex blood pressure control. *Proc. IEEE* 104, 432–443. doi: 10.1109/JPROC.2015.2496290

Karemaker, J. M., and Wesseling, K. H. (2008). Variability in cardiovascular control: the baroreflex reconsidered. *Cardiovasc. Eng.* 8, 23–29. doi: 10.1007/s10558-007-9046-4

Kienbaum, P., Karlsson, T., Sverrisdottir, Y. B., Elam, M., and Wallin, B. G. (2001). Two sites for modulation of human sympathetic activity by arterial baroreceptors. *J. Physiol.* 531, 861–869. doi: 10.1111/j.1469-7793.2001.0861h.x

La Rovere, M. T., Bigger, J. T. Jr., Marcus, F. I., Mortara, A., and Schwartz, P. J. (1998). Baroreflex sensitivity and heart-rate variability in prediction of total cardiac mortality after myocardial infarction. ATRAMI (Autonomic Tone and Reflexes After Myocardial Infarction) Investigators. *Lancet* 351, 478–484. doi: 10.1016/S0140-6736(97)11144-8

Laude, D., Elghozi, J. L., Girard, A., Bellard, F., Bouhaddi, M., Castiglioni, P., et al. (2004). Comparison of various techniques used to estimate spontaneous baroreflex sensitivity (the EuroBaVar study). *Am. J. Physiol.* 286, R226–R231. doi: 10.1152/ajpregu.00709.2002

Marchi, A., Bari, V., De Maria, B., Esler, M., Lambert, E., Baumert, M., et al. (2016). Simultaneous characterization of sympathetic and cardiac arms of the baroreflex through sequence techniques during incremental head-up tilt. *Front. Physiol.* 7:438. doi: 10.3389/fphys.2016.00438

Montano, N., Gnecchi-Ruscone, T., Porta, A., Lombardi, F., Pagani, M., and Malliani, A. (1994). Power spectrum analysis of heart rate variability to assess changes in sympatho-vagal balance during graded orthostatic tilt. *Circulation* 90, 1826–1831. doi: 10.1161/01.CIR.90.4.1826

O'Leary, D. D., Kimmerly, D. S., Cechetto, A. D., and Shoemaker, J. K. (2003). Differential effect of head-up tilt on cardiovagal and sympathetic baroreflex sensitivity in humans. *Exp. Physiol.* 88, 769–774. doi: 10.1113/eph8802632

Parati, G., di Rienzo, M., Bertinieri, G., Pomidossi, G., Casadei, R., Groppelli, A., et al. (1988). Evaluation of the baroreceptor-heart rate reflex by 24-hour intra-arterial blood pressure monitoring in humans. *Hypertension* 12, 214–222. doi: 10.1161/01.HYP.12.2.214

Pickering, T. G., Gribbin, B., and Sleight, P. (1972). Comparison of the reflex heart rate response to rising and falling arterial pressure in man. *Cardiovasc. Res.* 6, 277–283. doi: 10.1093/cvr/6.3.277

Porta, A., Bari, V., De Maria, B., Cairo, B., Vaini, E., Malacarne, M., et al. (2018). Peripheral resistance baroreflex during incremental bicycle ergometer exercise: characterization and correlation with cardiac baroreflex. *Front. Physiol.* 9:688. doi: 10.3389/fphys.2018.00688

Porta, A., Baselli, G., Rimoldi, O., Malliani, A., and Pagani, M. (2000). Assessing baroreflex gain from spontaneous variability in conscious dogs: role of causality and respiration. *Am. J. Physiol.* 279, H2558–H2567. doi: 10.1152/ajpheart.2000.279.5.H2558

Porta, A., Castiglioni, P., Di Rienzo, M., Bassani, T., Bari, V., Faes, L., et al. (2013). Cardiovascular control and time domain Granger causality: insights from selective autonomic blockade. *Phil. Trans. R Soc. A* 371:20120161. doi: 10.1098/rsta.2012.0161

Reyes del Paso, G. A., de la Coba, P., Martín-Vazquez, M., and Thayer, J. F. (2017). Time domain measurement of the vascular and myocardial branches of the baroreflex: a study in physically active versus sedentary individuals. *Psychophysiology* 54, 1528–1540. doi: 10.1111/psyp.12898

Robertson, D., Diedrich, A., and Chapleau, M. W. (2012). Editorial on arterial baroreflex issue. *Auton. Neurosci. -Basic Clin.* 172, 1–3. doi: 10.1016/j.autneu.2012.10.010

Rudas, L., Crossman, A. A., Morillo, C. A., Halliwill, J. R., Tahvanainen, K. U. O., Kuusela, T. A., et al. (1999). Human sympathetic and vagal baroreflex responses to sequential nitroprusside and phenylephrine. *Am. J. Physiol.* 276, H1691–H1698. doi: 10.1152/ajpheart.1999.276.5.H1691

Smith, M. L., Ellenbogen, K. A., Eckberg, D. L., Szentpetery, S., and Thames, M. D. (1989). Subnormal heart period variability in heart failure: effect of cardiac transplantation. *J. Am. Coll. Cardiol.* 14, 106–111. doi: 10.1016/0735-1097(89)90059-4

Smyth, H. S., Sleight, P., and Pickering, G. W. (1969). Reflex regulation of arterial pressure during sleep in man. A quantitative method of assessing baroreflex sensitivity. *Circ. Res.* 24,109–121. doi: 10.1161/01.RES.24.1.109

Sundlof, G., and Wallin, B. G. (1978). Human muscle nerve sympathetic activity at rest. Relationship to blood pressure and age. *J. Physiol.* 274, 621–637. doi: 10.1113/jphysiol.1978.sp012170

Taylor, C. E., Witter, T., El Sayed, K., Hissen, S. L., Johnson, A. W., and Macefield, V. G. (2015). Relationship between spontaneous sympathetic baroreflex sensitivity and cardiac baroreflex sensitivity in healthy young individuals. *Physiol. Rep.* 3:e12536. doi: 10.14814/phy2.12536

Vaschillo, E. G., Vaschillo, B., Buckman, J. F., Pandina, R. J., and Bates, M. E. (2012). Measurement of vascular tone and stroke volume baroreflex gain. *Psychophysiology* 49, 193–197. doi: 10.1111/j.1469-8986.2011.01305.x

Yasumasu, T., Abe, H., Oginosawa, Y., Takahara, K., and Nakashima, Y. (2005). Assessment of cardiac baroreflex function during fixed atrioventricular pacing using baroreceptor-stroke volume reflex sensitivity. *J. Cardiovasc. Electrophysiol.* 16, 727–731. doi: 10.1111/j.1540-8167.2005.40767.x

Conflict of Interest: The authors declare that the research was conducted in the absence of any commercial or financial relationships that could be construed as a potential conflict of interest.

frontiers in Neuroscience

ORIGINAL RESEARCH
published: 23 January 2019
doi: 10.3389/fnins.2019.00017

Revisiting the Sequence Method for Baroreflex Analysis

*Luiz Eduardo Virgilio Silva[1], Daniel Penteado Martins Dias[2], Carlos Alberto Aguiar da Silva[1], Hélio Cesar Salgado[1] and Rubens Fazan Jr.[1]**

[1] Department of Physiology, Ribeirão Preto Medical School, University of São Paulo, Ribeirão Preto, Brazil, [2] Barão de Mauá University Center, Ribeirão Preto, Brazil

The sequence method is an important approach to assess the baroreflex function, mainly because it is based on the spontaneous fluctuations of beat-by-beat arterial pressure (for example, systolic arterial pressure or SAP) and pulse interval (PI). However, some studies revealed that the baroreflex effectiveness index (BEI), calculated through the sequence method, shows an intriguing oscillatory pattern as function of the delay between SAP and PI. It has been hypothesized that this pattern is related to the respiratory influence on SAP and/or PI variability, limiting the SAP ramps to 3 or 4 beats of length. In this study, this hypothesis was tested by assessing the sequence method using raw (original) and filtered series. Results were contrasted to the well-established transfer function, estimated between SAP and PI. Continuous arterial pressure recordings were obtained from healthy rats (N = 61) and beat-by-beat series of SAP and PI were generated. Low-pass (LP) and high-pass (HP) filtered series of SAP and PI were created by filtering the original series with a cutoff frequency of 0.8 Hz. Original series were analyzed by either the sequence method or cross-spectral analysis (transfer function) at low- (LF) and high- (HF) frequency bands, while filtered series were evaluated only by the sequence method. Baroreflex sensitivity (BRS) and BEI of original series, calculated by sequence method, was highly (85–90%) determined by HP series, with no significant association between original and LP series. A high correlation (>0.7) was found between the BRS estimated from original series (sequence method) and HF band (transfer function), as well as for LP series (sequence method) and LF band (transfer function). These findings confirmed the hypothesis that the sequence method quantifies only the high-frequency components of the baroreflex, neglecting the low-frequency influences, such as the Mayer waves. Therefore, we propose using both the original and LP filtered time series for a broader assessment of the baroreflex function using the sequence method.

Keywords: heart rate variability, autonomic nervous system, baroreflex, sequence method, sensitivity, effectiveness index

OPEN ACCESS

Edited by:
Alberto Porta,
University of Milan, Italy

Reviewed by:
Michal Javorka,
Comenius University in Bratislava, Slovakia
Paolo Castiglioni,
Fondazione Don Carlo Gnocchi Onlus (IRCCS), Italy

****Correspondence:***
Rubens Fazan Jr.
rfazan@usp.br

Specialty section:
This article was submitted to Autonomic Neuroscience, a section of the journal Frontiers in Neuroscience

Received: *12 October 2018*
Accepted: *09 January 2019*
Published: *23 January 2019*

Citation:
Silva LEV, Dias DPM, da Silva CAA, Salgado HC and Fazan R Jr (2019) Revisiting the Sequence Method for Baroreflex Analysis. Front. Neurosci. 13:17. doi: 10.3389/fnins.2019.00017

INTRODUCTION

The sequence method, first described in the mid-1980s, was a milestone for the analysis of baroreflex function at both clinical and experimental levels (Bertinieri et al., 1985). First, because it relies on the spontaneous fluctuations of beat-by-beat arterial pressure (AP) and cardiac interval, i.e., this approach does not require the induction of blood pressure changes, avoiding many

drawbacks related to it. Second, the sequence method not only evaluates the baroreflex sensitivity (BRS) but also provides the baroreflex effectiveness index (BEI). In contrast to BRS, BEI reflects the percentage of beat-by-beat AP changes that are effectively translated into reflex changes of the heart rate (HR; Di Rienzo et al., 2001). Therefore, the BEI is considered a complementary index to the BRS, providing additional information regarding baroreflex function (Lataro et al., 2017; Silva and Katayama, 2017).

In the late 2000s, Laude and coworkers studied more in-depth the parameters of the sequence method to better understand their influence and the best choices for working with mice (Laude et al., 2008, 2009). They also reported an intriguing feature: when the BEI is calculated for increasing delays between beat-by-beat systolic AP (SAP) and pulse interval (PI), its value oscillates with a period of 3 to 4 beats. On the other hand, the BRS, also assessed with increasing delays, do not show any oscillatory pattern.

Even though these studies did not address the underlying causes of this oscillatory profile of BEI for incremental delays, we hypothesized that it might be a consequence of the respiratory influence on SAP, as highlighted in a recent study of our group (Lataro et al., 2017). The respiratory cycle in rats and mice lasts about 4 to 5 beats and the respiratory driven changes in SAP can often be easily identified (**Figure 1**). As consequence, SAP ramps (up or down) are usually limited to the length of 4 or 5 beats. In other words, a delay of 3 to 4 cardiac intervals is expected to separate SAP ramps. Since SAP ramps drive baroreflex-mediated changes in HR, one can expect the same 3 to 4 cardiac intervals separating one PI ramp to another. Although each SAP ramp is believed to elicit only one ramp of PI (the reflex response), the sequence method may erroneously associate many PI ramps at a given SAP ramp, leading, for instance, to oscillation of the BEI values every 3 or 4 PIs (see **Figure 1**).

Therefore, it seems that the sequence method is limited to assess spontaneous baroreflex function only at AP oscillations modulated by respiration, which limits the size of the SAP ramps. This concept carries important consequences, as the sequence method ignores the baroreflex responses to slow AP changes, such as the Mayer waves (Penaz, 1978). The current study evaluated the influence of low- and high-frequency oscillations of SAP and PI in the sequence method, and compared the BRS calculated using the sequence method to BRS obtained from the cross-spectral analysis. Also, we proposed an alternative approach to use the sequence method to calculate both the fast and slow components of the baroreflex.

MATERIALS AND METHODS

Animals

The dataset of this study is composed by revisited AP recordings ($N = 61$) from normal male young adult Wistar rats (250–300 g), obtained from previously published (Dias et al., 2016; Silva et al., 2017) and unpublished studies. In all experiments, the animals were maintained under controlled light (12–12 h light-dark cycle) and temperature (21°C) environment with water and food provided *ad libitum*. All experimental procedures adhered to the Guide for the Care and Use of Laboratory Animals prepared by the National Academy of Sciences and published by the National Institutes of Health and were approved by the Committee of Ethics in Animal Research from the Ribeirão Preto Medical School – University of São Paulo, Ribeirão Preto, SP, Brazil.

Experimental Procedures

Rats were anesthetized with a mixture of ketamine (50 mg/kg) and xylazine (10 mg/kg) and instrumented with a polyethylene catheter inserted into the carotid artery ($N = 7$), femoral artery ($N = 43$) or aorta ($N = 11$) for continuous direct AP recordings. Some rats also received a catheter inserted into the femoral vein (Silva et al., 2017) or subcutaneous electrodes for ECG recordings (Dias et al., 2016), according to the needs of the experimental protocol. 24 to 48 h after the surgical procedures, the arterial line of the animals was connected to a pressure transducer (MLT844, ADInstruments, Bella Vista, NSW, Australia) attached to a Bridge Amp (FE221, ADIstruments, Bella Vista, NSW, Australia) and the AP was continuously sampled (2 kHz) for 30 min, in an IBM/PC through an analogic to digital interface (Power Lab 4/40, ADInstruments, Bella Vista, NSW, Australia). All the recordings were performed in unanesthetized freely moving animals kept in individual cages and during basal conditions.

Data Pre-processing

Approximately 20 min of stable AP recordings from each rat was processed by computer software (LabChart Pro, ADInstruments, Bella Vista, NSW, Australia) to generate beat-by-beat series of SAP and PI values. Artifacts were removed from each series using the following procedure: a moving median window of 50 points was used to calculate the series *baseline*. Upper and lower thresholds were set as: $baseline \pm p * baseline$ ($0.05 < p < 0.20$). All values that exceeded the thresholds (upper or lower) were removed from the series. Removals never exceeded 1% of the original time series length. The average ± SD of series length is 8.240 ± 3.590 beats.

Low- and High-Pass Filtered Series

Filtered versions of the SAP and PI series were created by filtering the original series using a 9th order Butterworth filter with a cutoff frequency of 0.8 Hz. Low-pass (LP) and high-pass (HP) filtered series were created in order to determine the influence of low and high-frequency components of the baroreflex in the sequence method. The cutoff frequency was chosen according to the spectral components of the rat cardiovascular variability (Cerutti et al., 1991, 1994). **Figure 2** shows examples of the original and filtered SAP and PI series.

Sequence Method

The sequence method assumes that successive spontaneous increases or decreases in beat-by-beat AP values (here, SAP ramps) elicit baroreflex-mediated responses in the PI length (Laude et al., 2008). Therefore, to evaluate baroreflex function, this approach searches for SAP ramps linked (linearly correlated) to changes in PI. Some parameters need to be set in order to apply

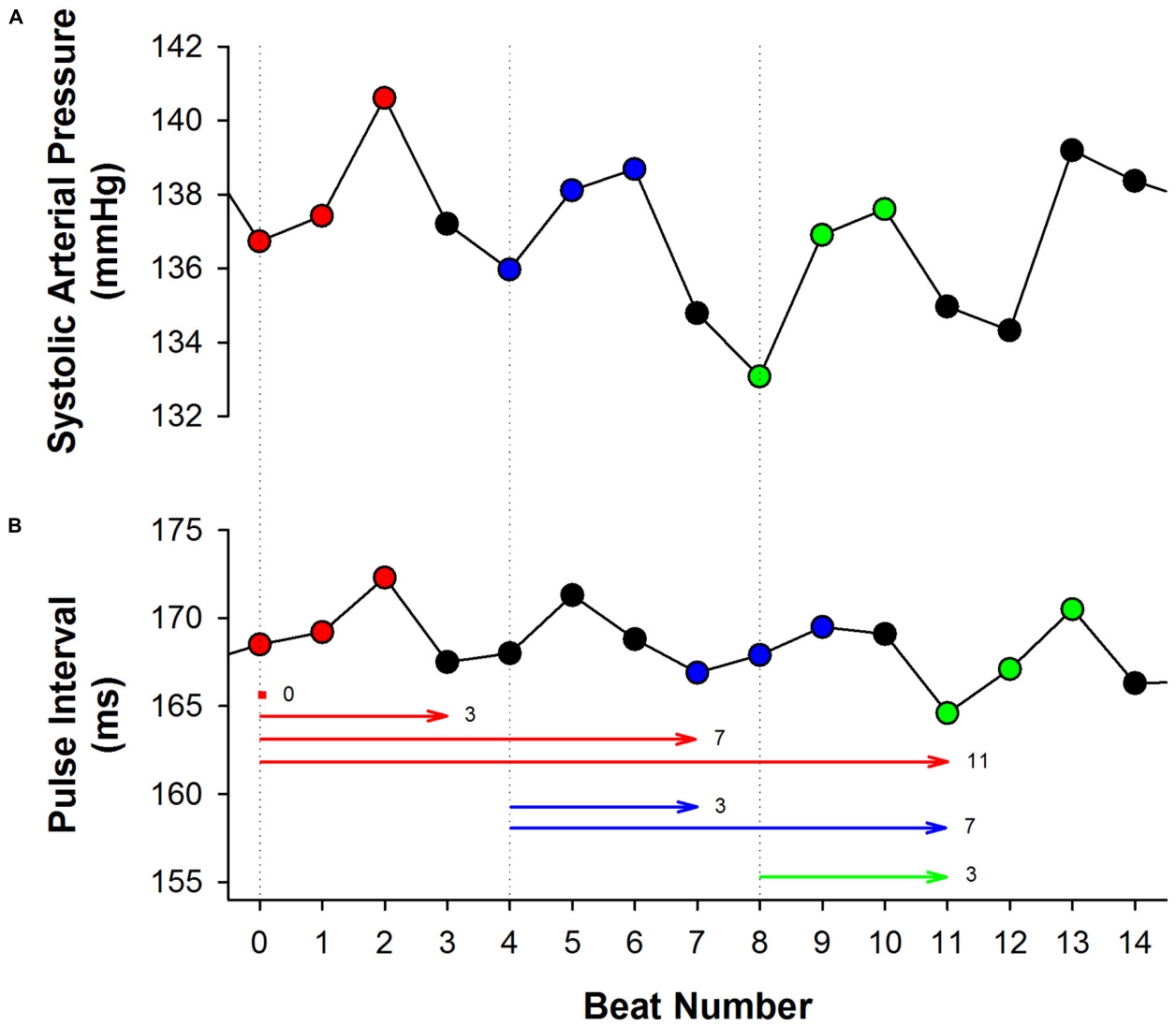

FIGURE 1 | The effect of respiration on the sequence method. In both excerpts of systolic arterial pressure (SAP, **A**) and pulse interval (PI, **B**) time series, obtained from a healthy rat, it is noticeable the influence of respiration, increasing and decreasing beat-by-beat SAP and PI with a period of three to four beats. Three up ramps were found in the SAP series, as shown in red (first ramp), blue (second ramp) and green (third ramp). The first up PI ramp found after each up SAP ramp was highlighted using the same color. Nevertheless, the sequence method may associate several PI ramps to a given SAP ramp, depending on the delay adopted (horizontal lines). For instance, the first up SAP ramp (red) can be associated with the PI ramps found in delays 0, 3, 7, and 11. Similarly, the second SAP ramp (blue) can be associated with the PI ramps found after 3 and 7 beats of delay. The same behavior occurs with the third SAP ramp. Therefore, BEI is expected to be higher for delays 0, 3, 7, and 11. In other words, BEI will oscillate with a period of three to four beats, due to the repetitive nature of the ramps imposed by the respiration.

the sequence method. First, a minimum variation (threshold) for SAP or PI change needs to be determined, i.e., the differences between the successive values of SAP or PI must meet a defined threshold. Second, the minimum sequence length (n), and the delay between SAP and PI ramps (d) must also be chosen. Finally, a minimum correlation coefficient (r) between SAP and PI ramps must be achieved to consider an actual baroreflex sequence. In other words, when an SAP ramp of n consecutive values (up or down) correlates with PI changes at the same direction, delayed by d beats from the SAP ramp, a baroreflex sequence has been found. The BRS (or gain) of each sequence is calculated by the slope of the regression line of PI vs. SAP, and the gain of the animal is the average slope, calculated from all the sequences found.

Besides the BRS, the sequence method also provides an additional index of baroreflex function, namely the BEI (Di Rienzo et al., 2001). BEI is the ratio of the number of sequences and the number of SAP ramps, occurring between 0 and 1. In brief, BEI depicts how many of the SAP changes are effectively translated into a change in PI, independently of its magnitude. Therefore, BEI and gain (i.e., slope) provide markers on different aspects of the spontaneous baroreflex function.

Following the guideline from a previous study (Laude et al., 2008, 2009), we set the correlation threshold to $r = 0.8$ and the

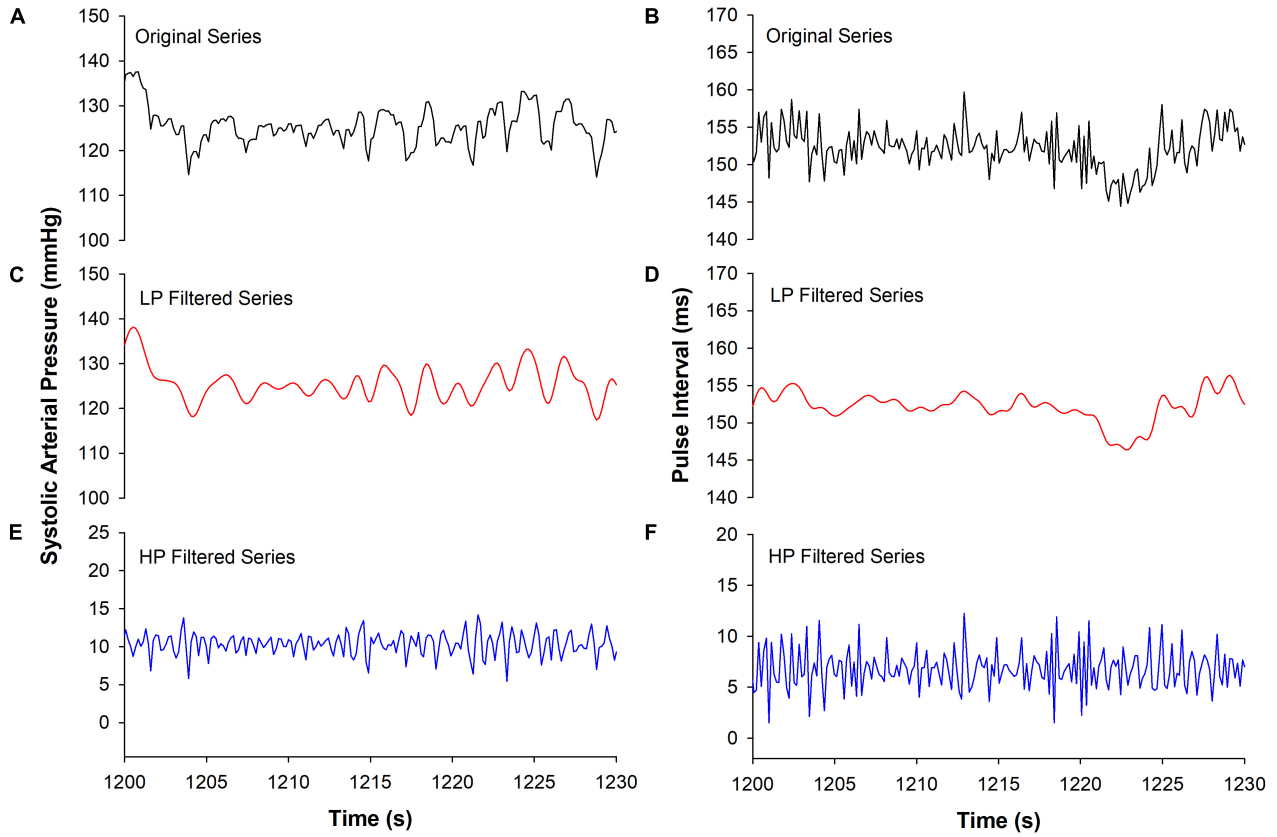

FIGURE 2 | Example of original and filtered series. Excerpts of SAP are shown for original **(A)**, low- (LP, **C**) and high-pass filtered (HP, **E**) series, as well as excerpts of PI for original **(B)**, low- **(D)** and high-pass filtered **(F)** series.

thresholds for SAP or PI changes were set to zero (i.e., any change in SAP or PI is considered). The delay between SAP and PI was assessed from 0 to 12 beats. The minimum sequence length was set to $n = 3$ for original time series and varied from $n = 3$ to $n = 9$ for filtered series. BRS and BEI were calculated using the computer software CardioSeries v2.4[1] (Dias et al., 2016).

Cross-Spectral Analysis by Transfer Function Estimation

The transfer function is a mathematical estimation that represents how a given system responds (output) to inputs (Pinna and Maestri, 2001). The baroreflex system is sensitive to AP changes (input), responding with changes in cardiac interval length. Therefore, estimating the transfer function between SAP and PI series provides information about the baroreflex function (Porta et al., 2013a).

The transfer function, which is defined in the frequency domain, can be estimated by the ratio of the PI-SAP cross-spectrum to SAP spectrum, and its modulus represents the gain of the baroreflex (Porta et al., 2013a). In addition to the transfer function, the coherence between SAP and PI can also be calculated to identify those frequencies where SAP and PI are more "coherent" or coupled. Therefore, under frequencies where those two signals are not coupled, the transfer function may be disregarded (Pinna and Maestri, 2001, 2002).

The original SAP and PI series were interpolated at 10 Hz (cubic spline) to become evenly spaced in time and were divided into half-overlapping segments of 4096 data points. This procedure is the well-known Welch protocol (Welch, 1967). A Hanning window was used to attenuate the spectral leakage in the side-lobes of the spectra, and the spectrum of each segment was calculated using the fast Fourier transform (FFT). The transfer function (gain or BRS) between SAP and PI was integrated into low (LF: 0.2–0.8 Hz) and high frequency (HF: 0.8–3.0 Hz) bands, accounting only for the frequencies where the coherence function was greater than 0.5. While the LF band carries relevant information about Mayer's waves of SAP, HF band mainly accounts for the respiratory oscillations of SAP (Julien, 2008). The transfer function was not estimated for the filtered time series.

Statistical Analysis

The normality of data distribution was verified by the Shapiro–Wilk test. Multiple linear regression was used to identify which oscillatory components of the original SAP and PI series are the

[1]www.danielpenteado.com

most relevant to the sequence method. For this purpose, the BRS (gain) of original series was modeled as a linear combination of the gain obtained from LP and HP filtered series, individually or combined. The same procedure was applied to BEI, i.e., it was modeled as a linear combination of the BEI estimated from LP and HP filtered series. The coefficient expressing how well each model describe the data (R^2) was reported. In addition, Bland–Altman plots were used to illustrate the agreement between the BRS, calculated using the sequence method, obtained from original and filtered series. The Spearman correlation coefficient was estimated between the sequence method BRS and the transfer function BRS (in LF and HF bands). The Wilcoxon Rank Sum Test and Friedman ANOVA on ranks were applied to check for differences between the BRS in LF and HF band (transfer function) and the BRS of original and filtered time series (sequence method). Significant differences were assumed when $P < 0.05$.

RESULTS

Both BRS and BEI, calculated using the sequence method, from the original (raw) and filtered series, are shown in **Figure 3**. As expected, BEI presented an oscillatory profile with a period of 3 to 4 beats for original (**Figure 3D**) and also for HP filtered series (**Figure 3E**). In the present study, BRS also showed periodic oscillation for increasing delays (**Figures 3A,B**). In contrast, for LP filtered series there is no clear oscillatory profile for either BEI or BRS (**Figures 3C,F**). However, the minimum sequence length markedly alters the BRS and BEI of LP filtered series. For $n = 3$ to $n = 9$, BRS changed from 1.2 to 0.8 ms/mmHg (**Figure 3C**), whereas the BEI varied from 0.8 to 0.2 (**Figure 3F**).

The Sequence Method Detects Only High-Frequency Oscillations

The BRS and BEI of the sequence method, calculated from original SAP and PI series, were modeled as a linear combination of the same index calculated from LP and HP filtered series. The squared multiple correlation index (R^2), representing the "quality" of each model, is reported in **Table 1**. Results show that the BRS (or BEI) of original series can be highly determined (explained) by the BRS (or BEI) of HP filtered series. When the BRS (or BEI) of LP filtered series is introduced into the model, no improvement is obtained. For the most used delays ($d = 1$ and $d = 3$), 85 to 90% of original BRS and BEI can be explained by the HP series, whereas only 5% could be attributed to LP filtered series. Even so, the association between original and LP filtered series is not significant for both the BRS and BEI.

The Bland–Altman plots of the sequence method BRS are shown in **Figure 4**. The plots represent the agreement (interchangeability of measurements) between the BRS obtained from the original series and the BRS obtained from filtered ones. The comparison was performed for original vs. LP (**Figure 4A,C**) and original vs. HP filtered series (**Figures 4B,D**), for delays of one and three beats ($d = 1$ and $d = 3$). The agreement between the BRS of original and HP series (-0.19 ± 0.79 for $d = 1$; 0.19 ± 0.77 for $d = 3$; mean difference $\pm$ SD) is significantly higher than the agreement between the BRS of original and LP series (1.95 ± 1.80 for $d = 1$; 2.54 ± 2.24 for $d = 3$; mean difference $\pm$ SD). Moreover, there is a clear higher proportional bias for the plots between original and LP filtered BRS, indicating that the higher the BRS, the higher the difference between the two measurements.

Correlation Between the Sequence Method and the Transfer Function

The correlation coefficients between BRS calculated using the sequence method (original and filtered series) and the BRS calculated using the transfer function (LF and HF bands) are shown in **Figure 5**. For original (**Figure 5A**) and HP series (**Figure 5B**), the BRS calculated by the sequence method was highly correlated to the BRS estimated by the transfer function at the HF band. In contrast, the correlation between the BRS estimated from the sequence method and the transfer function in the LF band was very low. For example, for delays equal to $d = 1$ or $d = 3$ (most common choices), the correlation between BRS obtained by the two methods was in the range 0.65 to 0.78 at HF band and 0.12 to 0.24 at LF band.

The opposite was found for LP filtered time series (**Figure 5C**). In this scenario, BRS examined by the sequence method was strongly correlated with the transfer function at the LF band. These results were consistent for all delays and sequence length (n), even though the correlation showed a tendency to be lower for longer sequences.

Figure 6 shows BRS calculated using the transfer function, in LF and HF bands (**Figure 6A**). For comparison, the BRS calculated by the sequence method is shown for some specific parameters (**Figures 6B,C**). We chose the minimum sequence length of $n = 3$ and delays of $d = 1$ or $d = 3$ beats for both original and filtered series. The mean BRS obtained by cross-spectral analysis at HF is more than three times higher compared to the mean BRS obtained at LF band (**Figure 6A**). The same behavior repeats for BRS calculated from original and filtered time series, using the sequence method, i.e., the BRS from original and HP filtered series are near three times higher than the BRS of LP filtered series, for both delays (**Figure 6B**, $d = 1$; **Figure 6C**, $d = 3$).

DISCUSSION

The analysis of spontaneous baroreflex has opened inestimable possibilities for better understanding the baroreflex function in a variety of situations. Although several methods have been designed for this purpose in the last years, the sequence method is still successfully applied and widely used (Laude et al., 2004; De Maria et al., 2018).

Nevertheless, the rupture of SAP ramps, as a consequence of the high-frequency (respiratory) fluctuations, seems to configure an important limitation of the sequence method. In other words, the method seems not to be capable of accounting for the slow components of the baroreflex. Some authors have previously reported the inability of the sequence method to account for the influence of the sympathetic system in the

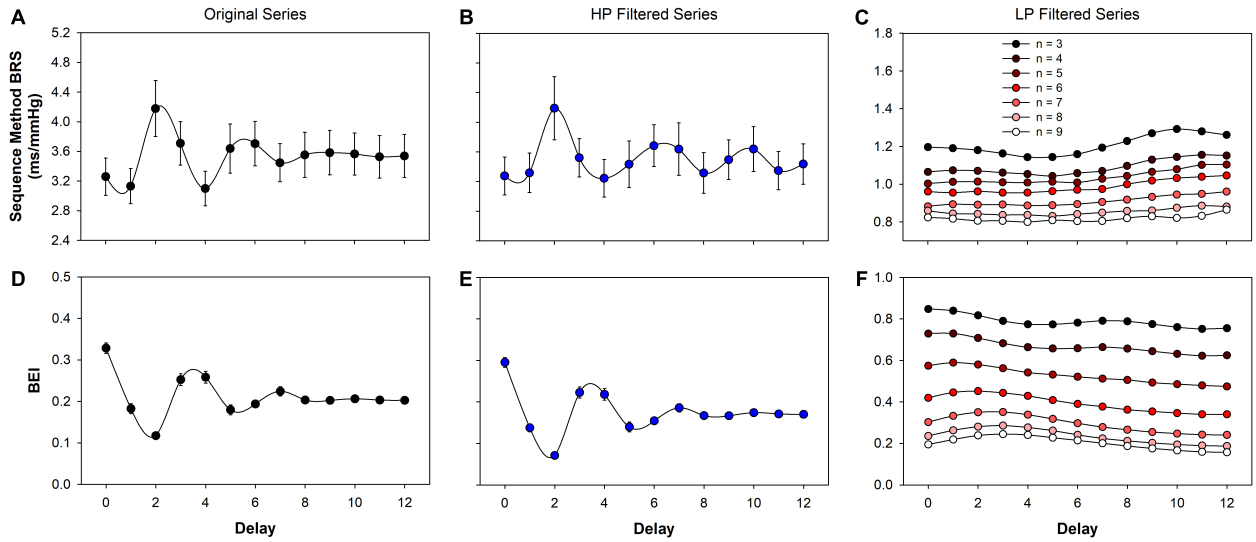

FIGURE 3 | Baroreflex function estimated using the sequence method. The baroreflex sensitivity (BRS) for original **(A)**, high- (HP, **B**) and low-pass (LP, **C**) filtered is shown as function of the delay between SAP and PI. The baroreflex effectiveness index (BEI) for original **(D)**, high- **(E)** and low-pass **(F)** filtered series are also shown as a function of the delay. The oscillatory profile of BEI observed in original and HP filtered series is a consequence of the restriction imposed by respiration on the sequence length (see **Figure 1**). For LP filtered series, both the BRS and the BEI monotonically decreases as *n* increases. The minimum sequence length was set as $n = 3$ for original and HP filtered series and varied from $n = 3$ to $n = 9$ for LP series. The delay was assessed from $d = 0$ to $d = 12$. Values are mean ± standard error.

TABLE 1 | Multiple linear regression of the BRS (gain) and BEI estimated by the sequence method for original SAP and PI series.

	LP filtered series only		HP filtered series only		LP + HP filtered series	
	BRS	**BEI**	**BRS**	**BEI**	**BRS**	**BEI**
d	R^2	R^2	R^2	R^2	R^2	R^2
0	0.06	0.06	0.89*	0.84*	0.89*	0.85*#
1	0.06	0.05	0.86*	0.84*	0.86*	0.84*
2	0.01	0.01	0.62*	0.80*	0.63*	0.80*
3	0.04	0.05	0.89*	0.86*	0.89*	0.86*
4	0.08#	0.00	0.76*	0.90*	0.76*	0.90*
5	0.03	0.16#	0.72*	0.91*	0.72*	0.91*
6	0.02	0.01	0.85*	0.80*	0.86*	0.80*
7	0.05	0.01	0.66*	0.81*	0.66*	0.82*
8	0.02	0.02	0.78*	0.82*	0.78*	0.82*
9	0.04	0.02	0.91*	0.81*	0.91*	0.81*
10	0.04	0.00	0.85*	0.83*	0.86*	0.83*
11	0.03	0.09#	0.84*	0.83*	0.84*	0.83*
12	0.04	0.15#	0.85*	0.67*	0.85*	0.69*

*The gain estimated from low-pass (LP) and high-pass (HP) filtered series were taken individually or combined as independent variables of the model. The same procedure was applied, separately, for the BEI. The minimum sequence length was set to n = 3. BRS: baroreflex sensitivity; BEI: baroreflex effectiveness index; SAP: systolic arterial pressure; PI: pulse interval; d: delay of the sequence method; R^2: the coefficient (between 0 and 1) expressing how well each model describe the dependent variable; #$P < 0.05$ for the association between the original (dependent) and LP series; *$P < 0.05$ for the association between the original (dependent) and HP series.*

baroreflex (Oosting et al., 1997; Stauss et al., 2006). Corroborating this hypothesis, the multiple linear regression and Bland–Altman plots employed here showed that the BRS and BEI, estimated from the sequence method, are strictly linked to the high-frequency components of the original series. In addition, the correlation analysis showed that the BRS calculated through the sequence method (original series) is highly related to the BRS derived from the cross-spectral analysis at high – but not low – frequency range. Considering the slower nature of adrenergic transmission, preventing the sympathetic influence in AP and HR at HF band (Stauss et al., 1997; Levick, 2000), it is reasonable to say that the sequence method does not measure the sympathetic-modulated component of the baroreflex.

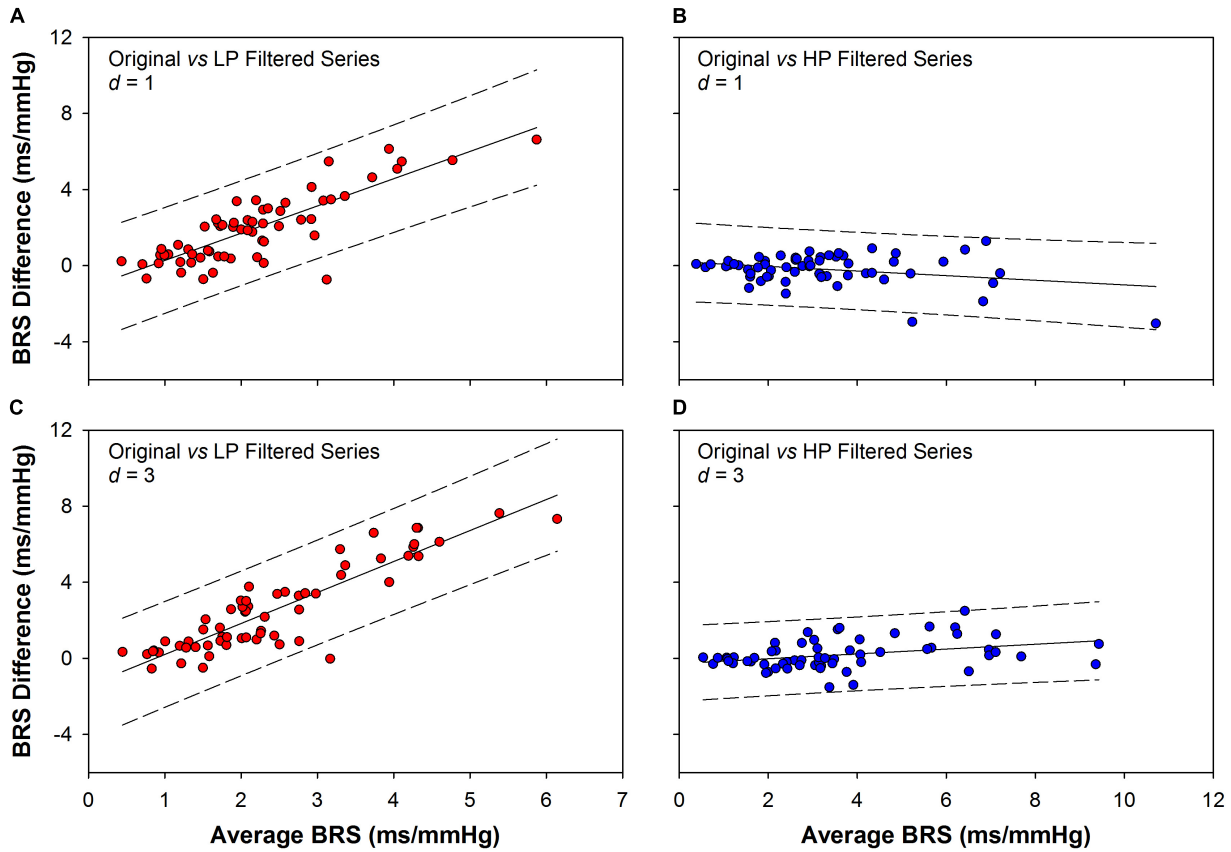

FIGURE 4 | Bland–Altman plots showing the agreement between the BRS obtained from original and filtered series. The BRS difference obtained between original and low-pass (LP) filtered series is higher than the BRS difference obtained between original and high-pass (HP) filtered ones, for both $d = 1$ (1.95 ± 1.80 vs. –0.19 ± 0.79) and $d = 3$ (2.54 ± 2.24 vs. 0.19 ± 0.77, mean difference ± SD). Moreover, there is a clear proportional bias in the BRS differences between original and LP filtered series, for both $d = 1$ **(A)** and $d = 3$ **(C)**. In contrast, there is no evidence of proportional bias for the BRS difference between original and HP filtered series, as the differences show opposite and small tendencies for $d = 1$ **(B)** or $d = 3$ **(D)**. *d*: delay between SAP and PI series.

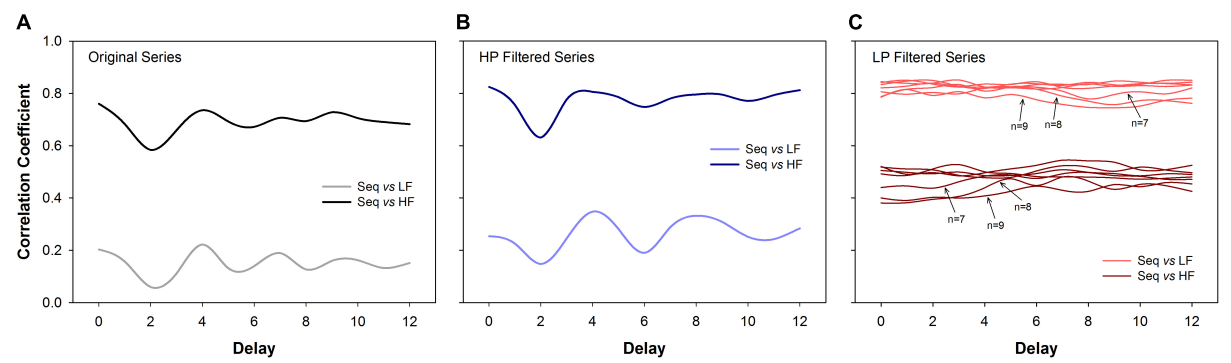

FIGURE 5 | Correlation analysis (Spearman coefficient) between the sequence method and the transfer function estimation (cross-spectral analysis). For original **(A)** and high-pass (HP) filtered series **(B)**, the BRS calculated using the sequence method is much more correlated to the HF component of BRS calculated through the transfer function. For low-pass (LP) filtered series **(C)** the BRS calculated by the sequence method is more correlated to the LF component of the BRS obtained by the transfer function. The results are consistent for all delays. For LP filtered series, the correlation values tend to decrease as *n* increases. The transfer function was always estimated using the original series. LF: low-frequency; HF: high-frequency; *n*: minimum sequence length; Seq: sequence method.

A reasonable alternative to measuring the slow components of the baroreflex using the sequence method is to filter out the high-frequency oscillations of SAP and PI time series (creating the LP filtered series) before applying the sequence method. In this case, the respiratory components will be removed, preventing SAP ramps to be broken every three or four beats. All analysis

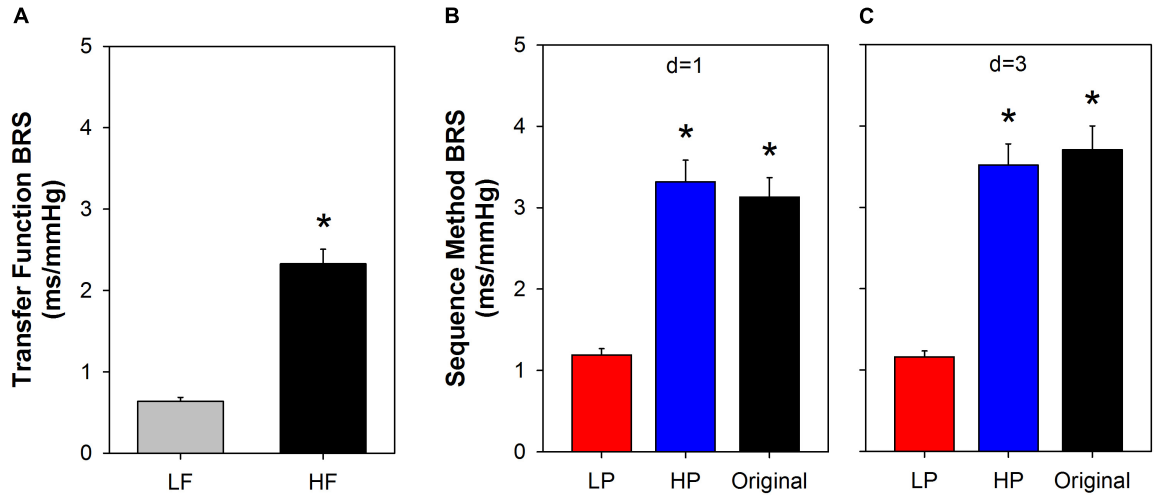

FIGURE 6 | Comparison between slow and fast BRS. The BRS calculated using the transfer function **(A)** indicates that the fast components of SAP oscillations (HF band) induce a BRS that is more than three times higher the sensitivity of the slow components of SAP (LF band). Very similar results were found with the sequence method when the original or high-pass (HP) filtered series were used to measure the fast BRS components and low-pass (LP) filtered series to measure the slow BRS **(B,C)**. The minimum sequence length was set to $n = 3$ for both original and filtered series. SAP: systolic arterial pressure; LF: low-frequency; HF: high-frequency; d: delay between arterial pressure and PI; * $P < 0.05$ compared to LF **(A)** or LP **(B,C)**. Values are mean ± standard error.

using LP filtered time series showed a very different scenario in comparison to the original and HP filtered ones. In one hand, the gain and BEI of HP filtered series (where only HF oscillations are present) is capable to describe, by itself, the BRS and BEI of original series; there is no significant association or agreement between the BRS of original and LP filtered series. On the other hand, the BRS of LP filtered series calculated with the sequence method is strongly correlated with the BRS at the low-frequency band of the cross-spectral analysis. Therefore, in order to measure both slow and fast components of the baroreflex utilizing the sequence method, it is conceivable to use not only the original but also the LP filtered series of SAP and PI. While results from the original series reflect the fast components of the baroreflex (the same obtained with HP filtered series), LP series will represent the slow components of the baroreflex. Of note, the cutoff frequency of filtered time series must be chosen according to the data under consideration, once the limits of LF and HF frequency bands may change for different species (Behar et al., 2018).

The best parameter choices for the sequence method was the subject of previous studies. Overall, a minimum sequence length of 3 cardiac intervals and delays of 1 or 3 beats are recommended (Laude et al., 2008, 2009). Those studies can be used as a guide for choosing the best parameters when the original time series are considered. For LP filtered time series, however, there was no guide for selecting the best values for the sequence length and delay. Moreover, the correlation between the transfer function (LF band) and sequence method (LP filtered series) was very similar for all parameters, giving no clues for their optimal values. Thus, for illustrating our proposal of using the sequence method for measuring both slow and fast components of the baroreflex, for LP filtered time series we selected the same parameters recommended for the original series, i.e., $n = 3$ and $d = 1$ or $d = 3$. However, a more comprehensive study on the effect of those two parameters must be carried out, using data obtained at diverse physiological conditions where the slow and fast baroreflex components can be controlled. For the data used here (healthy rats), only the minimum sequence length seems to play a role in the BRS and BEI of LP filtered time series. For example, the BEI showed a quite broad range of values, varying from 0.8 ($n = 3$) to 0.2 ($n = 9$) (**Figure 3F**). The decrease of BEI for increasing n is expected because the longer the SAP ramp, the lower the probability of finding a corresponding PI ramp. On the other hand, the decrease of BRS with n tells that shorter sequences give, in general, higher BRS than longer sequences. This is in agreement with the BRS calculated in LF and HF bands of the transfer function (higher BRS in HF band) and the overall higher BRS found for original and HP than LP filtered series, estimated by the sequence method (see **Figure 6**). Future studies are, therefore, necessary to identify which n is the best choice for the LP series, so that one can reliably quantify the BEI of the slow components of the baroreflex.

The sequence method was validated in situations of autonomic receptors blockade and by correlating the method to the classical pharmacological approach (Oxford method) (Oosting et al., 1997; Laude et al., 2004; Waki et al., 2006). However, such analyzes are not able to establish the causality between cardiovascular variables, especially when other important variables are not considered in the genesis of rhythms. For example, even though the high-frequency fluctuations of SAP and PI are highly correlated and coherent, they might be both driven by a third factor (respiration) instead of one modulating the another (Mancia et al., 1999; Faes et al., 2011). While several recent studies with causal approaches have confirmed the existence of a causal relation between SAP and PI, they also reported the existence of a causal relation from PI to SAP, as well as from respiration to SAP and respiration to PI (Faes et al., 2011; Porta et al., 2013b;

Helen Mary et al., 2018). Therefore, we cannot disregard the possibility that the sequence method, calculated over original or HP series, is overestimating the BRS by not disregarding the direct and parallel influence of the respiration into SAP and PI. On the other hand, a marked reduction of the number of sequences is observed when the baroreflex is surgically removed (Bertinieri et al., 1988; Di Rienzo et al., 2001). Thus, the sequence method is able to measure the baroreflex-mediated changes from SAP to PI at high-frequencies, indeed. However, the bias of this estimation due to the influence of other factors should be investigated in further studies. In this scenario, the use of LP filtered series may configure an advantage over HP filtered ones to evaluate the baroreflex function through the sequence method, as suggested by some authors (Fazan et al., 2005; Faes et al., 2006).

Extending the Findings to Humans

The evaluation of baroreflex function is a valuable tool in prognostic assessment and treatment strategies in a variety of cardiac diseases. However, most of the approaches developed to study baroreflex are not free of risk, requiring, for example, intravenous cannulation and use of vasoactive drugs which limits their use for a daily practice in clinical settings (La Rovere et al., 2008).

In this scenario, the sequence method emerges among the noninvasive alternatives to evaluate baroreflex in humans. Nevertheless, the concerns raised in this experimental study in rats should also be valuable for human subjects. Considering the average HR and respiratory frequency in humans, SAP ramps will also be limited to 3 to 4 cardiac beats. Therefore, similarly to what happens in rats, the sequence method in humans is also limited to assess spontaneous baroreflex function only at respiratory (fast) oscillations of SAP.

Therefore, the approaches suggested here to exclude the influences of respiration in spontaneous BRS in rats should also be applicable when the sequence method is used in signals from human beings.

In summary, we have confirmed the hypothesis that natural high-frequency components (in particular the respiration) of SAP and PI variability restricts the capability of the sequence method so that the slow components of the baroreflex are disregarded in the original method. To overcome this limitation, we proposed filtering out the high-frequency oscillations from SAP and PI series and use the sequence method with both original and LP filtered series, so that both slow and fast baroreflex function can be estimated. Nevertheless, different approaches could be considered to exclude the influence of respiration on SAP and PI (Topçu et al., 2018). Results point that our proposal seems to be a reasonable alternative to the classical approach. Further studies, with diversified datasets, are necessary to characterize the optimal parameters of the sequence method to be used with LP filtered time series.

DATA AVAILABILITY

The raw data supporting the conclusions of this manuscript will be made available by the authors, without undue reservation, to any qualified researcher.

AUTHOR CONTRIBUTIONS

LS and RF conceived the study. CdS and DD collected the data. LS and DD performed the data analysis. LS, DD, HS, and RF analyzed the data. LS drafted the manuscript. LS, DD, CdS, HS, and RF revised and approved the final version of the manuscript.

FUNDING

This study was financed in part by the Coordenação de Aperfeiçoamento de Pessoal de Nível Superior – Brasil (CAPES) – Finance Code 001, Fundação de Amparo à Pesquisa do Estado de São Paulo (FAPESP, Proc. 2013/20549-7), and Conselho Nacional de Desenvolvimento Científico e Tecnológico (CNPq, Proc. 402076/2016-8).

REFERENCES

Behar, J. A., Rosenberg, A. A., Shemla, O., Murphy, K. R., Koren, G., Billman, G. E., et al. (2018). A universal scaling relation for defining power spectral bands in mammalian heart rate variability analysis. *Front. Physiol.* 9:1001. doi: 10.3389/fphys.2018.01001

Bertinieri, G., di Rienzo, M., Cavallazzi, A., Ferrari, A. U., Pedotti, A., and Mancia, G. (1985). A new approach to analysis of the arterial baroreflex. *J. Hypertens. Suppl.* 3, S79–S81.

Bertinieri, G., Di Rienzo, M., Cavallazzi, A., Ferrari, A. U., Pedotti, A., and Mancia, G. (1988). Evaluation of baroreceptor reflex by blood pressure monitoring in unanesthetized cats. *Am. J. Physiol. Heart Circ. Physiol.* 254, H377–H383. doi: 10.1152/ajpheart.1988.254.2.H377

Cerutti, C., Barres, C., and Paultre, C. (1994). Baroreflex modulation of blood pressure and heart rate variabilities in rats: assessment by spectral analysis. *Am. J. Physiol.* 266, H1993–H2000. doi: 10.1152/ajpheart.1994.266.5.H1993

Cerutti, C., Gustin, M. P., Paultre, C. Z., Lo, M., Julien, C., Vincent, M., et al. (1991). Autonomic nervous system and cardiovascular variability in rats: a spectral analysis approach. *Am. J. Physiol. Heart Circ. Physiol.* 261, H1292–H1299. doi: 10.1152/ajpheart.1991.261.4.H1292

De Maria, B., Bari, V., Ranucci, M., Pistuddi, V., Ranuzzi, G., Takahashi, A. C. M., et al. (2018). Separating arterial pressure increases and decreases in assessing cardiac baroreflex sensitivity via sequence and bivariate phase-rectified signal averaging techniques. *Med. Biol. Eng. Comput.* 56, 1241–1252. doi: 10.1007/s11517-017-1765-0

Di Rienzo, M., Parati, G., Castiglioni, P., Tordi, R., Mancia, G., and Pedotti, A. (2001). Baroreflex effectiveness index: an additional measure of baroreflex control of heart rate in daily life. *Am. J. Physiol. Regul. Integr. Comp. Physiol.* 280, R744–R751. doi: 10.1152/ajpregu.2001.280.3.R744

Dias, D. P. M., Silva, L. E. V., Katayama, P. L., Silva, C. A., Salgado, H. C., and Fazan, R. (2016). Correlation between RR, inter-systolic and inter-diastolic intervals and their differences for the analysis of spontaneous heart rate variability. *Physiol. Meas.* 37, 1120–1128. doi: 10.1088/0967-3334/37/7/1120

Faes, L., Nollo, G., and Porta, A. (2011). Information domain approach to the investigation of cardio-vascular, cardio-pulmonary, and vasculo-pulmonary causal couplings. *Front. Physiol.* 2:80. doi: 10.3389/fphys.2011.00080

Faes, L., Widesott, L., Del Greco, M., Antolini, R., and Nollo, G. (2006). Causal cross-spectral analysis of heart rate and blood pressure variability for describing the impairment of the cardiovascular control in neurally mediated syncope. *IEEE Trans. Biomed. Eng.* 53, 65–73. doi: 10.1109/TBME.2005.859788

Fazan, R., de Oliveira, M., da Silva, V. J. D., Joaquim, L. F., Montano, N., Porta, A., et al. (2005). Frequency-dependent baroreflex modulation of blood pressure and heart rate variability in conscious mice. *Am. J. Physiol. Heart Circ. Physiol.* 289, H1968–H1975. doi: 10.1152/ajpheart.01224.2004

Helen Mary, M. C., Singh, D., and Deepak, K. K. (2018). Impact of respiration on cardiovascular coupling using Granger causality analysis in healthy subjects. *Biomed. Signal Proc. Control* 43, 196–203. doi: 10.1016/j.bspc.2018.03.008

Julien, C. (2008). Baroreflex control of sympathetic nerve activity and blood pressure variability. *Clin. Exp. Pharmacol. Physiol.* 35, 512–515. doi: 10.1111/j.1440-1681.2008.04907.x

La Rovere, M. T., Pinna, G. D., and Raczak, G. (2008). Baroreflex sensitivity: measurement and clinical implications. *Ann. Noninvas. Electrocardiol.* 13, 191–207. doi: 10.1111/j.1542-474X.2008.00219.x

Lataro, R. M., Silva, L. E. V., Silva, C. A. A., Salgado, H. C., and Fazan, R. (2017). Baroreflex control of renal sympathetic nerve activity in early heart failure assessed by the sequence method. *J. Physiol.* 595, 3319–3330. doi: 10.1113/JP274065

Laude, D., Baudrie, V., and Elghozi, J.-L. (2008). Applicability of recent methods used to estimate spontaneous baroreflex sensitivity to resting mice. *Am. J. Physiol. Regul. Integr. Comp. Physiol.* 294, R142–R150. doi: 10.1152/ajpregu.00319.2007

Laude, D., Baudrie, V., and Elghozi, J.-L. (2009). Tuning of the sequence technique. *IEEE Eng. Med. Biol. Mag.* 28, 30–34. doi: 10.1109/MEMB.2009.934630

Laude, D., Elghozi, J.-L., Girard, A., Bellard, E., Bouhaddi, M., Castiglioni, P., et al. (2004). Comparison of various techniques used to estimate spontaneous baroreflex sensitivity (the EuroBaVar study). *Am. J. Physiol. Regul. Integr. Comp. Physiol.* 286, R226–R231. doi: 10.1152/ajpregu.00709.2002

Levick, J. (2000). *Introduction to Cardiovascular Physiology*, 3rd Edn. New York, NY: CRC Press.

Mancia, G., Parati, G., Castiglioni, P., and di Rienzo, M. (1999). Effect of sinoaortic denervation on frequency-domain estimates of baroreflex sensitivity in conscious cats. *Am. J. Physiol. Heart Circ. Physiol.* 276, H1987–H1993. doi: 10.1152/ajpheart.1999.276.6.H1987

Oosting, J., Struijker-Boudier, H. A., and Janssen, B. J. (1997). Validation of a continuous baroreceptor reflex sensitivity index calculated from spontaneous fluctuations of blood pressure and pulse interval in rats. *J. Hypertens.* 15, 391–399. doi: 10.1097/00004872-199715040-00010

Penaz, J. (1978). Mayer waves: history and methodology. *Automedica* 2, 135–141.

Pinna, G. D., and Maestri, R. (2001). Reliability of transfer function estimates in cardiovascular variability analysis. *Med. Biol. Eng. Comput.* 39, 338–347. doi: 10.1007/BF02345289

Pinna, G. D., and Maestri, R. (2002). New criteria for estimating baroreflex sensitivity using the transfer function method. *Med. Biol. Eng. Comput.* 40, 79–84. doi: 10.1007/BF02347699

Porta, A., Bari, V., Bassani, T., Marchi, A., Pistuddi, V., and Ranucci, M. (2013a). Model-based causal closed-loop approach to the estimate of baroreflex sensitivity during propofol anesthesia in patients undergoing coronary artery bypass graft. *J. Appl. Physiol.* 115, 1032–1042. doi: 10.1152/japplphysiol.00537.2013

Porta, A., Castiglioni, P., Di Rienzo, M., Bassani, T., Bari, V., Faes, L., et al. (2013b). Cardiovascular control and time domain Granger causality: insights from selective autonomic blockade. *Philos. Trans. A Math. Phys. Eng. Sci.* 371:20120161. doi: 10.1098/rsta.2012.0161

Silva, L. E. V., Geraldini, V. R., de Oliveira, B. P., Silva, C. A. A., Porta, A., and Fazan, R. (2017). Comparison between spectral analysis and symbolic dynamics for heart rate variability analysis in the rat. *Sci. Rep.* 7:8428. doi: 10.1038/s41598-017-08888-w

Silva, L. E. V., and Katayama, P. L. (2017). Baroreflex-mediated sympathetic overactivation induced by mental stress in post-traumatic stress disorder depends on the type of stressor. *J. Physiol.* 595, 5757–5758. doi: 10.1113/JP274859

Stauss, H. M., Moffitt, J. A., Chapleau, M. W., Abboud, F. M., and Johnson, A. K. (2006). Baroreceptor reflex sensitivity estimated by the sequence technique is reliable in rats. *Am. J. Physiol. Heart Circ. Physiol.* 291, H482–H483. doi: 10.1152/ajpheart.00228.2006

Stauss, H. M., Persson, P. B., Johnson, A. K., and Kregel, K. C. (1997). Frequency-response characteristics of autonomic nervous system function in conscious rats. *Am. J. Physiol. Heart Circ. Physiol.* 273, H786–H795. doi: 10.1152/ajpheart.1997.273.2.H786

Topçu, Ç, Frühwirth, M., Moser, M., Rosenblum, M., and Pikovsky, A. (2018). Disentangling respiratory sinus arrhythmia in heart rate variability records. *Physiol. Meas.* 39:054002. doi: 10.1088/1361-6579/aabea4

Waki, H., Katahira, K., Polson, J. W., Kasparov, S., Murphy, D., and Paton, J. F. R. (2006). Automation of analysis of cardiovascular autonomic function from chronic measurements of arterial pressure in conscious rats. *Exp. Physiol.* 91, 201–213. doi: 10.1113/expphysiol.2005.031716

Welch, P. (1967). The use of fast fourier transform for the estimation of power spectra: a method based on time averaging over short, modified periodograms. *IEEE Trans. Audio Electroacoust.* 15, 70–73. doi: 10.1109/TAU.1967.1161901

Conflict of Interest Statement: The authors declare that the research was conducted in the absence of any commercial or financial relationships that could be construed as a potential conflict of interest.

frontiers in Neuroscience

ORIGINAL RESEARCH
published: 05 March 2019
doi: 10.3389/fnins.2019.00193

Novel Approach to Elucidate Human Baroreflex Regulation at the Brainstem Level: Pharmacological Testing During fMRI

Darius A. Gerlach[1], Jorge Manuel[2], Alex Hoff[1], Hendrik Kronsbein[1,3], Fabian Hoffmann[1,4], Karsten Heusser[1], Heimo Ehmke[3], André Diedrich[5], Jens Jordan[6], Jens Tank[1†] and Florian Beissner[2†]*

[1] Department of Cardiovascular Aerospace Medicine, Institute of Aerospace Medicine, German Aerospace Center (DLR), Cologne, Germany, [2] Somatosensory and Autonomic Therapy Research, Institute for Neuroradiology, Hannover Medical School, Hanover, Germany, [3] Institute of Cellular and Integrative Physiology, University Medical Center Hamburg-Eppendorf, Hamburg, Germany, [4] Division of Cardiology, Angiology and Pneumology, Cologne Heart Center, University Hospital Cologne, Cologne, Germany, [5] Division of Clinical Pharmacology, Department of Medicine, Autonomic Dysfunction Service, Vanderbilt University, Nashville, TN, United States, [6] Chair of Aerospace Medicine, Institute of Aerospace Medicine, German Aerospace Center (DLR), Helmholtz Association of German Research Centers, Cologne, Germany

Introduction: Brainstem nuclei govern the arterial baroreflex, which is crucial for heart rate and blood pressure control. Yet, brainstem function is difficult to explore in living humans and is therefore mostly studied using animal models or postmortem human anatomy studies. We developed a methodology to identify brainstem nuclei involved in baroreflex cardiovascular control in humans by combining pharmacological baroreflex testing with functional magnetic resonance imaging.

Materials and Methods: In 11 healthy men, we applied eight repeated intravenous phenylephrine bolus doses of 25 and 75 μg followed by a saline flush using a remote-controlled injector during multiband functional magnetic resonance imaging (fMRI) acquisition of the whole brain including the brainstem. Continuous finger arterial blood pressure, respiration, and electrocardiogram (ECG) were monitored. fMRI data were preprocessed with a brainstem-specific pipeline and analyzed with a general linear model (GLM) to identify brainstem nuclei involved in central integration of the baroreceptor input.

Results: Phenylephrine elicited a pressor response followed by a baroreflex-mediated lengthening of the RR interval (25 μg: 197 ± 15 ms; 75 μg: 221 ± 33 ms). By combining fMRI responses during both phenylephrine doses, we identified significant signal changes in the nucleus tractus solitarii (t = 5.97), caudal ventrolateral medulla (t = 4.59), rostral ventrolateral medulla (t = 7.11), nucleus ambiguus (t = 5.6), nucleus raphe obscurus (t = 6.45), and several other brainstem nuclei [$p < 0.0005$ family-wise error (few)-corr.].

OPEN ACCESS

Edited by:
Alberto Porta,
University of Milan, Italy

Reviewed by:
John M. Karemaker,
University Medical Center Amsterdam, Netherlands
Roberto Maestri,
IRCCS Istituti Clinici Scientifici Maugeri (ICS Maugeri), Italy
Antonio Roberto Zamunér,
Catholic University of the Maule, Chile

****Correspondence:***
Darius A. Gerlach
Darius.Gerlach@dlr.de

† These authors have contributed equally to this work as senior authors

Specialty section:
This article was submitted to Autonomic Neuroscience, a section of the journal Frontiers in Neuroscience

Received: *13 December 2018*
Accepted: *19 February 2019*
Published: *05 March 2019*

Citation:
Gerlach DA, Manuel J, Hoff A, Kronsbein H, Hoffmann F, Heusser K, Ehmke H, Diedrich A, Jordan J, Tank J and Beissner F (2019) Novel Approach to Elucidate Human Baroreflex Regulation at the Brainstem Level: Pharmacological Testing During fMRI. Front. Neurosci. 13:193. doi: 10.3389/fnins.2019.00193

Conclusion: Pharmacological baroreflex testing during fMRI allows characterizing central baroreflex regulation at the level of the brainstem in humans. Baroreflex-mediated activation and deactivation patterns are consistent with previous investigations in animal models. The methodology has the potential to elucidate human physiology and mechanisms of autonomic cardiovascular disease.

Keywords: baroreflex, fMRI, brainstem, blood pressure, regulation, cardiovascular, nuclei

INTRODUCTION

Cardiovascular control centers in the brainstem govern arterial baroreflexes, which are important for human blood pressure buffering (Jordan et al., 2002) and long-term blood pressure control (Bisognano et al., 2011). Careful physiological investigations in animals showed that the NTS is the primary relay station for afferent input from carotid and aortic baroreceptors (McAllen and Spyer, 1976; Dampney, 1994). Connections from there to the NA and DMN elicit counter regulatory adjustment in efferent cardiac vagal activity. Projections to the cVLM and from there to the rVLM adjust efferent sympathetic traffic (Dampney, 1994; Dampney et al., 2002). Damage to these brainstem nuclei results in profound abnormalities in human blood pressure control. A patient with ischemic lesions involving bilateral NTS featured afferent baroreflex failure (Biaggioni et al., 1994). Degeneration of brainstem nuclei including the rVLM in patients with multiple system atrophy is associated with severe orthostatic hypotension among other disabling symptoms of efferent baroreflex dysfunction (Benarroch et al., 1998). Even subtle abnormalities in the structure or function of these nuclei could substantially affect human cardiovascular regulation. Yet, while the overall integrity of arterial baroreflex function can be interrogated with physiological and pharmacological baroreflex tests (Bristow et al., 1971, 1974), baroreflex regulation at the level of the brainstem is very difficult to measure in humans. Our goal was to develop a novel approach to assess human baroreflex regulation at the level of the brainstem. Therefore, we combined fMRI of the BOLD, beat-by-beat blood pressure and heart rate monitoring, and phenylephrine bolus injections for pharmacological baroreflex loading. Phenylephrine increases blood pressure leading to baroreflex-mediated vagal activation and sympathoinhibition. Brainstem fMRI has previously been validated for several applications including trigeminal pain research (Schulte et al., 2016), resting state connectivity measurement (Beissner et al., 2014), characterization of the autonomic nervous system (Macefield and Henderson, 2010; Coulson et al., 2015), and studies on sleep apnea (Henderson et al., 2016).

Abbreviations: 12N, hypoglossal nucleus; ANTs, advanced normalization tools; BOLD, blood oxygenation level dependent contrast; cVLM, caudal ventrolateral medulla; DMN, dorsal motor nucleus of the vagus nerve; DPGi, dorsal paragigantocellular nucleus; ECG, electrocardiogram; EPI, echo planar imaging; FOV, field of view; fMRI, functional magnetic resonance imaging; FSL, FMRIB Software Library; FWR-corr., family-wise error correction; GLM, general linear model; IO, inferior olivary nucleus; IRt, intermediate reticular nucleus; LBNP,lower body negative pressure; LPGi, lateral paragigantocellular nucleus; LRt, lateral reticular nucleus; MNI, Montreal Neurological Institute standard space; MPRAGE, 3D magnetization prepared rapid acquisition gradient echo; MRI, magnetic resonance imaging; NA, nucleus ambiguus; NTS, nucleus tractus solitarii; ROb, nucleus raphe obscurus; rVLM, rostral ventrolateral medulla; SBP, systolic blood pressure; SP5, spinal trigeminal nucleus; SpO2, oxygen saturation; SpVe, spinal vestibular nucleus; TE, echo time; TI, inversion time; TR, repetition time.

MATERIALS AND METHODS

Subjects

We included 11 healthy, normotensive (125.7 ± 4.6/73.4 ± 5.5 mmHg, 57.6 ± 7.5 bpm), non-smoking, men aged 30.5 ± 6.3 years with a weight of 78.0 ± 10.6 kg ranging from 65 to 98 kg and a body mass index of 24.0 ± 1.9 kg/m^2. Subjects were normally active and non-sedentary. The study complied with the Declaration of Helsinki was approved by the ethics committee of the Ärztekammer Nordrhein, Düsseldorf, Germany, and all subjects had given their written informed consent before inclusion. We registered the study under clinical trials registration number DRKS00013101 prior to commencement.

Study Design

The study was a randomized controlled interventional trial in an ambulatory setting. Subjects visited the facility on three different days. On the first study day, subjects were familiarized with the MRI environment and physiological recording equipment and underwent medical examination. On the second study day, the subject's baroreflex response to phenylephrine boli was examined. Finally, pharmacological baroreflex testing during fMRI took place on the third study day. Subjects rested before the scan and had abstained from caffeine and alcohol for 24 h. After positioning and instrumentation of the subject followed by a resting period of 20 min in the scanner, we applied repeated intravenous phenylephrine (25 and 75 μg, n = 8) boli followed by a 10 ml normal saline flush using a programmable, MR-compatible remote-controlled injector. We repeated bolus administration every 120 s with n = 8 boli in total. Each fMRI run lasted 16 min 49 s. The 25 and 75 μg doses were applied in separate runs in randomized order. MRI measurements were carried out between 8:40 a.m. to 12:05 p.m. in an air conditioned room kept at a constant 21°C. All subjects were asked about their mood, sleep, and mental state using a customized non-standardized questionnaire before and after the examination. In particular, we asked about sleepiness, pain, and whether the subject perceived any effects of the injection.

MRI Acquisition

We obtained MRI acquisitions with a 3 T scanner (mMR Biograph PET-MRI scanner based on the Verio system, Siemens,

Erlangen, Germany) with a 32-channel head coil. T1-weighted images for anatomical references were acquired using a MPRAGE sequence with the following parameters: TR: 2400 ms, TE: 2.13 ms, TI: 1000 ms, flip angle: 8°, FOV: 246 mm∗192 mm, matrix: 246∗192, slice thickness: 1 mm. T2*-weighted functional images were acquired with an EPI sequence accelerated by multiband acquisition (TR/TE: 1180/32 ms, flip angle: 64°, FOV: 180 mm∗208 mm, matrix: 90∗104, slices: 78 with 2.0 mm slice thickness, voxel size: 2.0 mm isotropic, multiband factor: 6, volumes: 846; Xu et al., 2013; Todd et al., 2016). Unaccelerated single EPI images (TR: 6127 ms, flip angle: 90°) and B0-weighted spin echo EPI (TR/TE: 12,000/102.6 ms) with matched and 180° rotated phase encoding direction were acquired for better gray-white contrast and distortion correction, respectively. The flip angle was chosen according to the Ernst angle for shortened TR. Scans covered the whole brain including the brainstem. The total scan time was 45–50 min per intervention and subject. Image orientation was parallel to the anterior-posterior commissure line for T1-weighted images, whereas functional MRI images were additionally tilted by ∼35° to avoid signal drop-outs in areas of interest. The MRI protocol was optimized according to the findings and recommendations from the human connectome project (Ugurbil et al., 2013). Additional information on MR imaging sequences for the non-specialist can be found in Bitar et al. (2006).

Physiological Recordings

We recorded beat-to-beat finger blood pressure with a modified device based on a commercially available finger blood pressure monitor (NOVA®, FMS, Finapres Measurement Systems, Amsterdam, Netherlands). For MRI compatibility, the device was radio frequency shielded and the cuff to frontend distance was prolonged to increase the frontend's distance to the scanner. We also acquired the ECG and SpO_2 (MR400, PHILIPS, Orlando, FL, United States) as well as respiratory rate and end-tidal CO_2 ($etCO_2$; IVY 450C, Branford, CT, United States). Signals were collected after A/D conversion (WINDAQ, DATAQ, Akron, OH, United States) with a sampling frequency of 500 Hz. Data preprocessing included peak detection, outlier filtering, resampling to fMRI acquisition, and normalization. RR intervals, systolic and diastolic blood pressure values, and respiration rate for each heartbeat and breathing cycle were analyzed. Subjects were equipped with active noise canceling headphones during the fMRI scan (OptoACTIVE, Optoacustics Ltd., Mazor,

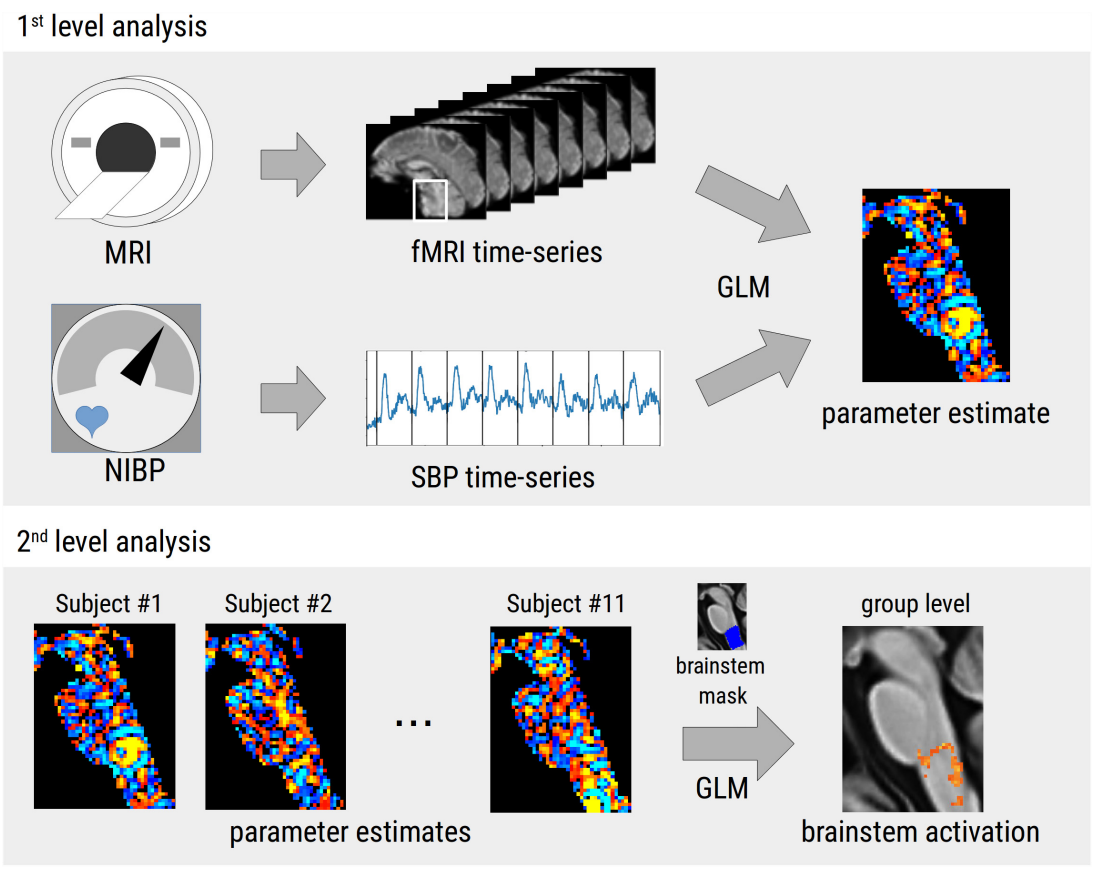

FIGURE 1 | Flow chart of the two-step statistical approach used in the study. In the first-level analysis, the time-course of systolic blood pressure (SBP) recorded during repeated phenylephrine bolus injections was used as regressor in a general linear model (GLM) on the functional MRI time-series leading to voxel-wise parameter estimate maps. In the second-level analysis, parameter estimates of all subjects were combined in a second GLM to calculate a group level statistical parametric map that was thresholded using family-wise error correction and threshold-free cluster enhancement. All analyses were restricted to the lower brainstem.

Israel). A fixed head position was maintained by inflatable pads around the headphones.

Image Analysis and Statistics

We preprocessed fMRI data with FSL tools, v5.0.11 (Oxford Centre for Functional MRI of the Brain, Oxford, United Kingdom; Smith et al., 2004; Woolrich et al., 2009). After conversion of fMRI images to NIFTI format, all multiband EPI were realigned to the unaccelerated EPI image using FSL MCFLIRT. This approach allows for motion correction. At the same time, unwarping was conducted with FSL TOPUP using the spin-echo EPI for distortion correction (Andersson et al., 2003). Multiband EPI were then brain extracted with FSL BET, high-pass filtered with 180 s cut-off, and spatially normalized to a study template made from the T1 and unaccelerated EPI images of all subjects. Template and transformation for registration were calculated using ANTs (Tustison and Avants, 2013). The final preprocessing step was the upsampling to the T1 study template with ANTs.

The preprocessed data were cropped to retain only the lower brainstem and a brainstem mask was applied to remove adjacent areas with high physiological noise (Beissner et al., 2014). However, no spatial smoothing was applied in our study.

Statistical analysis was done with a mixed-effect GLM (**Figure 1**). The full SBP time-course of 16.5 min was used as explanatory variable and regressed against the BOLD signal time-courses of individual voxels. First-level (single-subject) analyses were performed with FSL_GLM and the parameter estimates passed up to a second-level (group) analysis using non-parametric permutation testing with FSL RANDOMISE. Significance was assumed at $p < 0.0005$ corrected for multiple comparisons using family-wise error (FWE) correction and

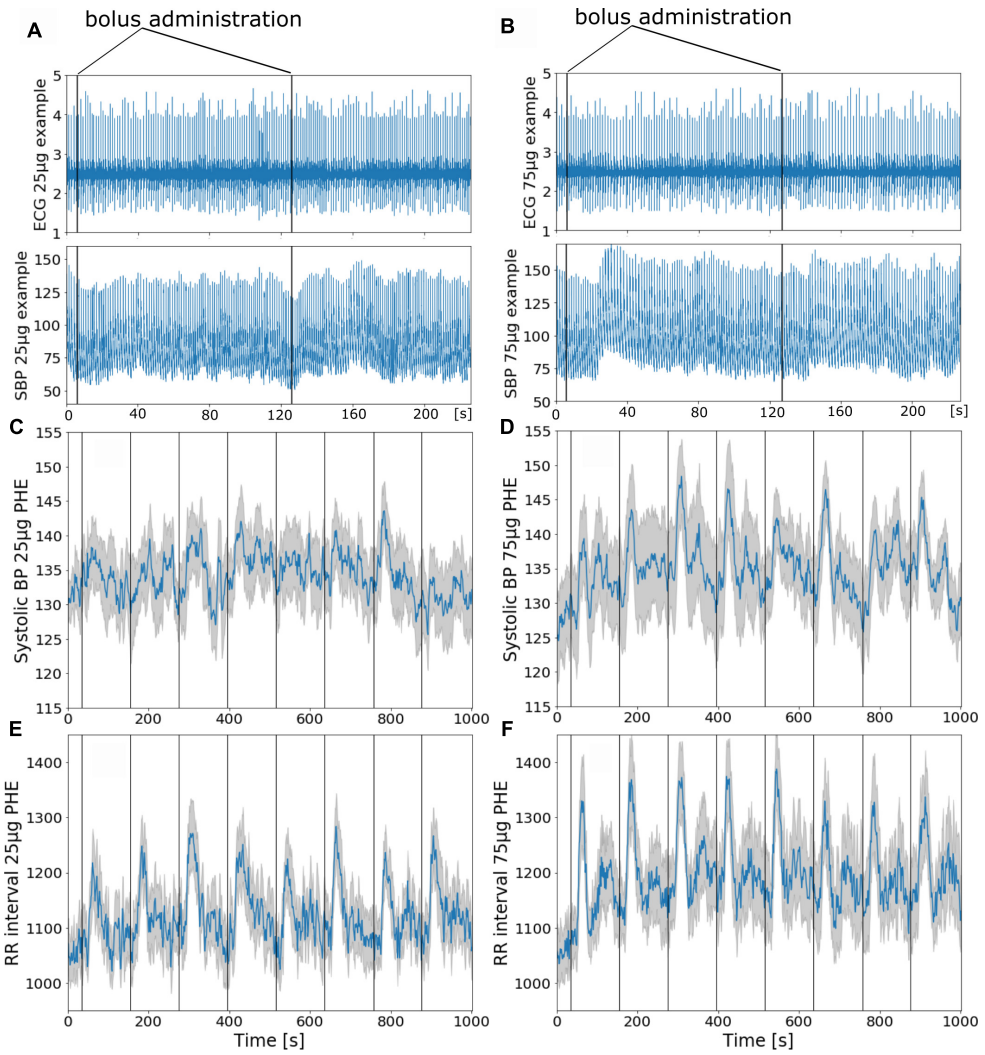

FIGURE 2 | (A,B) Phenylephrine bolus administration (**A**: 25 µg and **B**: 75 µg) with blood pressure and ECG recordings during functional MRI. The vertical black lines indicate bolus injections. **(C–F)** Group mean ± SE (gray curve) physiological recordings from 11 subjects with repeated phenylephrine administration. Systolic pressure **(C)** and RRI from ECG **(E)** recordings during 25 µg phenylephrine and systolic pressure **(D)** and RRI **(F)** recordings during 75 µg phenylephrine bolus administration.

threshold-free cluster enhancement (Smith and Nichols, 2009). Results were reported in the form of *t*-values (defined as the parameter estimate from the GLM divided by the error of the parameter estimate). After statistical analysis, results were transformed to standard space (Montreal Neurological Institute, MNI152 1 mm brain) using ANTs. We further analyzed the correlation between the averaged BOLD time-courses with the group mean SBP by extracting the BOLD signal from the masked lower brainstem.

RESULTS

Pharmacological Baroreflex Testing

All subjects reported to have slept well the night before the testing and were well motivated. None of the subjects reported pain provoked by the injection or by lying in the scanner, and all managed to stay awake throughout the test. We obtained good quality finger blood pressure recordings in most instances over the imaging period in 10 out of 11 subjects; in one subject, the signal drop outs were interpolated. Blood pressure traces deteriorated toward the end of the experiment in six of 11 subjects. To compensate for MRI induced artificial signal declines the regularly repeated level – and gain – calibration option (Physiocal^{TM}) was used in some subjects when needed. This resulted in a signal dropout of few seconds that was linearly interpolated. Still, all subjects could be considered for further analysis. **Figures 2A,B** illustrate continuous ECG and finger blood pressure recordings during administration of a 25 μg and a 75 μg phenylephrine bolus dose. **Figures 2C–F** illustrate averaged finger blood pressure RR interval responses to repeated phenylephrine doses; 25 and 75 μg doses increased SBP 5 ± 2 and 15 ± 2 mmHg, respectively. The pressor response elicited baroreflex-mediated heart rate reductions (RR interval lengthening 197 ± 15 ms with 25 μg: and 221 ± 33 ms with 75 μg). Despite the relatively short period between the repeated boli of only 2 min blood pressure did not increase over the 16.5 min imaging time. Baroreflex sensitivity estimation resulted in mean values13.8 ± 7.4 ms/mmHg for 25 μg and 14.1 ± 4.6 ms/mmHg for 75 μg ranging from 3.4 to 40.1 ms/mmHg. Baroreflex sensitivity was not always detectable especially during the 25 μg doses.

Brainstem fMRI

The GLM of the BOLD signal with SBP revealed significant activations (i.e., positive correlation) on the group level. Thus, an increase in SBP was related to an increase of the BOLD signal in the respective voxels. The analysis was first conducted separately for 25 and 75 μg phenylephrine doses, resulting in a single significant voxel for the 75 μg runs that was located in the NTS. A paired *t*-test between the 25 and 75 μg bolus administrations showed no differences, which led us to pool the data and improve statistical power. Based on this pooled analysis, we found significant activations in a number of brainstem nuclei that were subsequently identified using the Paxinos brainstem atlas (Paxinos et al., 2012). These nuclei comprised the NTS, cVLM and rVLM, ROb, DMN, nucleus hypoglossus (12N), inferior olive (IO), and different reticular nuclei. MNI coordinates and corresponding *t*-values are shown in **Table 1**.

TABLE 1 | Identified brainstem nuclei.

Side	*t*-value	MNI: *x* (mm)	MNI: *y* (mm)	MNI: *z* (mm)	Brainstem nuclei
r	7.21	5	−38	−60	Inferior olive (IO)
l	7.11	−8	−38	−46	Rostral ventrolateral medulla (rVLM)
					Lateral reticular nucleus (LRt)
					Lateral paragigantocellular nucleus (LPGi)
l/r	6.62	2	−43	−51	Hypoglossal nucleus (12N)
	6.45	1	−45	−57	Raphe obscurus nucleus (ROb)
l	6.29	−3	−43	−56	Intermediate reticular nucleus (IRt)
l	5.97	−1	−45	−54	Dorsal motor nucleus of the vagal nerve (DMN)
					Nucleus tractus solitarii(NTS)
r	5.67	7	−34	−45	Rostral ventrolateral medulla (rVLM)
r	5.67	2	−40	−44	Dorsal paragigantocellular nucleus (DPGi)
r	5.61	7	−42	−56	Spinal trigeminal nucleus (SP5)
r	5.6	6	−40	−48	Nucleus ambiguus (NA)
l	4.98	−7	−44	−56	Spinal trigeminal nucleus (SP5)
r	4.59	6	−38	−55	Caudal ventrolateral medulla (cVLM)
l	4.72	−5	−46	−53	Spinal vestibular nucleus (SpVe)
l	4.43	−6	−35	−55	Inferior olive (IO)
r	4.4	6	−45	−50	Medial vestibular nucleus
l	4.05	−5	−42	−48	Nucleus tractus solitarii (NTS)

All brainstem nuclei encompassed in the cluster were identified using a brainstem atlas. Active regions after $p < 0.0005$ threshold are reported in MNI standard space coordinates with the corresponding t-values for the local maxima. (Larger t-values indicate better correlation between fMRI signal and systolic blood pressure. The t-value is defined as the parameter estimate from the GLM divided by the error of the parameter estimate.) Cluster size: 1437 (mm^3), center of gravity x: 1.46, y: −40, z: −51.6. MNI: Montreal Neurological Institute.

The relationship between the averaged time-courses of the whole lower brainstem BOLD signal and SBP is depicted in **Figure 3**. Both signals exhibit strong variations and a poor correlation (R = 0.25). Thus, blood pressure changes alone are most likely not the only contributor to the fluctuations of the BOLD signal.

Figure 4 illustrates the significant group level activations. Overlaid anatomical atlas slices were used to identify the nuclei.

DISCUSSION

The important finding of our study is that pharmacological baroreflex testing combined with fMRI reveals brainstem nuclei

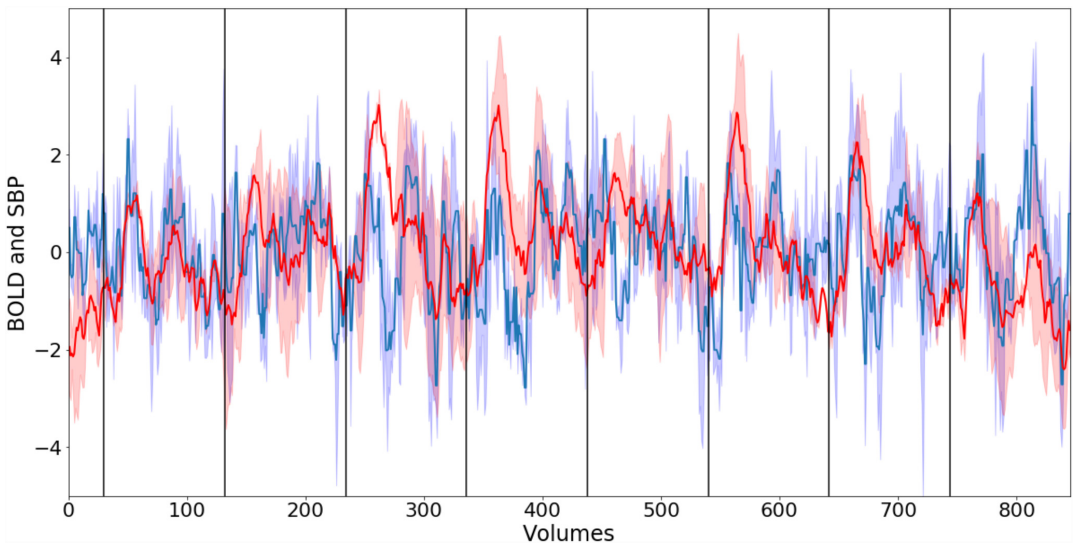

FIGURE 3 | Normalized smoothed group mean BOLD signal (blue) from lower brainstem and group mean systolic blood pressure (SBP) (red). Corresponding blue and red areas depict standard error. Black vertical lines indicate the start of phenylephrine bolus injections. The correlation R between both time-courses is 0.25.

involved in human baroreflex regulation. In humans, we identified with high sensitivity all of the brainstem nuclei that have previously been shown to contribute to the baroreflex circuit in animals. Our approach can now be applied to elucidate the role of the human brainstem in cardiovascular physiology and in the pathogenesis of human cardiovascular disease.

The combination of continuous cardiovascular monitoring and brainstem fMRI during baroreflex loading with phenylephrine is a particular strength of our study. Beat-by-beat blood pressure can so far only be assessed non-invasively with volume-clamp methods based on the Penàz servo-plethysmomanometer (Molhoek et al., 1984). Devices based on this principle (i.e., NOVA®, FMS, Finapres Measurement Systems, Amsterdam, Netherlands) are crucial for interrogating baroreflex function, need to be heavily modified for MRI studies and are only available in a few laboratories worldwide (Critchley et al., 2015). Other than the volume-clamp principle, there are commercially available non-invasive blood pressure systems for MRI (i.e., Biopac Systems Inc., Goleta, CA, United States) that are based on pulse decomposition analysis. The methodology is rather an indirect measure for the blood pressure (Baruch et al., 2011). Furthermore, brainstem fMRI is still challenging because of the strong physiological noise sources surrounding it (Beissner et al., 2014; Beissner, 2015). Due to the small size of brainstem nuclei, fMRI methods optimized for cortical structures cannot be applied (Beissner, 2015). Moreover, respiration, blood flow, and cerebrospinal fluid pulsations produce magnetic field distortions, out of phase spins and structural displacement (Brooks et al., 2013). Therefore, we aimed at maximizing statistical power by applying repeated stimulation with phenylephrine in a highly standardized fashion. To avoid non-specific effects of phenylephrine on brain circulation, we applied low and moderate phenylephrine doses (La Rovere et al., 1998). Baroreflex loading with phenylephrine produces an afferent signal that is conveyed to the NTS. Baroreflex afferent recordings in animal experiments and in patients during carotid surgery showed that signal time-course and magnitude were related to blood pressure. Since afferent nerve signals cannot be reasonably recorded in a human study, we utilized beat-by-beat blood pressure as input for our GLM analysis. We are aware that afferent baroreceptor input to NTS also feeds back on blood pressure. Compared with prior studies, our approach yields several advantages in delineating central baroreflex control. Previously applied autonomic challenges during fMRI include LBNP (Kimmerly et al., 2005), isometric handgrip testing (Coulson et al., 2015), Valsalva maneuver (Henderson et al., 2002), and slow breathing (Critchley et al., 2015). Handgrip and cold pressor testing engage central autonomic circuits through muscle afferents and pain fibers rather than baroreflex input. The Valsalva maneuver requires active participation likely confounding fMRI analysis and its effects are entangled with that of transient hypercapnia. The major challenge of LBNP is that it induces movement artifacts, when subjects are sucked down into the chamber. Moreover, the input stimulus for fMRI is commonly conceptualized as a boxcar time-course (on vs. off). Instead, we measured blood pressure time-course and magnitude during pharmacological baroreflex loading. It should be noted that BOLD contrast captures changes in neural activity but cannot readily differentiate neural inhibition and activation over time (Logothetis, 2008).

We reasoned that a methodology assessing brainstem baroreflex integration should recapitulate known baroreflex circuits. Indeed, baroreflex loading with phenylephrine yielded positive correlations between BOLD signals in the NTS and SBP. We also observed baroreflex-related BOLD signal changes in the NA which governs efferent cardiac vagal activity. Furthermore, baroreflex loading significantly changed BOLD signals in nuclei involved in sympathetic control including cVLM, rVLM,

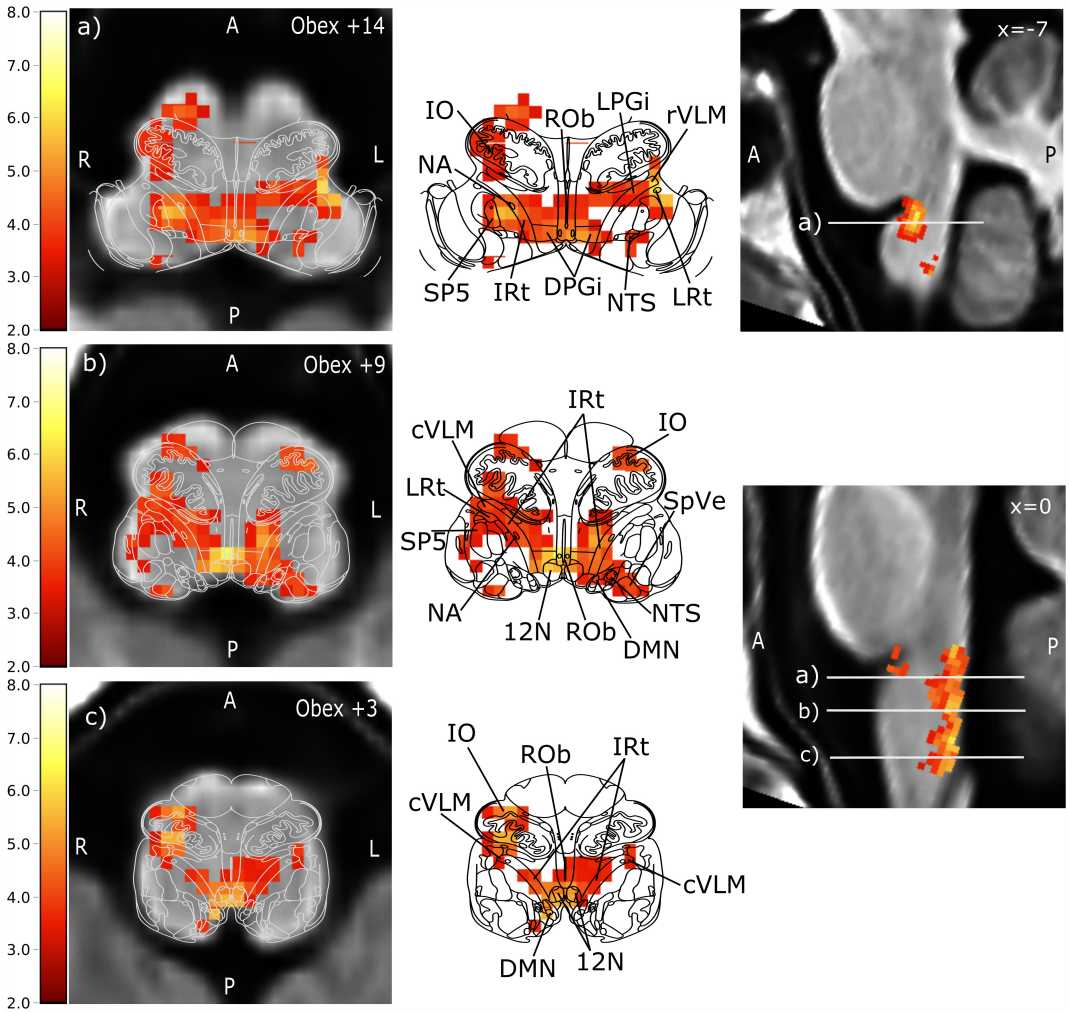

FIGURE 4 | Brainstem regions showing activations associated with blood pressure changes elicited by phenylephrine bolus injections. Group level results of all 11 subjects using data from all 16 boli. For visualization purposes, the images were tilted such that the resulting sections were perpendicular to the rostro-caudal brainstem axis to match the anatomical atlas. Left: transversal lower brainstem slices with of anatomical group template overlaid with the statistical parametric map of the positive BOLD correlation with SBP (*t*-values encoded by color scale) and the corresponding atlas slice (modified from Paxinos brainstem atlas). Middle: BOLD overlay with the Paxinos brainstem atlas (Paxinos et al., 2012). Right: sagittal view of the brainstem. The corresponding transversal slices are marked by white lines with the letters of the sub-figure. Prominent activation maxima include **(a)** left rostral ventrolateral medulla (rVLM), Ncl. raphe obscurus (ROb), and right Ncl. ambiguus (NA), **(b)** Ncl. raphe obscurus (ROb), left intermediate reticular nucleus (IRt) extending to nucleus tractus solitarii, and right caudal ventrolateral medulla (cVLM), and **(c)** Ncl. hypoglossus (12N) extending to IRt and dorsal motor nucleus of the vagal nerve (DMN), right inferior olive extending to the cVLM. Further activated nuclei are: lateral reticular nucleus (LRt), dorsal paragigantocellular nucleus (DPGi), lateral paragigantocellular nucleus (LPGi), spinal trigeminal nucleus (SP5) and spinal vestibular nucleus (SpVe). A: anterior, P: posterior, L: left, R: right.

and raphe obscurus and provided more detailed coverage of baroreflex-regulated brainstem nuclei compared with previous fMRI studies in humans. Thus, fMRI resting state measurements combined with consecutively recorded muscle sympathetic nerve activity (Macefield and Henderson, 2010) suggested positive correlations between efferent sympathetic activity and the rVLM BOLD signal and negative correlations between sympathetic activity and NTS, cVLM BOLD signals. In another study, BOLD signals increased in broad regions including rVLM and decreased in cVLM and in medullary dorsomedial regions during inspiratory capacity apnea compared to relaxed breathing conditions (Macefield et al., 2006). Activation of higher cortical centers was reported in a baroreceptor unloading study with LBNP including insular frontoparietal cortex, and cerebellum (Kimmerly et al., 2005). Our localization of the rVLM, one of the central regions of baroreflex regulation, shows excellent correspondence with coordinates previously reported from a study correlating BOLD and blood pressure responses during hypoxia and normoxia and various breathing maneuvers (Critchley et al., 2015). Additionally, the IO, different reticular nuclei, 12N, and ROb were activated although they are traditionally not linked to blood pressure regulation. Even though some investigators suggested that these nuclei contribute to blood pressure control (Smith and Nathan, 1966; Miura and Reis, 1971),

their role is not fully understood, yet. Because our methodology reliably identified previously known baroreflex-related brainstem nuclei, now human brain areas not previously accessible or not considered to relate to baroreflex activity can be interrogated.

Limitations

The BOLD signal is altered with changes in cerebral blood volume and blood flow (Logothetis, 2008). We cannot fully exclude that phenylephrine indirectly or directly affected cerebral circulation, which could affect fMRI analysis. In rabbits, phenylephrine increased blood pressure and cerebral blood flow while cerebral blood volume and de- and oxyhemoglobin were left unchanged (Koyama et al., 1990). The finding is reassuring since the latter influence the BOLD signal. Moreover, phenylephrine did not produce cerebral vasoconstriction in patients during anesthesia whereas the volatile anesthetic isoflurane increased cerebral blood flow (Strebel et al., 1998). In contrast, cerebral tissue oxygenation decreased with phenylephrine during anesthesia patients with unchanged cerebrovascular volume (Meng et al., 2012). However, none of these responses could explain specific BOLD signal changes in brainstem baroreflex circuits. Indeed, phenylephrine was also applied to elucidate baroreflex-mediated BOLD signal responses in cats before and after baroreceptor denervation (Henderson et al., 2004).

The number of subjects in our study is relatively low in comparison to conventional cortical fMRI studies, even though we were able to demonstrate significant activations based on the high number of stimuli used. Thus, our sample may not represent the average population, which should be considered when generalizing our results. However, most of our results are consistent with previous studies applying LBNP, Valsalva maneuver, hand grip, or inspiratory load (Macey et al., 2015). Finally, our spatial resolution of 2 mm isotropic limits our ability to clearly separate nuclei that are in close vicinity. For example, we cannot rule out that the activation of the DMN observed in our study was not based on signal spreading from the neighboring NTS. Future technological developments may mitigate this problem as may improved experimental designs.

Perspectives

We developed a novel approach to elucidate human baroreflex regulation at the level of the brainstem. The methodology can be applied to investigate human physiology. Indeed, much of our knowledge on central nervous baroreflex integration relies on animal studies and it has been difficult translating these findings to human subjects. Furthermore, the methodology can now be applied to investigate conditions associated with altered baroreflex function, dissect out the localization of the dysfunction, and, perhaps, target treatments in a more rational fashion. For example, fMRI-based baroreflex testing could be utilized to differentiate rare central and peripheral autonomic failure syndromes at an earlier stage. In common cardiovascular disorders such as heart failure, impaired baroreflex function heralds a poor prognosis (La Rovere et al., 1998, 2013). Better mechanistic understanding may beget new treatment approaches. Finally, device-based therapies targeting baroreflex afferents through electrical carotid sinus stimulation have been recently developed and tested in patients with resistant arterial hypertension and with heart failure (Heusser et al., 2010; Scheffers et al., 2010; Gronda et al., 2014). However, the response to electrical carotid sinus stimulation is variable and the proportion of non-responders is unacceptably high. Perhaps, brainstem studies could be developed further and then utilized to identify patients that are more or less likely to respond. To achieve these goals, the methodology should be tested in more detail, particularly in conditions associated with baroreflex impairment. Furthermore, the imaging methodology should be further refined. For example, more sophisticated analyses like masked independent component analysis (Moher Alsady et al., 2016) and frequency-based analysis of BOLD signals in resting-state settings (Chang and Glover, 2010) could prove useful.

DATA AVAILABILITY

The raw data supporting the conclusions of this manuscript will be made available by the authors, without undue reservation, to any qualified researcher. The datasets generated for this study are available on request to the corresponding author.

AUTHOR CONTRIBUTIONS

DG was the study coordinator and contributed to fMRI physiological data acquisition and analysis and writing of the manuscript. JM contributed to scripting of preprocessing, discussion of analysis and results, and revision of the manuscript. AH contributed to adjustment of fMRI compatible setup and physiological data acquisition. HK contributed to subject recruitment and physiological data acquisition. FH contributed to subject supervision and physiological data acquisition. KH contributed to data review and interpretation and revision of the manuscript. HE revised the manuscript. AD contributed to physiological data analysis. JJ contributed to data discussion and revision of the manuscript and was the supervisor. JT contributed to study idea and revision of the manuscript and was the project supervisor. FB contributed to study idea, statistical analysis, discussion of analysis and results, and revision of the manuscript.

FUNDING

This study was funded by the DLR internal cost object 2475023. FH was funded by University Hospital Cologne grant: 50WB1816 and DLR grant: 50WB1517.

ACKNOWLEDGMENTS

We are grateful for receiving the sequence "multibanded slice accelerated EPI with controlled aliasing" from the University of Minnesota Center for Magnetic Resonance Research. Furthermore, we are grateful to Finapres Measurement Systems (FMS, Amsterdam, Netherlands) for the extensive cooperation permitting customization of the finger blood pressure device NOVA® for MRI compatibility.

REFERENCES

Andersson, J. L. R., Skare, S., and Ashburner, J. (2003). How to correct susceptibility distortions in spin-echo echo-planar images: application to diffusion tensor imaging. *Neuroimage* 20, 870–888. doi: 10.1016/S1053-8119(03)00336-7

Baruch, M. C., Warburton, D. E., Bredin, S. S., Cote, A., Gerdt, D. W., and Adkins, C. M. (2011). Pulse Decomposition Analysis of the digital arterial pulse during hemorrhage simulation. *Nonlinear Biomed. Phys.* 5:1. doi: 10.1186/1753-4631-5-1

Beissner, F. (2015). Functional MRI of the brainstem: common problems and their solutions. *Clin. Neuroradiol.* 25(Suppl. 2), 251–257. doi: 10.1007/s00062-015-0404-0

Beissner, F., Schumann, A., Brunn, F., Eisentrager, D., and Bar, K. J. (2014). Advances in functional magnetic resonance imaging of the human brainstem. *Neuroimage* 86, 91–98. doi: 10.1016/j.neuroimage.2013.07.081

Benarroch, E. E., Smithson, I. L., Low, P. A., and Parisi, J. E. (1998). Depletion of catecholaminergic neurons of the rostral ventrolateral medulla in multiple systems atrophy with autonomic failure. *Ann. Neurol.* 43, 156–163. doi: 10.1002/ana.410430205

Biaggioni, I., Whetsell, W. O., Jobe, J., and Nadeau, J. H. (1994). Baroreflex failure in a patient with central nervous system lesions involving the nucleus tractus solitarii. *Hypertension* 23, 491–495. doi: 10.1161/01.HYP.23.4.491

Bisognano, J. D., Bakris, G., Nadim, M. K., Sanchez, L., Kroon, A. A., Schafer, J., et al. (2011). Baroreflex activation therapy lowers blood pressure in patients with resistant hypertension: results from the double-blind, randomized, placebo-controlled rheos pivotal trial. *J. Am. Coll. Cardiol.* 58, 765–773. doi: 10.1016/j.jacc.2011.06.008

Bitar, R., Leung, G., Perng, R., Tadros, S., Moody, A. R., Sarrazin, J., et al. (2006). MR pulse sequences: what every radiologist wants to know but is afraid to ask. *Radiographics* 26, 513–537. doi: 10.1148/rg.262055063

Bristow, J. D., Brown, E. B., Cunningham, D. J. C., Goode, R. C., Howson, M. G., and Sleight, P. (1971). The effects of hypercapnia, hypoxia and ventilation on the baroreflex regulation of the pulse interval. *J. Physiol.* 216, 281–302. doi: 10.1113/jphysiol.1971.sp009525

Bristow, J. D., Brown, E. B., Cunningham, D. J. C., Howson, M. G., Lee, M. J. R., Pickering, T. G., et al. (1974). The effects of raising alveolarPCO2and ventilation separately and together on the sensitivity and setting of the baroreceptor cardiodepressor reflex in man. *J. Physiol.* 243, 401–425. doi: 10.1113/jphysiol.1974.sp010760

Brooks, J. C., Faull, O. K., Pattinson, K. T., and Jenkinson, M. (2013). Physiological noise in brainstem FMRI. *Front. Hum. Neurosci.* 7:623. doi: 10.3389/fnhum.2013.00623

Chang, C., and Glover, G. H. (2010). Time-frequency dynamics of resting-state brain connectivity measured with fMRI. *Neuroimage* 50, 81–98. doi: 10.1016/j.neuroimage.2009.12.011

Coulson, J. M., Murphy, K., Harris, A. D., Fjodorova, M., Cockcroft, J. R., and Wise, R. G. (2015). Correlation between baseline blood pressure and the brainstem FMRI response to isometric forearm contraction in human volunteers: a pilot study. *J. Hum. Hypertens.* 29, 449–455. doi: 10.1038/jhh.2014.103

Critchley, H. D., Nicotra, A., Chiesa, P. A., Nagai, Y., Gray, M. A., Minati, L., et al. (2015). Slow breathing and hypoxic challenge: cardiorespiratory consequences and their central neural substrates. *PLoS One* 10:e0127082. doi: 10.1371/journal.pone.0127082

Dampney, R. A. (1994). Functional organization of central pathways regulating the cardiovascular system. *Physiol. Rev.* 74, 323–364. doi: 10.1152/physrev.1994.74.2.323

Dampney, R. A. L., Coleman, M. J., Fontes, M. A. P., Hirooka, Y., Horiuchi, J., Li, Y. W., et al. (2002). Central mechanisms underlying short- and long-term regulation of the cardiovascular system. *Clin. Exp. Pharmacol. Physiol.* 29, 261–268. doi: 10.1046/j.1440-1681.2002.03640.x

Gronda, E., Seravalle, G., Brambilla, G., Costantino, G., Casini, A., Alsheraei, A., et al. (2014). Chronic baroreflex activation effects on sympathetic nerve traffic, baroreflex function, and cardiac haemodynamics in heart failure: a proof-of-concept study. *Eur. J. Heart Fail.* 16, 977–983. doi: 10.1002/ejhf.138

Henderson, L. A., Fatouleh, R. H., Lundblad, L. C., Mckenzie, D. K., and Macefield, V. G. (2016). Effects of 12 months continuous positive airway pressure on sympathetic activity related brainstem function and structure in obstructive sleep apnea. *Front. Neurosci.* 10:90. doi: 10.3389/fnins.2016.00090

Henderson, L. A., Macey, P. M., Macey, K. E., Frysinger, R. C., Woo, M. A., Harper, R. K., et al. (2002). Brain responses associated with the Valsalva maneuver revealed by functional magnetic resonance imaging. *J. Neurophysiol.* 88, 3477–3486. doi: 10.1152/jn.00107.2002

Henderson, L. A., Richard, C. A., Macey, P. M., Runquist, M. L., Yu, P. L., Galons, J. P., et al. (2004). Functional magnetic resonance signal changes in neural structures to baroreceptor reflex activation. *J. Appl. Physiol.* 96, 693–703. doi: 10.1152/japplphysiol.00852.2003

Heusser, K., Tank, J., Engeli, S., Diedrich, A., Menne, J., Eckert, S., et al. (2010). Carotid baroreceptor stimulation, sympathetic activity, baroreflex function, and blood pressure in hypertensive patients. *Hypertension* 55, 619–626. doi: 10.1161/HYPERTENSIONAHA.109.140665

Jordan, J., Tank, J., Shannon, J. R., Diedrich, A., Lipp, A., SchröDer, C., et al. (2002). Baroreflex buffering and susceptibility to vasoactive drugs. *Circulation* 105, 1459–1464. doi: 10.1161/01.CIR.0000012126.56352.FD

Kimmerly, D. S., O'leary, D. D., Menon, R. S., Gati, J. S., and Shoemaker, J. K. (2005). Cortical regions associated with autonomic cardiovascular regulation during lower body negative pressure in humans. *J. Physiol.* 569, 331–345. doi: 10.1113/jphysiol.2005.091637

Koyama, K., Mito, T., Takashima, S., and Suzuki, S. (1990). Effects of phenylephrine and dopamine on cerebral blood flow, blood volume, and oxygenation in young rabbits. *Pediatr. Neurol.* 6, 87–90. doi: 10.1016/0887-8994(90)90039-4

La Rovere, M. T., Bigger, J. T., Marcus, F. I., Mortara, A., and Schwartz, P. J. (1998). Baroreflex sensitivity and heart-rate variability in prediction of total cardiac mortality after myocardial infarction. *Lancet* 351, 478–484. doi: 10.1016/S0140-6736(97)11144-8

La Rovere, M. T., Pinna, G. D., Maestri, R., and Sleight, P. (2013). Clinical value of baroreflex sensitivity. *Neth. Heart J.* 21, 61–63. doi: 10.1007/s12471-012-0349-8

Logothetis, N. K. (2008). What we can do and what we cannot do with fMRI. *Nature* 453, 869–878. doi: 10.1038/nature06976

Macefield, V. G., Gandevia, S. C., and Henderson, L. A. (2006). Neural sites involved in the sustained increase in muscle sympathetic nerve activity induced by inspiratory capacity apnea: a fMRI study. *J. Appl. Physiol.* 100, 266–273. doi: 10.1152/japplphysiol.00588.2005

Macefield, V. G., and Henderson, L. A. (2010). Real-time imaging of the medullary circuitry involved in the generation of spontaneous muscle sympathetic nerve activity in awake subjects. *Hum. Brain Mapp.* 31, 539–549. doi: 10.1002/hbm.20885

Macey, P. M., Ogren, J. A., Kumar, R., and Harper, R. M. (2015). Functional imaging of autonomic regulation: methods and key findings. *Front. Neurosci.* 9:513. doi: 10.3389/fnins.2015.00513

McAllen, R. M., and Spyer, K. M. (1976). The location of cardiac vagal preganglionic motoneurones in the medulla of the cat. *J. Physiol.* 258, 187–204. doi: 10.1113/jphysiol.1976.sp011414

Meng, L., Gelb, A. W., Alexander, B. S., Cerussi, A. E., Tromberg, B. J., Yu, Z., et al. (2012). Impact of phenylephrine administration on cerebral tissue oxygen saturation and blood volume is modulated by carbon dioxide in anaesthetized patients. *Br. J. Anaesth.* 108, 815–822. doi: 10.1093/bja/aes023

Miura, M., and Reis, D. J. (1971). The paramedian reticular nucleus: a site of inhibitory interaction between projections from fastigial nucleus and carotid sinus nerve acting on blood pressure. *J. Physiol.* 216, 441–460. doi: 10.1113/jphysiol.1971.sp009534

Moher Alsady, T., Blessing, E. M., and Beissner, F. (2016). MICA-A toolbox for masked independent component analysis of fMRI data. *Hum. Brain Mapp.* 37, 3544–3556. doi: 10.1002/hbm.23258

Molhoek, G. P., Wesseling, K. H., Settels, J. J., Van Vollenhoven, E., Weeda, H. W., De Wit, B., et al. (1984). Evaluation of the Penàz servo-plethysmo-manometer for the continuous, non-invasive measurement of finger blood pressure. *Basic Res. Cardiol.* 79, 598–609. doi: 10.1007/BF01910489

Paxinos, G., Huang, X., Sengul, G., and Watson, C. (2012). "Organization of brainstem nuclei. The human nervous system," in *The Human Nervous System*, eds J. Mai and G. Paxinos (Amsterdam: Elsevier Academic Press), 260–327. doi: 10.1016/B978-0-12-374236-0.10008-2

Scheffers, I. J., Kroon, A. A., Schmidli, J., Jordan, J., Tordoir, J. J., Mohaupt, M. G., et al. (2010). Novel baroreflex activation therapy in resistant hypertension:

results of a European multi-center feasibility study. *J. Am. Coll. Cardiol.* 56, 1254–1258. doi: 10.1016/j.jacc.2010.03.089

Schulte, L. H., Sprenger, C., and May, A. (2016). Physiological brainstem mechanisms of trigeminal nociception: an fMRI study at 3T. *Neuroimage* 124, 518–525. doi: 10.1016/j.neuroimage.2015.09.023

Smith, O. A. Jr., and Nathan, M. A. (1966). Inhibition of the carotid sinus reflex by stimulation of the inferior olive. *Science* 154, 674–675. doi: 10.1126/science.154.3749.674

Smith, S. M., Jenkinson, M., Woolrich, M. W., Beckmann, C. F., Behrens, T. E., Johansen-Berg, H., et al. (2004). Advances in functional and structural MR image analysis and implementation as FSL. *Neuroimage* 23(Suppl. 1), S208–S219. doi: 10.1016/j.neuroimage.2004.07.051

Smith, S. M., and Nichols, T. E. (2009). Threshold-free cluster enhancement: addressing problems of smoothing, threshold dependence and localisation in cluster inference. *Neuroimage* 44, 83–98. doi: 10.1016/j.neuroimage.2008.03.061

Strebel, S. P., Kindler, C., Bissonnette, B., Tschaler, G., and Deanovic, D. (1998). The impact of systemic vasoconstrictors on the cerebral circulation of anesthetized patients. *Anesthesiology* 89, 67–72. doi: 10.1097/00000542-199807000-00012

Todd, N., Moeller, S., Auerbach, E. J., Yacoub, E., Flandin, G., and Weiskopf, N. (2016). Evaluation of 2D multiband EPI imaging for high-resolution, whole-brain, task-based fMRI studies at 3T: sensitivity and slice leakage artifacts. *Neuroimage* 124, 32–42. doi: 10.1016/j.neuroimage.2015.08.056

Tustison, N. J., and Avants, B. B. (2013). Explicit B-spline regularization in diffeomorphic image registration. *Front. Neuroinform.* 7:39. doi: 10.3389/fninf.2013.00039

Ugurbil, K., Xu, J., Auerbach, E. J., Moeller, S., Vu, A. T., Duarte-Carvajalino, J. M., et al. (2013). Pushing spatial and temporal resolution for functional and diffusion MRI in the human connectome project. *Neuroimage* 80, 80–104. doi: 10.1016/j.neuroimage.2013.05.012

Woolrich, M. W., Jbabdi, S., Patenaude, B., Chappell, M., Makni, S., Behrens, T., et al. (2009). Bayesian analysis of neuroimaging data in FSL. *Neuroimage* 45, S173–S186. doi: 10.1016/j.neuroimage.2008.10.055

Xu, J., Moeller, S., Auerbach, E. J., Strupp, J., Smith, S. M., Feinberg, D. A., et al. (2013). Evaluation of slice accelerations using multiband echo planar imaging at 3 T. *Neuroimage* 83, 991–1001. doi: 10.1016/j.neuroimage.2013.07.055

Conflict of Interest Statement: The authors declare that the research was conducted in the absence of any commercial or financial relationships that could be construed as a potential conflict of interest.

frontiers in Physiology

ORIGINAL RESEARCH
published: 02 April 2019
doi: 10.3389/fphys.2019.00342

Characterization of the Asymmetry of the Cardiac and Sympathetic Arms of the Baroreflex From Spontaneous Variability During Incremental Head-Up Tilt

*Beatrice De Maria[1], Vlasta Bari[2], Beatrice Cairo[3], Emanuele Vaini[2], Murray Esler[4], Elisabeth Lambert[4,5], Mathias Baumert[6], Sergio Cerutti[7], Laura Dalla Vecchia[1] and Alberto Porta[2,3]**

[1] IRCCS Istituti Clinici Scientifici Maugeri, Milan, Italy, [2] Department of Cardiothoracic, Vascular Anesthesia and Intensive Care, IRCCS Policlinico San Donato, Milan, Italy, [3] Department of Biomedical Sciences for Health, University of Milan, Milan, Italy, [4] Human Neurotransmitters Laboratory, Baker IDI Heart and Diabetes Institute, Melbourne, VIC, Australia, [5] Faculty of Health, Arts and Design, Iverson Health Innovation Research Institute, Swinburne University of Technology, Hawthorn, VIC, Australia, [6] School of Electrical and Electronic Engineering, The University of Adelaide, Adelaide, SA, Australia, [7] Department of Electronics Information and Bioengineering, Politecnico di Milano, Milan, Italy

OPEN ACCESS

Edited by:
Tijana Bojić,
University of Belgrade, Serbia

Reviewed by:
Helio Cesar Salgado,
University of São Paulo, Brazil
Evan L. Matthews,
Montclair State University, United States

***Correspondence:**
Alberto Porta
alberto.porta@unimi.it

Specialty section:
This article was submitted to Autonomic Neuroscience, a section of the journal Frontiers in Physiology

Received: *24 November 2018*
Accepted: *13 March 2019*
Published: *02 April 2019*

Citation:
De Maria B, Bari V, Cairo B, Vaini E, Esler M, Lambert E, Baumert M, Cerutti S, Dalla Vecchia L and Porta A (2019) Characterization of the Asymmetry of the Cardiac and Sympathetic Arms of the Baroreflex From Spontaneous Variability During Incremental Head-Up Tilt. Front. Physiol. 10:342. doi: 10.3389/fphys.2019.00342

Hysteresis of the baroreflex (BR) is the result of the different BR sensitivity (BRS) when arterial pressure (AP) rises or falls. This phenomenon has been poorly studied and almost exclusively examined by applying pharmacological challenges and static approaches disregarding causal relations. This study inspects the asymmetry of the cardiac BR (cBR) and vascular sympathetic BR (sBR) in physiological closed loop conditions from spontaneous fluctuations of physiological variables, namely heart period (HP) and systolic AP (SAP) leading to the estimation of cardiac BRS (cBRS) and muscle sympathetic nerve activity (MSNA) and diastolic AP (DAP) leading to the estimation of vascular sympathetic BRS (sBRS). The assessment was carried out in 12 young healthy subjects undergoing incremental head-up tilt with table inclination gradually increased from 0 to 60°. Two analytical methods were exploited and compared, namely the sequence (SEQ) and phase-rectified signal averaging (PRSA) methods. SEQ analysis is based on the detection of joint causal schemes representing the HP and MSNA burst rate delayed responses to spontaneous SAP and DAP modifications, respectively. PRSA analysis averages HP and MSNA burst rate patterns after aligning them according to the direction of SAP and DAP changes, respectively. Since cBRSs were similar when SAP went up or down, hysteresis of cBR was not detected. Conversely, hysteresis of sBR was evident with sBRS more negative when DAP was falling than rising. sBR hysteresis was no longer visible during sympathetic activation induced by the orthostatic challenge. These results were obtained via the SEQ method, while the PRSA technique appeared to be less powerful in describing the BR asymmetry due to the strong association between BRS estimates computed over positive and negative AP variations. This study

suggests that cBR and sBR provide different information about the BR control, sBR exhibits more relevant non-linear features that are evident even during physiological changes of AP, and the SEQ method can be fruitfully exploited to characterize the BR hysteresis with promising applications to BR branches different from cBR and sBR.

Keywords: hysteresis, muscle sympathetic nerve activity, MSNA, baroreflex sequence analysis, phase-rectified signal averaging, heart rate variability, autonomic nervous system, cardiovascular control

INTRODUCTION

The baroreflex (BR) can be seen as a composite reflex formed by several arms simultaneously adjusting multiple physiological variables in response to the same arterial pressure (AP) variation. Among these branches the cardiac BR (cBR) and the vascular sympathetic BR (sBR) react to AP changes, respectively, with parallel variations of heart period (HP) (Smyth et al., 1969; Pickering et al., 1972) and antiparallel variations of sympathetic nerve activity. Sympathetic traffic is commonly surrogated in humans with muscle sympathetic nerve activity (MSNA) recorded via microneurographic technique (Sundlof and Wallin, 1978). The characterization of BR is usually based on the estimation of the BR sensitivity (BRS) representing the variation of the target variable, such as HP or MSNA, per unit change of AP. Cardiac BRS (cBRS) is mostly estimated by observing the variation of HP in response to a unit modification of systolic AP (SAP) (Smyth et al., 1969; Pickering et al., 1972), while vascular sympathetic BRS (sBRS) is more frequently assessed by measuring the variation of MSNA, or probability of occurrence of the MSNA burst, per unit change of diastolic AP (DAP) (Sundlof and Wallin, 1978; Kienbaum et al., 2001). The cBRS is positive because HP decreases in response to a SAP fall and HP increases in reaction to a SAP rise. Conversely, sBRS is negative given that the amplitude (or area) and the likelihood of the occurrence of the MSNA burst increase in response to DAP drops and they rise when DAP decreases.

Pharmacological studies in young healthy individuals suggested that the cBR and sBR arms exhibit an asymmetric behavior with different BRS computed over positive and negative AP changes (Pickering et al., 1972; Sundlof and Wallin, 1978; Studinger et al., 2007; Studinger et al., 2009). This asymmetry leads to the phenomenon of hysteresis with distinct trajectories covered by the set point in the planes (SAP,HP) and (DAP,MSNA) when AP rises and falls (Rudas et al., 1999; Studinger et al., 2007, 2009; Hart et al., 2011). More specifically, the cBR responds to the same absolute variation of SAP with a larger absolute variation of HP during SAP rise than fall (Pickering et al., 1972; Rudas et al., 1999). Conversely, the sBR reacts to the same absolute variation of DAP with a larger probability of observing an MSNA burst during DAP decrease than increase. These results are evident when important variations of AP are imposed via the administration of vasoactive drugs (Pickering et al., 1972; Sundlof and Wallin, 1978; Rudas et al., 1999; Studinger et al., 2007, 2009), but it is unclear whether they can be confirmed in presence of spontaneous, and likely small, AP changes. Indeed, the studies that computed BRS by separating positive and negative AP variations provided an incomplete answer given that the issue of testing BR hysteresis was not straightly tackled (Parati et al., 1988; De Maria et al., 2018), or the analysis was limited to a single arm of the BR (Martin-Vazquez and Reyes Del Paso, 2010; Davydov et al., 2018) or a static approach was exploited with limited possibility to explore causal relations (Hart et al., 2011). This lack limits the comprehension of the BR functioning and its arms in physiological conditions (Taylor et al., 2015; Marchi et al., 2016b).

Therefore, the aim of this study is to perform the simultaneous characterization of cBR hysteresis from spontaneous variability of HP and SAP and sBR hysteresis from spontaneous fluctuations of MSNA burst rate and DAP during incremental head-up tilt in young healthy individuals (Lambert et al., 2008). cBRS and sBRS are computed via the sequence (SEQ) method (Bertinieri et al., 1985) and via the phase-rectified signal averaging (PRSA) (Bauer et al., 2010; Muller et al., 2012). The SEQ technique extracts joint causal parallel HP-SAP ramps (Parati et al., 1988) and joint causal antiparallel MSNA-DAP ramps (Marchi et al., 2016b), while PRSA aligns HP and MSNA burst rate patterns according to the sign of SAP and DAP changes, respectively. The assessment of cBRS and sBRS is carried out by separately considering positive and negative AP variations (De Maria et al., 2018). The simultaneous application of both SEQ and PRSA methods allows us to compare the ability of the two approaches in typifying the BR hysteresis, while the simultaneous description of cBR and sBR hystereses allows us to stress peculiarity of different BR arms in physiological conditions.

MATERIALS AND METHODS

Experimental Protocol

Twelve young healthy subjects (9 females; age from 20 to 36 years, median = 22.5 years; body mass index from 18.6 to 28.4 $kg{\cdot}m^{-2}$, median = 24.2 $kg{\cdot}m^{-2}$) were enrolled in the study. The experimental protocol was fully described in Lambert et al. (2008). Briefly, incremental graded head-up tilt test, starting from 0 to 60°, was performed. Subjects were consecutively tilted at 0, 20, 30, 40, and 60° (T0, T20, T30, T40, and T60, respectively) and maintained in each position for 10 min. The subjects never returned to the supine position and tilt table inclination was incremented from the previous one. The test was performed in the morning, 1 h after a light breakfast and after at least a 12-h caffeine free period. The subjects breathed spontaneously but they were not allowed to talk. The experimental protocol was approved by the Alfred Hospital Ethics Review Committee (no. 144/06) and conformed

to the relevant guidelines of the National Health and Medical Research Council of Australia and to the principles of the Declaration of Helsinki. All subjects signed written informed consent before the test.

Electrocardiogram (ECG), invasive AP, and MSNA signals were recorded for the overall duration of the test. ECG was monitored using a single III lead amplifier (ADInstruments, Castle Hill, NSW, Australia). AP signal was obtained by cannulating percutaneously the radial artery (3F, 5 cm, Cook catheter). A clinical microneurography (IOWA Nerve Traffic Analyzer, model 662C-3, Department of Bioengineering, The University of Iowa, Iowa, IA, United States) was used to record the multiunit sympathetic nerve discharges in postganglionic fibers distributed to the skeletal muscle vasculature. A tungsten microelectrode (FHC, Bowdoinham, Maine, United States) was percutaneously inserted in the peroneal nerve and adjusted in order to obtain a satisfactory MSNA signal (Lambert et al., 2008). The raw MSNA signal was band-pass filtered (700–2000 Hz), amplified, rectified and integrated (time constant of 0.1 s). The integrated MSNA signal was utilized for further analysis. The sampling rate of the recorded signals (i.e., ECG, AP and integrated MSNA) was 1000 Hz (PowerLab system, model ML785/8SP, ADInstruments, Castle Hill, NSW, Australia). Out of all 12 subjects, the recordings of one subject during T30 and T40 were excluded for poor quality, while 5 subjects did not complete the experimental protocol during T60.

Beat-to-Beat Variability Series Extraction

The kth HP, $HP(k)$, where k is the cardiac beat counter, was calculated as the temporal distance between two consecutive R-wave peaks detected on the ECG signal. QRS complexes were identified when the absolute first derivative of the ECG overcame a predefined threshold. R-wave peaks were fixed by means of parabolic interpolation. The minimum and maximum values of the AP signal within $HP(k)$ were considered as the kth DAP, $DAP(k)$, and the kth SAP, $SAP(k)$, respectively. $DAP(k)$ preceded in time $SAP(k)$. All the identified fiduciary points (i.e., R peaks, SAP and DAP values) were visually checked and manually corrected in case of erroneous or missed detections. In presence of ectopic beats, corrections were performed over the series via cubic spline interpolation taking as onset and offset the closest values unaffected by the ectopies. No more than 5% of correction was allowed.

From the integrated MSNA signal the variability of the MSNA burst rate was obtained as described in Marchi et al. (2016a). The first step was the detection of the MSNA bursts over the entire recording. To account for the latency of the sBR the MSNA bursts were searched in a temporal window ranging from 0.9 to 1.7 s from the R-wave peak (Sundlof and Wallin, 1978; Kienbaum et al., 2001; Diedrich et al., 2009). A running threshold calculated as a fraction of the maximum burst amplitude in the overall signal and updated on a beat-to-beat basis, allowed the detection of the MSNA bursts by overcoming the problems related to bursts amplitude variation and baseline wandering (Diedrich et al., 2009). The second step to obtain the MSNA burst rate variability series was the counting of the previously detected MSNA bursts in a moving time window of 5 s that was advanced in steps of 1 ms. The obtained step-wise burst-count MSNA signal was filtered with a cut-off frequency equal to 0.5 Hz, thus focusing the typical range of frequencies of spontaneous variability in humans (Task Force of the European Society of Cardiology the North American Society of Pacing Electrophysiology, 1996) and the filtered signal was sampled at the occurrence of the first R-wave peak representing the onset of the $HP(k)$ and the correspondent value was indicated as $MSNA(k)$. The values of the MSNA burst rate variability series were divided by the frame length (i.e., 5 s), thus representing the number of bursts occurring in 1 s and its units are bursts·s^{-1}. Analyses were carried out over the beat-to-beat series HP = $\{HP(k), k = 1,\ldots,N\}$, SAP = $\{SAP(k), k = 1,\ldots,N\}$, DAP = $\{DAP(k), k = 1,\ldots,N\}$, and MSNA = $\{MSNA(k), k = 1,\ldots,N\}$, where $N = 300$ cardiac beats according to the typical sequence length exploited in short-term analysis of cardiovascular control (Task Force of the European Society of Cardiology the North American Society of Pacing Electrophysiology, 1996).

cBRS Estimation via the SEQ Method

cBRS was computed according to the SEQ method (Bertinieri et al., 1985) as implemented in Porta et al. (2000). More specifically, the SEQ method for the cBR analysis is based on the search of ordered HP and SAP sequences $\boldsymbol{HP}(k + \tau_{cBR}) = [HP(k + \tau_{cBR}), HP(k + \tau_{cBR} - 1), HP(k + \tau_{cBR} - 2), HP(k + \tau_{cBR} - 3)]$ and $\boldsymbol{SAP}(k) = [SAP(k), SAP(k - 1), SAP(k - 2), SAP(k - 3)]$ formed by four consecutive HP and SAP values corresponding to three HP and SAP variations defined as $\Delta HP(k + \tau_{cBR}) = HP(k + \tau_{cBR}) - HP(k + \tau_{cBR} - 1)$ and $\Delta SAP(k) = SAP(k) - SAP(k - 1)$. The sequence $\boldsymbol{SAP}(k)$ precedes $\boldsymbol{HP}(k + \tau_{cBR})$, where τ_{cBR} represents the cBR latency expressed in cardiac beats. If $\boldsymbol{HP}(k + \tau_{cBR})$ and $\boldsymbol{SAP}(k)$ sequences feature all positive variations, they were referred to as SEQ+. Therefore, SEQ+ is a joint HP-SAP scheme formed by positive HP and SAP ramps. Conversely, if $\boldsymbol{HP}(k + \tau_{cBR})$ and $\boldsymbol{SAP}(k)$ sequences feature all negative variations they were termed as SEQ−. Therefore, SEQ− is a joint HP-SAP scheme formed by negative HP and SAP ramps. All SEQ+ and SEQ− joint schemes were considered of cBR origin regardless of the magnitude of total, or partial, SAP and HP variations and the strength of the linear association between HP and SAP values (Porta et al., 2013). The robustness of the results was checked by applying more usual thresholds, namely absolute total SAP variation > 1 mmHg; absolute total HP variation > 5 ms; correlation coefficient > 0.85 (Parati et al., 1988). The latency τ_{cBR} was optimized on an individual basis according to procedure proposed in Porta et al. (2018b) in the range from 0 to 4 beats according to the rapidity of the vagal arm of the cBR acting within the next cardiac beat following the current SAP (i.e., $\tau_{cBR} = 0$ beats) (Eckberg, 1976; Baselli et al., 1994) and the slower actions that should be exhausted within a time interval of 3–4 s (Baskerville et al., 1979). The cBRS was separately computed over SEQ+ and SEQ− patterns. Over each type of joint pattern (i.e., SEQ+ and SEQ−), the slope of the linear regression in the plane $[SAP(k), HP(k + \tau_{cBR}{}^{o})]$, where $\tau_{cBR}{}^{o}$ is the optimal τ_{cBR}, was computed and its average value over all joint HP-SAP patterns

belonging to the same family (i.e., SEQ+ or SEQ−) was taken as an estimate of the cBRS. cBRS was labeled as $cBRS_{SEQ+}$ and $cBRS_{SEQ-}$ according to the type of joint HP-SAP pattern. Both $cBRS_{SEQ+}$ and $cBRS_{SEQ-}$ were non-negative and expressed in ms·mmHg^{-1}.

sBRS Estimation via the SEQ Method

sBRS was computed according to the SEQ method proposed in Marchi et al. (2016b). More specifically, the SEQ method for the sBR analysis is based on the search of ordered MSNA burst rate and DAP sequences $\boldsymbol{MSNA}(k + \tau_{sBR}) = [MSNA(k + \tau_{sBR}), MSNA(k + \tau_{sBR} - 1), MSNA(k + \tau_{sBR} - 2), MSNA(k + \tau_{sBR} - 3)]$ and $\boldsymbol{DAP}(k) = [DAP(k), DAP(k - 1), DAP(k - 2), DAP(k - 3)]$ formed by four consecutive MSNA burst rate and DAP values corresponding to three MSNA burst rate and DAP variations $\Delta MSNA(k + \tau_{sBR}) = MSNA(k + \tau_{sBR}) - MSNA(k + \tau_{sBR} - 1)$ and $\Delta DAP(k) = DAP(k) - DAP(k - 1)$. The sequence $\boldsymbol{DAP}(k)$ precedes $\boldsymbol{MSNA}(k + \tau_{sBR})$, where τ_{sBR} represents the sBR latency expressed in cardiac beats. If the $\boldsymbol{MSNA}(k + \tau_{sBR})$ sequence features all negative variations, while the $\boldsymbol{DAP}(k)$ one exhibits all positive variations, it is referred to as SEQ+. Therefore, SEQ+ is a joint MSNA-DAP scheme formed by negative MSNA and positive DAP ramps. Conversely, if the $\boldsymbol{MSNA}(k + \tau_{sBR})$ sequence features all positive variations, while the $\boldsymbol{DAP}(k)$ one exhibits all negative variations, it is termed SEQ−. Therefore, SEQ− is a joint MSNA-DAP scheme formed by positive MSNA and negative DAP ramps. All SEQ+ and SEQ− joint schemes were considered to be of sBR origin regardless of the magnitude of total, or partial, DAP and MSNA burst rate variations and the strength of the linear association between MSNA burst rate and DAP values. The robustness of the results was checked by applying standard thresholds, namely absolute total DAP variation > 1 mmHg; absolute total MSNA burst rate variation > 0 bursts·s^{-1}; absolute correlation coefficient > 0.85 (Marchi et al., 2016b). The latency τ_{sBR} was optimized on an individual basis according to procedure proposed in Porta et al. (2018b) in the range from 0 to 3 beats according to the delay of sBR in acting on MSNA after sensing AP (Sundlof and Wallin, 1978; Kienbaum et al., 2001; Diedrich et al., 2009). The sBRS was separately computed over SEQ+ and SEQ− patterns by following the same regression line approach as in the cases of cBR but applied in the plane $[DAP(k), MSNA(k + \tau_{sBR}{}^{o})]$, where $\tau_{sBR}{}^{o}$ is the optimal τ_{sBR}. sBRS was labeled as $sBRS_{SEQ+}$ and $sBRS_{SEQ-}$ according to the type of joint MSNA-DAP pattern. Both $sBRS_{SEQ+}$ and $sBRS_{SEQ-}$ were non-positive and expressed in bursts·s^{-1}·mmHg^{-1}.

cBRS Estimation via the PRSA Method

The PRSA method for the cBRS estimation was originally described in Bauer et al. (2010) and Muller et al. (2012). Defined as the anchor time the cardiac beat index k where SAP increases [i.e., $\Delta SAP(k) > 0$], a sequence of 15 consecutive HPs around the anchor time $k + \tau_{cBR}$ was selected, where τ_{cBR} is the cBR latency. Each HP sequence was composed by the seven HPs preceding $HP(k + \tau_{cBR})$, $HP(k + \tau_{cBR})$, and the seven HPs following $HP(k + \tau_{cBR})$. All the identified HP segments were aligned at the anchor times. Defined $X(0)$ as the mean of all HPs at the anchor time, $X(-1)$ as the mean of the HPs preceding the anchor time, $X(-2)$ as the mean of the HPs at two beats before the anchor time, and $X(1)$ as the mean of the HPs immediately following the anchor time, the PRSA estimate of cBRS driven by positive SAP variations ($cBRS_{PRSA+}$) was calculated as $cBRS_{PRSA+} = 1/4\ [X(0) + X(1) - X(-1) - X(-2)]$. $cBRS_{PRSA+}$ was expressed in ms. Given that $cBRS_{PRSA+}$ was not expressed in usual cBRS units, a normalized version of the original PRSA method (nPRSA) was devised (Muller et al., 2012). nPRSA estimate of $cBRS_{PRSA+}$ ($cBRS_{nPRSA+}$) was obtained by dividing $cBRS_{PRSA+}$ by the averaged ΔSAP(k). $cBRS_{nPRSA+}$ was expressed in ms·mmHg^{-1}. In the original version anchor times were defined exclusively in correspondence of $\Delta SAP(k) > 0$. In De Maria et al. (2018) it was proposed to compute $cBRS_{PRSA-}$ and $cBRS_{nPRSA-}$ as well by simply repeating the same procedure as before over the anchor times where $\Delta SAP(k) < 0$. The sign of $cBRS_{PRSA-}$ was inverted to preserve the non-negativity of cBRS estimates. $cBRS_{PRSA-}$ was expressed in ms, while $cBRS_{nPRSA-}$ in ms·mmHg^{-1}. In agreement with the fastness of vagal arm of cBR τ_{cBR} was assigned to 0 beats (Eckberg, 1976; Baselli et al., 1994).

sBRS Estimation via the PRSA Method

In this study we applied the PRSA method (Bauer et al., 2010; Muller et al., 2012) with the extension proposed in De Maria et al. (2018) to perform sBR analysis by separating the contributions given by positive and negative DAP variations. Briefly, the procedure described in previous *Section* was repeated by substituting SAP with DAP and HP with MSNA burst rate. Markers computed via the PRSA method over positive and negative DAP variations were labeled as $sBRS_{PRSA+}$ and $sBRS_{PRSA-}$, respectively, and those calculated via the nPRSA technique were termed as $sBRS_{nPRSA+}$ and $sBRS_{nPRSA-}$, respectively. The sign of $sBRS_{PRSA-}$ was inverted to preserve the non-positivity of sBRS estimates. $sBRS_{PRSA+}$ and $sBRS_{PRSA-}$ were expressed in bursts·s^{-1}, and $sBRS_{nPRSA+}$ and $sBRS_{nPRSA-}$ in bursts·s^{-1}·mmHg^{-1}.

Statistical Analysis

After pooling together all the data regardless of the experimental condition, the significance of the difference between cBRS, or sBRS, computed over positive and negative AP variations was tested by means of paired *t*-test, or Wilcoxon signed rank test when appropriate. If paired analysis could not be carried out because cBRS, or sBRS, could not be computed over both positive and negative AP changes, unpaired *t*-test, or Mann–Whitney rank sum test when appropriate, was applied. Two-way analysis of variance (Holm–Sidak test for multiple comparisons) was used to check the significance of the differences between cBRS, or sBRS, indexes computed separately according to the sign of the AP variation within the same experimental condition (i.e., T0, T20, T30, T40, and T60) and between-condition differences (T20, T30, T40, and T60 versus T0) within the same type of marker (i.e., calculated over positive or negative AP changes). Pearson correlation analysis was carried out to assess the significance of the association between cBRS, or sBRS, estimates and the sine of the tilt table angle (i.e., 0, 20, 30, 40, and 60°) taken as an effective marker of the magnitude of the orthostatic challenge. After pooling together all the data regardless of the

experimental condition, the same tool was carried out to assess the correlation between the cBRS estimates derived from positive and negative SAP changes, and between the sBRS estimates derived from positive and negative DAP variations. Pearson product moment correlation coefficient r and type I error probability p were calculated. Statistical analysis was repeated for all the methods utilized to estimate cBRS and sBRS (i.e., SEQ, PRSA, and nPRSA techniques). A $p < 0.05$ was always deemed as significant. Statistical analysis was carried out using a commercial statistical program (Sigmaplot, Systat Software, Inc., Chicago, IL, United States, version 11.0).

RESULTS

cBRS and sBRS were computed in all the subjects in all the experimental conditions by PRSA and nPRSA methods (i.e., 100% of the recordings) and this performance held regardless of the sign of the AP change. Conversely, SEQ approach had more limited performance and was able to measure cBRS and sBRS, respectively, in 88 and 92% of the recordings over positive AP variations and, respectively, in 92 and 98% of the recordings over negative AP variations. The reason for this inability was the lack of SEQ+ or SEQ− patterns in some subjects in some experimental conditions.

The simple error bar graphs of **Figure 1** show cBRS (**Figures 1A–C**) and sBRS (**Figures 1D–F**) estimates as a function of the type of AP variation, namely positive or negative SAP and DAP change in **Figures 1A–F**, respectively. cBRS and sBRS are estimated via SEQ (**Figures 1A,D**), PRSA (**Figures 1B,E**), and nPRSA (**Figures 1C,F**) techniques. Data are pooled together regardless of the experimental condition (i.e., T0, T20, T30, T40, and T60) and reported as mean plus standard deviation. cBRS markers were similar when computed over positive and negative SAP variations regardless of the method utilized to estimate cBRS (**Figures 1A–C**). Conversely, sBRS was more negative when computed over negative than positive DAP variations (**Figure 1D**). However, this result was obtained exclusively using the SEQ method, while PRSA and nPRSA approaches were not able to differentiate sBRS according to the sign of the DAP change (**Figures 1E,F**). Results given in **Figure 1**. are summarized in **Table 1** as well.

The grouped error bar graphs of **Figure 2** show cBRS (**Figures 2A–C**) and sBRS (**Figures 2D–F**) estimates as a function of experimental condition (i.e., T0, T20, T30, T40, and T60). cBRS estimates are differentiated according to the sign of SAP variations, while sBRS are separated according to the direction of DAP changes. In all panels black and white bars indicate BRS estimate computed over, respectively, positive and negative AP variations. cBRS and sBRS are estimated via SEQ (**Figures 2A,D**), PRSA (**Figures 2B,E**), and nPRSA (**Figures 2C,F**) techniques. Data are reported as mean plus standard deviation. Regardless of the method, cBRS markers moved toward 0 with the magnitude of the orthostatic challenge. Significant cBRS decreases were observed with tilt table inclination angles higher than, or equal to,

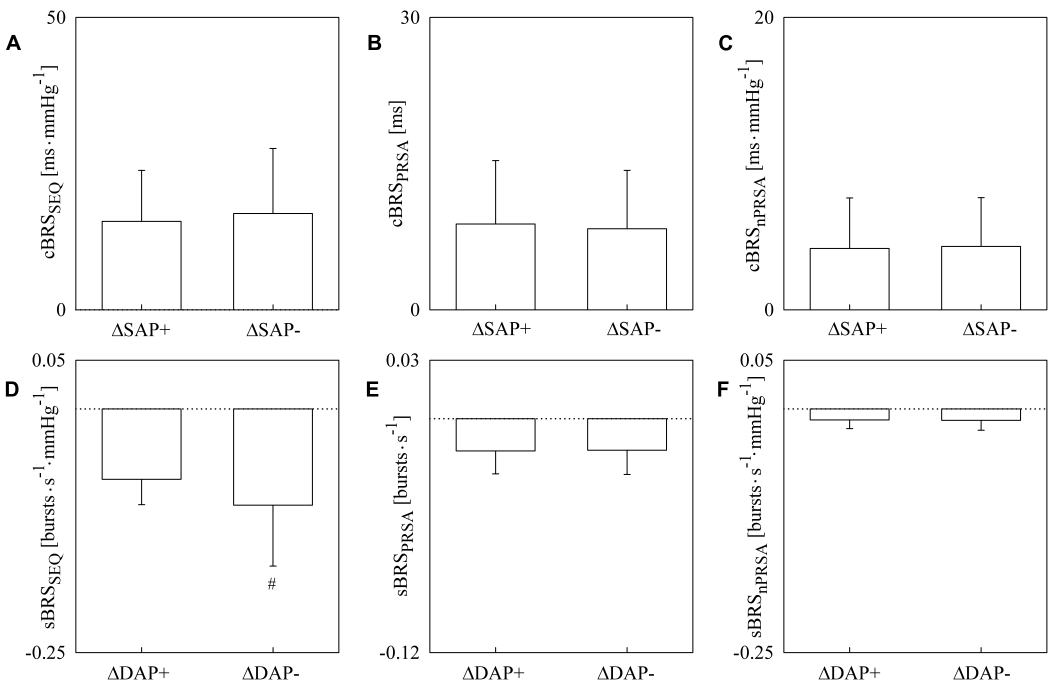

FIGURE 1 | The simple error bar graphs show cBRS **(A–C)** and sBRS **(D–F)** in young healthy subjects undergoing incremental head-up tilt as a function of the sign of, respectively, SAP **(A–C)** and DAP **(D–F)** variations. cBRS and sBRS were estimated using three different approaches, namely SEQ **(A,D)**, PRSA **(B,E)**, and nPRSA **(C,F)** methods. Data were pooled together regardless of the experimental condition (i.e., T0, T20, T30, T40, and T60). The results are presented as mean plus standard deviation. The symbol # indicates $p < 0.05$ versus positive AP variations.

TABLE 1 | cBRS and sBRS as a function of the method and sign of AP variation.

Index	ΔAP+	ΔAP−
$cBRS_{SEQ}$ [ms·mmHg^{-1}]	15.11 ± 8.74	16.45 ± 11.12
$cBRS_{PRSA}$ [ms]	8.79 ± 6.51	8.31 ± 5.99
$cBRS_{nPRSA}$ [ms·mmHg^{-1}]	4.20 ± 3.45	4.336 ± 3.33
$sBRS_{SEQ}$ [bursts·s^{-1}·mmHg^{-1}]	−0.072 ± 0.026	−0.099 ± 0.062#
$sBRS_{PRSA}$ [bursts·s^{-1}]	−0.017 ± 0.012	−0.016 ± 0.012
$sBRS_{nPRSA}$ [bursts·s^{-1}·mmHg^{-1}]	−0.011 ± 0.009	−0.012 ± 0.010

AP, arterial pressure; BR, baroreflex; cBR, cardiac BR; sBR, sympathetic BR; cBRS, cBR sensitivity; sBRS, sBR sensitivity; ΔAP+, positive AP variation; ΔAP−, negative AP variation; SEQ, sequence method; PRSA, phase rectified signal averaging method; nPRSA, normalized PRSA. Data are presented as mean ± standard deviation. The symbol # indicates $p < 0.05$ versus ΔAP+. ΔAP is intended as ΔSAP for the computation of cBRS and ΔDAP for the computation of sBRS.

40° (**Figures 2A–C**). This result held regardless of the sign of SAP changes utilized to assess cBRS. Remarkably, no significant differences were observed within the same experimental condition between cBRS estimates computed over positive and negative SAP variations. sBRS was more stable with the magnitude of the orthostatic challenge (**Figures 2D–F**). Indeed, no significant changes versus T0 were observed when sBRS was computed via SEQ, PRSA and nPRSA methods (**Figures 2D–F**). Remarkably, sBRS computed over negative DAP variations was more negative than that derived from positive DAP changes and this difference was significant at T0 (**Figure 2D**). The finding was detected only by SEQ method: indeed, when sBRS was computed via PRSA and nPRSA techniques, its value did not depend on the direction of DAP changes in any of the considered experimental conditions (**Figures 2E,F**). Results given in **Figure 2** are summarized in **Table 2** as well.

Figure 3 reports the scatter plots of the cBRS on the magnitude of the orthostatic challenge quantified by the sine of the tilt table angles. Each open circle represents the cBRS computed in a specific subject in a given experimental condition. cBRS is estimated according to SEQ (**Figures 3A,D**), PRSA (**Figures 3B,E**), and nPRSA (**Figures 3C,F**) techniques. Panels on the top (**Figures 3A–C**) are relevant to cBRS computed over positive SAP changes, while those at the bottom (**Figures 3D–F**) are relevant to cBRS calculated over negative SAP changes. The linear regression (solid line) is drawn along with its 95% confidence interval (dotted lines) if a significant linear association between the two variables was found. All the cBRS estimates were significantly and negatively correlated with the magnitude of the orthostatic challenge regardless of the method and sign of the SAP variation. Pearson correlation coefficient r and type I error probability p were $r = -0.486$; $p = 7.16 \cdot 10^{-4}$ (**Figure 2A**), $r = -0.518$; $p = 9.74 \cdot 10^{-5}$ (**Figure 2B**), $r = -0.481$; $p = 3.15 \cdot 10^{-4}$ (**Figure 2C**), $r = -0.531$; $p = 1.22 \cdot 10^{-4}$ (**Figure 2D**), $r = -0.545$; $p = 3.56 \cdot 10^{-5}$ (**Figure 2E**), and $r = -0.509$; $p = 1.36 \cdot 10^{-4}$ (**Figure 2F**).

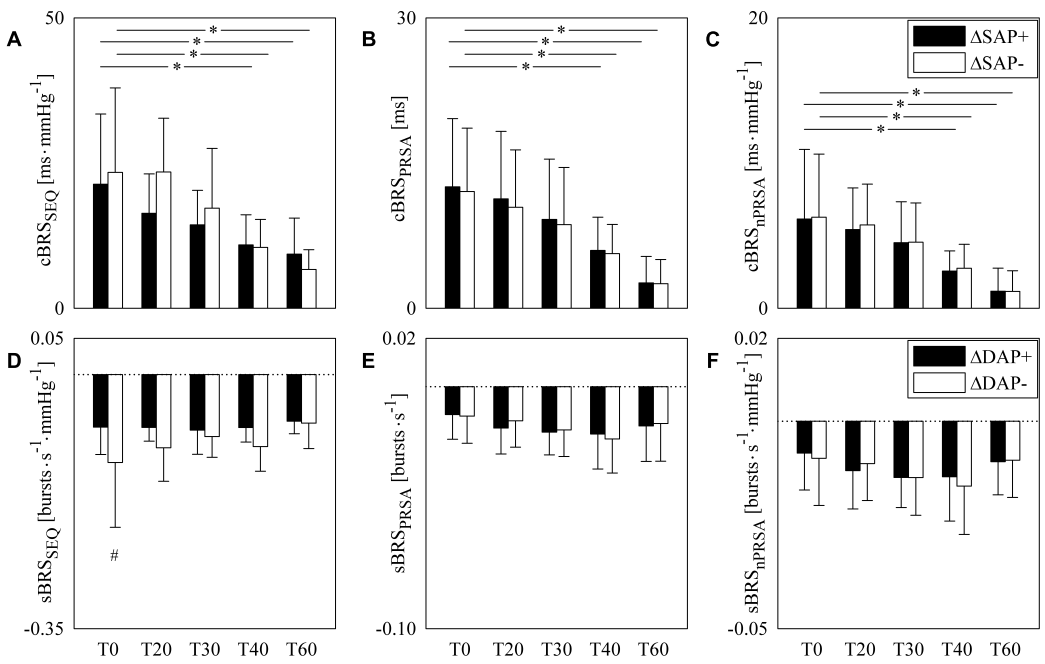

FIGURE 2 | The grouped error bar graphs show cBRS **(A–C)** and sBRS **(D–F)** in young healthy subjects undergoing incremental head-up tilt as a function of the experimental condition (i.e., T0, T20, T30, T40, and T60). cBRS and sBRS were estimated using three different approaches, namely SEQ **(A,D)**, PRSA **(B,E)**, and nPRSA **(C,F)** methods, and reported by separately considering positive (black bars) and negative (white bars) SAP variations in **(A–C)** and DAP changes in **(D–F)**. The results are presented as mean plus standard deviation. The symbol # indicates a significant change of cBRS **(A–C)**, or sBRS **(D–F)**, versus positive AP variations with $p < 0.05$ within the same experimental condition (i.e., T0, T20, T30, T40, or T60). The symbol * indicates a significant change with $p < 0.05$ versus T0 within the same type of cBRS **(A–C)**, or sBRS **(D–F)**.

TABLE 2 | cBRS and sBRS as a function of the method, sign of AP variation and title table inclination.

Index	T0		T20		T30		T40		T60	
	ΔAP+	ΔAP−	ΔAP+	ΔAP−	ΔAP+	ΔAP−	ΔAP+	ΔAP−	ΔAP+	ΔAP−
$cBRS_{SEQ}$ [ms·mmHg^{-1}]	21.35 ± 12.08	23.39 ± 14.55	16.35 ± 6.78	23.46 ± 9.25	14.38 ± 5.91	17.24 ± 10.29	10.91 ± 5.18*	10.47 ± 4.83*	9.32 ± 6.21*	6.69 ± 3.39#*
$cBRS_{PRSA}$ [ms]	12.54 ± 7.05	12.06 ± 6.55	11.30 ± 6.97	10.43 ± 5.93	9.18 ± 6.23	8.64 ± 5.9	5.97 ± 3.43*	5.64 ± 3.02*	2.62 ± 2.73*	2.54 ± 2.5*
$cBRS_{nPRSA}$ [ms·mmHg^{-1}]	6.15 ± 4.79	6.27 ± 4.34	5.43 ± 2.86	5.74 ± 2.80	4.52 ± 2.81	4.54 ± 2.71	2.56 ± 1.39*	2.75 ± 1.65*	1.17 ± 1.59*	1.16 ± 1.42*
$sBRS_{SEQ}$ [bursts·s^{-1}·mmHg^{-1}]	−0.072 ± 0.038	−0.121 ± 0.089#	−0.073 ± 0.019	−0.101 ± 0.046	−0.077 ± 0.033	−0.085 ± 0.028	−0.073 ± 0.020	−0.099 ± 0.034	−0.064 ± 0.017	−0.067 ± 0.035
$sBRS_{PRSA}$ [bursts·s^{-1}]	−0.011 ± 0.010	−0.012 ± 0.011	−0.017 ± 0.011	−0.014 ± 0.011	−0.019 ± 0.009	0.018 ± 0.011	−0.020 ± 0.014	−0.022 ± 0.014	−0.016 ± 0.015	−0.015 ± 0.015
$sBRS_{nPRSA}$ [bursts·s^{-1}·mmHg^{-1}]	−0.008 ± 0.009	−0.009 ± 0.011	−0.012 ± 0.009	−0.010 ± 0.009	−0.014 ± 0.007	−0.014 ± 0.009	−0.013 ± 0.011	−0.016 ± 0.012	−0.010 ± 0.008	−0.009 ± 0.009

*AP, arterial pressure; BR, baroreflex; cBR, cardiac BR; sBR, sympathetic BR; cBRS, cBR sensitivity; sBRS, sBR sensitivity; ΔAP+, positive AP variation; ΔAP−, negative AP variation; SEQ, sequence method; PRSA, phase rectified signal averaging method; nPRSA, normalized PRSA. Data are presented as mean ± standard deviation. The symbol * indicates $p < 0.05$ versus T0 within the same type of ΔAP variation. The symbol # indicates $p < 0.05$ versus ΔAP+ within the same experimental condition. ΔAP is intended as ΔSAP for the computation of cBRS and ΔDAP for the computation of sBRS.*

Figure 4 has the same structure as **Figure 3** but reports sBRS as a function of the sine of the tilt table angles. A linear association of sBRS derived from SEQ method with the magnitude of the orthostatic challenge was detected only when sBRS was assessed over negative DAP changes (**Figure 4D**). Pearson correlation coefficient r was positive (i.e., r = 0.286) and type I error probability p was $4.43 \cdot 10^{-2}$. Conversely, no significant linear association was found when sBRS was derived from the SEQ method over positive DAP variations (**Figure 4A**). The same conclusion was drawn when sBRS was estimated via PRSA and nPRSA techniques and held regardless of the sign of the DAP changes (**Figures 4B,C,E,F**).

Figure 5 reports the scatter plots of the cBRS derived from negative SAP variations on that obtained from positive SAP changes (**Figures 5A–C**) and the scatter plots of the sBRS derived from negative DAP variations on that obtained from positive DAP changes (**Figures 5D–F**). Each open circle represents a pair of cBRS (**Figures 5A–C**), or sBRS (**Figures 5D–F**), estimates computed in a specific subject in a given experimental condition. cBRS and sBRS are estimated according to SEQ (**Figures 5A,D**), PRSA (**Figures 5B,E**), and nPRSA (**Figures 5C,F**) methods. Data are pooled together regardless of the experimental condition. The linear regression (solid line) is drawn along with its 95% confidence interval (dotted lines) if a significant linear association between the two variables was found. A significant positive association between cBRS computed over positive and negative SAP variations was found regardless of the method (**Figures 5A–C**): the Pearson correlation coefficient r and the type I error probability p were 0.413 and $6.62 \cdot 10^{-3}$ in **Figure 5A**, 0.974 and $1.87 \cdot 10^{-33}$ in **Figure 5B**, and 0.985 and $6.04 \cdot 10^{-39}$ in **Figure 5C**. Conversely, a significant linear association between sBRS calculated over positive and negative DAP changes was detected only when sBRS was derived via PRSA and nPRSA techniques (i.e., r = 0.943, $p = 5.65 \cdot 10^{-25}$ in **Figure 5E** and $r = 0.938$, $p = 3.11 \cdot 10^{-24}$ in **Figure 5F**). No significant correlation was found between sBRS computed over positive and negative DAP variations via the SEQ method (**Figure 5D**).

Results remained valid when gender disproportion was fixed by considering only females (see **Supplementary Tables S1**, **S2**). Remarkably, the exclusion of the three men reduced the age dispersion to 20–28 years (min–max range, median = 22 years), thus limiting the impact of age spreading. Moreover, findings of the SEQ method were confirmed (see **Supplementary Tables S3**, **S4**) when prerequisites for selection of joint SEQ+ and SEQ− patterns were applied according to standard setting of minimal absolute total variations of SAP or DAP, minimal absolute total variations of HP or MSNA burst rate and minimal absolute value of the correlation coefficient.

DISCUSSION

The main findings of this work can be summarized as follows: (i) the asymmetry of the cBR is not detectable from spontaneous fluctuations of HP and SAP during incremental head-up tilt maneuver; (ii) the asymmetry of the sBR is detectable from spontaneous variations of MSNA burst rate and DAP at rest in

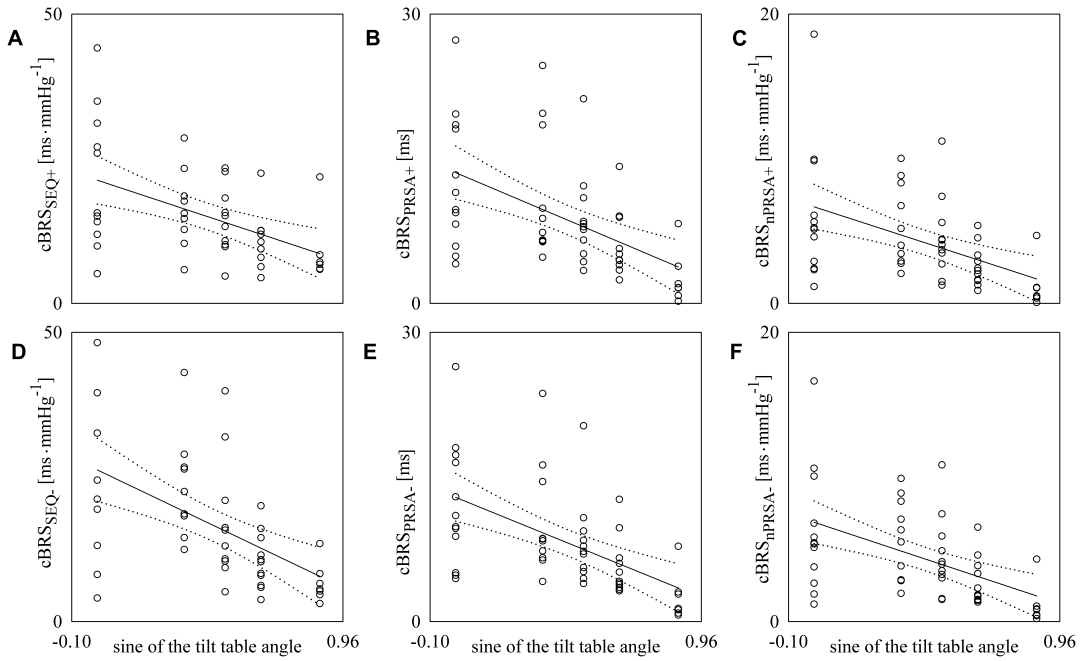

FIGURE 3 | The scatter plots show the results of the linear correlation analysis between cBRS estimates and the sine of the tilt table angles. Each circle represents the cBRS estimate computed in a subject in the assigned experimental condition. cBRS was estimated via SEQ **(A,D)**, PRSA **(B,E)**, and nPRSA **(C,F)** methods. The cBRS estimates were obtained by separately considering positive **(A–C)** and negative **(D–F)** SAP variations. The linear regression line (solid line) and its 95% confidence interval (dotted lines) are plotted only if the Pearson correlation coefficient is significantly different from 0 with $p < 0.05$.

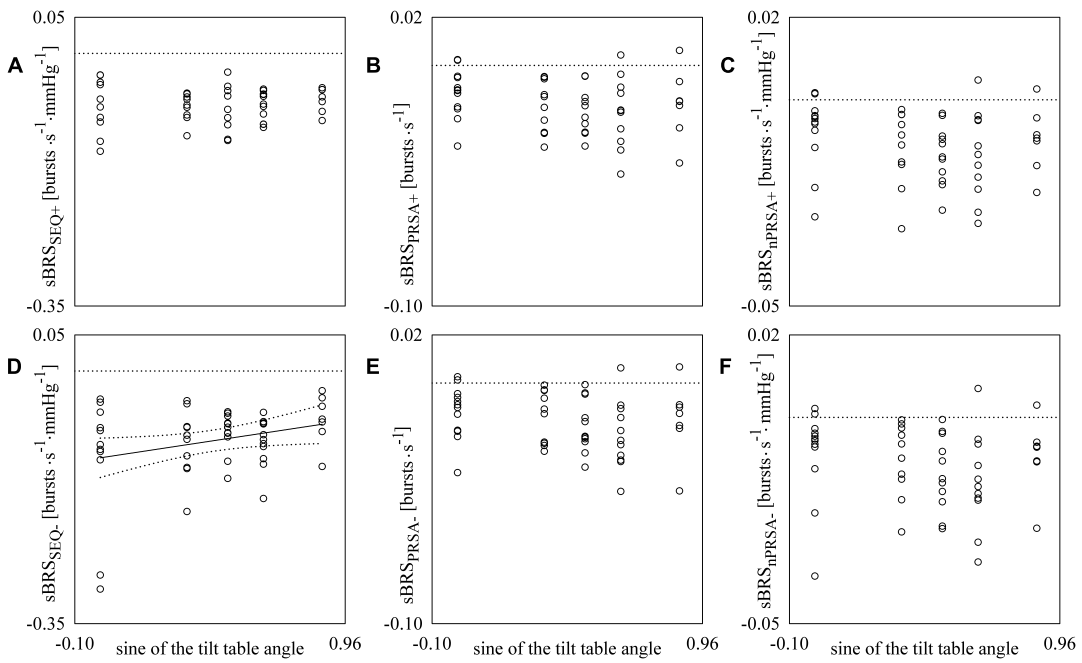

FIGURE 4 | The scatter plots show the results of the linear correlation analysis between sBRS estimates and the sine of the tilt table angles. Each circle represents the sBRS estimate computed in a subject in the assigned experimental condition. sBRS was estimated via SEQ **(A,D)**, PRSA **(B,E)**, and nPRSA **(C,F)** methods. The sBRS estimates were obtained by separately considering positive **(A–C)** and negative **(D–F)** DAP variations. The linear regression line (solid line) and its 95% confidence interval (dotted lines) are plotted only if the Pearson correlation coefficient is significantly different from 0 with $p < 0.05$.

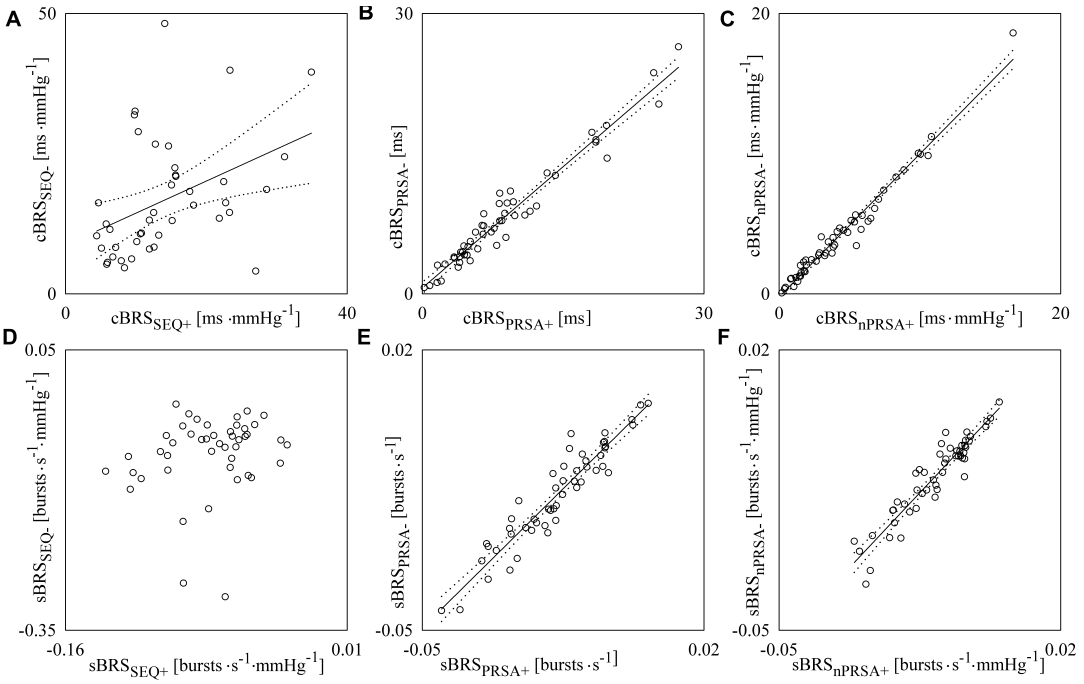

FIGURE 5 | The scatter plots show the results of linear correlation analysis in the planes ($cBRS_{SEQ+}$, $cBRS_{SEQ-}$) **(A)**, ($cBRS_{PRSA+}$, $cBRS_{PRSA-}$) **(B)** and ($cBRS_{nPRSA+}$, $cBRS_{nPRSA-}$) **(C)**, ($sBRS_{SEQ+}$, $sBRS_{SEQ-}$) **(D)**, ($sBRS_{PRSA+}$, $sBRS_{PRSA-}$) **(E)**, and ($sBRS_{nPRSA+}$, $sBRS_{nPRSA-}$) **(F)** in young healthy subjects undergoing incremental head-up tilt. Each circle represents the pair of cBRS **(A–C)** or sBRS **(D–F)** estimates computed in a subject in a given experimental condition. Data were pooled together regardless of the experimental condition (i.e., T0, T20, T30, T40, and T60). The linear regression line (solid line) and its 95% confidence interval (dotted lines) are plotted only if the Pearson correlation coefficient is significantly different from 0 with $p < 0.05$.

supine conditions and it is lost in response to the sympathetic activation and vagal withdrawal induced by the postural challenge; (iii) the SEQ method is much more powerful than the PRSA technique in describing the cBR and sBR hysteresis.

The cBR Hysteresis Is Not Detectable From Spontaneous Variability of SAP and HP

The cBR responds to an AP drop with an HP shortening and to an AP rise with an HP lengthening (Smyth et al., 1969). The cBR is traditionally characterized through an interventional approach imposing a large AP drop or rise via the administration of a vasoactive drug (Smyth et al., 1969; Pickering et al., 1972) or the stimulation of the barosensory areas in the carotid arteries via a neck chamber (Eckberg, 1980). In the interventional analysis the gain of the HP-AP relation, usually referred to as cBRS, was obtained as the slope of the linear regression of HP on SAP. Linear relation is estimated starting from the highest SAP value just after the intervention and ending to the SAP nadir in the case of induced SAP falls or starting from the lowest SAP value just after the intervention and ending to the SAP peak in the case of induced SAP rises. cBRS is non-negative because cBR buffers SAP changes with parallel HP variations and a migration of cBRS toward 0 indicates a weak buffering. The cBR exhibits an asymmetric behavior resulting from the dependence of the cBRS on the sign of the SAP changes: the linear portion of the relation of HP on SAP is steeper when SAP is rising than falling. This feature leads to a longer HP just after a SAP change immediately followed by an opposite sign SAP variation of the same absolute magnitude (Pickering et al., 1972; Rudas et al., 1999; Studinger et al., 2007). As a consequence, the trajectory followed by the point in the plane (SAP, HP) is not a straight line, even for small variations of SAP, but an elliptical HP-SAP pattern. This typical phenomenon is termed hysteresis (Studinger et al., 2007; Hart et al., 2011). The cBR hysteresis suggests that cBR buffers more efficiently SAP increases than decreases. The asymmetry of the cBR originates from the viscoelastic properties of the barosensory vessels, as assessed from the diameter-pressure relation, leading to larger carotid artery diameter changes, and consequently to a greater stretch of the barosensitive vessels, when SAP is rising than falling (Bonyhay et al., 1997; O'Leary et al., 2005). However, it was suggested that the asymmetric behavior of the diameter-pressure relation could not be the sole mechanism responsible for the cBR hysteresis. Indeed, an important role is played by the asymmetric behavior of the neural component as assessed from the HP-diameter relation (Studinger et al., 2007). While cBR hysteresis was frequently studied using interventional analysis (Pickering et al., 1972; Rudas et al., 1999; Studinger et al., 2007), the cBRS was rarely computed by separately considering positive and negative SAP variations over spontaneous fluctuations of HP and SAP (Parati et al., 1988; Martin-Vazquez and Reyes Del Paso, 2010; Davydov et al., 2018; De Maria et al., 2018).

This lack is much more evident when searching for studies featuring the contemporaneous application of different BR characterization methods and an analysis over multiple BR arms. In the present study, SEQ and PRSA techniques were exploited for the analysis of the cBR hysteresis from spontaneous fluctuations of SAP and HP. The SEQ method, scanning HP and SAP variabilities to search for short sequences of assigned length featuring consecutive and parallel variations of SAP and HP, was applied by separately considering positive and negative changes (Bertinieri et al., 1985; De Maria et al., 2018). The PRSA approach, usually anchoring the analysis of HP variability to a specific direction of the SAP changes (i.e., positive) (Bauer et al., 2010; Muller et al., 2012), was applied even in the opposite direction (i.e., negative) (De Maria et al., 2018). We found no significant dependency of the cBRS over the direction of SAP changes when both the data were pooled together regardless of the experimental condition and they were analyzed separately in each experimental session. The inability of cBRS estimates based on spontaneous fluctuations to detect the asymmetric behavior of the cBR might be related to the smallness of the SAP changes that are insufficient for exploring portions of the HP-SAP relation with significantly different slopes. The lack of the cBR asymmetry was confirmed even when the slopes of the linear regression of cBRS estimated over positive and negative SAP variations on the sine of the tilt table angle were compared: indeed, regardless of the method utilized to extract cBRS, the slopes were similar, thus suggesting that both cBRS estimates computed over positive and negative SAP changes contribute equally in closed loop conditions to the decrease of cBRS with the magnitude of the orthostatic challenge (Cooke et al., 1999; Furlan et al., 2000; O'Leary et al., 2003; Dalla Vecchia et al., 2013; Marchi et al., 2016b; De Maria et al., 2018). We advocate the assessment of the impact of HP-SAP causality (Porta et al., 2000) on this conclusion: a possibility is to limit the eventual effect of HP variability rhythms that might be of origin different from cBR, such as the respiratory sinus arrhythmia, via low-pass filtering the series (Oosting et al., 1997).

The sBR Hysteresis Is Detectable From Spontaneous Variability of DAP and MSNA Burst Rate

The sBR buffers DAP changes by reducing the probability of observing a MSNA burst when AP is high and by increasing it when DAP is low. The probability is usually expressed as the number of MSNA bursts per 100 cardiac beats, termed burst incidence (Sundlof and Wallin, 1978; Ebert and Cowley, 1992; Ichinose et al., 2004; Keller et al., 2006; Taylor et al., 2015) or percentage, termed burst threshold (Kienbaum et al., 2001; Hart et al., 2010, 2011; Barbic et al., 2015). This MSNA-DAP relation holds as well when total MSNA (Matsukawa et al., 1996; O'Leary et al., 2003), or total MSNA per cardiac beat (Halliwill et al., 1996; Ichinose et al., 2004; Fu et al., 2006; Dutoit et al., 2010), or total MSNA per 100 beats (Studinger et al., 2009), or parameters describing the MSNA burst strength, such as the average amplitude (Sundlof and Wallin, 1978; Ebert and Cowley, 1992; Taylor et al., 2015) or area of the MSNA burst (Rudas et al., 1999; Kienbaum et al., 2001; Ichinose et al., 2004; O'Leary et al., 2005; Keller et al., 2006), were considered. The sBR was first typified by exploiting the spontaneous fluctuations of DAP and MSNA in absence of any pharmacological intervention inducing AP rises or falls (Sundlof and Wallin, 1978) and later by applying pharmacological approaches (Ebert and Cowley, 1992; Halliwill et al., 1996; Matsukawa et al., 1996; Rudas et al., 1999; Studinger et al., 2009; Dutoit et al., 2010; Hart et al., 2010). In the sBR analysis, regardless of the exploitation of spontaneous or pharmacological approach, the gain of the MSNA-AP relation, usually referred to as sBRS, was obtained as the slope of the linear regression of burst incidence, burst strength, or total MSNA at a given DAP level on DAP value. sBRS is non-positive because it is less likely to find a MSNA burst associated with higher DAP values and a migration of sBRS toward 0 indicates a reduced buffering of DAP variations with appropriate MSNA modifications. Like the cBR, the sBR exhibits an asymmetric behavior resulting from the dependence of the sBRS on the sign of the DAP changes: indeed, the linear portion of the relation of probability of finding a MSNA burst at an assigned DAP level on DAP is steeper when DAP is falling than rising. This feature leads to a lower likelihood of MSNA burst just after a DAP change immediately followed by an opposite sign DAP variation of the same absolute magnitude (Sundlof and Wallin, 1978; Studinger et al., 2009; Hart et al., 2011). This phenomenon is referred to as sBR hysteresis in analogy to the cBR one (Studinger et al., 2009; Hart et al., 2011) and suggests that sBR buffers more efficiently DAP decreases than increases. Remarkably, the sBR hysteresis was found to be evident when both spontaneous (Sundlof and Wallin, 1978; Hart et al., 2011) and pharmacologically driven (Studinger et al., 2009) MSNA and DAP variations were considered. Moreover, it was more easily detectable via burst incidence parameters (Sundlof and Wallin, 1978; Studinger et al., 2009; Hart et al., 2011) than via burst strength markers (Rudas et al., 1999; O'Leary et al., 2005). In this study, we applied a recently proposed dynamical approach to the characterization of sBR (Marchi et al., 2016b) that appears also suitable for the assessment of sBR hysteresis. This analysis exploits the definition of MSNA variability representing the variations of MSNA burst rate over time (Marchi et al., 2016a), scans MSNA and DAP series to search for short antiparallel joint ramps, and computes sBRS as the average slope of the regression line of MSNA burst rate on DAP over these joint MSNA-DAP patterns. In the present study, this approach was applied by separately considering joint MSNA-DAP patterns featuring positive and negative DAP variations. Also, the PRSA approach (Bauer et al., 2010; Muller et al., 2012) was applied to the MSNA burst rate variability series and its analysis was anchored separately to positive and negative DAP changes (De Maria et al., 2018). Given that SEQ and PRSA methods do not require pharmacological challenges they provide an alternative to pharmacological methods for the assessment of the sBR hysteresis (Rudas et al., 1999; Studinger et al., 2009). SEQ and PRSA techniques provide an alternative to non-pharmacological methods for the evaluation of sBR asymmetry as well (Hart et al., 2011). Indeed, the traditional

method based on spontaneous variability (Kienbaum et al., 2001) is useless to study the sBR hysteresis because it does not account for MSNA-DAP causal interactions along sBR (i.e., the association between the MSNA burst rate and DAP could occur according to schemes not necessarily linking MSNA burst rate increases to DAP decreases and *vice versa*). As a consequence, the traditional method (Kienbaum et al., 2001) was adapted in Hart et al. (2011) to embed the flow of time in the analysis by conditioning the probability of occurrence of the MSNA burst at a given DAP to the sign of the DAP modification. However, this strategy reduces the reliability of the sBRS estimate, especially over short data sequences, as a consequence of the reduced consistency of the estimate of the probability of observing an MSNA burst at given DAP when the direction of the DAP change is accounted for.

In our study, when data were pooled together regardless of the experimental condition, we found a significant dependency of the sBRS on the direction of DAP changes with more negative sBRS values while DAP falling than rising. Therefore, our dynamical approach to the characterization of sBR from spontaneous variability confirms the findings obtained via static non-pharmacological and pharmacological approaches (Sundlof and Wallin, 1978; Studinger et al., 2009; Hart et al., 2011). When the experimental conditions were considered separately, this result was significant only in supine condition. Indeed, during the orthostatic challenge and the consequent increase of MSNA burst rate (Cooke et al., 1999; Furlan et al., 2000; O'Leary et al., 2003; Marchi et al., 2016a), the asymmetric behavior of the sBR was no longer evident. This finding is not surprising given that the sBR asymmetry depends on the MSNA burst rate and was lost when the mean MSNA burst rate is increased (i.e., sBR tends to improve its ability to respond to DAP rises than falls at high MSNA levels) (Sundlof and Wallin, 1978; Rudas et al., 1999; Studinger et al., 2009; Hart et al., 2011). The different behavior of sBR in response to DAP ups and downs was stressed by the separate analysis of the dependency of sBRS on sine of the tilt table angle. Indeed, the positive linear relation of sBRS on the magnitude of the orthostatic challenge, reported in Marchi et al. (2016b) when sBRS was assessed regardless of the direction of the DAP changes, was confirmed in our study only when sBRS was evaluated over DAP drops. It seems that the ability to counteract DAP falls was more and more reduced with tilt table angles, while that to counteract DAP rises was preserved. This finding might result in a reduced tolerance of compensating AP drops during the postural challenge at high tilt table inclination. However, even though the tendency to move toward 0 with the magnitude of the challenge is confirmed (Marchi et al., 2016b), we note that this tendency did not produce a significant variation of the sBRS. This result supports the notion of a preserved sBRS with the magnitude of the hypovolemic challenge (Ichinose et al., 2004; Barbic et al., 2015) and suggests a general maintenance of sBR control (Porta et al., 2017). This result is in disagreement with studies assessing sBRS during head-up tilt (Halliwill et al., 1996; Fu et al., 2006). Indeed, these studies observed more negative sBRS values during the postural challenge compared to baseline but sBRS was expressed in different units of measurement (i.e., arbitrary units per mmHg), thus suggesting a possible dependency of the conclusions on the type of the monitored quantity (Kienbaum et al., 2001; Keller et al., 2006) and stressing the importance of using approaches that are independent of normalizing factors (Marchi et al., 2016b) necessary to compensate MSNA amplitude parameters for the variable proximity of the electrode to the nerve fascicle (Sundlof and Wallin, 1978; Kienbaum et al., 2001). A similar observation holds when comparing studies supporting (Sundlof and Wallin, 1978; Hart et al., 2011) and not supporting (Rudas et al., 1999; O'Leary et al., 2005) the existence of sBR hysteresis.

The SEQ Method Is More Powerful Than the PRSA Technique in Assessing Hysteresis of BR Arms

Both the SEQ and PRSA methods (Bertinieri et al., 1985; Bauer et al., 2010; Muller et al., 2012) can provide BRS estimates by differentiating positive and negative AP variations (De Maria et al., 2018). However, we confirm that SEQ and PRSA methods cannot be considered equivalent (De Maria et al., 2018). Indeed, the correlations between cBRS estimates computed over positive and negative SAP variations via the PRSA and nPRSA methods are much stronger than those observed through the SEQ technique, as suggested by the wider scattering in **Figure 5A** than in **Figures 5B,C**. This behavior has been interpreted as a hallmark of a greater rigidity of the PRSA methods compared to the SEQ one in evaluating the gain of the HP-SAP relation from spontaneous fluctuations of HP and SAP variables (De Maria et al., 2018). This conclusion is strengthened in the present study by the analysis of the sBR. Indeed, while the sBRS estimates derived from positive and negative DAP variations computed via the SEQ method are uncorrelated, those derived from PRSA techniques are again strictly correlated. However, the uncorrelation between the sBRS estimates detected by the SEQ analysis is expected, given that the sBR hysteresis detected from the spontaneous fluctuations of DAP and MSNA burst rate is likely to limit the correlation between sBRS markers. Therefore, the strong correlation between sBRS derived from positive and negative DAP variations pointed out by PRSA techniques seems to be artificial. The higher rigidity of the PRSA techniques might have contributed to the inability of these methods to suggest the asymmetric behavior of the sBR. Therefore, we recommend the use of the SEQ method for the assessment of the BR hysteresis from spontaneous fluctuations of cardiovascular variables because the SEQ method is more prone to provide independent descriptors of the BR functioning when this reflex is solicited by positive and negative AP variations. The better performance of the SEQ method may lie in its focus on particularly rare patterns lasting several beats and more likely of BR origin, while the PRSA utilizes basic AP variations from one beat to the next one that might not necessarily drive HP or MSNA responses. Conversely, the PRSA method should be preferred for its robustness and repeatability of the results, when BRS estimates are assessed regardless of the sign of the AP variations (Bauer et al., 2010; Maestri et al., 2017; Pinna et al., 2017).

CONCLUSION

Two dynamical approaches for the characterization of the BR hysteresis, namely the SEQ and PRSA methods, from spontaneous fluctuations of cardiovascular variables were applied simultaneously to cBR and sBR. We recommend the use of the SEQ method for future studies on the BR hysteresis given that this approach is much more powerful than the PRSA technique in typifying the different responses of BR arms to positive and negative AP spontaneous changes. The expected asymmetric behavior of sBR and cBR was detected exclusively in the sBR and in absence of an orthostatic stimulus, thus stressing the much more inherent asymmetry, and non-linearity, of the sBR visible even for small variations of AP and in unstressed conditions. The detection of sBR asymmetry demonstrates that the BR hysteresis phenomenon can be studied from spontaneous fluctuations of cardiovascular variables, thus prompting for the application of this approach to other branches of BR, such as the peripheral resistance (Porta et al., 2018a) and stroke volume (Casadei et al., 1992). Moreover, the different behavior between cBR and sBR makes evident the complementary information that can be derived from the simultaneous characterization of different arms of the BR control. We advocate future applications in healthy subjects under different experimental challenges and in a more numerous healthy group to confirm the inability of detecting the asymmetric behavior of cBR from spontaneous variability and check whether the eventual maintenance of sBR asymmetry during an orthostatic challenge could identify some pathological conditions, such as orthostatic intolerance. Even though results of this study are confirmed after reducing gender and age variability, the present findings need to be corroborated by specific studies accounting explicitly for age and gender factors (Ng et al., 1993; Laitinen et al., 1998; Fisher et al., 2012). This exploration is important because the majority of the studies present in literature about the modifications of BRS with age and gender does not taken into account the BRS hysteresis phenomenon. At this regard the present approach, fully grounded on spontaneous fluctuations of physiological variables, could be of help by setting an analysis framework useful in retrospective studies.

DATA AVAILABILITY

The datasets generated for this study are available on request to the corresponding author.

AUTHOR CONTRIBUTIONS

BDM analyzed the data. BDM and AP drafted the manuscript. ME and EL performed the experiments. BDM, VB, BC, EV, ME, EL, MB, SC, LDV, and AP interpreted the data, revised the manuscript, and approved the final version of the manuscript.

SUPPLEMENTARY MATERIAL

The Supplementary Material for this article can be found online at: https://www.frontiersin.org/articles/10.3389/fphys.2019.00342/full#supplementary-material

REFERENCES

Barbic, F., Heusser, K., Marchi, A., Zamuner, A., Gauger, P., Tank, J., et al. (2015). Cardiovascular parameters and neural sympathetic discharge variability before orthostatic syncope: role of sympathetic baroreflex control to the vessels. *Physiol. Meas.* 36, 633–641. doi: 10.1088/0967-3334/36/4/633

Baselli, G., Cerutti, S., Badilini, F., Biancardi, L., Porta, A., Pagani, M., et al. (1994). Model for the assessment of heart period and arterial pressure variability interactions and respiratory influences. *Med. Biol. Eng. Comput.* 32, 143–152. doi: 10.1007/BF02518911

Baskerville, A. L., Eckberg, D. L., and Thompson, M. A. (1979). Arterial pressur.e and pulse interval responses to repetitive carotid baroreceptor stimuli in man. *J. Physiol.* 297, 61–71. doi: 10.1113/jphysiol.1979.sp013027

Bauer, A., Morley-Davies, A., Barthel, P., Muller, A., Ulm, K., Malik, M., et al. (2010). Bivariate phase-rectified signal averaging for assessment of spontaneous baroreflex sensitivity: pilot study of the technology. *J. Electrocardiol.* 43, 649–653. doi: 10.1016/j.jelectrocard.2010.05.012

Bertinieri, G., di Rienzo, M., Cavallazzi, A., Ferrari, A. U., Pedotti, A., and Mancia, G. (1985). A new approach to analysis of the arterial baroreflex. *J. Hypertens.* 33, S79–S81.

Bonyhay, I., Jokkel, G., Karlocai, K., Reneman, R., and Kollai, M. (1997). Effect of vasoactive drugs on carotid diameter in humans. *Am. J. Physiol.* 273, H1629–H1636. doi: 10.1152/ajpheart.1997.273.4.H1629

Casadei, B., Meyer, T. E., Coats, A. J., Conway, J., and Sleight, P. (1992). Baroreflex control of stroke volume in man: an effect mediated by the vagus. *J. Physiol.* 448, 539–550. doi: 10.1113/jphysiol.1992.sp019056

Cooke, W. H., Hoag, J. B., Crossman, A. A., Kuusela, T. A., Tahvanainen, K. U., and Eckberg, D. L. (1999). Human responses to upright tilt: a window on central autonomic integration. *J. Physiol.* 517(Pt 2), 617–628. doi: 10.1111/j.1469-7793.1999.0617t.x

Dalla Vecchia, L., Barbic, F., Galli, A., Pisacreta, M., Gornati, R., Porretta, T., et al. (2013). Favorable effects of carotid endarterectomy on baroreflex sensitivity and cardiovascular neural modulation: a 4-month follow-up. *Am. J. Physiol.* 304, R1114–R1120. doi: 10.1152/ajpregu.00078.2013

Davydov, D. M., Naliboff, B., Shahabi, L., and Shapiro, D. (2018). Asymmetries in reciprocal baroreflex mechanisms and chronic pain severity: Focusing on irritable bowel syndrome. *Neurogastroenterol. Motil.* 30:e13186. doi: 10.1111/nmo.13186

De Maria, B., Bari, V., Ranucci, M., Pistuddi, V., Ranuzzi, G., Takahashi, A. C. M., et al. (2018). Separating arterial pressure increases and decreases in assessing cardiac baroreflex sensitivity via sequence and bivariate phase-rectified signal averaging techniques. *Med. Biol. Eng. Comput.* 56, 1241–1252. doi: 10.1007/s11517-017-1765-0

Diedrich, A., Porta, A., Barbic, F., Brychta, R. J., Bonizzi, P., Diedrich, L., et al. (2009). Lateralization of expression of neural sympathetic activity to the vessels and effects of carotid baroreceptor stimulation. *Am. J. Physiol.* 296, H1758–H1765. doi: 10.1152/ajpheart.01045.2008

Dutoit, A. P., Hart, E. C., Charkoudian, N., Wallin, B. G., Curry, T. B., and Joyner, M. J. (2010). Cardiac baroreflex sensitivity is not correlated to sympathetic baroreflex sensitivity within healthy young humans. *Hypertension* 56, 1118–1123. doi: 10.1161/HYPERTENSIONAHA.110.158329

Ebert, T. J., and Cowley, A. W. (1992). Baroreflex modulation of sympathetic outflow during physiological increases of vasopressin in humans. *Am. J. Physiol.* 262, H1372–H1378. doi: 10.1152/ajpheart.1992.262.5.H1372

Eckberg, D. L. (1976). Temporal response patterns of the human sinus node to brief carotid baroreceptor stimuli. *J. Physiol.* 258, 769–782. doi: 10.1113/jphysiol.1976.sp011445

Eckberg, D. L. (1980). Nonlinearities of the human carotid baroreceptor-cardiac reflex. *Circ. Res.* 47, 208–216. doi: 10.1161/01.RES.47.2.208

Fisher, J. P., Kim, A., Hartwich, D., and Fadel, P. J. (2012). New insights into the effects of age and sex on arterial baroreflex function at rest and during exercise in humans. *Auton. Neurosci. Basic Clin.* 172, 13–22. doi: 10.1016/j.autneu.2012.10.013

Fu, Q., Shook, R. P., Okazaki, K., Hastings, J. L., Shibata, S., Conner, C. L., et al. (2006). Vasomotor sympathetic neural control is maintained during sustained upright posture in humans. *J. Physiol.* 577(pt 2), 679–687. doi: 10.1113/jphysiol.2006.118158

Furlan, R., Porta, A., Costa, F., Tank, J., Baker, L., Schiavi, R., et al. (2000). Oscillatory patterns in sympathetic neural discharge and cardiovascular variables during orthostatic stimulus. *Circulation* 101, 886–892. doi: 10.1161/01.CIR.101.8.886

Halliwill, J. R., Taylor, J. A., and Eckberg, D. L. (1996). Impaired sympathetic vascular regulation in humans after acute dynamic exercise. *J. Physiol.* 495(pt 1), 279–288. doi: 10.1113/jphysiol.1996.sp021592

Hart, E. C., Joyner, M. J., Wallin, B. G., Karlsson, T., Curry, T. B., and Charkoudian, N. (2010). Baroreflex control of muscle sympathetic nerve activity: a nonpharmacological measure of baroreflex sensitivity. *Am. J. Physiol.* 298, H816–H822. doi: 10.1152/ajpheart.00924.2009

Hart, E. C., Wallin, B. G., Curry, T. B., Joyner, M. J., Karlsson, T., and Charkoudian, N. (2011). Hysteresis in the sympathetic baroreflex: role of baseline nerve activity. *J. Physiol.* 589(pt 1), 3395–3404. doi: 10.1113/jphysiol.2011.208538

Ichinose, M., Saito, M., Ogawa, T., Hayashi, K., Kondo, N., and Nishiyasu, T. (2004). Modulation of control of muscle sympathetic nerve activity during orthostatic stress in humans. *Am. J. Physiol.* 287, H2147–H2153. doi: 10.1152/ajpheart.00215.2004

Keller, D. M., Cui, J., Davis, S. L., Low, D. A., and Crandall, C. G. (2006). Heat stress enhances arterial baroreflex control of muscle sympathetic nerve activity via increased sensitivity of burst gating, not burst area, in humans. *J. Physiol.* 573(pt 2), 445–451. doi: 10.1113/jphysiol.2006.108662

Kienbaum, P., Karlsson, T., Sverrisdottir, Y. B., Elam, M., and Wallin, B. G. (2001). Two sites for modulation of human sympathetic activity by arterial baroreceptors. *J. Physiol* 531(pt 3), 861–869. doi: 10.1111/j.1469-7793.2001.0861h.x

Laitinen, T., Hartikainen, J., Vanninen, E., Niskanen, L., Geelen, G., and Länsimies, E. (1998). Age and sex dependency of baroreflex sensitivity in healthy subjects. *J. Appl. Physiol.* 84, 576–583. doi: 10.1152/jappl.1998.84.2.576

Lambert, E., Eikelis, N., Esler, M., Dawood, T., Schlaich, M., Bayles, R., et al. (2008). Altered sympathetic nervous reactivity and norepinephrine transporter expression in patients with postural tachycardia syndrome. *Circ. Arrhythm Electrophysiol.* 12, 103–109. doi: 10.1161/CIRCEP.107.750471

Maestri, R., La Rovere, M. T., Raczak, G., Danilowicz-Szymanowicz, L., and Pinna, G. D. (2017). Estimation of baroreflex sensitivity by the bivariate phase rectified signal averaging method: a comparison with the phenylephrine method. *Physiol. Meas.* 38, 1874–1884. doi: 10.1088/1361-6579/aa8b5a

Marchi, A., Bari, V., De Maria, B., Esler, M., Lambert, E., Baumert, M., et al. (2016a). Calibrated variability of muscle sympathetic nerve activity during graded head-up tilt in humans and its link with noradrenaline data and cardiovascular rhythms. *Am. J. Physiol.* 310, R1134–R1143. doi: 10.1152/ajpregu.00541.2015

Marchi, A., Bari, V., De Maria, B., Esler, M., Lambert, E., Baumert, M., et al. (2016b). Simultaneous characterization of sympathetic and cardiac arms of the baroreflex through sequence techniques during incremental head-up tilt. *Front. Physiol.* 7:438.

Martin-Vazquez, M., and Reyes Del Paso, G. A. (2010). Physical training and the dynamics of the cardiac baroreflex: a comparison when blood pressure rises and falls. *Int. J. Psychophysiol.* 76, 142–147. doi: 10.1016/j.ijpsycho.2010.03.004

Matsukawa, T., Sugiyama, Y., and Mano, T. (1996). Age-related changes in baroreflex control of heart rate and sympathetic nerve activity in healthy humans. *J. Auton. Nerv. Syst.* 60, 209–212. doi: 10.1016/0165-1838(96)00057-4

Muller, A., Morley-Davies, A., Barthel, P., Hnatkova, K., Bauer, A., Ulm, K., et al. (2012). Bivariate phase-rectified signal averaging for assessment of spontaneous baroreflex sensitivity: normalization of the results. *J. Electrocardiol.* 45, 77–81. doi: 10.1016/j.jelectrocard.2011.07.010

Ng, A. V., Callister, R., Johnson, D. G., and Seals, D. R. (1993). Age and sex influence muscle sympathetic nerve activity at rest in healthy humans. *Hypertension* 21, 498–503. doi: 10.1161/01.HYP.21.4.498

O'Leary, D. D., Kimmerly, D. S., Cechetto, A. D., and Shoemaker, J. K. (2003). Differential effect of head-up tilt on cardiovagal and sympathetic baroreflex sensitivity in humans. *Exp. Physiol.* 88, 769–774. doi: 10.1113/eph8802632

O'Leary, D. D., Steinback, C. D., Cechetto, A. D., Foell, B. T., Topolovec, J. C., Gelb, A. W., et al. (2005). Relating drug-induced changes in carotid artery mechanics to cardiovagal and sympathetic baroreflex control. *Can. J. Physiol. Pharmacol.* 83, 439–446. doi: 10.1139/y05-030

Oosting, J., Struijker-Boudier, H. A. J., and Janssen, B. J. A. (1997). Validation of a continuous baroreceptor reflex sensitivity index calculated from spontaneous fluctuations of blood pressure and pulse interval in rats. *J. Hypertens.* 15, 391–399. doi: 10.1097/00004872-199715040-00010

Parati, G., Di Rienzo, M., Bertinieri, G., Pomidossi, G., Casadei, R., Groppelli, A., et al. (1988). Evaluation of the baroreceptor-heart rate reflex by 24-hour intra-arterial blood pressure monitoring in humans. *Hypertension* 12, 214–222. doi: 10.1161/01.HYP.12.2.214

Pickering, T. G., Gribbin, B., and Sleight, P. (1972). Comparison of the reflex heart rate response to rising and falling arterial pressure in man. *Cardiovasc. Res.* 63, 277–283. doi: 10.1093/cvr/6.3.277

Pinna, G. D., Porta, A., Maestri, R., De Maria, B., Dalla Vecchia, L. A., and La Rovere, M. T. (2017). Different estimation methods of spontaneous baroreflex sensitivity have different predictive value in heart failure patients. *J. Hypertens.* 35, 1666–1675. doi: 10.1097/HJH.0000000000001377

Porta, A., Bari, V., Bassani, T., Marchi, A., Pistuddi, V., and Ranucci, M. (2013). Model-based causal closed-loop approach to the estimate of baroreflex sensitivity during propofol anesthesia in patients undergoing coronary artery bypass graft. *J. Appl. Physiol.* 115, 1032–1042. doi: 10.1152/japplphysiol.00537.2013

Porta, A., Bari, V., De Maria, B., Cairo, B., Vaini, E., Malacarne, M., et al. (2018a). Peripheral resistance baroreflex during incremental bicycle ergometer exercise: characterization and correlation with cardiac baroreflex. *Front. Physiol.* 9:688. doi: 10.3389/fphys.2018.00688

Porta, A., Bari, V., De Maria, B., Cairo, B., Vaini, E., Perseguini, N. M., et al. (2018b). Comparison between probabilistic and wiener-granger causality in assessing modifications of the cardiac baroreflex control with age. *Physiol. Meas.* 39:104004. doi: 10.1088/1361-6579/aae0ec

Porta, A., Baselli, G., Rimoldi, O., Malliani, A., and Pagani, M. (2000). Assessing baroreflex gain from spontaneous variability in conscious dogs: role of causality and respiration. *Am. J. Physiol.* 279, H2558–H2567. doi: 10.1152/ajpheart.2000.279.5.H2558

Porta, A., Marchi, A., Bari, V., De Maria, B., Esler, M., Lambert, E., et al. (2017). Assessing the strength of cardiac and sympathetic baroreflex controls via transfer entropy during orthostatic challenge. *Phil. Trans. R. Soc. A* 375:20160290. doi: 10.1098/rsta.2016.0290

Rudas, L., Crossman, A. A., Morillo, .the search of ordered MSNA burst rate and C A., Halliwill, J. R., Tahvanainen, K. U., Kuusela, T. A., et al. (1999). Human sympathetic and vagal baroreflex responses to sequential nitroprusside and phenylephrine. *Am. J. Physiol.* 276, H1691–H1698. doi: 10.1152/ajpheart.1999.276.5.H1691

Smyth, H. S., Sleight, P., and Pickering, G. W. (1969). Reflex regulation of the arterial pressure during sleep in man. A quantitative method of assessing baroreflex sensitivity. *Circ. Res.* 24, 109–121. doi: 10.1161/01.RES.24.1.109

Studinger, P., Goldstein, R., and Taylor, J. A. (2007). Mechanical and neural contributions to hysteresis in the cardiac vagal limb of the arterial baroreflex. *J. Physiol.* 583(pt 3), 1041–1048. doi: 10.1113/jphysiol.2007.139204

Studinger, P., Goldstein, R., and Taylor, J. A. (2009). Age- and fitness-related alterations in vascular sympathetic control. *J. Physiol.* 587(pt 9), 2049–2057. doi: 10.1113/jphysiol.2009.170134

Sundlof, G., and Wallin, B. G. (1978). Human muscle nerve sympathetic activity at rest. Relationship to blood pressure and age. *J. Physiol.* 274, 621–637. doi: 10.1113/jphysiol.1978.sp012170

Task Force of the European Society of Cardiology the North American Society of Pacing Electrophysiology (1996). Heart rate variability – standards of measurement, physiological interpretation and clinical use. *Circulation* 93, 1043–1065. doi: 10.1161/01.CIR.93.5.1043

Taylor, C. E., Witter, T., El Sayed, K., Hissen, S. L., Johnson, A. W., and Macefield, V. G. (2015). Relationship between spontaneous sympathetic baroreflex sensitivity and cardiac baroreflex sensitivity in healthy young individuals. *Physiol. Rep.* 3:e12536. doi: 10.14814/phy2.12536

Conflict of Interest Statement: The authors declare that the research was conducted in the absence of any commercial or financial relationships that could be construed as a potential conflict of interest.

frontiers in Physiology

ORIGINAL RESEARCH
published: 11 April 2019
doi: 10.3389/fphys.2019.00381

Sickle Cell Disease Subjects Have a Distinct Abnormal Autonomic Phenotype Characterized by Peripheral Vasoconstriction With Blunted Cardiac Response to Head-Up Tilt

*Patjanaporn Chalacheva[1], Roberta M. Kato[2], Payal Shah[3], Saranya Veluswamy[3], Christopher C. Denton[3], John Sunwoo[1], Wanwara Thuptimdang[1], John C. Wood[4], Jon A. Detterich[4], Thomas D. Coates[3] and Michael C. K. Khoo[1]**

[1] Department of Biomedical Engineering, University of Southern California, Los Angeles, CA, United States, [2] Divisions of Pulmonology, Children's Hospital Los Angeles, Los Angeles, CA, United States, [3] Hematology Section, Children's Center for Cancer, Blood Disease and Bone Marrow Transplantation, Children's Hospital Los Angeles, Keck School of Medicine of University of Southern California, Los Angeles, CA, United States, [4] Divisions of Cardiology, Children's Hospital Los Angeles, Los Angeles, CA, United States

OPEN ACCESS

Edited by:
Alberto Porta,
University of Milan, Italy

Reviewed by:
Giuseppe Baselli,
Politecnico di Milano, Italy
Michal Javorka,
Comenius University in Bratislava, Slovakia
Paolo Castiglioni,
Fondazione Don Carlo Gnocchi Onlus (IRCCS), Italy

***Correspondence:**
Michael C. K. Khoo
khoo@usc.edu

Specialty section:
This article was submitted to Autonomic Neuroscience, a section of the journal Frontiers in Physiology

Received: *20 January 2019*
Accepted: *19 March 2019*
Published: *11 April 2019*

Citation:
Chalacheva P, Kato RM, Shah P, Veluswamy S, Denton CC, Sunwoo J, Thuptimdang W, Wood JC, Detterich JA, Coates TD and Khoo MCK (2019) Sickle Cell Disease Subjects Have a Distinct Abnormal Autonomic Phenotype Characterized by Peripheral Vasoconstriction With Blunted Cardiac Response to Head-Up Tilt. Front. Physiol. 10:381. doi: 10.3389/fphys.2019.00381

In sickle cell disease (SCD), prolonged capillary transit times, resulting from reduced peripheral blood flow, increase the likelihood of rigid red cells entrapment in the microvasculature, predisposing to vaso-occlusive crisis. Since changes in peripheral flow are mediated by the autonomic nervous system (ANS), we tested the hypothesis that the cardiac and peripheral vascular responses to head-up tilt (HUT) are abnormal in SCD. Heart rate, respiration, non-invasive continuous blood pressure and finger photoplethysmogram (PPG) were monitored before, during, and after HUT in SCD, anemic controls and healthy subjects. Percent increase in heart rate from baseline was used to quantify cardiac ANS response, while percent decrease in PPG amplitude represented degree of peripheral vasoconstriction. After employing cluster analysis to determine threshold levels, the HUT responses were classified into four phenotypes: (CP) increased heart rate and peripheral vasoconstriction; (C) increased heart rate only; (P) peripheral vasoconstriction only; and (ST) subthreshold cardiac and peripheral vascular responses. Multinomial logistic regression (MLR) was used to relate these phenotypic responses to various parameters representing blood properties and baseline cardiovascular activity. The most common phenotypic response, CP, was found in 82% of non-SCD subjects, including those with chronic anemia. In contrast, 70% of SCD subjects responded abnormally to HUT: C-phenotype = 22%, P-phenotype = 37%, or ST-phenotype = 11%. MLR revealed that the HUT phenotypes were significantly associated with baseline cardiac parasympathetic activity, baseline peripheral vascular variability, hemoglobin level and SCD diagnosis. Low parasympathetic activity at baseline dramatically increased the probability of belonging to the P-phenotype in SCD subjects, even after adjusting for hemoglobin level, suggesting a characteristic autonomic dysfunction that is independent of anemia. Further analysis using a mathematical model of heart rate variability revealed that the low parasympathetic

activity in P-phenotype SCD subjects was due to impaired respiratory-cardiac coupling rather than reduced cardiac baroreflex sensitivity. By having strong peripheral vasoconstriction without compensatory cardiac responses, P-phenotype subjects may be at increased risk for vaso-occlusive crisis. The classification of autonomic phenotypes based on HUT response may have potential use for guiding therapeutic interventions to alleviate the risk of adverse outcomes in SCD.

Keywords: sickle cell anemia, autonomic dysfunction, orthostatic stress, phenotypic response, peripheral vasoconstriction

INTRODUCTION

Sickle cell disease (SCD) is an inherited hemoglobin disorder characterized by transformation of flexible biconcave disk shaped red blood cells into rigid sickle shaped cells caused by polymerization of the abnormal hemoglobin-S once oxygen is released into tissue (Rees et al., 2010). These rigid sickle cells can obstruct microvascular blood flow. Subsequent regional blood flow obstructions can clinically manifest as vaso-occlusive crisis (VOC), resulting in attendant pain, organ damage or death. The mechanism that triggers the transformation from steady-state to VOC remains elusive and the frequency of crises is highly variable among patients. However, onset of VOC events are often associated with emotional stress, cold exposure and pain (Coates et al., 2018), all of which can alter the balance in autonomic nervous system (ANS) activity. In 1976, Eaton et al. (1976) proposed that VOC was triggered by events that prolong red cell transit time in the microvasculature because sickle hemoglobin polymerization would occur in smaller vessels where entrapment was likely. It is known that ANS plays a major role in the regulation of blood flow as blood vessels, particularly arterioles, are innervated with sympathetic neurons (Thomas, 2011). So, abnormal autonomic control of peripheral vascular resistance may predispose SCD patients to prolonged vasoconstriction in response to stressful stimuli. Without compensatory changes in cardiac output, this increases the chance of microvascular blood flow obstruction and VOC.

To date, there is growing evidence of abnormal ANS function in SCD. The interest in autonomic dysfunction in SCD stemmed in part from the increased risk of sudden death in this population (Coates et al., 2018; James et al., 1994; Mestre et al., 1997). Decreased beat-to-beat cardiac variability is common in SCD. Low cardiac variability is a marker of autonomic dysfunction and was found to be a significant predictor of mortality after acute myocardial infarction in non-SCD patients (Kleiger et al., 1987). Our group previously showed that SCD subjects had marked parasympathetic withdrawal in response to transient hypoxia (Sangkatumvong et al., 2011). Other studies found that decreased parasympathetic activity was associated with higher frequency of painful VOC (Nebor et al., 2011) and reported increased sympathetic activity in SCD during VOC compared to their steady state (Charlot et al., 2017). While many studies have employed heart rate variability (HRV) analysis to assess autonomic function, HRV provides information that is directly representative of only cardiac autonomic activity but not peripheral vascular control. In fact, there is a dearth of studies exploring peripheral vascular function in SCD patients. We previously found that SCD subjects had higher frequency of sympathetically-mediated sigh-vasoconstriction (Sangkatumvong et al., 2011) and subsequently, others found that SCD children had stronger vasoconstriction in response to inspiratory breath hold (L'Esperance et al., 2013).

Head-up tilt (HUT) is a potent sympathetic stimulus that triggers both cardiac and peripheral responses and has long been used to assess autonomic function in the context of postural syncope (Zaqqa and Massumi, 2000; Stewart, 2012). During HUT, orthostatic stress causes transient hemodynamic changes which are restored by rapid cardiovascular adjustments through sympathetic activation and parasympathetic withdrawal. As one assumes the upright posture, blood initially shifts toward abdomen and legs, leading to transient drop in stroke volume, cardiac output and subsequently blood pressure. Cardiac and peripheral vascular baroreflexes then act to increase heart rate and peripheral resistance, restoring blood pressure.

In this study, we used HUT as the means to provide an all-encompassing assessment of cardiac and/or peripheral autonomic function in normal controls, SCD subjects and non-SCD subjects with chronic anemia. We hypothesized that by identifying different categories of HUT response among these subjects, we would be able to isolate the autonomic phenotypes that might place SCD subjects at increased risk for microvascular occlusion and VOC. We then employed the causal modeling approach, which utilizes signal analysis and system identification techniques, to probe and disentangle the functional mechanisms involved in the cardiovascular control system (Xiao et al., 2005; Batzel et al., 2009; Khoo, 2018). These advanced analyses provided additional clues into which mechanisms were responsible for predisposing SCD subjects to having different HUT response phenotypes, thereby enabling us to identify the source of the autonomic abnormality in SCD most likely to increase risk of VOC.

MATERIALS AND METHODS

Participants

All experiments were conducted at Children's Hospital Los Angeles (CHLA). The study protocol was approved by the Committee on Clinical Investigations, the institutional review board (IRB) of CHLA. Participants, who were at least 13 years old, were selected from ethnically matched family members,

SCD subjects and other patients followed in the red cell and hemoglobinopathy program at CHLA. Exclusion criteria were any known acute or chronic illnesses including cardiovascular disease that may compromise subject safety or data integrity, significant sickling symptoms and/or vaso-occlusive crisis less than 4 weeks from the scheduled study and known pregnancy. However, non-SCD subjects with chronic anemia were included in order to help disentangle the effect of having SCD from low hemoglobin level. In accordance with CHLA IRB policies, written informed consent or assent (for subjects < 14 years old) was obtained before participation in the study. In addition, parental consent was obtained if the subject was less than 18 years old. Data acquired from total of 66 subjects were studied. Subject characteristics are summarized in **Table 1**.

Protocols and Data Preprocessing

Subjects were asked to stay hydrated and get adequate sleep the day before the study and avoid caffeinated beverages on the day of the study. The study was always carried out in the morning, starting between 9 and 11 am. The study took place in the autonomic lab, a quiet, dimmed light and temperature-controlled room. After the subject had rested quietly for at least 5 min, we recorded heart rate, blood pressure and oxygen saturation (SpO_2). Then up to 30 ml of blood was drawn for complete blood count, reticulocyte count, hemoglobin electrophoresis, plasma hemoglobin, plasma free heme and hemopexin.

The subject was positioned on the tilt table. Before the actual study protocol started, the subjects underwent a short HUT (<1 min) to familiarize them with the protocol as well as to let them position themselves properly as they transitioned from supine to 70° upright position. The subjects were then returned to supine position. After all vital signals stabilized, we began collecting baseline (no intervention) data for 7 min. The subjects underwent a battery of autonomic challenges, such as induced hypoxia, handgrip and controlled breathing, which were not related to the HUT protocol presented in this paper. Each of these challenges, including HUT, was separated by a washout period. The HUT protocol started with 5-min pre-HUT recording in supine position. The subject was then tilted up to 70° upright position at a rate of approximately 5°/s and remained in that position for 7 min before being returned to supine. Following stabilization of all signals, recording continued post-HUT for at least 5 min.

The electrocardiogram (ECG), continuous blood pressure (Nexfin; BMEYE, Amsterdam, Netherlands), photoplethysmogram (Nonin Medical Inc., United States), and respiratory airflow using a pneumotachometer (Hans Rudolph, Inc., Kansas City, MO, United States) were monitored. Blood pressure and photoplethysmogram (PPG) were measured on the index finger and the thumb on the right hand, respectively. Cutaneous blood flow using laser Doppler flowmetry (Perimed, Jarfalla, Sweden) was also measured on the right ring finger for consistency checks with the PPG measurements but was not used in the analyses (see section "Discussion"). In addition, an accelerometer was attached to the tilt table to capture the exact moment when HUT occurred. All measurements were digitized synchronously and continuously through Biopac MP150 data acquisition system (Biopac, United States) at 250 Hz. The beat-to-beat variables were extracted in relation to the R-waves on the ECG. R–R interval (RRI) was defined as the time between two consecutive R-waves. Diastolic and systolic blood pressure (DBP and SBP) were the nadir and the peak of the blood pressure pulse within each RRI. The mean arterial pressure (MAP) for each beat was calculated from the average of the continuous blood pressure

TABLE 1 | Subject characteristics and baseline physiological measurements.

	Non-SCD (*N* = 39)	SCD (*N* = 27)	*P*-value
Diagnosis	Healthy 11	Homozygous SS 25	–
	Sickle cell trait 8	S-β0 thalassemia 1	
	Hereditary spherocytosis 7	S-β+ thalassemia 1	
	Beta thalassemia major 4		
	Hemoglobin H 5		
	Hemoglobin H constant spring 4		
Age (years)	22.0 (1.2)	23.6 (1.5)	0.40
Sex (M/F)	19/20	13/14	0.96†
BMI (kg/m^2)	24.7 (1.0)	22.6 (0.9)	0.13
Hemoglobin (g/dL)	12.2 (0.4)	9.5 (0.3)	**<0.0001**
Hematocrit (%)	37.2 (0.94)	27.7 (1.03)	**<0.0001**
Reticulocyte* (%)	1.59 (2.97)	9.02 (9.86)	**<0.0001**
Hemoglobin S‡ (%)	–	57 (5.6)	–
Plasma hemoglobin* (mg/dL)	38.3 (59.8)	71.9 (63.5)	**0.0019**
Free heme* (μM)	0.18 (1.69)	1.26 (1.23)	**0.0016**
Hemopexin* (μg/mL)	451 (481)	310 (333)	0.14
SpO_2* (%)	98 (0.0)	97 (2)	**<0.0001**

*Normally distributed data are shown as mean (standard error of mean) with p-value from t-test. Non-normally distributed data, indicated by *, are shown as median (interquartile range) with p-values from Wilcoxon test. †indicates chi-squared test. Bolded p-values indicate statistical significance ($p < 0.05$). ‡Hemoglobin S that can polymerize under normal conditions such as in SCD patients, unlike in sickle cell trait patients.*

values over the cardiac cycle. The pulse amplitude of the PPG (PPGa) was derived as the difference between the peak and nadir of PPG signal within each beat. PPGa reflects pulsatile change in finger blood volume caused by arterial blood flow in the fingertip (Allen, 2007; Elgendi, 2012) and is related to blood flow and arterial compliance (Beene and Eggers, 1974; Babchenko et al., 2001). The modulation of arterial compliance is primarily governed by the sympathetic nervous system as previous studies have demonstrated that PPGa increases significantly during sympathetic blockade (Beene and Eggers, 1974; Kim et al., 1975; Babchenko et al., 2001). As such, we took the decreases/increases in PPGa to represent vasoconstriction/dilation in response to neural inputs. Since PPGa is a relative measurement, it was normalized to its own 95th percentile value of its full study recording and expressed in normalized unit (nu). Lastly, the respiratory airflow was integrated to produce instantaneous lung volume (ILV) change.

For subsequent spectral and modeling analyses, all beat-to-beat variables, namely RRI, SBP, DBP, MAP, and PPGa, and the corresponding respiration signal (ILV), were converted into uniformly sampled time series, with 0.5 s as the interval between samples, using interpolation and resampling algorithm of Berger et al. (1986).

HUT Response Quantification

Tachycardia and peripheral vasoconstriction are the compensatory responses to transient drop in blood pressure during HUT. We defined the cardiac response (decrease in mean RRI) and peripheral response (decrease in mean PPGa) as percent change relative to their own supine values:

$$\Delta \text{ RRI or } \Delta \text{ PPGa } = \left(\frac{\text{mean supine} - \text{mean HUT}}{\text{mean supine}} \times 100 \right) \quad (1)$$

Higher ΔRRI and ΔPPGa signified stronger tachycardic and vasoconstrictive responses, respectively. To avoid including transient HUT-related responses, the mean values of RRI, PPGa, and SBP were derived from 3-min during the pre-HUT period at least 60 s before HUT onset, during HUT 150 s after HUT onset, and during post-HUT 90 s after returning to supine (**Figure 1**). We chose the post-HUT means rather than pre-HUT values to be the reference supine values for RRI and PPGa as they were more consistent with the baseline recorded at the very beginning of the entire study session (see **Supplementary Materials**). Mean SBP was carefully monitored to determine whether the subjects could restore their blood pressure level during HUT.

HUT Response Classification

Determination of thresholds for response to HUT was first done by examination of the frequency distributions of percent change in RRI and PPGa in response to HUT. The RRI and PPGa data during both supine and HUT were expressed as percent change relative to the subject's own supine value. The null distributions for fluctuations in RRI and PPGa while supine (expressed in %) were constructed for all subjects, reflecting the

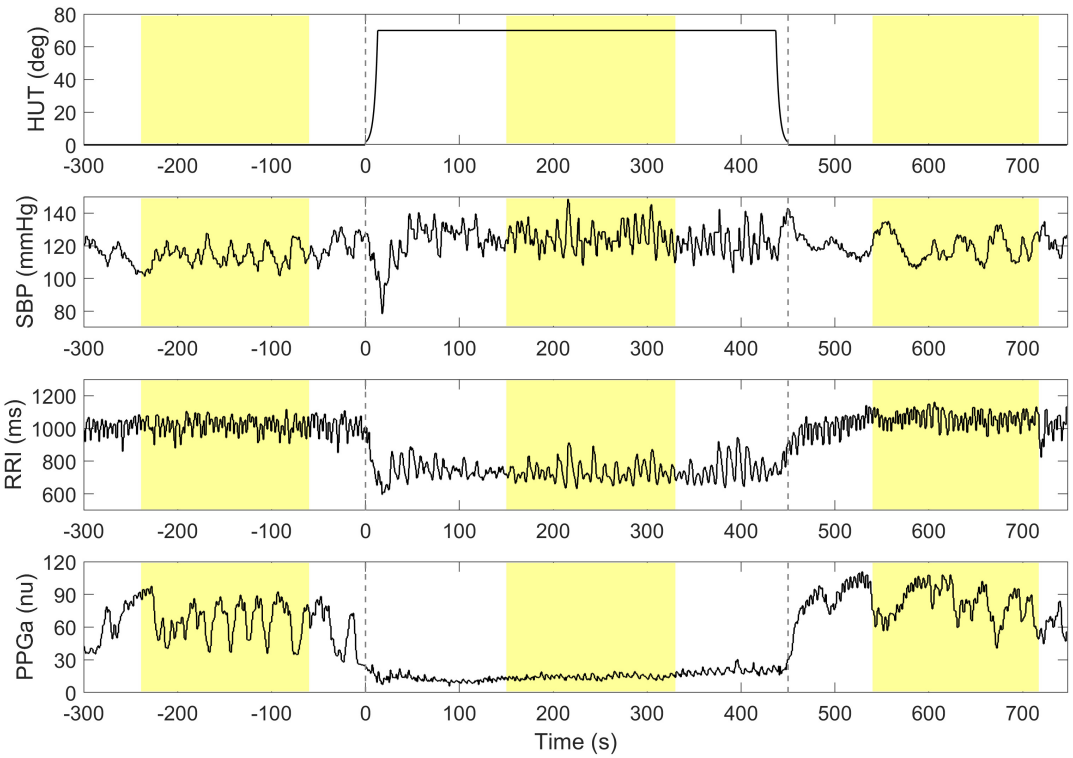

FIGURE 1 | A representative data segment pre-, during and post-HUT. Vertical dashed lines indicate the onset and the end of HUT. The mean values of SBP, RRI and PPGa during pre-, during and post-HUT are calculated from the shaded areas.

"population" spontaneous fluctuations in RRI and PPGa. The subject was considered as having a substantial HUT response (i.e., the responses exceeded spontaneous fluctuations) if the ΔRRI or ΔPPGa during HUT (expressed in %) was greater than 1 standard deviation (SD) of the supine null distribution (**Figure 2**, dashed lines). Based on a cutoff at 1 SD, the subjects were initially classified into four groups (combinations of having ΔRRI and ΔPPGa during HUT above or below the thresholds).

These thresholds were further refined by first visualizing ΔRRI and ΔPPGa of each subject as a data pair. The scatter plot of ΔRRI vs. ΔPPGa is shown in **Figure 3**. Next, we searched for the RRI and PPGa thresholds that best separated the data pairs into four quadrants (i.e., four groups) by minimizing the dispersion of data pairs from the center of each group (Everitt et al., 2011). We allowed the RRI and PPGa thresholds to vary from 1 to 3 SDs. One SDs of RRI and PPGa were selected as the minimal thresholds to ensure that the responses at least exceeded spontaneous fluctuations. The combination of these thresholds that yielded the minimal total dispersion of data pairs in all groups was selected as the optimal cutoff RRI and PPGa thresholds. We used these final thresholds to classify subjects into 4 phenotypic responses to SBP recovery during HUT: (1) dual cardiac rate and peripheral vasoconstriction responses (CP), (2) only cardiac rate response (C), (3) only peripheral

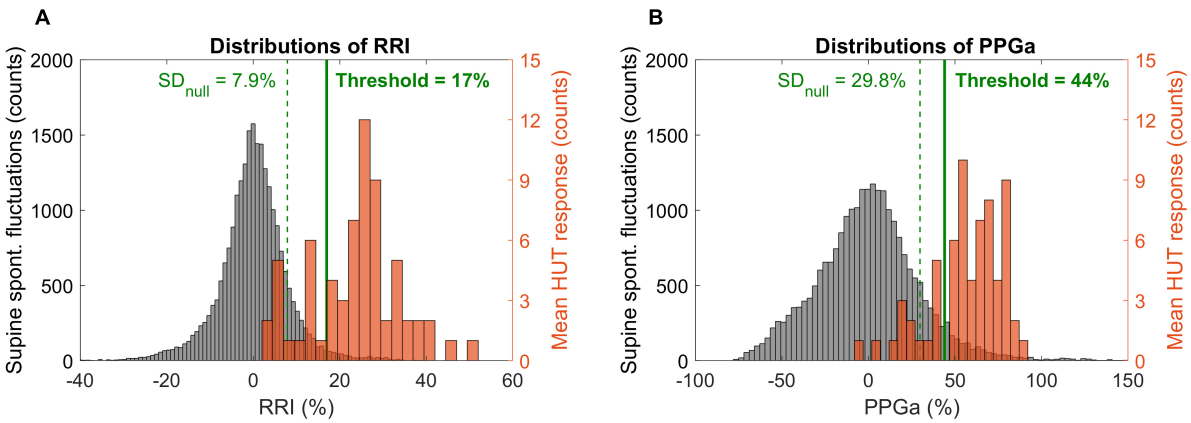

FIGURE 2 | Distributions of spontaneous fluctuations during supine (null distributions, gray) and distributions of the mean change during HUT (orange) in RRI **(A)** and PPGa **(B)**. Note that the distributions of spontaneous fluctuations consider all sample points during supine while the mean HUT response distributions constitute of one value of ΔRRI or ΔPPGa per subject. Dashed vertical lines indicate 1 standard deviation of the null distributions (level of spontaneous fluctuations during supine). Solid lines indicate the optimal thresholds in RRI and PPGa for HUT response classification.

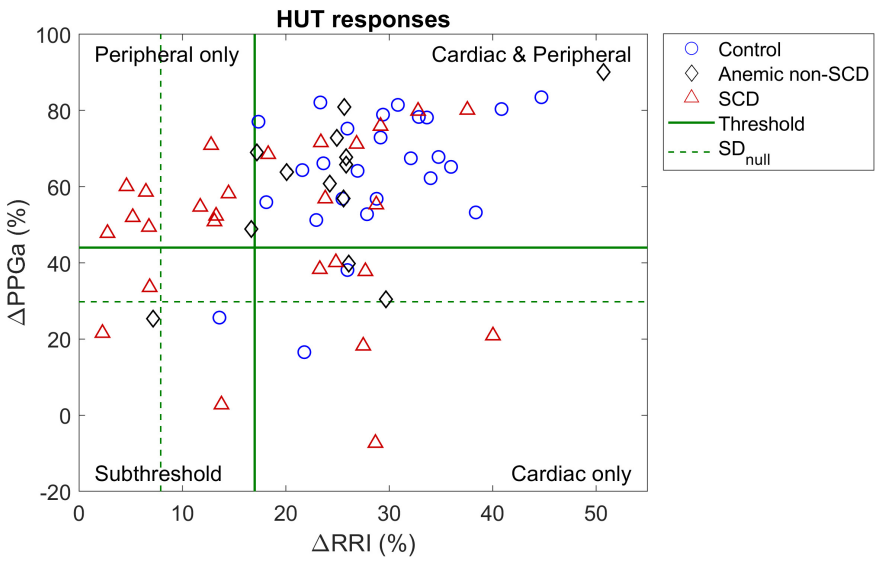

FIGURE 3 | Scatter plot of percent mean change in RRI and PPGa during HUT relative to supine value. Dash lines (SD_{null}) represent the level of spontaneous fluctuations during supine in RRI and PPGa. Solid lines are the optimal thresholds that divide subjects into clusters of different HUT response phenotypes. Most subjects were classified into the dual cardiac and peripheral response phenotype (CP, upper right quadrant). However, the peripheral vasoconstriction only phenotype (P, upper left quadrant) consisted of mainly SCD subjects.

vasoconstriction response (P) and (4) subthreshold cardiac rate and peripheral vasoconstriction responses (ST). SBP, RRI, and PPGa of representative subjects with different HUT responses are shown in **Figure 4**.

Baseline Physiological and Autonomic Parameters

To assess how the individuals' baseline physiological characteristics affected their HUT responses, we calculated mean RRI, SBP, DBP, and PPGa and autonomic indices from their corresponding study baseline. The autonomic indices were derived from heart rate variability, blood pressure variability and peripheral vascular variability as follows:

1. Normalized high-frequency power of RRI ($HFP_{RRI,n}$): RRI spectral power in 0.15–0.4 Hz region divided by the square of mean RRI, representing parasympathetic modulation of RRI (ESC/NASPE Task Force, 1996; Sacha, 2013).
2. Low-to-high ratio (LHR_{RRI}): ratio of low-frequency RRI spectral power (0.04–0.15 Hz) to high-frequency RRI spectral power, representing sympatho-vagal balance (ESC/NASPE Task Force, 1996).
3. Low-frequency power of SBP (LFP_{SBP}): SBP spectral power in 0.04–0.15 Hz region, representing sympathetic modulation on blood pressure (Parati et al., 1995; Pagani et al., 1996; Malpas, 2002).
4. Baroreflex sensitivity (BRS): determined using the sequence method (Parati et al., 2000), reflecting how much RRI changes in response to spontaneous changes in SBP.
5. Low frequency power of PPGa (LFP_{PPGa}): PPGa spectral power in 0.04–0.15 Hz region, reflecting vascular variability in response to stimuli such as sympathetic nerve inputs.

The spectral powers were computed using the Welch method (Mitra, 2006). These physiological and autonomic parameters, along with subject characteristics, were then used to predict the HUT response phenotypes in SCD and non-SCD subjects using multinomial logistic regression (MLR) analysis. Details of the MLR analysis are described in the Statistical tests section.

Model-Derived Autonomic Indices

To further explore what functional mechanisms might account for the differences in baseline autonomic characteristics among HUT response phenotypes, we employed an input-output modeling approach to capture the functional dependencies among the various key physiological variables (Khoo, 2018). The mathematical model allows us to disentangle the effect of each model input, e.g., blood pressure and respiration, on the model output, e.g., heart rate and vascular responses. An important

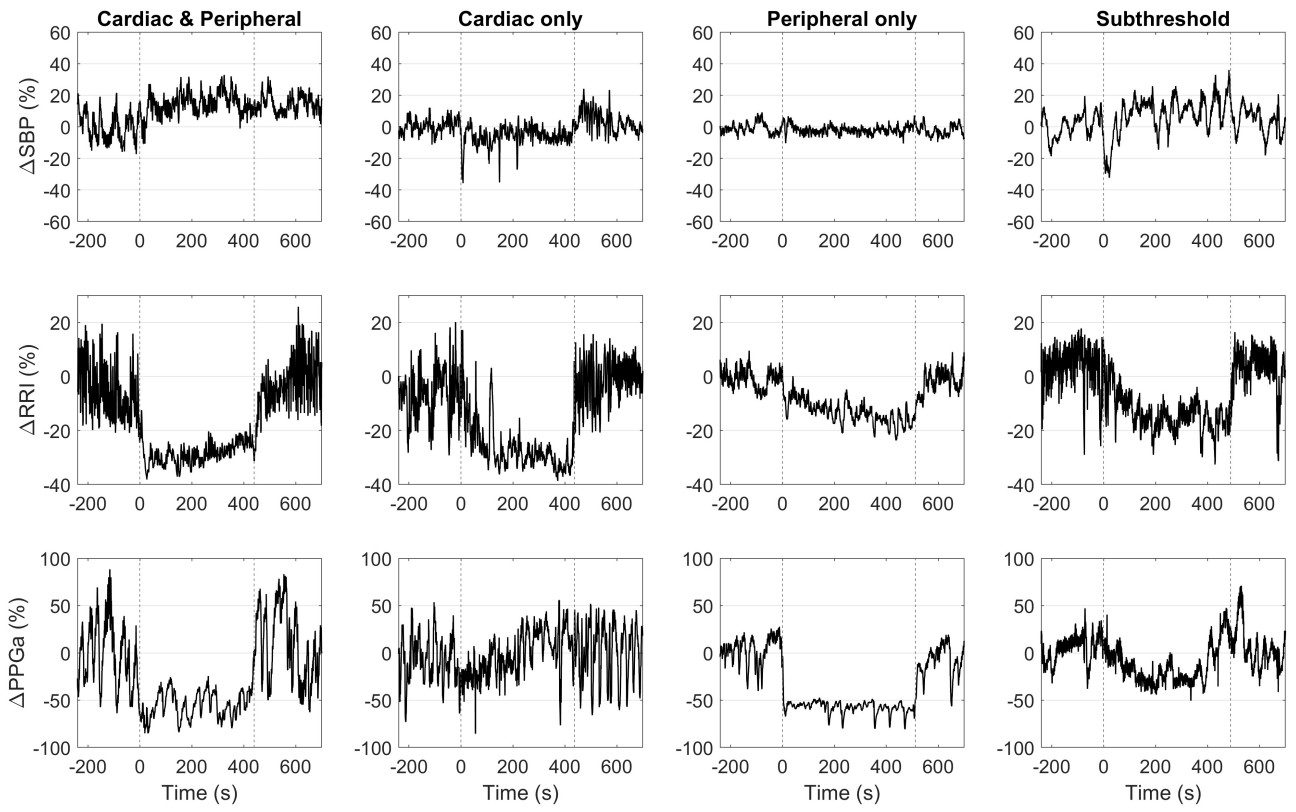

FIGURE 4 | Representative data of four subjects with different HUT response phenotypes. Vertical dashed lines mark the onset and the end of HUT.

feature of this approach is that the model can have multiple inputs but the dynamics between each input and the output have to be "causal" – i.e., changes in the output at the present time can only be ascribed to changes in one or more of the inputs that occurred in the past. Based on our understanding of the underlying physiology, we assumed that fluctuations in RRI (δRRI) are derived from two main mechanisms: the arterial baroreflex (ABR), relating changes in SBP (δSBP) to δRRI, and respiratory-cardiac coupling (RCC). RCC could represent a broad variety of physiological mechanisms through which respiration can affect heart rate. These include central respiratory entrainment of cardiovagal traffic from the medulla, vagal feedback from the pulmonary stretch receptors, mechanical stretching of the sinoatrial node, and contributions from the cardiopulmonary reflexes due to respiratory changes in venous return (Lucini et al., 2000; Belozeroff et al., 2003). The mathematical representation of the model of heart rate variability is

$$\delta RRI(t) = \sum_{i=0}^{M-1} h_{\mathrm{ABR}}(i) \cdot \delta SBP(t - i - T_{\mathrm{ABR}}) + \sum_{i=0}^{M-1} h_{\mathrm{RCC}}(i) \cdot \delta ILV(t - i - T_{\mathrm{RCC}}) + \varepsilon_{\mathrm{RRI}}(t) \quad (2)$$

In similar fashion, peripheral vascular variability was assumed to be derived from two main mechanisms: blood pressure-peripheral vascular coupling (BPC) and the respiratory-peripheral vascular coupling (RPC) (Chalacheva and Khoo, 2014; Khoo and Chalacheva, 2016). BPC relates the fluctuations in mean arterial blood pressure (δMAP) to fluctuations in PPGa (δPPG_{a}) through sympathetically mediated baroreflex control of peripheral resistance (Guyenet, 2006) and through local regulation of blood flow (Davis and Hill, 1999; Secomb, 2008). RPC relates changes in respiration (δILV) to PPGa fluctuations through respiratory modulation of sympathetic neural activity, which in turn affects peripheral vascular resistance (Seals et al., 1993; Malpas et al., 2001). The mathematical representation for peripheral vascular variability is:

$$\delta PPGa(t) = \sum_{i=0}^{M-1} h_{\mathrm{BPC}}(i) \cdot \delta MAP(t - i - T_{\mathrm{BPC}}) + \sum_{i=0}^{M-1} h_{\mathrm{RPC}}(i) \cdot \delta ILV(t - i - T_{\mathrm{RPC}}) + \varepsilon_{\mathrm{PPGa}}(t) \quad (3)$$

Equations (2) and (3) describe how δRRI and $\delta PPGa$ at the current time, represented by sample index t, are influenced by the cumulative effects of past (up to M + latency T) values of δSBP, δMAP, and δILV. h_{ABR}, h_{RCC}, h_{BPC}, and h_{RPC} represent the "standardized" RRI or PPGa responses to unit pulse increases in the corresponding inputs. These are also known as the "impulse responses" (Khoo, 2018). M denotes the system memory or the time (number of samples) it takes for an impulse response to decay to zero. $\varepsilon_{\mathrm{RRI}}$ and $\varepsilon_{\mathrm{PPGa}}$ represent the model residuals, the extraneous influences on RRI or PPGa fluctuations that are not accounted for by the models. T_{ABR}, T_{RCC}, T_{BPC}, T_{RPC} denote the latencies (in number of samples) associated with the corresponding functional mechanisms.

The above mathematical models were applied to data collected from all SCD subjects during the baseline period to quantify the underlying autonomic characteristics for each of the subjects. The impulse responses were estimated using the basis function expansion technique (Khoo and Chalacheva, 2016), where the impulse response was represented as a weighted sum of a set of basis functions as follows

$$h_{\mathrm{x}}(t) = \sum_{i=1}^{q_{\mathrm{x}}} c_{\mathrm{x}}(i) B_i^{(n_{\mathrm{x}})}(t) \quad (4)$$

h_{x} represents the impulse response relating input x to the output. In this case, x represents δSBP, δMAP, or δILV. q_{x} is the number of basis functions used in the expansion of an impulse response. $B_i^{(n)}(t)$ represents the orthonormal sets of Meixner functions with nth order of (Asyali and Juusola, 2005). c_{x} represents each of the expansion coefficients of the basis functions for the impulse response. Further details of the procedures for solving Equations (2), (3), and (4) to estimate the impulse responses may be found in Belozeroff et al. (2003) and Khoo (2018).

Once the impulse responses of these mechanisms were obtained, the transfer functions were determined by taking the Fourier transforms of the estimated impulse responses. The average transfer function magnitudes in the high-frequency (0.15–0.4 Hz) region, $\mathrm{ABR_{HF}}$ and $\mathrm{RCC_{HF}}$, were calculated and taken to represent the gains through which SBP fluctuations and respiration, respectively, contribute to parasympathetic modulation of RRI (i.e., $\mathrm{HFP_{RRI}}$). Similarly, the average transfer function magnitudes in the low-frequency (0.04–0.15 Hz) region, $\mathrm{BPC_{LF}}$ and $\mathrm{RPC_{LF}}$, were computed and taken to represent the gains with which SBP fluctuations and respiration, respectively, contribute to sympathetic modulation of fluctuations in PPGa. Previous studies by us (Belozeroff et al., 2003) and others (Lucini et al., 2000) have shown that $\mathrm{ABR_{HF}}$ correlates well with the more broadly used measure of BRS derived from the sequence technique. However, an important difference between the model-based method and sequence technique for assessing baroreflex gain is that estimates of $\mathrm{ABR_{HF}}$ are obtained after computationally adjusting for the direct influence of respiration [see Equation (2) above].

Statistical Tests

Student's t-test (or Wilcoxon test if data were not normally distributed) was used to test for differences in subject characteristics between SCD and non-SCD subjects. Paired t-test was used to compare the SBP values to determine if these subjects could restore their blood pressure level during HUT.

The relation among subject characteristics, baseline autonomic indices and the HUT response phenotypes were examined in two stages by multinomial logistic regression (MLR) analysis (Domínguez-Almendros et al., 2011). Candidate variables for the MLR were included if $p < 0.20$ in the univariate analysis. Log-transformation was applied to highly skewed variables to satisfy assumptions of logistic regression.

TABLE 2 | Baseline physiological and autonomic indices.

	Non-SCD	SCD	*P*-value
RRI (ms)	906 (22)	875 (28)	0.37
SBP (mmHg)	117 (1.8)	113 (2.2)	0.20
DBP (mmHg)	68.5 (1.5)	66.0 (1.3)	0.23
PPGa (nu)	66.4 (3.0)	66.0 (3.7)	0.93
$HFP_{RRI,n}$* (nu/Hz)	0.00187 (0.0020)	0.00178 (0.0028)	0.81
LHR_{RRI}* (unitless)	0.40 (0.34)	0.48 (0.80)	0.12
LFP_{SBP}* ($mmHg^2$/Hz)	6.83 (7.48)	4.89 (6.23)	0.22
BRS* (ms/mmHg)	17.2 (11.4)	15.0 (12.9)	0.32
LFP_{PPGa}* (nu)	35.7 (47.9)	54.1 (47.8)	0.27

*Normally distributed data are shown as mean (standard error of mean) with p-value from t-test. Non-normally distributed data, indicated by *, are shown as median (interquartile range) with p-values from Wilcoxon test. RRI, R-R interval; SBP, systolic blood pressure; DBP, diastolic blood pressure; PPGa, photoplethysmogram amplitude; $HFP_{RRI,n}$, normalized high-frequency power of RRI; LHR_{RRI}, low-to-high ratio of RRI; LFP_{SBP}, low-frequency power of SBP; BRS, baroreflex sensitivity; LFP_{PPGa}, low-frequency power of PPGa.*

The selected candidate variables were entered in a stepwise regression. If the candidate variables were correlated with each other (e.g., hemoglobin, plasma free hemoglobin and free heme), the variable were added to the model one at a time to avoid multicollinearity. Finally, a set of significant predictors constituted the final MLR model. For all MLR analyses, we let the CP phenotype be the reference category for the HUT response phenotypes. Using the final MLR model, we also calculated the predicted probability of falling into different HUT response phenotypes as each covariate varied at different levels: low (10th percentile), moderate (median) and high (90th percentile), to investigate the effect of each covariate while controlling for other factors, i.e., holding other parameters at their median values.

Analysis of variance (ANOVA) was used to test the model-derived autonomic indices of SCD subjects for differences among HUT response phenotypes. If the variables were not normally distributed, the variables were log-transformed to satisfy the ANOVA assumption (Shapiro–Wilk normality test, assuming normality if $p > 0.05$). Dunnett's test was applied *post hoc* if ANOVA detects significant difference among phenotypes with the CP-phenotype being the control group.

For all statistical tests, the statistical significance was defined as $p < 0.05$. All statistical analyses were performed using JMP statistical software, version 13.0 (SAS Institute Inc., Cary, NC, United States).

RESULTS

Subject Characteristics

Tables 1, **2** summarize subject characteristics and baseline physiological and autonomic indices. There was no difference in age, sex, body mass index (BMI), mean baseline RRI, SBP, DBP, PPGa or any autonomic indices between SCD and non-SCD subjects. However, SCD subjects had lower hemoglobin, hematocrit and SpO_2, and higher reticulocyte count, plasma free hemoglobin and free heme than non-SCD subjects.

HUT Responses

In most patients there was an initial drop in SBP at the onset of tilt; there was no significant difference ($p = 0.1961$) between pre-HUT SBP (119 mmHg) and during HUT SBP (117 mmHg), suggesting that most subjects were able to restore their blood pressure during HUT. However, there were 5 subjects with >20% drop in SBP during HUT from their pre-HUT SBP: 3 from the CP group, 1 from the P group and 1 from the ST group. None of the subjects showed or reported any signs of syncope.

The scatter plot of ΔRRI (cardiac response to HUT) vs. ΔPPGa (peripheral vascular response to HUT) is shown in **Figure 3**. The spontaneous fluctuations in RRI and PPGa during supine were 7.9 and 29.8%, respectively (dashed lines, denoted as SD_{null}). The optimal thresholds that best separate subjects into four HUT phenotypes were 17 and 44% for RRI and PPGa, respectively (solid lines). **Table 3** tabulates the number of SCD and non-SCD subjects in different HUT groups. Most subjects were classified as having dual cardiac and peripheral vascular responses to HUT; however, subjects with only peripheral vasoconstriction response were primarily patients with SCD (likelihood ratio $\chi^2 = 22.4$, $p < 0.0001$).

Effects of Baseline Characteristics on HUT Responses

Univariate associations predicting the response to HUT were examined and the potential candidates for stepwise regression analysis were: diagnosis, age, sex, SpO_2, hemoglobin, hematocrit, reticulocyte, free heme, baseline DBP, PPGa, $HFP_{RRI,n}$, LFP_{SBP}, BRS and LFP_{PPGa} (**Table 4**). Stepwise regression analysis selected the following as the covariates in the final MLR model of HUT response phenotypes: diagnosis, hemoglobin, baseline $HFP_{RRI,n}$ and baseline LFP_{PPGa} ($p < 0.0001$, $\chi^2 = 61.96$, DF = 12, $R^2 = 0.43$). These variables predict 43% of the variance with a

TABLE 3 | SCD and non-SCD subjects by HUT response classification: count (row %).

		HUT phenotype			
	CP	C	P	ST	Total
SCD	8 (29.6)	6 (22.2)	10 (37.0)	3 (11.1)	27
Non-SCD	32 (82.1)	4 (10.3)	1 (2.6)	2 (5.1)	39
Total	40	10	11	5	66

The contingency table shows the number of SCD and non-SCD subjects in different HUT phenotypes (likelihood ratio $\chi^2 = 22.4$, $p < 0.0001$). CP, having both cardiac and peripheral responses; C, having only cardiac response; P, having only peripheral response; ST, having subthreshold cardiac and peripheral response.

TABLE 4 | Univariate analysis for HUT response groups.

Parameters	*P*-value
Diagnosis	**<0.0001**
Age	**0.1674**
Sex	**0.1725**
Height	0.26
Weight	0.37
BMI	0.21
SpO_2	**0.0034**
Hemoglobin	**0.0004**
Hematocrit	**0.0002**
Reticulocyte*	**0.0328**
Plasma hemoglobin*	0.21
Free heme*	**0.0569**
Hemopexin*	0.93
Baseline RRI	0.23
Baseline SBP	0.24
Baseline DBP	**0.0416**
Baseline PPGa	**0.0077**
Baseline $HFP_{RRI,n}$*	**0.0002**
Baseline LHR_{RRI}*	0.35
Baseline LFP_{SBP}*	**0.1669**
Baseline BRS	**0.0226**
Baseline LFP_{PPGa}*	**0.1883**

*P-value column shows the significance of each parameter in estimating HUT phenotypes. Bolded parameters are parameters that will enter the stepwise regression analysis ($p < 0.20$) for selection of the covariate set of the final multinomial regression model. *indicates log-transformed data. SpO_2, oxygen saturation; RRI, R–R interval; SBP, systolic blood pressure; DBP, diastolic blood pressure; PPGa, photoplethysmogram amplitude; $HFP_{RRI,n}$, normalized high-frequency power of RRI; LHR_{RRI}, low-to-high ratio of RRI; LFP_{SBP}, low-frequency power of SBP; BRS, baroreflex sensitivity; LFP_{PPGa}, low-frequency power of PPGa.*

TABLE 5 | Parameter estimates of the final multinomial logistic regression of HUT phenotypes.

Parameter	HUT phenotypes	Estimate	*SE*	*P*-value
Intercept	C	23.18	7.99	0.0037
Intercept	P	−7.56	6.30	0.23
Intercept	ST	13.03	7.92	0.10
Diagnosis				**0.0082**†
Diagnosis [SCD]	C	0.70	1.14	0.54
Diagnosis [SCD]	P	3.50	1.28	**0.0065**
Diagnosis [SCD]	ST	1.21	1.22	0.32
Hemoglobin				**0.0096**†
Hemoglobin	C	−0.69	0.32	**0.0322**
Hemoglobin	P	−0.27	0.26	0.31
Hemoglobin	ST	−0.83	0.37	**0.0242**
Baseline $HFP_{RRI,n}$*				**<0.0001**†
Baseline $HFP_{RRI,n}$*	C	4.17	1.57	**0.0080**
Baseline $HFP_{RRI,n}$*	P	−2.64	1.28	**0.0394**
Baseline $HFP_{RRI,n}$*	ST	0.49	1.61	0.76
Baseline LFP_{PPGa}*				**0.0032**†
Baseline LFP_{PPGa}*	C	−4.59	1.61	**0.0044**
Baseline LFP_{PPGa}*	P	−0.49	1.75	0.78
Baseline LFP_{PPGa}*	ST	−3.89	1.72	**0.0243**

*The global multinomial logistic regression model test was significant ($\chi^2 = 61.96$, $DF = 12$, $p < 0.0001$). *indicates log-transformed data. †indicates p-value of the overall effect test (the change in fit resulting from discarding one of the covariates). P-value column shows the significance of each parameter estimate, with CP group being the reference HUT phenotype. Bolded p-values indicate statistical significance ($p < 0.05$). CP, having both cardiac and peripheral responses; C, having only cardiac response; P, having only peripheral response; ST, having subthreshold cardiac and peripheral response; $HFP_{RRI,n}$, normalized high-frequency power of RRI; LFP_{PPGa}, low-frequency power of photoplethysmogram amplitude.*

misclassification rate of 22% suggesting that this model predicts the HUT response phenotypes with 78% accuracy.

The parameter estimates of the MLR analysis of HUT responses and their corresponding *p*-values are listed in **Table 5**. We found that SCD subjects were 33 times more likely to have only peripheral vasoconstriction in response to HUT than non-SCD subjects, after controlling for hemoglobin, baseline $HFP_{RRI,n}$ and LFP_{PPGa}. **Figure 5** summarizes the effect of the independent predictors of HUT response phenotype. The middle pair of bars in **Figures 5A–C** are the same, and show that the probability of SCD subjects having only peripheral vasoconstriction as a primary mechanism for SBP recovery during HUT (P category) is 29% when hemoglobin, $HFP_{RRI,n}$ and LFP_{PPGa} are all at their respective median levels. When hemoglobin alone is decreased to the 10th percentile (**Figure 5A**), the probability of having dual response to HUT (CP) is reduced to 27% in SCD and to 64% in non-SCD. In contrast, when the hemoglobin level is at the 90th percentile, almost all SCD and non-SCD subjects have dual response. When $HFP_{RRI,n}$ by itself is lowered to the 10th percentile (**Figure 5B**), indicating decreased baseline parasympathetic activity, the probability of having dual response is reduced to 23% in SCD while the probability of having only peripheral vasoconstriction response (P) increases to 76%. In contrast, when $HFP_{RRI,n}$ is at the 90th percentile, the probability of having only tachycardic response to HUT (C) increases to 29% in SCD and the probability of having only peripheral vasoconstriction (P) is reduced to 5%. When LFP_{PPGa}, reflecting vascular variability at baseline, is at the 10th percentile (**Figure 5C**), the probability of having subthreshold response (ST) is significantly increased for both SCD and non-SCD with little effect on the probability of having peripheral vasoconstriction only (P). However, when the vascular variability is at the 90th percentile, most subjects have normal dual response to HUT regardless of diagnosis.

Baseline Characteristics of SCD Subjects With P Phenotype

Although the SCD subjects we studied displayed all 4 HUT phenotypes, the P phenotype consisted overwhelmingly of SCD subjects (**Figure 3**). So what baseline characteristics distinguished the P-phenotype SCD subjects from the other SCD subjects? Based on the MLR analysis, the probability of having the P phenotype in SCD subjects substantially increased if those subjects were to have low baseline parasympathetic activity (**Figure 5B**). $HFP_{RRI,n}$ was indeed lower in SCD subjects with the P phenotype compared SCD subjects with normal (CP) response ($p = 0.0144$). We used mathematical modeling

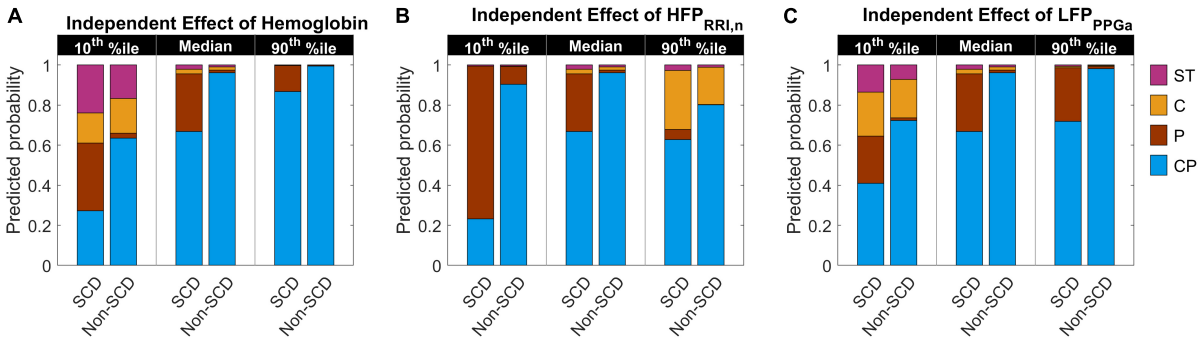

FIGURE 5 | Predicted probability of having certain HUT response phenotype as hemoglobin level, $HFP_{RRI,n}$ and LFP_{PPGa} independently vary from low (10th percentile) to high (90th percentile) level. The middle pair of bars in each subfigure are the same and show the probability when hemoglobin **(A)**, $HFP_{RRI,n}$ **(B)**, and LFP_{PPGa} **(C)** are all at their respective median levels. CP, having dual cardiac and peripheral response; P, having only peripheral response; C, having only cardiac response; and ST, having subthreshold cardiac and peripheral responses to HUT. The height of each colored column in each stacked bar represents the probability of having the corresponding phenotypic response to HUT.

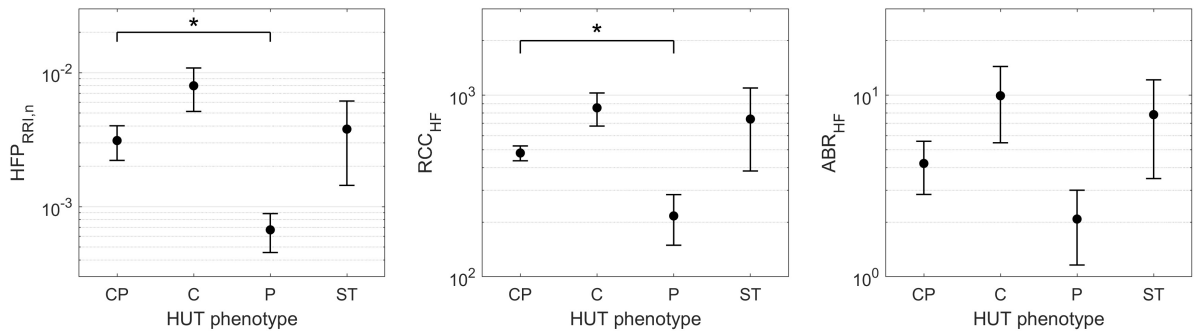

FIGURE 6 | $HFP_{RRI,n}$ and model-derived cardiac autonomic indices of SCD subjects across HUT phenotypes (mean ± SEM). *indicates significant pairwise difference from the CP phenotype. SCD subjects with the P phenotype had significantly lower baseline parasympathetic activity ($HFP_{RRI,n}$, **left**) than those with typical HUT response (CP phenotype). The mathematical modeling analysis revealed that the low parasympathetic activity in SCD subjects with the P phenotype was due to impaired respiratory-cardiac coupling (RCC_{HF}, **middle**). The arterial baroreflex gain (ABR_{HF}, **right**) followed similar trend to $HFP_{RRI,n}$ across phenotypes but the difference did not reach statistical significance.

TABLE 6 | Model-derived autonomic indices in SCD subjects by HUT phenotype.

	CP	C	P	ST	*P*-value
RCC_{HF} (ms/L)	487 (224)	698 (744)	148 (156)*	451 (1132)	**0.0010**
ABR_{HF} (ms/mmHg)	3.9 (5.7)	6.2 (17.3)	1.7 (3.6)	3.9 (13.4)	0.14
RPC_{LF} (nu/L)	136 (295)	70 (95)	114 (178)	274 (162)	0.13
BPC_{LF} (nu/mmHg)	4.8 (5.2)	2.9 (0.6)	5.4 (2.2)	2.5 (2.3)	0.08

*Data are shown as median (interquartile range) with p-value from ANOVA. Bolded p-values indicate statistical significance ($p < 0.05$). * indicates significant pairwise difference from the CP phenotype ($p = 0.010$, Dunnett's test). RCC_{HF}, high-frequency respiratory-cardiac coupling gain; ABR_{HF}, high-frequency arterial baroreflex gain; RPC_{LF}, low-frequency respiratory-peripheral vascular coupling gain; BPC_{LF}, low-frequency blood pressure-peripheral vascular coupling gain.*

to delineate which functional mechanisms might account for the low $HFP_{RRI,n}$ in P-phenotype subjects. We found that the P-phenotype SCD subjects had significantly lower high-frequency RCC gain (RCC_{HF}) than those with CP phenotype ($p = 0.010$, **Figure 6**). The high-frequency ABR gain (ABR_{HF}) also followed similar trends to those of $HFP_{RRI,n}$ but this parameter was not significantly different from CP phenotype (**Table 6**). As a consistency check, we found that the BRS across SCD phenotypes agreed with ABR_{HF} and did not show any significant difference from the CP phenotype.

Another significant autonomic predictor of HUT phenotypes was baseline LFP_{PPGa}, representing vascular variability. The probability of having the C phenotype increased as LFP_{PPGa} became lower (**Figure 5C**). This was, however, the case for both SCD and non-SCD subjects. The SCD subgroup analysis showed that there was no difference in LFP_{PPGa} across HUT phenotypes. Consistent with this finding, model-based analysis of the functional mechanisms governing vascular variability confirmed that low-frequency BPC and RPC gains (BPC_{LF} and RPC_{LF}), were not different across phenotypes (**Table 6**).

DISCUSSION

Autonomic Responses to Head Up Tilt

The HUT test is commonly used to evaluate orthostatic intolerance (Zaqqa and Massumi, 2000; Stewart, 2012) but it has also been employed to assess autonomic function in various disease states (Chandler and Mathias, 2002; Wang et al., 2012). During HUT, the shift in blood volume from the upper to lower parts of the body leads to a transient drop in blood pressure, triggering the arterial and cardiopulmonary reflexes. These reflexes result in parasympathetic withdrawal, thereby increasing heart rate, and increased sympathetic drive, which increases vascular tone and peripheral resistance, along with heart rate and cardiac contractility. In subjects without orthostatic intolerance, the net effect of all these reflex actions is the maintenance of blood pressure at or close to pre-tilt levels. However, the relative changes in vagal control of heart rate and sympathetic control of vascular resistance and tone within and across individuals have not been systematically studied, and particularly so on a quantitative basis.

In this study, we used PPGa as a surrogate measure of peripheral vascular conductance. Implicit in this is the assumption that the changes in PPGa we measured represent primarily changes resulting from peripheral vasoconstriction/dilation. However, a fraction of the changes in PPGa could also have been due to changes in pulse pressure, secondary to changes in stroke volume during HUT. Pulse pressure was indeed reduced during HUT (∼40.7 mmHg) compared to supine (∼47.5 mmHg). However, in terms of percent change from supine levels, the mean decrease in pulse pressure was 13.1%, substantially smaller than the corresponding 56.7% reduction in PPGa, suggesting that stroke volume played a secondary role in contributing to the decrease in PPGa during HUT. Additional analysis of cutaneous blood flow (based on laser Doppler flowmetry) in the same hand showed that the mean percent decrease in microvascular flow from supine to HUT was 30.5%. Since this estimate was based on beat-averaged values of the flow signal and did not take into account the amplitude of the pulsatile component, it represents changes in mean microvascular flow with minimal direct influence from pulse pressure. This decrease in mean cutaneous blood flow provides further support to the notion that the reduction in PPGa during HUT was mainly due to peripheral vasoconstriction rather than changes in stroke volume.

Phenotyping the Responses to HUT

In the current study, we measured the responses of SCD, anemic non-SCD and healthy subjects to HUT, and classified them on the basis of the corresponding relative changes in heart rate and peripheral vascular responses. As mentioned in the Section "Materials and Methods," the responses were divided into four different phenotypes: (1) dual cardiac and peripheral vascular responses (CP), (2) primarily cardiac rate response (C), (3) primarily peripheral vascular response (P) and (4) subthreshold cardiac and peripheral vascular responses (ST). We found that the majority of subjects (∼60%) regardless of diagnosis belonged to the CP phenotype. However, the group with P phenotype consisted predominantly of SCD subjects. This remained true even after adjusting for the effects of anemia. In SCD subjects, low cardiac parasympathetic activity at baseline dramatically increased the probability of having P-phenotype response (**Figure 5B**). This suggests there is a characteristic autonomic dysfunction that is unique to subjects with SCD compared to healthy and anemic controls. Further analysis, using a multivariate dynamic model of heart rate variability, suggests that the low baseline parasympathetic activity in these SCD subjects is more likely to be due to impaired respiratory-cardiac coupling, rather than the decreased cardiac baroreflex sensitivity (**Figure 6**). On the opposite side of the spectrum, the subset of subjects with augmented cardiac parasympathetic activity (elevated $HFP_{RRI,n}$) but low vascular variability (low LFP_{PPGa}) at baseline tended to have C-phenotype response to HUT (increased heart rate without concurrent peripheral vasoconstriction). It is possible that subjects with low baseline vascular variability would have low sympathetic modulation of peripheral resistance but high sympathetic tone, because their vessels are already largely constricted. As such, dynamic modulations of sympathetic input will not have much effect in eliciting further peripheral vasoconstriction, such as during HUT in this subset of subjects.

Abnormal Autonomic Activity and Vasoreactivity in SCD

Imbalance between parasympathetic and sympathetic activity in SCD has been reported in multiple studies (Sangkatumvong et al., 2011; L'Esperance et al., 2013; Chalacheva et al., 2015, 2017; Khaleel et al., 2017). Our research group previously found that SCD subjects had stronger parasympathetic withdrawal to transient hypoxia (Sangkatumvong et al., 2011) and blunted cardiac baroreflex to cold face stimulation (Chalacheva et al., 2015). Others found relative sympathetic dominance in SCD (Mestre et al., 1997; Pearson et al., 2005). Martins et al. (2012) investigated HUT responses in SCD, iron deficiency anemic and healthy subjects and found also that SCD subjects did not have a large increase in heart rate compared to other subject groups, consistent with our results. We also showed previously that SCD subjects had higher frequency of vasoconstriction in response to sigh (Sangkatumvong et al., 2011), a reflex which is sympathetically mediated (Bolton et al., 1936). Similarly, another group reported that SCD subjects had stronger vasoconstriction in response to inspiratory breath hold, also a sympathetically mediated stimulus, compared to controls (L'Esperance et al., 2013). In our recent studies, we found that SCD subjects had stronger vasoreactivity to heat pain compared to controls (Chalacheva et al., 2017; Khaleel et al., 2017). These previous findings all point toward higher tendency to having peripheral vasoconstriction in response to autonomic stimuli in SCD. However, our current study suggests that the peripheral vasoconstriction responses to HUT are not different between SCD and non-SCD subjects. Moreover, further investigation using model-based analysis of baseline peripheral vascular variability found no differences in sympathetic vascular baroreflex gain among the different

autonomic phenotypes in SCD subjects. On the other hand, it should be pointed out that peripheral vascular variability may not be influenced only by sympathetic nerve inputs but also vasoactive substances, such as nitric oxide and endothelin-1 (Kinlay et al., 2001). Thus low nitric oxide bioavailability, a common pathological condition in SCD (Reiter et al., 2002), could have negative impact on vascular variability. Bourque et al. (2011) suggested that nitric oxide tonically inhibits the vasoconstrictive effect of endothelin-1. With imbalance between these two mediators, endothelin-1 actions become dominant when there is low nitric oxide bioavailability, resulting in sustained vasoconstriction.

The key findings that have emerged from this study are that: (a) P-phenotype responses (peripheral vasoconstriction without significant heart rate increase) were found overwhelmingly in SCD subjects, and (b) the SCD subjects with P phenotype had lower baseline cardiac parasympathetic activity than those who displayed typical HUT responses (CP phenotype). The latter finding is consistent with previous reports that SCD subjects tend to have impaired parasympathetic activity. Further investigation using model-based analysis suggests that the low cardiac parasympathetic activity in the P-phenotype SCD subjects was due to impaired respiratory-cardiac coupling rather than decreased baroreflex gain. The physiological mechanisms underlying this finding remain to be elucidated. On the peripheral vascular control side, we could not detect any difference in baseline vascular variability in SCD subjects among HUT phenotypes. The autonomic indices of SCD subjects derived from the peripheral vascular control model also did not show any difference among HUT phenotypes. However, it should be emphasized that the lack of differences in baseline vascular variability across subject groups or phenotypes does not necessarily imply that there were no differences in sympathetic vascular tone (Malpas, 2002).

Role of Anemia

Anemia is another significant predictor of the autonomic response to HUT. The body compensates for anemia by increasing cardiac output in order to maintain oxygen delivery. Chronic anemia leads to chronic dilation of the left ventricle in SCD (Lester et al., 1990; Gladwin and Sachdev, 2012). At the same time, anemic patients tend to have low peripheral resistance (Metivier et al., 2000). These alterations in cardiac output, oxygen delivery and peripheral resistance have direct effects on autonomic control of cardiovascular system. In this study, we found that anemia decreased the probability of having dual cardiac and peripheral vascular responses to HUT (CP phenotype) in both SCD and non-SCD subjects (**Figure 5A**). However, anemia and low vascular variability strongly predicts subthreshold response to HUT (ST phenotype) in SCD patients. Martins et al. (2012) reported that SCD and anemic controls had lower increase in DBP than normal controls during HUT, when hemoglobin level in SCD and anemic controls were comparable. Their finding suggests that anemia lessens the ability to vasoconstrict in response to orthostatic stress, which explains why those subjects could not sufficiently vasoconstrict to increase DBP.

Clinical Implications for SCD

How is all this relevant to SCD? We know that decreased regional blood flow from any cause will increase the likelihood of deoxygenated HbS polymerizing within the microvasculature before they can escape to larger diameter vessels, triggering vaso-occlusion. Thus, we speculate that the P-phenotype subset of SCD subjects with prolonged peripheral vasoconstriction, but without compensatory changes in heart rate, in response to HUT would be more likely to have reduced microvascular blood flow, and thus have the highest risk of VOC. The low baseline levels of parasympathetic activity in these subjects may explain the inability of the heart to respond sufficiently to stimuli that activate the sympathetic nervous system. Under conditions of decreased peripheral vascular flow, the transit time of red blood cells through the capillary beds would be elevated, increasing the probability of rigid sickle red cell entrapment in the microvasculature and subsequent VOC. This could explain why SCD subjects tend to associate stress, cold and pain as factors that trigger VOC. A recent study has shown that hypnosis lessened the vasoconstrictive effect during pain and anticipation to pain (Bhatt et al., 2017), suggesting that interventions that reduce sympathetic drive can potentially alleviate the risk of VOC. It is possible that ST-phenotype SCD subjects may also be at increased risk for VOC because they are already peripherally vasoconstricted and, at the same time, unable to raise cardiac output to increase peripheral blood flow in response to orthostatic stress. But our ability to draw conclusions on the ST-phenotype subjects is severely limited by the small sample size of this category in the present study. Nevertheless, our finding of distinct autonomic phenotypes is consistent with clinical observations that the frequency and severity of pain crises can vary substantially across individuals with SCD (Coates et al., 2018).

One significant limitation of this study is that we included SCD and anemic non-SCD subjects who received regular transfusion therapy. While inclusion of these transfused subjects allows us to investigate a larger range of hemoglobin level and its effect on HUT responses, we could not look at the VOC frequency in SCD subjects as a function of HUT response phenotype. This is because VOC are generally prevented by chronic transfusion therapy. Nonetheless, there was a significantly greater probability of having P phenotype response in SCD than controls, independent of hemoglobin level.

Future Perspectives

While our findings provide insight into which functional mechanisms predispose SCD subjects to having atypical HUT response, further investigations would enable us to pinpoint the cause of autonomic abnormalities in SCD subjects. In particular, it would be important to determine which underlying physiological mechanisms are primarily responsible for the decreased respiratory-cardiac coupling in the P-phenotype SCD subjects. For instance, could this difference be due to impairment of the cardiopulmonary receptors in the atrial wall or abnormality in neural

transmission of respiratory drive to cardiac vagal efferents? As well, measurements that can delineate the separate contributions of sympathetic outflow, cardiac contractility and vasomotion will provide a more comprehensive understanding of the underlying basis of the different autonomic phenotypes.

CONCLUSION

We have shown that SCD subjects are much more likely than non-SCD subjects to have impaired cardiac, but intact peripheral responses to orthostatic stress induced by HUT. These abnormal responses are associated with low baseline cardiac parasympathetic activity, independent of hemoglobin level. The classification of autonomic phenotypes based on HUT response may have potential use for predicting disease severity, guiding and targeting treatments/interventions to alleviate the risk of adverse outcomes in SCD.

ETHICS STATEMENT

All experiments were conducted at Children's Hospital Los Angeles (CHLA). The study protocol was approved by the Committee on Clinical Investigations (institutional review board of CHLA). In accordance with CHLA IRB policies, written informed consent or assent (for subjects < 14 years old) was obtained before participation in the study. In addition, parental consent was obtained if the subject was less than 18 years old.

AUTHOR CONTRIBUTIONS

TC, MK, RK, JW, and JD designed the study protocols. PC, RK, PS, and JS performed the experimental device setup. PC, RK, PS, SV, CD, and JD ran patient studies and collected the data. PC analyzed the data and wrote the manuscript. WT assisted with software used for data pre-processing. PC, MK, TC, JD, JW, PS, RK, SV, and CD interpreted the results. MK, TC, JW, and JD critically reviewed and edited the manuscript. RK, PS, SV, CD, and JS edited the manuscript.

FUNDING

This work was supported by National Institutes of Health grants U01 HL117718 and P41 EB001978.

ACKNOWLEDGMENTS

We thank Maha Khaleel and Justin Abbott for assistance in data collection, and Honglei Liu and Silvie Suriany for analyzing blood samples.

SUPPLEMENTARY MATERIAL

The Supplementary Material for this article can be found online at: https://www.frontiersin.org/articles/10.3389/fphys.2019.00381/full#supplementary-material

REFERENCES

Allen, J. (2007). Photoplethysmography and its application in clinical physiological measurement. *Physiol. Meas.* 28, R1–R39. doi: 10.1088/0967-3334/28/3/R01

Asyali, M. H., and Juusola, M. (2005). Use of meixner functions in estimation of volterra kernels of nonlinear systems with delay. *IEEE Trans. Biomed. Eng.* 52, 229–237. doi: 10.1109/TBME.2004.840187

Babchenko, A., Davidson, E., Ginosar, Y., Kurz, V., Faib, I., Adler, D., et al. (2001). Photoplethysmographic measurement of changes in total and pulsatile tissue blood volume, following sympathetic blockade. *Physiol. Meas.* 22, 389–396. doi: 10.1088/0967-3334/22/2/310

Batzel, J., Baselli, G., Mukkamala, R., and Chon, K. H. (2009). Modelling and disentangling physiological mechanisms: linear and nonlinear identification techniques for analysis of cardiovascular regulation. *Philos. Trans. R. Soc. A Math. Phys. Eng. Sci.* 367, 1377–1391. doi: 10.1098/rsta.2008.0266

Beene, T. K., and Eggers, G. W. (1974). Use of the pulse monitor for determining sympathetic block of the arm. *Anesthesiology* 40, 412–414. doi: 10.1097/00000542-197404000-00023

Belozeroff, V., Berry, R. B., and Khoo, M. C. (2003). Model-based assessment of autonomic control in obstructive sleep apnea syndrome. *Sleep* 26, 65–73. doi: 10.1093/sleep/26.1.65

Berger, R. D., Akselrod, S., Gordon, D., and Cohen, R. J. (1986). An efficient algorithm for spectral analysis of heart rate variability. *IEEE Trans. Biomed. Eng.* 33, 900–904. doi: 10.1109/TBME.1986.325789

Bhatt, R., Martin, S., Evans, S., Lung, K., Coates, T., Zeltzer, L., et al. (2017). The effect of hypnosis on pain and peripheral blood flow in sickle-cell disease: a pilot study. *J. Pain Res.* 10, 1635–1644. doi: 10.2147/JPR.S131859

Bolton, B., Carmichael, E. A., and Sturup, G. (1936). Vaso-constriction following deep inspiration. *J. Physiol.* 86, 83–94. doi: 10.1113/jphysiol.1936.sp003345

Bourque, S. L., Davidge, S. T., and Adams, M. A. (2011). The interaction between endothelin-1 and nitric oxide in the vasculature: new perspectives. *Am. J. Physiol. Integr. Comp. Physiol.* 300, R1288–R1295. doi: 10.1152/ajpregu.00397.2010

Chalacheva, P., Kato, R. M., Sangkatumvong, S., Detterich, J., Bush, A., Wood, J. C., et al. (2015). Autonomic responses to cold face stimulation in sickle cell disease: a time-varying model analysis. *Physiol. Rep.* 3:e12463. doi: 10.14814/phy2.12463

Chalacheva, P., Khaleel, M., Sunwoo, J., Shah, P., Detterich, J. A., Kato, R. M., et al. (2017). Biophysical markers of the peripheral vasoconstriction response to pain in sickle cell disease. *PLoS One* 12:e0178353. doi: 10.1371/journal.pone.0178353

Chalacheva, P., and Khoo, M. C. K. (2014). Estimating the baroreflex and respiratory modulation of peripheral vascular resistance. *Conf. Proc. IEEE Eng. Med. Biol. Soc.* 2014, 2936–2939. doi: 10.1109/EMBC.2014.6944238

Chandler, M. P., and Mathias, C. J. (2002). Haemodynamic responses during head-up tilt and tilt reversal in two groups with chronic autonomic failure: pure autonomic failure and multiple system atrophy. *J. Neurol.* 249, 542–548. doi: 10.1007/s004150200062

Charlot, K., Hierso, R., Lemonne, N., Romana, M., Tressières, B., Lalanne-Mistrih, M.-L., et al. (2017). Changes in autonomic nervous activity during vaso-occlusive crisis in patients with sickle cell anaemia. *Br. J. Haematol.* 177, 484–486. doi: 10.1111/bjh.14064

Coates, T. D., Chalacheva, P., Zeltzer, L., and Khoo, M. C. K. (2018). Autonomic nervous system involvement in sickle cell disease. *Clin. Hemorheol. Microcirc.* 68, 251–262. doi: 10.3233/CH-189011

Davis, M. J., and Hill, M. A. (1999). Signaling mechanisms underlying the vascular myogenic response. *Physiol. Rev.* 79, 387–423. doi: 10.1152/physrev.1999.79.2.387

Domínguez-Almendros, S., Benítez-Parejo, N., and Gonzalez-Ramirez, A. R. (2011). Logistic regression models. *Allergol. Immunopathol.* 39, 295–305. doi: 10.1016/j.aller.2011.05.002

Eaton, W. A., Hofrichter, J., and Ross, P. D. (1976). Editorial: delay time of gelation: a possible determinant of clinical severity in sickle cell disease. *Blood* 47, 621–627.

Elgendi, M. (2012). On the analysis of fingertip photoplethysmogram signals. *Curr. Cardiol. Rev.* 8, 14–25. doi: 10.2174/157340312801215782

Everitt, B. S., Landau, S., Leese, M., and Stahl, D. (2011). *Cluster Analysis*, 5th Edn. Chichester: Wiley. doi: 10.1002/9780470977811

Gladwin, M. T., and Sachdev, V. (2012). Cardiovascular abnormalities in sickle cell disease. *J. Am. Coll. Cardiol.* 59, 1123–1133. doi: 10.1016/j.jacC.2011.10.900

Guyenet, P. G. (2006). The sympathetic control of blood pressure. *Nat. Rev. Neurosci.* 7, 335–346. doi: 10.1038/nrn1902

James, T. N., Riddick, L., and Massing, G. K. (1994). Sickle cells and sudden death: morphologic abnormalities of the cardiac conduction system. *J. Lab. Clin. Med.* 124, 507–520.

Khaleel, M., Puliyel, M., Shah, P., Sunwoo, J., Kato, R. M., Chalacheva, P., et al. (2017). Individuals with sickle cell disease have a significantly greater vasoconstriction response to thermal pain than controls and have significant vasoconstriction in response to anticipation of pain. *Am. J. Hematol.* 92, 1137–1145. doi: 10.1002/ajh.24858

Khoo, M. C. K. (2018). *Physiological Control Systems: Analysis, Simulation, and Estimation*, 2nd Edn. Hoboken, NJ: John Wiley and Sons, Inc. doi: 10.1002/9781119058786

Khoo, M. C. K., and Chalacheva, P. (2016). Model-derived markers of autonomic cardiovascular dysfunction in sleep-disordered breathing. *Sleep Med. Clin.* 11, 489–501. doi: 10.1016/j.jsmc.2016.07.003

Kim, J. M., Arakawa, K., and VonLintel, T. (1975). Use of the pulse-wave monitor as a measurement of diagnostic sympathetic block and of surgical sympathectomy. *Anesth. Analg.* 54, 289–296. doi: 10.1213/00000539-197505000-00005

Kinlay, S., Creager, M. A., Fukumoto, M., Hikita, H., Fang, J. C., Selwyn, A. P., et al. (2001). Endothelium-derived nitric oxide regulates arterial elasticity in human arteries in vivo. *Hypertension* 38, 1049–1053. doi: 10.1161/hy1101.095329

Kleiger, R. E., Miller, J. P., Bigger, J. T., and Moss, A. J. (1987). Decreased heart rate variability and its association with increased mortality after acute myocardial infarction. *Am. J. Cardiol.* 59, 256–262. doi: 10.1016/0002-9149(87)90795-8

L'Esperance, V. S., Cox, S. E., Simpson, D., Gill, C., Makani, J., Soka, D., et al. (2013). Peripheral vascular response to inspiratory breath hold in paediatric homozygous sickle cell disease. *Exp. Physiol.* 98, 49–56. doi: 10.1113/expphysiol.2011.064055

Lester, L. A., Sodt, P. C., Hutcheon, N., and Arcilla, R. A. (1990). Cardiac abnormalities in children with sickle cell anemia. *Chest* 98, 1169–1174. doi: 10.1378/CHEST.98.5.1169

Lucini, D., Porta, A., Milani, O., Baselli, G., and Pagani, M. (2000). Assessment of arterial and cardiopulmonary baroreflex gains from simultaneous recordings of spontaneous cardiovascular and respiratory variability. *J. Hypertens.* 18, 281–286. doi: 10.1097/00004872-200018030-00007

Malpas, S. C. (2002). Neural influences on cardiovascular variability: possibilities and pitfalls. *Am. J. Physiol. Heart Circ. Physiol.* 282, H6–H20. doi: 10.1152/ajpheart.2002.282.1.H6

Malpas, S. C., Leonard, B. L., Guild, S. J., Ringwood, J. V., Navakatikyan, M., Austin, P. C., et al. (2001). The sympathetic nervous system's role in regulating blood pressure variability. *IEEE Eng. Med. Biol. Mag.* 20, 17–24. doi: 10.1109/51.917720

Martins, W. D. A., Lopes, H. F., Consolim-Colombo, F. M., Gualandro, S. D. F. M., Arteaga-Fernández, E., and Mady, C. (2012). Cardiovascular autonomic dysfunction in sickle cell anemia. *Auton. Neurosci.* 166, 54–59. doi: 10.1016/j.autneu.2011.07.011

Mestre, J. C. R., Hernández, A., Agramonte, O., and Hernández, P. (1997). Cardiovascular autonomic dysfunction in sickle cell anemia: a possible risk factor for sudden death? *Clin. Auton. Res.* 7, 121–125. doi: 10.1007/BF02308838

Metivier, F., Marchais, S. J., Guerin, A. P., Pannier, B., and London, G. M. (2000). Pathophysiology of anaemia: focus on the heart and blood vessels. *Nephrol. Dial. Transplant.* 15(Suppl. 3), 14–18. doi: 10.1093/oxfordjournals.ndt.a027970

Mitra, S. K. (2006). *Digital Signal Processing: a Computer Based Approach*, 3rd Edn. Boston, MA: McGraw-Hill.

Nebor, D., Bowers, A., Hardy-Dessources, M.-D., Knight-Madden, J., Romana, M., Reid, H., et al. (2011). Frequency of pain crises in sickle cell anemia and its relationship with the sympatho-vagal balance, blood viscosity and inflammation. *Haematologica* 96, 1589–1594. doi: 10.3324/haematol.2011.047365

ESC/NASPE Task Force (1996). Heart rate variability: standards of measurement, physiological interpretation and clinical use. Task force of the european society of cardiology and the North American society of pacing and electrophysiology. *Eur. Heart J.* 17, 1043–1065.

Pagani, M., Lucini, D., Rimoldi, O., Furlan, R., Piazza, S., Porta, A., et al. (1996). Low and high frequency components of blood pressure variability. *Ann. N. Y. Acad. Sci.* 783, 10–23. doi: 10.1111/j.1749-6632.1996.tb26704.x

Parati, G., Di Rienzo, M., and Mancia, G. (2000). How to measure baroreflex sensitivity: from the cardiovascular laboratory to daily life. *J. Hypertens.* 18, 7–19. doi: 10.1097/00004872-200018010-00003

Parati, G., Saul, J. P., Di Rienzo, M., and Mancia, G. (1995). Spectral analysis of blood pressure and heart rate variability in evaluating cardiovascular regulation. A critical appraisal. *Hypertension* 25, 1276–1286. doi: 10.1161/01.HYP.25.6.1276

Pearson, S. R., Alkon, A., Treadwell, M., Wolff, B., Quirolo, K., and Boyce, W. T. (2005). Autonomic reactivity and clinical severity in children with sickle cell disease. *Clin. Auton. Res.* 15, 400–407. doi: 10.1007/s10286-005-0300-9

Rees, D. C., Williams, T. N., and Gladwin, M. T. (2010). Sickle-cell disease. *Lancet* 376, 2018–2031. doi: 10.1016/S0140-6736(10)61029-X

Reiter, C. D., Wang, X., Tanus-Santos, J. E., Hogg, N., Cannon, R. O. III, Schechter, A. N., et al. (2002). Cell-free hemoglobin limits nitric oxide bioavailability in sickle-cell disease. *Nat. Med.* 8, 1383–1389. doi: 10.1038/nm799

Sacha, J. (2013). Why should one normalize heart rate variability with respect to average heart rate. *Front. Physiol.* 4:306. doi: 10.3389/fphys.2013.00306

Sangkatumvong, S., Khoo, M. C. K., Kato, R., Detterich, J. A., Bush, A., Keens, T. G., et al. (2011). Peripheral vasoconstriction and abnormal parasympathetic response to sighs and transient hypoxia in sickle cell disease. *Am. J. Respir. Crit. Care Med.* 184, 474–481. doi: 10.1164/rccm.201103-0537OC

Seals, D. R., Suwarno, N. O., Joyner, M. J., Iber, C., Copeland, J. G., and Dempsey, J. A. (1993). Respiratory modulation of muscle sympathetic nerve activity in intact and lung denervated humans. *Circ. Res.* 72, 440–454. doi: 10.1161/01.RES.72.2.440

Secomb, T. W. (2008). Theoretical models for regulation of blood flow. *Microcirculation* 15, 765–775. doi: 10.1080/10739680802350112

Stewart, J. M. (2012). Mechanisms of sympathetic regulation in orthostatic intolerance. *J. Appl. Physiol.* 113, 1659–1668. doi: 10.1152/japplphysiol.00266.2012

Thomas, G. D. (2011). Neural control of the circulation. *Adv. Physiol. Educ.* 35, 28–32. doi: 10.1152/advan.00114.2010

Wang, S., Randall, D. C., Knapp, C. F., Patwardhan, A. R., Nelson, K. R., Karounos, D. G., et al. (2012). Blood pressure regulation in diabetic patients with and without peripheral neuropathy. *Am. J. Physiol. Regul. Integr. Comp. Physiol.* 302, R541–R550. doi: 10.1152/ajpregu.00174.2011

Xiao, X., Mullen, T. J., and Mukkamala, R. (2005). System identification: a multi-signal approach for probing neural cardiovascular regulation. *Physiol. Meas.* 26, R41–R71. doi: 10.1088/0967-3334/26/3/R01

Zaqqa, M., and Massumi, A. (2000). Neurally mediated syncope. *Tex. Heart Inst. J.* 27, 268–272.

Conflict of Interest Statement: The authors declare that the research was conducted in the absence of any commercial or financial relationships that could be construed as a potential conflict of interest.

frontiers in Neuroscience

ORIGINAL RESEARCH
published: 18 April 2019
doi: 10.3389/fnins.2019.00339

Baroreflex Sensitivity Measured by Pulse Photoplethysmography

Jesús Lázaro[1,2,3]*, *Eduardo Gil*[2,3], *Michele Orini*[4], *Pablo Laguna*[2,3] and *Raquel Bailón*[2,3]

[1] Department of Biomedical Engineering, University of Connecticut, Storrs, CT, United States, [2] Biomedical Signal Interpretation and Computational Simulation (BSICoS) Group, Aragón Institute of Engineering Research (I3A), IIS Aragón, University of Zaragoza, Zaragoza, Spain, [3] Centro de Investigación Biomédica en Red en Bioingeniería, Biomateriales y Nanomedicina (CIBER-BBN), Madrid, Spain, [4] Department of Mechanical Engineering, University College London, London, United Kingdom

Novel methods for assessing baroreflex sensitivity (BRS) using only pulse photoplethysmography (PPG) signals are presented. Proposed methods were evaluated with a data set containing electrocardiogram (ECG), blood pressure (BP), and PPG signals from 17 healthy subjects during a tilt table test. The methods are based on a surrogate of α index, which is defined as the power ratio of RR interval variability (RRV) and that of systolic arterial pressure series variability (SAPV). The proposed α index surrogates use pulse-to-pulse interval series variability (PPV) as a surrogate of RRV, and different morphological features of the PPG pulse which have been hypothesized to be related to BP, as series surrogates of SAPV. A time-frequency technique was used to assess BRS, taking into account the non-stationarity of the protocol. This technique identifies two time-varying frequency bands where RRV and SAPV (or their surrogates) are expected to be coupled: the low frequency (LF, inside 0.04–0.15 Hz range), and the high frequency (HF, inside 0.15–0.4 Hz range) bands. Furthermore, time-frequency coherence is used to identify the time intervals when the RRV and SAPV (or their surrogates) are coupled. Conventional α index based on RRV and SAPV was used as Gold Standard. Spearman correlation coefficients between conventional α index and its PPG-based surrogates were computed and the paired Wilcoxon statistical test was applied in order to assess whether the indices can find significant differences ($p < 0.05$) between different stages of the protocol. The highest correlations with the conventional α index were obtained by the α-index-surrogate based on PPV and pulse up-slope (PUS), with 0.74 for LF band, and 0.81 for HF band. Furthermore, this index found significant differences between rest stages and tilt stage in both LF and HF bands according to the paired Wilcoxon test, as the conventional α index also did. These results suggest that BRS changes induced by the tilt test can be assessed with high correlation by only a PPG signal using PPV as RRV surrogate, and PPG morphological features as SAPV surrogates, being PUS the most convenient SAPV surrogate among the studied ones.

Keywords: baroreflex, photoplethysmography, alpha index, autonomic nervous system, blood pressure, cardiovascular assessment

OPEN ACCESS

Edited by:
Alberto Porta,
University of Milan, Italy

Reviewed by:
Roberto Maestri,
IRCCS Scientific Clinical Institutes Maugeri (ICS Maugeri), Italy
Luiz Eduardo Virgilio Silva,
University of São Paulo, Brazil
Mathias Baumert,
University of Adelaide, Australia

***Correspondence:**
Jesús Lázaro
jlazarop@unizar.es

Specialty section:
This article was submitted to Autonomic Neuroscience, a section of the journal Frontiers in Neuroscience

Received: *20 January 2019*
Accepted: *22 March 2019*
Published: *18 April 2019*

Citation:
Lázaro J, Gil E, Orini M, Laguna P and Bailón R (2019) Baroreflex Sensitivity Measured by Pulse Photoplethysmography. Front. Neurosci. 13:339. doi: 10.3389/fnins.2019.00339

1. INTRODUCTION

The baroreflex system plays an important role in regulating short-term fluctuations of arterial blood pressure (BP) (La Rovere et al., 2008; Robertson et al., 2012). Arterial baroreceptors (placed in the wall of the carotid sinuses and aortic arch) sense changes in BP and modulate efferent autonomic neural activity to the central nervous system accordingly. A rise in sensed BP leads to an increase of vagal neurons discharge and a decrease in the discharge of sympathetic neurons, resulting in decreased heart rate (HR), cardiac contractility and peripheral vascular resistance. On the contrary, decreased BP enhances sympathetic and inhibits vagal activity, leading to increased HR, cardiac contractility and peripheral vascular resistance.

Cardiovascular diseases are frequently associated to an impairment of baroreflex mechanisms, resulting in chronic adrenergic activation. Reduced baroreflex control of HR has been reported in coronary artery disease, heart failure, hypertension and myocardial infarction (La Rovere et al., 2008; Pinna et al., 2017). Assessment of baroreflex in humans is usually approached measuring the changes in HR in response to changes in BP, the so-called baroreflex sensitivity (BRS). Alternatively, spontaneous beat-to-beat fluctuations of systolic arterial pressure and RR interval can be analyzed, allowing BRS assessment during daily-life. A wide spectrum of techniques has been used for spontaneous beat-to-beat BRS assessment. Traditional approaches, such as the sequence technique and those based on the spectral analysis of systolic arterial pressure and RR interval series (α index), were reviewed in La Rovere et al. (2008).

In order to deal with the nonstationary nature of cardiovascular variability, methods based on wavelet transform (Nowak et al., 2008; Keissar et al., 2010) and quadratic time-frequency representations (Orini et al., 2011) have been proposed. In Orini et al. (2012) a framework for nonstationary BRS assessment, based on a time-frequency distribution, was presented, taking into account the strength and prevalent direction of local coupling between RR variability (RRV) and systolic arterial pressure variability (SAPV) series. Alternatively, in Chen et al. (2011) dynamic assessment of BRS is accomplished based on a closed loop model within a point process framework. A critical review of clinical studies using spontaneous BRS was reported in Pinna et al. (2017). Despite some limitations, such as the lack of standards and the poor measurability in some patient populations, published studies support spontaneous BRS as a powerful tool for prognostic prediction in diseases such as hypertension, myocardial infarction, chronic heart failure and diabetes (La Rovere et al., 2008; Di Rienzo et al., 2009; de Moura-Tonello et al., 2016).

Abbreviations: BP, Blood pressure; BRS, Baroreflex sensitivity; ECG, Electrocardiograml; HF, High frequency; HR, Heart rate; HRV, Heart rate variability; LF, Low frequency; PA, Pulse amplitude; PAT, Pulse arrival time; PATV, Pulse arrival time variability; PDA, Pulse decomposition analysis; PEP, Pre-ejection period; PPG, Pulse photoplethysmography; PPV, Pulse-to-pulse variability; PSTT, Pulse slope transit time; PTT, Pulse transit time; PUS, Pulse up-slope; PW, Pulse width; RRV, RR interval variability; SAPV, Systolic arterial pressure variability; SD, Standard deviation.

Spontaneous BRS assessment and monitoring during daily life is limited by the requirement of continuous BP recording, which is usually accomplished by the volume-clamp method or tonometry method, neither of them being suitable for ubiquitous monitoring (Mukkamala et al., 2015). This limitation may be overcome by using a surrogate of systolic arterial pressure which does not require the BP recording. Many works have attempted BP estimation based on pulse transit time (PTT), which is the time delay for the pressure wave to travel between two arterial sites. Most of these approaches, reviewed in Mukkamala et al. (2015), are based on models of arterial wall mechanics and wave propagation in the artery. Due to ease of measurement, pulse arrival time (PAT), which is the time delay between the electrocardiogram (ECG) waveform and a distal arterial waveform, has been widely used instead of PTT for BP estimation. PAT is the sum of PTT and the pre-ejection period (PEP), which varies beat-to-beat depending on ventricular and arterial pressures, short-term physiologic control and medication. Although the effect of PEP modulation makes PAT more inconvenient than PTT for BP estimation, half of the studies reviewed in Mukkamala et al. (2015) used PAT as a surrogate of PTT. Some of these methods have been used for BRS assessment. For instance, in Abe et al. (2015) it was proposed to evaluate baroreflex function using the maximum normalized cross-correlation between the LF components of HRV and PAT, derived from ECG and pulse photoplethysmographic (PPG) signals.

In Liu et al. (2011) it was suggested that PAT can track BP variations in HF range, but was inadequate to follow the LF variations. To overcome this limitation (Ding et al., 2016) proposed to estimate BP combining PAT with a new index, the photoplethysmogram intensity ratio (PIR), which can reflect changes in arterial diameter due to arterial vasomotion. In order to avoid PEP influence in BP estimation, PTT has been derived from impedance plethysmography recorded at the wrist and PPG at the finger (Huynh et al., 2018), or from a ballistocardiogram and PPG at the foot (Martin et al., 2016). Alternatively, PTT was estimated from two PPG signals recorded at ear and toe in Chen et al. (2009) and at forearm and wrist in Wang et al. (2018). Some works have investigated the correlation between PAT and PTT estimated from PPG signals at finger and forehead at rest (Liu et al., 2015) and during a tilt-test (Lázaro et al., 2016). In Li et al. (2014) different PPG indices were investigated for BP estimation. The time ratio of systole to diastole, time span of PPG cycle, diastolic time duration and area ratio of systole to diastole are at least as good as PTT for BP estimation, and can be derived from just one PPG signal.

The PPG signal can be acquired with a sensor placed in many places of the body. Furthermore, its recording is very simple, economical, and comfortable for the subject. Thus, PPG signal is a very interesting signal for ambulatory scenarios and wearable devices, and assessing BRS from PPG signal may have significant impact in such applications. Moreover, several studies have compared pulse rate variability (PRV), derived from the PPG to HRV derived from the ECG, reporting good agreement even in non-stationary situations and during abrupt autonomic nervous system changes (Gil et al., 2010; Wong et al., 2012;

Posada-Quintero et al., 2013; Schfer and Vagedes, 2013). In this work we investigate the feasibility of assessing BRS solely from one PPG signal. The proposed approach is based on using PPG-based surrogates of RRV and SAPV series. On one hand, pulse-to-pulse variability (PPV) series was used as surrogate of RRV series. On the other hand, different PPG morphological features which are hypothesized to be related to the BP were used for generating series that were used as surrogates of SAPV. The ability of the proposed methods to capture changes in autonomic nervous system control was evaluated in a tilt-test database.

2. MATERIALS AND METHODS

2.1. Data and Preprocessing

A data set containing ECG, BP, and PPG recordings from 17 healthy subjects (11 men), aged 28.5 ± 2.5 years, during a tilt table test was used for method evaluation. The protocol started with 4 min in supine position (Rest1), followed with 5 min in 70°-tilt-up position (Tilt), and ended with 4 min back to supine position (Rest2). The table took 18 s for automatic transitions between stages.

ECG lead V4 was recorded by Biopac ECG100C with a sampling rate of 1,000 Hz, BP signal ($x_{\mathrm{BP}}(n)$) was recorded by Finometer system with a sampling rate of 250 Hz, and PPG signal was recorded from the index finger by BIOPAC OXY100C with a sampling rate of $F_s = 250$ Hz. A low-pass filter with a cut-off frequency of 35 Hz was applied to the PPG in order to attenuate noise. This preprocessed PPG signal is denoted $x_{\mathrm{PPG}}(n)$ in this paper. Several points were measured over the PPG pulses. Some of them were measured directly over the pulse as those described in section 2.1.1, and others over the waves extracted from the pulse by the pulse decomposition analysis (PDA) technique described in section 2.1.2.

2.1.1. Pulse Delineation

Several points of the ith PPG pulse were detected in order to take different morphological measurements. All these points are illustrated in **Figure 1**. First, PPG pulses were detected by an algorithm based on a low-pass derivative and a time-varying threshold (Lázaro et al., 2014). This algorithm detects the maximum up-slope point (n_{U_i}), and later it is used for detecting the pulse apex point (n_{A_i}) and the pulse basal point (n_{B_i}) as:

$$n_{\mathrm{A}_i} = \arg\max_n \left\{x_{\mathrm{PPG}}(n)\right\}, \qquad n \in \left[n_{\mathrm{U}_i}, n_{\mathrm{U}_i} + 0.3F_s\right] \quad (1)$$

$$n_{\mathrm{B}_i} = \arg\min_n \left\{x_{\mathrm{PPG}}(n)\right\}, \qquad n \in \left[n_{\mathrm{U}_i} - 0.3F_s, n_{\mathrm{U}_i}\right]. \quad (2)$$

Subsequently, n_{A_i} and n_{B_i} are used to compute the medium-amplitude point (n_{M_i}). This point is considered as a robust measure of PPG pulse location because it is located during the interval of the steepest slope of the PPG pulse, and it is set as:

$$n_{\mathrm{M}_i} = \arg\min_n \left\{\left|x_{\mathrm{PPG}}(n) - \frac{x_{\mathrm{PPG}}(n_{\mathrm{A}_i}) + x_{\mathrm{PPG}}(n_{\mathrm{B}_i})}{2}\right|\right\}, \quad n \in \left[n_{\mathrm{B}_i}, n_{\mathrm{A}_i}\right]. \quad (3)$$

Pulse onset n_{O_i} and end n_{E_i} points were detected based on the first derivative (Lázaro et al., 2013). In addition, pulse up-slope end n_{SE_i} was detected in a similar way. Let $x'_{\mathrm{PPG}}(n)$ be the first derivative of $x_{\mathrm{PPG}}(n)$ computed by successive differences, after a 5-Hz-low-pass filter. Then, n_{SE_i} is set as:

$$n_{\mathrm{SE}_i} = \arg\min_n \left\{\left|x'_{\mathrm{PPG}}(n) - \eta x'_{\mathrm{PPG}}(n_{\mathrm{U}_i})\right|\right\}, \qquad n \in \left[n_{\mathrm{U}_i}, n_{\mathrm{A}_i}\right], \quad (4)$$

where η was set to 0.05 similarly to the case of n_{O_i} and n_{E_i} (Lázaro et al., 2013).

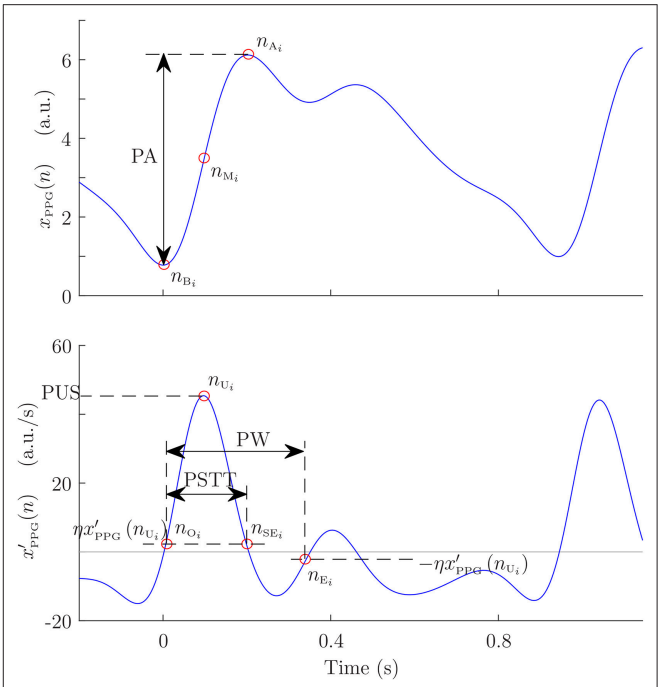

FIGURE 1 | Example of PPG pulse with its automatically detected points, and morphological measures taken from them: pulse amplitude (PA), pulse width (PW), and pulse slope transit time (PSTT).

2.1.2. Pulse Decomposition Analysis

PDA is a field in PPG signal proccessing that consits of modeling the PPG pulse as a main wave superposed with several reflected waves, increasing the robustness of some morphological measurements and even allowing others that would not be possible directly over the pulse. Several models can be found in the literature, based on different shapes including Gaussians (Baruch et al., 2011), LogNormal (Huotari et al., 2011), and Rayleight (Goswami et al., 2010). In this work, a modification to the PDA technique presented in Lázaro et al. (2018) is proposed. The main difference of this technique with respect to other PDA techniques in the literature is that the waves are extracted one-by-one, instead of fitting a several-waves-model at once. The modification proposed in this paper consists of not assuming a specific shape for the superposed waves, although it is assumed that they are symmetrical.

First, the baseline of the PPG signal was estimated by cubic-spline-interpolation of $x_{\mathrm{PPG}}(n_{\mathrm{B}_i})$, and subsequently subtracted

from $x_{\mathrm{PPG}}(n)$. This baseline-removed version of PPG signal is denoted $x^{\mathrm{b}}_{\mathrm{PPG}}(n)$ in this manuscript. Then, the beginning and the end of the ith PPG pulse were considered to be n_{B_i} and $n_{\mathrm{B}_{i+1}}$, respectively. Note that this criterion ensures that each PPG pulse begins and ends with zero amplitude, as subtracted baseline was estimated at those n_{B_i}. Later, the algorithm extracts recursively the jth inner wave of the pulse by the following steps:

1. Set the beginning of the up-slope of the jth wave ($n^{\mathrm{b}}_{\mathrm{SO}_{j,i}}$) as the previous to the first non-zero-amplitude sample. Note that in case of $j = 1$ (the main wave), this corresponds to n_{B_i}.
2. Set the end of the up-slope of the jth wave ($n^{\mathrm{b}}_{\mathrm{SE}_{j,i}}$) as the first relative maximum.
3. Estimate the jth wave $y^{\mathrm{b}}_{j,i}(n)$ by concatenating the up-slope with itself horizontally flipped, assuming that it is symmetric:

$$x^{\mathrm{b}}_{j,i}(n) = \begin{cases} x^{\mathrm{b}}_{\mathrm{PPG}}(n), & n \in \left[n^{\mathrm{b}}_{\mathrm{SO}_{j,i}}, n^{\mathrm{b}}_{\mathrm{SE}_{j,i}}\right] \\ 0, & \text{otherwise} \end{cases} \quad (5)$$

$$y^{\mathrm{b}}_{j,i}(n) = x^{\mathrm{b}}_{j,i}(n) + x^{\mathrm{b}}_{j,i}(-n + 2n^{\mathrm{b}}_{\mathrm{SE}_{j,i}} + 1), \quad (6)$$

4. Substract $y^{\mathrm{b}}_{j,i}(n)$ to $x^{\mathrm{b}}_{\mathrm{PPG}}(n)$ and go back to step 1 to continue extracting the $(j + 1)$th wave.

Once the desired number of waves have been extracted, they can be modeled in order to measure morphological features. In this work, three waves were extracted per PPG pulse. Subsequently, these $y^{\mathrm{b}}_{j,i}(n)$ were normalized to the unit in amplitude and to 1,000 samples by spline interpolation, and then they were modeled as Gaussian waves, each one defined by an amplitude, a mean, and a standard deviation (SD). Once these values are estimated, they were re-converted to the original scales of amplitude and time. An illustration of the steps of this algorithm can be observed in **Figure 2**.

2.2. PPG-Based Surrogates of Systolic Arterial Pressure Variability for BRS Estimation

2.2.1. Systolic Arterial Pressure Variability Surrogates Based on Pulse Signal

Four pulse morphological features that have been related to the BP and/or to the arterial stiffness in the literature were measured from each PPG pulse: amplitude (PA), width (PW), up-slope (PUS), and slope transit time (PSTT). Pulse amplitude and width were measured as in Lázaro et al. (2013). The pulse amplitude corresponds to that amplitude reached by n_{A_i} with respect to n_{B_i}, and the pulse width was measured as the time interval between n_{O_i} and n_{E_i}. Pulse up-slope was measured as the first derivative value at n_{U_i}, and PSTT was measured as the time interval between n_{O_i} and n_{SE_i}. Later, PA, PW, PUS, and PSTT series were computed as:

$$d^{u}_{\mathrm{PA}}(n) = \sum_i \left[x_{\mathrm{PPG}}\left(n_{\mathrm{A}_i}\right) - x_{\mathrm{PPG}}\left(n_{\mathrm{B}_i}\right)\right] \delta\left(n - n_{\mathrm{M}_i}\right) \quad (7)$$

$$d^{u}_{\mathrm{PW}}(n) = \sum_i \left[n_{\mathrm{E}_i} - n_{\mathrm{O}_i}\right] \delta\left(n - n_{\mathrm{M}_i}\right) \quad (8)$$

$$d^{u}_{\mathrm{PUS}}(n) = \sum_i \left[x'_{\mathrm{PPG}}\left(n_{\mathrm{U}_i}\right)\right] \delta\left(n - n_{\mathrm{M}_i}\right) \quad (9)$$

$$d^{u}_{\mathrm{PSTT}}(n) = \sum_i \left[n_{\mathrm{SE}_i} - n_{\mathrm{O}_i}\right] \delta\left(n - n_{\mathrm{M}_i}\right), \quad (10)$$

where $\delta(\cdot)$ denotes the Kronecker delta function, and the superscript "u" denotes that the signals are unevenly sampled, as the PPG pulses occur unevenly in time. A median-absolute-deviation outlier-rejection (Bailón et al., 2006) rule was applied to each one of these series, rejecting those points of the series that are outside the boundaries defined as the median ± 5 times the SD of the previous 50 points. Subsequently, a 4-Hz-evenly sampled version of each one of them was obtained by linear interpolation. The resulting signals are denoted using the same nomenclature, this time without the superscript "u" [e.g., $d_{\mathrm{PA}}(n)$].

2.2.2. Systolic Arterial Pressure Variability Surrogates Based on Pulse Decomposition Analysis

Seven morphological features were extracted from each PDA-based modeled PPG pulse. Specifically, the amplitude, mean, and twice the SD of the Gaussian-function fitted to the main wave were studied (m_{A1}, m_{B1}, and m_{C1}, respectively). Moreover, the feature related to twice the SD of the first reflected wave were also studied (m_{C2}), as well as the time delay between the main wave occurrence m_{B1} and those of reflected ones m_{B2} and m_{B3} (m_{T12} and m_{T13}, respectively). Furthermore, the percentage of amplitude that it is lost in the first reflection was also estimated as:

$$m_{\mathrm{A12}} = \frac{m_{\mathrm{A1}} - m_{\mathrm{A2}}}{m_{\mathrm{A1}}}. \quad (11)$$

Figure 3 illustrate these measures. These features extracted from the PDA are also hypothesized to be related to the BP and/or to the arterial stiffness since they are related to amplitude, relative position between the waves, and waves dispersion by SD. Their associated series were computed as:

$$d^{u}_{\{\mathrm{A1,\,B1,\,C1,\,C2,\,T12,\,T13,\,A12}\}}(n) = \sum_i m_{\{\mathrm{A1,\,B1,\,C1,\,C2,\,T12,\,T13,\,A12}\}}\, \delta\left(n - n_{\mathrm{B}_i}\right). \quad (12)$$

The outliers of these series were rejected by the same median-absolute-deviation-based rule applied in the case of the features which were measured over the pulse (see section 2.2.1), and similarly, they were linearly interpolated obtaining a 4 Hz evenly sampled version of each one of them denoted without the superscript "u".

2.3. Baroreflex Sensitivity Indices

The BRS indices were computed based on the α index, which is computed from a spectral analysis of RRV and SAPV. Several α-index surrogates based on PPG signal were computed, using PPV as RRV surrogate, and the SAPV surrogates described above.

The PPV was estimated using n_{M_i} as fiducial point:

$$d^{u}_{\mathrm{PPV}}(n) = \sum_i \frac{1}{F_s}\left[n_{\mathrm{M}_i} - n_{\mathrm{M}_{i-1}}\right] \delta\left(n - n_{\mathrm{M}_i}\right). \quad (13)$$

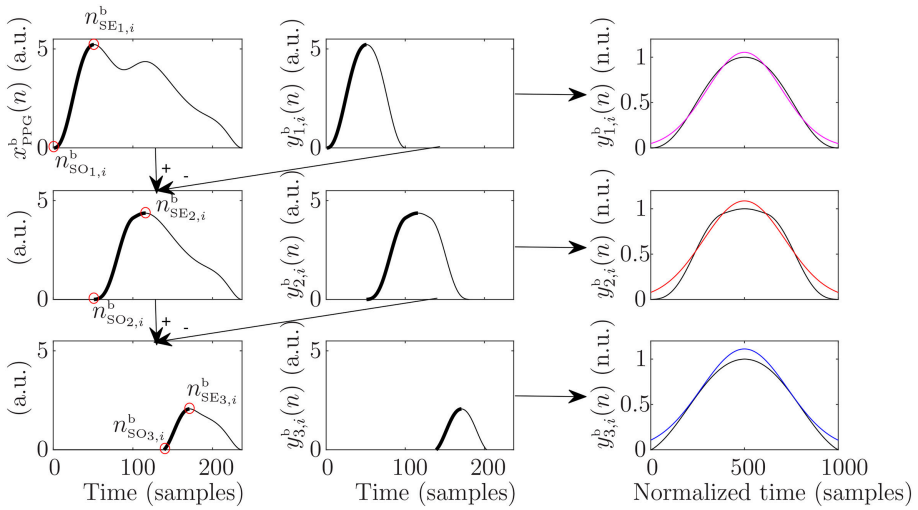

FIGURE 2 | Example of the steps for the pulse decompostion analysis that lead to extraction of main wave (first row), first reflected wave (second row), and second reflected wave (third row). In addition, the subsequent modeling of the extracted waves can be observed in the third column in magenta, red, and blue for the main, first reflected, and second reflected waves, respectively.

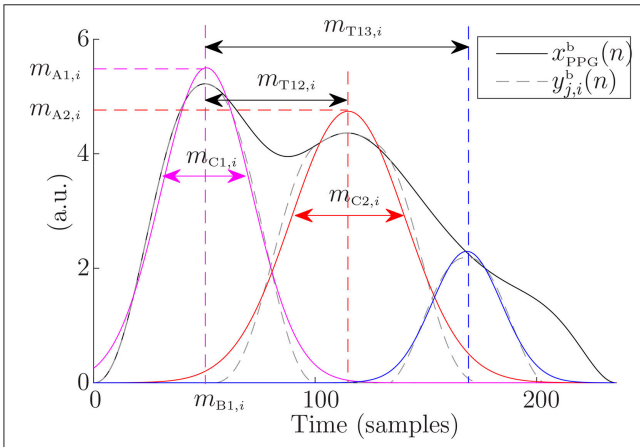

FIGURE 3 | Measures over the extracted waves of an example PPG pulse. Gaussians fitted to these waves are shown in color.

These series were also outlier-rejected and linearly interpolated to an even sampling rate of 4 Hz. Then, a power spectrum was computed from $d_{\mathrm{PPV}}(n)$, obtaining $\bar{S}_{\mathrm{PPV}}(f)$, and from the kth SAPV surrogates, obtaining $S_k(f)$, for each one of the stages of the protocol, where k can be PA, PW, PUS, PSTT, A1, B1, C1, C2, T12, T13, and A12. These power spectra were obtained by the Welch periodogram, using a 2 min Hamming window and 50% of overlap. Then, the PPG-based surrogates of the α index were extracted from these spectra, within LF ([0.04, 0.15] Hz) and HF ([0.15, 0.4] Hz) bands:

$$\alpha_k^{\{\mathrm{LF,HF}\}} = \sqrt{\int_{\Omega_{\{\mathrm{LF,HF}\}}} S_{\mathrm{PPV}}(f)df \Big/ \int_{\Omega_{\{\mathrm{LF,HF}\}}} S_k(f)df}, \qquad (14)$$

where Ω_{LF} and Ω_{HF} denote the LF and HF bands, respectively.

In addition, in order to take into account the non-stationarity of the protocol, the BRS indices were computed using a time-frequency technique for instantaneous measurement of α index, described in Orini et al. (2012). A time-frequency distribution was applied to $d_{\mathrm{PPV}}(n)$ obtaining $S_{\mathrm{PPV}}(n,f)$, and to each one of the PPG-morphology series used as SAPV surrogates obtaining $S_k(n,f)$. In addition, a cross time-frequency spectrum $S_{\mathrm{PPV},k}(n,f)$ was also computed as in Orini et al. (2012). The instantaneous frequencies of the main components of $S_{\mathrm{PPV},k}(n,f)$ within [0.04, 0.15] Hz [for LF band, $f_{\mathrm{LF}}(n)$] and [0.15, 0.4] Hz [for HF band $f_{\mathrm{HF}}(n)$] were computed as the frequencies where $S_{\mathrm{PPV},k}(n,f)$ is maximum within those bands. Then, $\Omega_{\mathrm{LF}}(n)$ and $\Omega_{\mathrm{HF}}(n)$ were defined as the frequency bands centered at $f_{\mathrm{LF}}(n)$ and $f_{\mathrm{HF}}(n)$, respectively, with a bandwidth equal to the frequency resolution of the used time-frequency distribution. Then, the PPG-based surrogate of α index was computed for each $S_k(n,f)$ as the square root of the ratio between the powers of $d_{\mathrm{PPV}}(n)$ (as a surrogate of RRV) and $d_k(n)$, for each one of the defined bands:

$$\alpha_k^{\{\mathrm{LF,HF}\}}(n) = \sqrt{\int_{\Omega_{\{\mathrm{LF,HF}\}}} S_{\mathrm{PPV}}(n,f)df \Big/ \int_{\Omega_{\{\mathrm{LF,HF}\}}} S_k(n,f)df}. \qquad (15)$$

Figure 4 shows inter-subject median and interquartile range (IQR) of $\alpha_k^{\{\mathrm{LF,HF}\}}(n)$ during the protocol. For BRS assessment, it is convenient to measure these indices only when PPV and k series are coupled. In order to detect these time courses, a time-frequency coherence ($\gamma_{\mathrm{PPV},k}(n,f)$) was computed, and PPV and k series were considered to be coupled in those areas where $\gamma_{\mathrm{PPV},k}(n,f)$ is over a significance level. The indices $\alpha_k^{\mathrm{LF}}(n)$ and $\alpha_k^{\mathrm{HF}}(n)$ measured only when $\gamma_{\mathrm{PPV},k}(n,f)$ is significant within Ω_{LF} and Ω_{HF}, respectively, are denoted $\alpha_k^{\mathrm{LF}_\gamma}(n)$ and

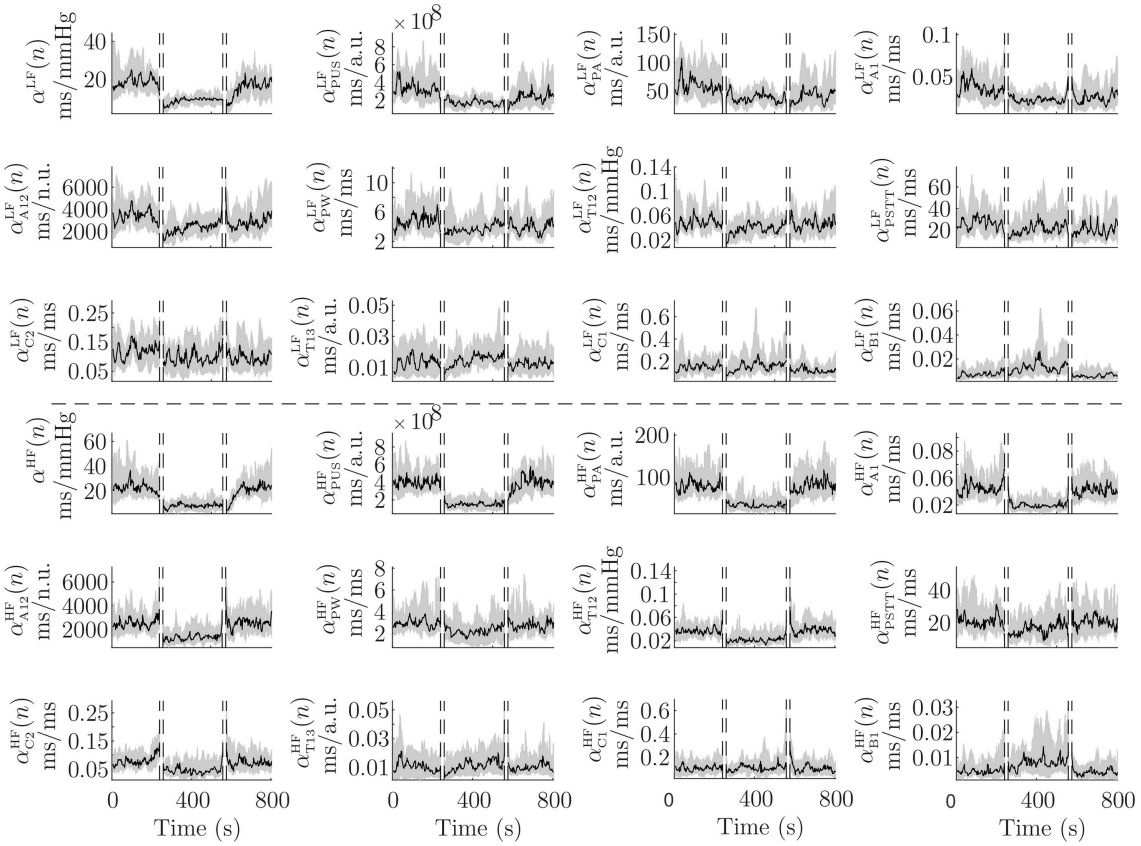

FIGURE 4 | Median (black) and IQR (shaded area) of $\alpha^{LF}(n)$, $\alpha^{HF}(n)$, and their PPG-based surrogates, during the whole protocol. First 3 rows are related to the LF band and last 3 rows are related to the HF band.

$\alpha_k^{HF_\gamma}(n)$, respectively, in this paper. Further details are given in Orini et al. (2012).

For validation purposes, the conventional α index was also computed from the RRV and the SAPV, denoted with no subindex $[\alpha^{\{LF,HF,LF_\gamma,HF_\gamma\}}(n)]$, and taken as reference. The RRV was computed by the interval function using the R points (n_{R_i}) determined from the ECG by Martínez et al. (2004):

$$d^u_{RRV}(n) = \sum_i \frac{1}{F_s}\left[n_{R_i} - n_{R_{i-1}}\right]\delta\left(n - n_{R_i}\right). \tag{16}$$

The SAPV was computed from the maximum of BP pulses ($\check{n}_{A_i}$), which were detected similarly to the case of the PPG pulses (see section 2.1.1):

$$d^u_{SAPV}(n) = \sum_i x_{BP}\left(\check{n}_{A_i}\right)\delta\left(n - \check{n}_{A_i}\right). \tag{17}$$

2.4. Performance Metrics

A unique value per subject and stage of the protocol (Rest1, Tilt, and Rest2) was obtained for each one of the three studied α-index estimation methods:

1. Welch-periodogram approach ($\alpha^{\{LF,HF\}}$): As it is based on a non-time-frequency technique, a unique value per subject and stage is available.
2. Time-frequency approach ($\bar{\alpha}^{\{LF,HF\}}$): The median of $\alpha^{\{LF,HF\}}(n)$ within each stage and each subject was taken as the unique value per subject and stage.
3. Time-frequency-coherence approach ($\bar{\alpha}^{\{LF_\gamma,HF_\gamma\}}$): The median of $\alpha^{\{LF_\gamma,HF_\gamma\}}(n)$ within each stage and each subject was taken as the unique value per subject and stage.

Then, correlation between the indices (α and α_k) obtained from the 17 subjects and the 3 stages of the protocol (Rest1, Tilt, and Rest2) were computed. The distributions of these indices were found to be not normal by the Kolmogorov-Smirnov test. Thus, the Spearman's correlation coefficient was used. Furthermore, the Wilcoxon signed-rank test was applied to see if the indices can find significant ($p < 0.05$) differences between the different stages of the protocol.

As the SAPV surrogates, the α-index surrogates have different units and magnitude than classical α index. Thus, these surrogates cannot be directly compared to the classical α index, but their evolution can be compared. In order to do this, the relative variation of the α-index between consecutive stages was computed for

each subject:

$$\Delta\alpha = \frac{\alpha_{S2} - \alpha_{S1}}{\alpha_{S1}}, \quad (18)$$

where α_{S1} and α_{S2} represent the studied index within stages S1 and S2, respectively.

A linear regression of the α-index surrogates which obtained best results in terms of correlation (those based on PUS, as it can be observed in section 3) was performed, obtaining similar units than those of the conventional α index (ms/mmHg). This linear regression was performed in order to compare those indices in a Bland-Altman plot. In addition, a multiple linear regression was performed using all the studied α-index surrogates in order to study whether their information is complementary or redundant. The combined α-index surrogates are denoted $\hat{\alpha}^{\{LF,HF\}}$ (Welch-periodogram approach), $\hat{\bar{\alpha}}^{\{LF,HF\}}$ (time-frequency approach), and $\hat{\bar{\alpha}}^{\{LF_\gamma,HF_\gamma\}}$ (time-frequency-coherence approach).

TABLE 1 | Inter-subject Spearman correlations of $\alpha^{\{LF,HF\}}$ and $\alpha_k^{\{LF,HF\}}$ obtained in the different stages of the protocol.

	α and α_k		$\bar{\alpha}$ and $\bar{\alpha}_k$		$\bar{\alpha}^\gamma$ and $\bar{\alpha}_k^\gamma$	
k	**LF**	**HF**	**LF**	**HF**	**LF**	**HF**
PUS	0.81	0.80	0.74	0.76	0.74	0.81
A1	0.80	0.87	0.69	0.80	0.69	0.76
PA	0.77	0.79	0.67	0.79	0.67	–
A12	0.61	0.68	0.50	0.62	0.50	0.61
T12	0.48	0.53	0.48	0.61	0.48	0.56
PW	0.32	0.48	0.14	0.49	0.14	0.36
PSTT	0.48	0.36	0.39	0.27	0.39	0.29
C2	0.39	0.50	0.17	0.30	0.17	–
T13	0.20	0.18	0.14	0.10	0.14	–
C1	0.31	0.24	0.36	0.35	0.36	–
B1	0.03	0.02	0.10	0.05	0.10	–0.06

In addition, inter-subject Spearman correlations of medians of $\tilde{\alpha}^{\{LF,HF\}}$ and $\tilde{\alpha}_k^{\{LF,HF\}}$ obtained in the different stages of the protocol are also shown, as well as the inter-subject Spearman correlations of medians of $\tilde{\alpha}^{\{LF_\gamma,HF_\gamma\}}$ and $\tilde{\alpha}_k^{\{LF_\gamma,HF_\gamma\}}$.

3. RESULTS

Table 1 shows inter-subject Spearman's correlation coefficients between $\alpha^{\{LF,HF\}}$ and $\alpha_k^{\{LF,HF\}}$, between $\bar{\alpha}^{\{LF,HF\}}$ and $\bar{\alpha}_k^{\{LF,HF\}}$, and between $\bar{\alpha}^{\{LF_\gamma,HF_\gamma\}}$ and $\bar{\alpha}_k^{\{LF_\gamma,HF_\gamma\}}$. The highest correlations were obtained for the α-index surrogates based on PUS. A scatterplot of these indices is shown in **Figure 5**. In addition, a Bland-Altmant plot of these indices and their associated conventional α indices is shown in **Figure 6**, after a linear regression in order to obtain similar units and magnitudes. The obtained limits of agreement were 0.94 ± 21.90 ms/mmHg (mean of the two values $\pm$ 1.96 $\times$ SD), –8.99E–15 $\pm$ 60.90, 1.29 $\pm$ 20.13, 4.56E–15 $\pm$ 40.49, 1.40 $\pm$ 18.43, 5.92E–15 $\pm$ 46.89 ms/mmHg, for α_{PUS}^{LF}, α_{PUS}^{HF}, $\bar{\alpha}_{PUS}^{LF}$, $\bar{\alpha}_{PUS}^{HF}$, $\bar{\alpha}_{PUS}^{LF_\gamma}$, and $\bar{\alpha}_{PUS}^{HF_\gamma}$, respectively.

The Bland-Altmant plot obtained from the multiple linear regression using all the studied indices is shown in **Figure 7**. The obtained limits of agreement were 1.31 $\pm$ 20.38, 2.61E–15 $\pm$ 25.48, 1.12 $\pm$ 19.68, –6.30E–15 $\pm$ 20.00, 0.89 $\pm$ 10.25, –6.85E–15 $\pm$ 15.80 ms/mmHg, for α_{PUS}^{LF}, α_{PUS}^{HF}, $\bar{\alpha}_{PUS}^{LF}$, $\bar{\alpha}_{PUS}^{HF}$, $\bar{\alpha}_{PUS}^{LF_\gamma}$, and $\bar{\alpha}_{PUS}^{HF_\gamma}$, respectively.

Table 2 shows the inter-subject median and interquartile ranges of $\alpha^{\{LF,HF\}}$ and $\alpha_k^{\{LF,HF\}}$, for those indices which showed

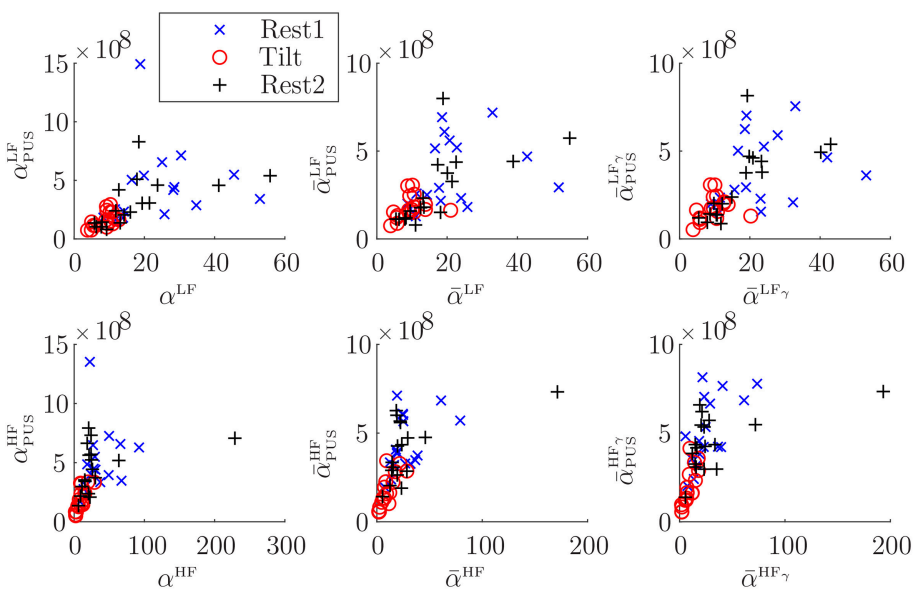

FIGURE 5 | Scatterplots of α vs. α_{PUS} indices (first column), of $\bar{\alpha}$ vs. $\bar{\alpha}_{PUS}$ indices (second column), and of $\bar{\alpha}^\gamma$ vs. $\bar{\alpha}_{PUS}^\gamma$ indices (third column).

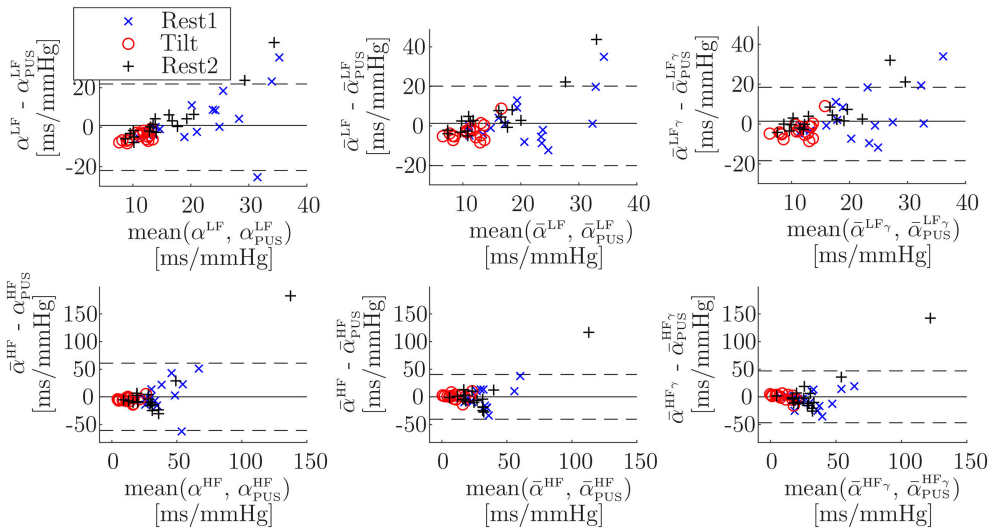

FIGURE 6 | Bland-Altman plots of α vs. α_{PUS} indices (Welch-periodogram approach, first column), of $\bar{\alpha}$ vs. $\bar{\alpha}_{PUS}$ indices (time-frequency approach, second column), and of $\bar{\alpha}^{\gamma}$ vs. $\bar{\alpha}^{\gamma}_{PUS}$ indices (time-frequency coherence approach, third column), after a linear regression to convert all units to ms/mmHg. Note that scales are not the same for LF band (first row) than for HF band (second row).

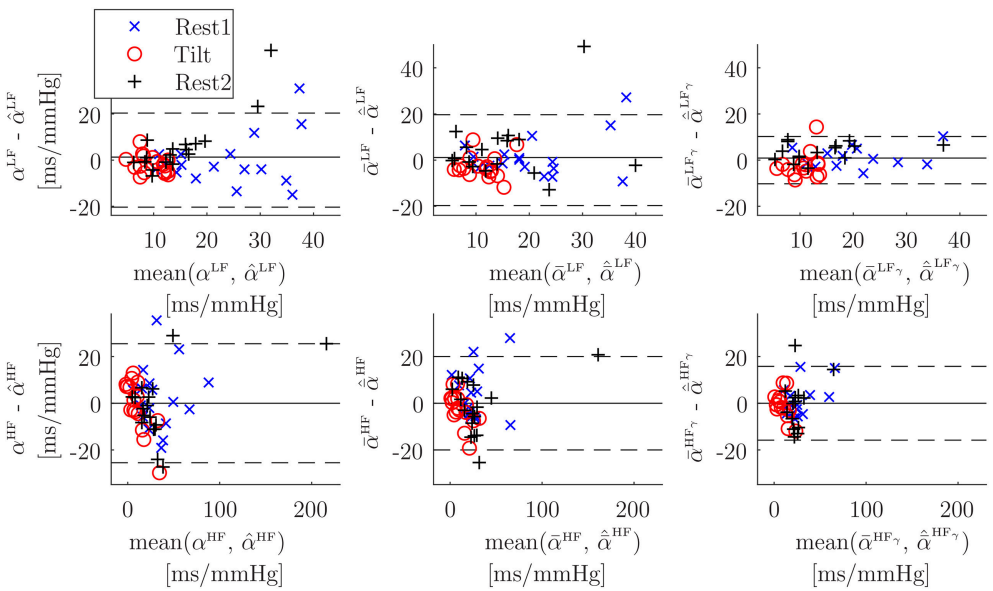

FIGURE 7 | Bland-Altman plots of α vs. its multiple-linear-regression-based combination of surrogates $\hat{\alpha}$ (Welch-periodogram approach, first column), of $\bar{\alpha}$ vs. its multiple-linear-regression-based combination of surrogates $\hat{\bar{\alpha}}$ (time-frequency approach, second column), and of $\bar{\alpha}^{\gamma}$ vs. its multiple-linear-regression-based combination of surrogates $\hat{\bar{\alpha}}^{\gamma}$ (time-frequency coherence approach, third column). Note that scales are not the same for LF band (first row) than for HF band (second row).

at least moderate Spearman's correlation coefficients (>0.50), and their relative increments (Δ). Significant differences ($p < 0.05$) of these indices between Tilt and rest stages are denoted with*. Similarly, the inter-subject median and interquartile ranges of medians of $\bar{\alpha}^{\{LF,HF\}}$ and $\bar{\alpha}_k^{\{LF,HF\}}$ are shown in **Table 3**, and interquartile ranges of medians of $\bar{\alpha}^{\{LF_\gamma,HF_\gamma\}}$ and $\bar{\alpha}_k^{\{LF_\gamma,HF_\gamma\}}$ are shown in **Table 4**.

4. DISCUSSION

Novel methods for measuring BRS using a PPG signal have been presented. They are based on surrogates of the α index, defined as the ratio of the power of RRV series and the power of SAPV series. In this work, PPV is used as a surrogate of RRV, and the SAPV is surrogated by different morphological features of the PPG pulse which have been related to BP in the literature. Some

TABLE 2 | Inter-subject median and interquartile ranges of $\alpha^{\{LF,HF\}}$ and $\alpha_k^{\{LF,HF\}}$.

	α					
	Median					
	[First quartile, Third quartile]					
k	**LF**			**HF**		
	Rest1	**Tilt**	**Rest2**	**Rest1**	**Tilt**	**Rest2**
α	1.99*	0.93	1.42*	2.79*	0.91	2.13*
(ms/mmHg $\times 10$)	[1.35, 2.90]	[0.60, 1.05]	[0.89, 1.99]	[1.82, 4.93]	[0.47, 1.19]	[1.54, 2.50]
Δ	−106.58		37.87	−220.44		52.45
(%)	[−250.08, −64.39]		[22.20, 58.03]	[−552.97, −147.87]		[41.72, 77.60]
PUS	3.41*	1.54	2.41*	4.41*	1.46	4.44*
(ms^2/a.u. $\times 10^8$)	[2.04, 5.43]	[1.15, 2.29]	[1.37, 4.58]	[3.28, 6.33]	[1.17, 2.62]	[2.83, 5.94]
Δ	−122.90		42.46	−115.58		64.53
(%)	[−203.55, −30.42]		[3.56, 57.68]	[−305.99, −98.13]		[37.04, 74.70]
A1	3.71*	2.07	2.56	4.78*	1.87	4.42*
(ms/a.u. $\times 10^{-2}$)	[2.58, 6.84]	[1.51, 2.94]	[1.28, 4.44]	[3.11, 7.61]	[1.32, 2.92]	[2.89, 5.11]
Δ	−81.94		27.65	−92.90		50.78
(%)	[−194.28, −17.10]		[−29.56, 50.62]	[−256.82, −75.16]		[26.26, 64.68]
PA	5.25*	3.05	4.39*	6.94*	3.41	8.69*
(ms/a.u. $\times 10$)	[4.00, 9.81]	[2.55, 4.91]	[2.28, 7.54]	[6.46, 11.15]	[2.18, 5.53]	[4.86, 12.34]
Δ	−77.63		30.97	−93.94		48.55
(%)	[−176.46, −15.02]		[−22.42, 50.93]	[−331.49, −52.50]		[33.52, 73.50]
A12	2.00*	1.08	1.44	1.11*	0.63	1.21*
(ms/n.u. $\times 10^3$)	[1.57, 2.17]	[0.76, 1.55]	[0.87, 1.92]	[0.85, 1.50]	[0.47, 0.93]	[0.95, 1.52]
Δ	−45.69		20.47	−82.31		47.74
(%)	[−235.27, −5.27]		[−42.09, 51.86]	[−277.89, −26.75]		[15.44, 57.68]
T12	4.70	4.16	4.08	3.24*	2.32	3.46*
(ms/ms $\times 10^{-2}$)	[4.08, 6.60]	[2.77, 5.80]	[3.30, 6.23]	[2.86, 4.13]	[1.45, 3.39]	[2.70, 3.99]
Δ	−34.22		18.80	−45.43		38.66
(%)	[−121.33, 10.56]		[−3.63, 37.65]	[−179.21, −8.12]		[0.58, 52.76]

Significant differences ($p < 0.05$) of these intra-subject medians between Tilt and rest stages are denoted with $*$. In addition, the median and interquartile ranges of the relative increments (Δ) of these intra-subject medians between consecutive stages of the protocol (Rest1 and Tilt, and Tilt and Rest2) are also shown.

of these features are based on a novel PDA technique that has been presented in this paper. Many modeling functions have been applied to fit the PPG pulses in the literature. The novelty of the proposed PDA technique is that the used modeling function does not affect to the decomposition, as it is applied individually to the already extracted waves. It is worthy to note that the goal in this paper is not to obtain a very accurate measure of the studied morphological features, but in deriving a measure which is proportional to those features (as only their variability is needed). Keeping this in mind, a Gaussian function was used because it satisfies de goal while being a simple function that makes sense from the physiological point of view.

Three approaches were studied for estimating the α index from RRV and SAPV (or their surrogates): one based on Welch periodogram ($\alpha^{\{LF,HF\}}$), and two based on a time-frequency distribution which takes into account the non-stationarity of the protocol (Orini et al., 2012). This method redefines both LF and HF bands, making them time-varying following the dominant frequencies in such bands ($\bar{\alpha}^{\{LF,HF\}}$). Alternatively, this method computes a time-frequency coherence between the RRV and the SAPV (or their surrogates), and estimates the α index in restricted areas where the obtained coherence is statistically significant, i.e., in those areas evidencing that RRV and SAPV (or their surrogates) are coupled ($\bar{\alpha}^{\{LF_\gamma,HF_\gamma\}}$).

The correlation analysis shows how the PPG-based surrogates of α index track the changes of the conventional (ECG-and-BP-based) α index. Five out of the eleven SAPV surrogates leaded to α-index surrogates which obtained at least moderate correlation (>0.5). Those SAPV surrogates are, in order of cases getting the highest correlation: PUS, A1, PA, A12, and T12. Specifically, those α-index surrogates based on PUS obtained high correlation (>0.7) in all the cases. Those α-index surrogates based on A1 also obtained high correlation in four out of the six cases (α_{A1}^{LF}, α_{A1}^{HF}, $\bar{\alpha}_{A1}^{HF}$ and $\bar{\alpha}_{A1}^{HF_\gamma}$), while the remaining two ($\bar{\alpha}_{A1}^{LF}$ and $\bar{\alpha}_{A1}^{LF_\gamma}$) were very close to obtain it (correlation was 0.69 in both cases).

Results regarding the BRS assessment are shown in **Table 2** for the Welch-periodogram approach ($\alpha^{\{LF,HF\}}$), **Table 3** for the time-frequency approach ($\bar{\alpha}^{\{LF,HF\}}$), and **Table 4** for the time-frequency-coherence ($\bar{\alpha}^{\{LF_\gamma,HF_\gamma\}}$). The conventional α indices showed significant differences between both rest stages and Tilt within both LF and HF, and for the 3 approaches. The highest difference was observed between Rest1 and Tilt within HF band

TABLE 3 | Inter-subject median and interquartile ranges of intra-subject median of $\bar{\alpha}^{\{LF,HF\}}$ and $\bar{\alpha}_k^{\{LF,HF\}}$.

	$\bar{\alpha}$					
	Median					
	[First quartile, Third quartile]					
k	**LF**			**HF**		
	Rest1	**Tilt**	**Rest2**	**Rest1**	**Tilt**	**Rest2**
α	1.86*	0.94	1.34*	2.47*	0.85	1.96*
(ms/mmHg $\times 10$)	[1.35, 2.44]	[0.59, 1.06]	[0.92, 2.04]	[1.77, 3.31]	[0.41, 1.30]	[1.52, 2.48]
Δ	−100.04		31.21	−178.17		53.36
(%)	[−172.82, −74.32]		[6.35, 58.64]	[−355.59, −117.53]		[39.64, 77.75]
PUS	2.91*	1.63	1.81*	3.84*	1.58	4.27*
(ms^2/a.u. $\times 10^8$)	[2.13, 5.30]	[1.47, 2.09]	[1.18, 4.26]	[3.28, 5.79]	[0.98, 2.40]	[2.80, 5.61]
Δ	−101.90		7.67	−146.59		53.28
(%)	[−159.25, −58.17]		[−9.30, 56.29]	[−332.19, −81.41]		[40.21, 70.44]
A1	2.95*	2.03	2.23	4.72*	1.96	4.28*
(ms/a.u. $\times 10^{-2}$)	[2.35, 6.05]	[1.86, 2.96]	[1.34, 4.16]	[3.22, 6.09]	[1.39, 3.03]	[2.98, 6.35]
Δ	−71.93		−11.96	−91.35		42.31
(%)	[−88.72, −22.61]		[−47.85, 49.40]	[−263.31, −53.42]		[25.53, 70.41]
PA	4.76*	3.31	3.68	8.68*	3.62	7.87*
(ms/a.u. $\times 10$)	[3.93, 9.94]	[2.98, 5.22]	[2.27, 6.73]	[6.05, 10.45]	[2.21, 5.05]	[5.73, 11.51]
Δ	−64.68		−10.13	−113.09		50.80
(%)	[−99.06, −17.93]		[−55.90, 44.17]	[−319.85, −62.92]		[24.07, 69.72]
A12	1.88*	1.16	1.41	1.30*	6.78	1.31*
(ms/n.u. $\times 10^3$)	[1.11, 2.25]	[0.82, 1.54]	[0.97, 2.19]	[0.93, 1.56]	[0.5, 0.95]	[0.92, 1.80]
Δ	−30.61		11.47	−89.39		45.56
(%)	[−96.71, −8.05]		[−36.23, 51.83]	[−161.07, −34.94]		[−4.30, 57.83]
T12	4.88*	4.21	4.63	3.58*	2.27	4.01*
(ms/ms $\times 10^{-2}$)	[3.46, 6.65]	[2.66, 5.79]	[3.20, 6.93]	[3.17, 4.23]	[1.57, 3.05]	[2.56, 4.73]
Δ	−33.02		25.21	−84.19		41.15
(%)	[−144.80, 11.64]		[7.39, 46.72]	[−158.29, −19.44]		[9.53, 59.66]

Significant differences ($p < 0.05$) of these intra-subject medians between Tilt and rest stages are denoted with $*$. In addition, the median and interquartile ranges of the relative increments (Δ) of these intra-subject medians between consecutive stages of the protocol (Rest1 and Tilt, and Tilt and Rest2) are also shown.

(-220.44% for α^{HF}, -178.17% for $\bar{\alpha}^{HF}$, and -189.00% for $\bar{\alpha}^{HF_\gamma}$), while the smallest difference was observed between Rest2 and Tilt within LF band (37.87% for α^{LF}, 31.21% for $\bar{\alpha}^{LF}$, and 35.37% for $\bar{\alpha}^{LF_\gamma}$).

The only SAPV surrogate which led to α-index surrogates showing the same behavior than the conventional α-index was PUS. None of the other SAPV surrogates led to α-index surrogates finding significant differences between Rest2 and Tilt within LF (the smallest observed change) with the exception of PA when using the Welch-periodogram approach (α_{PA}^{LF}). However, PUS, A1, PA, and A12-based α-index surrogates found significant Rest1 and Tilt within both the LF and HF band, and between Rest2 and Tilt within the HF band, for the 3 approaches. The T12-based α-index surrogates also found these differences for both the time-frequency and the time-frequency-coherence approaches while they found significant differences only within HF band for the Welch-periodogram approach. In general, those PPG-based-α-index surrogates exploiting the pulse amplitude (PA, A1, and A12) obtained better results than those exploiting the pulse dispersion (PSTT, B1, C1, C2, T12, and T13) for BRS assessment, with the exception of T12. However, the best results were obtained for the index derived from PUS, which exploits both PPG amplitude and pulse dispersion. Another possible reason of the better results obtained by PUS is that it is measured at the beginning of the pulse, which would be the part related to a unique wave (main wave, before superposition of reflections) containing the BP information better expressed than the reflected waves.

The Bland-Altman plots (**Figure 6**) for PUS-based α-index surrogates (after converting units to ms/mmHg by a linear regression) are wider for HF ($\pm$60.90 ms/mmHg, $\pm$40.49 ms/mmHg, and $\pm$46.89 ms/mmHg, for Welch-periodogram, time-frequency, and time-frequency-coherence approaches, respectively) than for LF ($\pm$21.90, $\pm$20.13, and $\pm$18.43 ms/mmHg, for Welch-periogram-, time-frequency-, and time-frequency-coherence approaches, respectively). When combining all the PPG-based α-index surrogates by a multiple-linear regression, these limits of agreement are narrower, specially for within HF ($\pm$25.48, $\pm$20.00, and $\pm$15.80 mm/mmHg, for Welch-periogram-, time-frequency-, and time-frequency-coherence approaches, respectively). These results suggest that there is complementary

TABLE 4 | Inter-subject median and interquartile ranges of intra-subject median of $\tilde{\alpha}^{\{LF_\gamma,HF_\gamma\}}$ and $\tilde{\alpha}_k^{\{LF_\gamma,HF_\gamma\}}$.

	$\tilde{\alpha}^{\gamma}$ Median [First quartile, Third quartile]					
k	**LF**			**HF**		
	Rest1	**Tilt**	**Rest2**	**Rest1**	**Tilt**	**Rest2**
α	1.90*	0.96	1.49*	2.29*	0.72	2.12*
(ms/mmHg ×10)	[1.46, 2.90]	[0.58, 1.12]	[1.03, 2.15]	[1.57, 3.71]	[0.45, 1.25]	[1.54, 2.94]
Δ	−117.50		35.37	−189.00		57.92
(%)	[−192.77, −82.71]		[14.80, 59.37]	[−379.50, −121.44]		[45.78, 78.53]
PUS	2.94*	1.74	2.38*	4.56*	1.63	4.35*
(ms^2/a.u. $\times10^8$)	[2.06, 5.42]	[1.18, 2.18]	[1.37, 4.63]	[3.74, 6.90]	[1.15, 2.73]	[3.21, 5.54]
Δ	−110.81		26.90	−149.21		61.31
(%)	[−161.04, −65.23]		[−5.61, 60.80]	[−337.87, −111.69]		[36.88, 76.98]
A1	3.53*	2.18	2.77	4.63*	1.98	4.03*
(ms/a.u. $\times10^{-2}$)	[2.47, 5.65]	[1.76, 2.95]	[1.47, 4.37]	[3.19, 6.06]	[1.53, 3.09]	[3.15, 5.86]
Δ	−73.33		11.92	−98.35		39.30
(%)	[−143.21, −26.44]		[−45.15, 58.81]	[−214.68, −57.39]		[30.64, 64.98]
PA	6.54*	3.63	5.11	8.52*	3.50	7.94*
(ms/a.u. ×10)	[3.94, 10.01]	[2.71, 4.75]	[2.29, 7.35]	[6.43, 11.54]	[2.15, 5.59]	[5.72, 12.16]
Δ	−80.12		16.64	−122.46		60.19
(%)	[−135.09, −20.67]		[−32.66, 56.67]	[−289.82, −75.74]		[28.98, 74.27]
A12	1.78*	1.25	1.53	1.24*	0.77	1.33*
(ms/n.u. $\times10^3$)	[1.20, 2.15]	[0.83, 1.62]	[0.93, 2.07]	[1.17, 1.87]	[0.54, 1.07]	[0.91, 1.81]
Δ	−49.07		13.43	−90.11		40.77
(%)	[−107.14, −15.78]		[−10.92, 55.82]	[−150.88, −21.83]		[19.90, 57.58]
T12	4.99*	3.78	4.74	3.62*	2.36	3.89*
(ms/ms $\times10^{-2}$)	[3.64, 6.09]	[2.75, 5.77]	[3.22, 6.95]	[3.28, 5.11]	[1.57, 3.79]	[2.78, 4.82]
Δ	−26.56		28.52	−67.77		42.34
(%)	[−109.23, 6.28]		[5.59, 45.66]	[−206.71, −15.50]		[0.64, 59.04]

*Significant differences ($p < 0.05$) of these intra-subject medians between Tilt and rest stages are denoted with *. In addition, the median and interquartile ranges of the relative increments (Δ) of these intra-subject medians between consecutive stages of the protocol (Rest1 and Tilt, and Tilt and Rest2) are also shown.*

information among the SAPV surrogates and thus, they could be combined for improving the α-index surrogate. However, this combination may require a calibration process which may be subject-specific in a final application. Further studies including data from same subjects during different days must be elaborated in order to explore techniques to combine the information of the different α-index surrogates.

Comparing the correlations obtained by the PUS-based α-index surrogates among the three α-index estimation approaches, the highest correlation within LF was obtained when using the Welch-periodogram approach (0.81), while the highest correlation within HF was obtained when using the time-frequency-coherence approach (0.81). However, given the intrinsic non-stationarity of the cardiovascular system, our recommendation is to use the time-frequency-coherence approach (Orini et al., 2012) because it takes into account the time-varying dominant frequencies and the strength of the coupling between RRV and SAPV (or their surrogates) and thus, its estimates are more related to the BRS than the estimates from the other two approaches.

Based on these results, our recommendation for PPG-based BRS assessment is $\bar{\alpha}_{\mathrm{PUS}}^{\{LF_\gamma,HF_\gamma\}}$. First, $\bar{\alpha}_{\mathrm{PUS}}^{LF_\gamma}$ presented a significant decrease of more than 100% in median in tilt with respect to supine, which is in concordance with the decrease in reference $\bar{\alpha}^{LF_\gamma}$. Second, $\bar{\alpha}_{\mathrm{PUS}}^{HF_\gamma}$ also presented a significant decrease in tilt with respect to supine, in this case around 2 times lower with respect to Rest1 (26.90%) than to Rest2 (61.31%), and these results are also in accordance to the reference $\bar{\alpha}^{HF_\gamma}$ (with 35.37% and 57.92%, respectively). It is worthy to note that the best α surrogate may be not derived from the best SAPV surrogate, because PPV was used as RRV surrogate while it is the sum of RRV and PAT variability (PATV) (Gil et al., 2010). Thus, for obtaining a exact surrogate for the ratio RRV/SAPV using PPV as numerator of the ratio, the best denominator is not exactly SAPV, but SAPV×(1+PATV/RRV).

These results support the potential value of the proposed index as a surrogate of BRS to monitor baroreflex impairment in certain applications. For example, in de Moura-Tonello et al. (2016) the square root of the RR and systolic BP series power (α index) at rest was significantly reduced (around 50%) in type

2 diabetes mellitus patients without cardiovascular autonomic neuropathy with respect to healthy controls of similar age and antropometric characteristics. In Ranucci et al. (2017) preoperative BRS was evaluated in 150 patients undergoing coronary surgery and related to postoperative complications such as atrial fibrillation, renal function impairment and low cardiac output syndrome. The α index was significantly lower (around 30% in median) in patients experiencing postoperative acute kidney dysfunction, as well as in patients with low cardiac output state (around 50% in median). However, clinical studies have to be elaborated in order to evaluate the proposed indices in different applications. To the best of our knowledge, this is the first time that these indices are studied for BRS assessment, so healthy volunteers with presumably efficient baroreflex were used in order to observe actual changes along the protocol. Different results may be obtained with patients of different diseases, specially taking into account that coherence is reduced in heart disease patients.

Results reported in this work suggest that BRS can be assessed with high correlation by only a PPG signal based on PPV (as RRV surrogate), and PPG-amplitude-based and/or PPG-dispersion-based features (as SAPV surrogates), being PUS the most convenient SAPV surrogate for BRS assessment. The PPG signal recording is simple, economical, and comfortable for the subject. Moreover, PPG signal can be acquired in many places of the body. Thus, these results are very interesting for ambulatory scenarios and for wearable devices. Future studies may include an surrogate of the α index using a combination of different PPG-based SAPV surrogates, specially amplitude- and dispersion-based features.

ETHICS STATEMENT

This study was carried out in accordance with the recommendations of Comité Ètico de Investigación Clínica de Aragón (CEICA) with written informed consent from all subjects. All subjects gave written informed consent in accordance with the Declaration of Helsinki. This study was exempt from approval of the ethical committee because no new data were registered for its development.

AUTHOR CONTRIBUTIONS

JL and RB wrote the first draft in the manuscript preparation. All authors participated in the design of the proposed methods, as well of the statistical analysis for their evaluation, reviewed, and critiqued the manuscript preparation.

FUNDING

This project has received funding from the European Union's Framework Programme for Research and Innovation Horizon 2020 (2014-2020) under the Marie Skłodowska-Curie Grant Agreement No. 745755. This work was supported also by projects DPI2016-75458-R and RTI2018-097723-B-I00 funded by MINECO and FEDER, by Gobierno de Aragón (Reference Group BSICoS T39-17R) cofunded by FEDER 2014-2020 Building Europe from Aragon, and by CIBER in Bioengineering, Biomaterials and Nanomedicine (CIBER-BBN) through Instituto de Salud Carlos III. The computation was performed by the ICTS NANBIOSIS, specifically by the High Performance Computing Unit of CIBER-BBN at University of Zaragoza.

REFERENCES

Abe, M., Yoshizawa, M., Obara, K., Sugita, N., Homma, N., and Yambe, T. (2015). Evaluation of baroreflex function using green light photoplethysmogram in consideration of resistance to artifacts. *Adv. Biomed. Eng.* 4, 1–6. doi: 10.14326/abe.4.1

Bailón, R., Sörnmo, L., and Laguna, P. (2006). A robust method for ecg-based estimation of the respiratory frequency during stress testing. *IEEE Trans. Biomed. Eng.* 53, 1273–1285. doi: 10.1109/TBME.2006.871888

Baruch, M. C., Warburton, D. E. R., Bredin, S. S. D., Cote, A., Gerdt, D. W., and Adkins, C. M. (2011). Pulse decomposition analysis of the digital arterial pulse during hemorrhage simulation. *Nonlinear Biomed. Phys.* 5, 1–15. doi: 10.1186/1753-4631-5-1

Chen, Y., Wen, C., Tao, G., Bi, M., and Li, G. (2009). Continuous and noninvasive blood pressure measurement: a novel modeling methodology of the relationship between blood pressure and pulse wave velocity. *Ann. Biomed. Eng.* 37, 2222–2233. doi: 10.1007/s10439-009-9759-1

Chen, Z., Purdon, P. L., Harrell, G., Pierce, E. T., Walsh, J., Brown, E. N., et al. (2011). Dynamic assessment of baroreflex control of heart rate during induction of propofol anesthesia using a point process method. *Ann. Biomed. Eng.* 39, 260–276. doi: 10.1007/s10439-010-0179-z

de Moura-Tonello, S., Porta, A., Marchi, A., de Almeida Fagundes, A., Francisco, C., Rehder-Santos, P., et al. (2016). Analysis and baroreflex estimation in patients with type 2 diabetes in absence of any manifest neuropathy. *PLoS ONE* 11:e0148903. doi: 10.1371/journal.pone.0148903

Di Rienzo, M., Parati, G., Radaelli, A., and Castiglioni, P. (2009). Baroreflex contribution to blood pressure and heart rate oscillations: time scales, time-variant characteristics and nonlinearities. *Philos. Trans. A Math. Phys. Eng. Sci.*, 367:1301–18. doi: 10.1098/rsta.2008.0274

Ding, X., Zhang, Y., Liu, J., Dai, W., and Tsang, H. K. (2016). Continuous cuffless blood pressure estimation using pulse transit time and photoplethysmogram intensity ratio. *IEEE Trans. Biomed. Eng.* 63, 964–972. doi: 10.1109/TBME.2015.2480679

Gil, E., Orini, M., Bailn, R., Vergara, J. M., Mainardi, L., and Laguna, P. (2010). Photoplethysmography pulse rate variability as a surrogate measurement of heart rate variability during non-stationary conditions. *Physiol. Measure.* 31, 1271–1290. doi: 10.1088/0967-3334/31/9/015

Goswami, D., Chaudhuri, K., and Mukherjee, J. (2010). A new two-pulse synthesis model for digital volume pulse signal analysis. *Cardiovasc. Eng.* 10, 109–117. doi: 10.1007/s10558-010-9098-8

Huotari, M., Vehkaoja, A., Mtt, K., and Kostamovaara, J. (2011). Photoplethysmography and its detailed pulse waveform analysis for arterial stiffness. *J. Mechan. Mater. Struct.* 44, 345–362. Available online at: http://rmseura.tkk.fi/rmlehti/2011/nro4/RakMek_44_4_2011_4.pdf

Huynh, T. H., Jafari, R., and Chung, W. (2018). Noninvasive cuffless blood pressure estimation using pulse transit time and impedance plethysmography. *IEEE Trans. Biomed. Eng.* 66, 967-976. doi: 10.1109/TBME.2018.2865751

Keissar, K., Maestri, R., Pinna, G., T La Rovere, M., and Gilad, O. (2010). Non-invasive baroreflex sensitivity assessment using wavelet transfer function-based time-frequency analysis. *Physiol. Measure.* 31, 1021–1036. doi: 10.1088/0967-3334/31/7/011

La Rovere, M. T., Pinna, G. D., and Raczak, G. (2008). Baroreflex sensitivity: measurement and clinical implications. *Ann. Noninvas. Electrocard.* 13, 191–207. doi: 10.1111/j.1542-474X.2008.00219.x

Lázaro, J., Gil, E., Bailón, R., Mincholé, A., and Laguna, P. (2013). Deriving respiration from photoplethysmographic pulse width. *Med. Biol. Eng. Comput.* 51, 233–242. doi: 10.1007/s11517-012-0954-0

Lázaro, J., Gil, E., Vergara, J. M., and Laguna, P. (2014). Pulse rate variability analysis for discrimination of sleep-apnea-related decreases in the amplitude fluctuations of pulse photoplethysmographic signal in children. *IEEE J. Biomed. Health Inform.* 18, 240–246. doi: 10.1109/JBHI.2013.2267096

Lázaro, J., Kontaxis, S., Bailón, R., Laguna, P., and Gil, E. (2018). "Respiratory rate derived from pulse photoplethysmographic signal by pulse decomposition analysis," in *2018 40th Annual International Conference of the IEEE Engineering in Medicine and Biology Society (EMBC)* (Honolulu, HI), 5282–5285.

Lázaro, J., Bailón, R., Laguna, P., Marozas, V., Rapalis, A., and Gil, E. (2016). "Difference in pulse arrival time at forehead and at finger as a surrogate of pulse transit time," in *2016 Computing in Cardiology Conference (CinC)* (Vancouver, BC), 269–272.

Li, Y., Wang, Z., Zhang, L., Yang, X., and Song, J. (2014). Characters available in photoplethysmogram for blood pressure estimation: beyond the pulse transit time. *Australas. Phys. Eng. Sci. Med.* 37, 367–376. doi: 10.1007/s13246-014-0269-6

Liu, H., Ivanov, K., Wang, Y., and Wang, L. (2015). Toward a smartphone application for estimation of pulse transit time. *Sensors* 15, 27303–27321. doi: 10.3390/s151027303

Liu, Q., Poon, C., and Zhang, Y. (2011). Time frequency analysis of variabilities of heart rate, systolic blood pressure and pulse transit time before and after exercise using the recursive autoregressive model. *Biomed. Signal Proc. Control* 6, 364–369.

Martin, S. L.-O., Carek, A. M., Kim, C.-S., Ashouri, H., Inan, O. T., and Hahn, Jin-Oh amd Mukkamala, R. (2016). Weighing scale-based pulse transit time is a superior marker of blood pressure than conventional pulse arrival time. *Sci. Rep.* 6:39273. doi: 10.1038/srep39273

Martínez, J., Almeida, R., Olmos, S., and Rocha, A. P., L. P. (2004). A wavelet-based ecg delineator: evaluation on standard databases. *IEEE Trans. Biomed. Eng.* 51, 570–581. doi: 10.1109/TBME.2003.821031

Mukkamala, R., Hahn, J., Inan, O. T., Mestha, L. K., Kim, C., Treyin, H., and Kyal, S. (2015). Toward ubiquitous blood pressure monitoring via pulse transit time: Theory and practice. *IEEE Trans. Biomed. Eng.* 62, 1879–1901. doi: 10.1109/TBME.2015.2441951

Nowak, J., Ocon, A., Taneja, I., Medow, M., and Stewart, J. (2008). Multi-resolution wavelet analysis of time-dependent physiological responses in syncopal youths. *Am. J. Phys. Heart Circ. Phys.* 296, H171–H179. doi: 10.1152/ajpheart.00963.2008

Orini, M., Bail, R., Mainardi, L., Laguna, P., and Flandrin, P. (2011). Characterization of dynamic interactions between cardiovascular signals by time-frequency coherence. *IEEE Trans. Biomed. Eng.* 59, 663–673. doi: 10.1109/TBME.2011.2171959

Orini, M., Laguna, P., Mainardi, L. T., and Bailón, R. (2012). Assessment of the dynamic interactions between heart rate and arterial pressure by the cross time frequency analysis. *Physiol. Measure.* 33, 315–331. doi: 10.1088/0967-3334/33/3/315

Pinna, G. D., Porta, A., Maestri, R., De Maria, B., Dalla Vecchia, L. A., and La Rovere, M. T. (2017). Different estimation methods of spontaneous baroreflex sensitivity have different predictive value in heart failure patients. *J. Hyperten.* 35, 1666–1675. doi: 10.1097/HJH.0000000000001377

Posada-Quintero, H. F., Delisle-Rodriguez, D., Cuadra-Sanz, M. B., and de la Vara-Prieto, R. R. F. (2013). Evaluation of pulse rate variability obtained by the pulse onsets of the photoplethysmographic signal. *Physiol. Meas.* 34, 179–187. doi: 10.1088/0967-3334/34/2/179

Ranucci, M., Porta, A., Bari, V., Pistuddi, V., and La Rovere, M. T. (2017). Baroreflex sensitivity and outcomes following coronary surgery. *PLoS ONE* 12:e175008. doi: 10.1371/journal.pone.0175008

Robertson, D., Diedrich, A., and Chapleau, M. (2012). Afferent baroreflex failure. *Auton. Neurosci.* 172, 1–3. doi: 10.1016/j.autneu.2012.10.010

Schfer, A. and Vagedes, J. (2013). How accurate is pulse rate variability as an estimate of heart rate variability?: A review on studies comparing photoplethysmographic technology with an electrocardiogram. *Int. J. Cardiol.* 166, 15–29. doi: 10.1016/j.ijcard.2012.03.119

Wang, Y., Liu, Z., and Ma, S. (2018). Cuff-less blood pressure measurement from dual-channel photoplethysmographic signals via peripheral pulse transit time with singular spectrum analysis. *Physiol. Measure.* 39:025010. doi: 10.1088/1361-6579/aa996d

Wong, J. S., Lu, W. A., Wu, K. T., Liu, M., Chen, G. Y., and Kuo, C. D. (2012). A comparative study of pulse rate variability and heart rate variability in healthy subjects. *J. Clin. Monitor. Comput.* 26, 107–114. doi: 10.1007/s10877-012-9340-6.

Conflict of Interest Statement: The authors declare that the research was conducted in the absence of any commercial or financial relationships that could be construed as a potential conflict of interest.

frontiers in Physiology

ORIGINAL RESEARCH
published: 30 April 2019
doi: 10.3389/fphys.2019.00478

Cardiac Baroreflex, HRV, and Statistics: An Interdisciplinary Approach in Hypertension

*Nadia Solaro[1], Mara Malacarne[2], Massimo Pagani[2] and Daniela Lucini[2]**

[1] Department of Statistics and Quantitative Methods, University of Milano-Bicocca, Milan, Italy, [2] BIOMETRA Department, University of Milan, Milan, Italy

Interests about the fine underpinnings of cardiovascular beat-by-beat variability have historical roots. Over the last decades, various aspects of the relationships between arterial pressure and heart period were taken as a proxy of the baroreflex in physiology and medicine, stimulating the interest of investigators in several interconnected scientific fields, in particular, bioengineering, neurophysiology, and clinical medicine. Studies of the overall system facilitated the emergence of a simplified negative (vagal) feedback model of the baroreflex and overshadowed the simultaneous interaction with excitatory, sympathetic positive-feedback mechanisms that would, however, better suit the model of a "paired antagonistic (parasympathetic/sympathetic) innervation of the internal organs." From the bioengineering side, the simplicity of obtaining the series of subsequent RR intervals stimulated the analysis of beat-by-beat variations, providing a multitude of heart rate variability (HRV) indices considered as proxies of the underlying sympatho-vagal balance, and participating to the management of several important clinical conditions, such as hypertension. In this context, advanced statistical methods, used in an integrated manner and controlling for age and gender biases, might help shed new light on the relationship between cardiac baroreflex, assessed by the frequency domain index α, and the HRV indices with the varying of systolic arterial pressure (SAP) levels. The focus is also on a novel unitary Autonomic Nervous System Index (ANSI) built as a synthesis of HRV considering its three most informative proxies [RR, RR variance, and the rest-stand difference in the normalized power of low-frequency (LF) variability component]. Data from a relatively large set of healthy subjects (n = 1154) with a broad range of SAP [from normal (n_{Nt} = 778) to elevated (n_{Ht} = 232)] show that, e.g., α and ANSI significantly correlate overall (r = 0.523, $p < 0.001$), and that this correlation is lower in hypertensives (r = 0.444, $p < 0.001$) and higher in pre-hypertensives (r = 0.618, $p < 0.001$) than in normotensives (r = 0.5, $p < 0.001$). That suggests the existence of curvilinear "umbrella" patterns that might better describe the effects of the SAP states on the relationships between baroreflex and HRV. By a mix of robust, non-parametric and resampling statistical techniques, we give empirical support to this study hypothesis and show that the pre-hypertensive group results at the apex/bottom in most of the studied trends.

Keywords: neural control, non-parametric bootstrap, non-parametric inference, patterned alternatives, physiopathology, sympathetic activity, vagal activity, Winsorized correlation coefficient

OPEN ACCESS

Edited by:
Maja Elstad,
University of Oslo, Norway

Reviewed by:
Jens Tank,
Helmholtz Association of German Research Centres (HZ), Germany
Alessandro Silvani,
Università degli Studi di Bologna, Italy

****Correspondence:***
Daniela Lucini
daniela.lucini@unimi.it

Specialty section:
This article was submitted to Autonomic Neuroscience, a section of the journal Frontiers in Physiology

Received: *20 December 2018*
Accepted: *05 April 2019*
Published: *30 April 2019*

Citation:
Solaro N, Malacarne M, Pagani M and Lucini D (2019) Cardiac Baroreflex, HRV, and Statistics: An Interdisciplinary Approach in Hypertension. Front. Physiol. 10:478. doi: 10.3389/fphys.2019.00478

INTRODUCTION

Since seminal studies by Sayers (1973) and Akselrod et al. (1981) a few decades ago it became clear that beat-by-beat oscillations in RR interval [usually alluded to as heart rate variability (HRV; Task Force of the European Society of Cardiology and the North American Society of Pacing, and Electrophysiology, 1996)] contain hidden information on underlying neural control mechanisms, based on the instantaneous balance between parasympathetic and sympathetic (inhibitory, excitatory) mechanisms (Malliani et al., 1991). Slowly initially, and faster subsequently, the increasing number of studies, now surpassing 23,000 in the Medline database, witness beyond doubt the growing interest on HRV as a *de facto* standard.

Even a simple cursory look at available literature, it appears that HRV may spark interest for different reasons, i.e., biological and technical, alone or combined, risking to favor debates about semantics rather than substance (Brown, 2017):

(1) First of all semantics: HRV (i.e., variability of heart rate computed as the number of beats/time in minutes) is frequently used interchangeably with RR V (i.e., variability of RR interval, in ms). RR V is taken as a proxy of PP interval (with some imprecision; Takahashi et al., 2016), and considered dependent of the dynamical interaction between the efferent vagal and sympathetic firing, combined with the humoral milieu and genetic substratum (D'Souza et al., 2014).

(2) HRV may be conceived as a proxy of the powerful beat-by-beat neural regulation of cardiovascular system in health and disease, providing a simple, non-invasive, means to estimate the changing equilibrium of the "paired antagonistic innervation" (Hess, 2014) (sympathetic and parasympathetic) governing RR interval. Contrary to historical considerations that "all autonomic nerves [are] motor" (Langley, 1921), evidence suggests that cardiac innervation can be represented by a dual pathway (sympathetic and parasympathetic) (Malliani et al., 1991) made up of mixed (efferent, i.e., motor, and afferent, i.e., sensory) nerves, subserving negative (mostly vagal) and positive (essentially sympathetic – Pagani et al., 1982; Malliani and Montano, 2002) feedback reflexes. Central structures (such as the recently highlighted Central Autonomic Network – Benarroch, 1993) coordinate and govern a number of nuclei exiting in a continuous flow of inhibitory and excitatory activity regulating the (sympatho-vagal) balance, hence eventually determining hemodynamic performance. Accordingly, any given setting of peripheral demands corresponds to a parallel distribution of arterial pressures and flows throughout the peripheral circulation. In physiological conditions at rest vagal activity prevails over sympathetic activity (White and Raven, 2014), approximately 4:1, and during activation, such as with exercise, the relationship is reversed, but even at maximal stimulation some level of vagal activity remains.

(3) HRV may be treated within a bioengineering ontology (Task Force of the European Society of Cardiology and the North American Society of Pacing, and Electrophysiology, 1996), considering the variability signal and various modalities of its management. Accordingly, mathematical manipulations may help define best ways to extract information (Haken, 1983) on the relative inhibitory and excitatory drives to the SA node, but also as a more subtle indicator of the underlying balance between positive and negative feedback circuits. Modeling and computing should not, however, be overemphasized against more attention and clinical sense (Karemaker, 1997) as suggested by a series of recent and older reviews and debates (e.g., Eckberg, 1997; Malliani et al., 1998; Paton et al., 2005; Billman, 2013; Pagani et al., 2018).

(4) In this context, advanced statistical analysis approaches combining non-parametric, robust, and resampling techniques might prove helpful to provide practical tools (e.g., graphical analysis) for easier clinical applications, or to extract unexpected relationships between variables (Lucini et al., 2018). Concurrently since initial studies, it was clear that the proxies of autonomic regulation were carrying different types of encoded information. For instance, limiting our considerations to a linear ontology, years ago we explored the use of a synthetic descriptor of the sympatho-vagal balance employing the numerical ratio between low frequency (LF) and high frequency (HF) components detected with spectral analysis of the RR variability signal (Pagani et al., 1986). Subsequently, it was also clear that amplitude (such as HRV) and frequency coding (particularly well represented by LF and HF in normalized units) provide different types of information (Pagani and Malliani, 2000). As suggested by electroneurographic recordings (Schwartz et al., 1973) and complex multivariate statistics (Lucini et al., 2018), amplitude and frequency codes should both be considered in the modeling of RR V. In this way, it is possible to reduce the number of significant proxies and minimize redundancy.

(5) Recently, we applied factor analysis in order to reduce the large number of indices that are provided by spectral analysis of RR V and found that the major part of information (82.7%) embedded in RR V is carried by three clusters of indices of homogeneous meaning (Sala et al., 2017). Factor loadings suggest the following clusters: normalized autonomic indices, absolute indices, and heart period. The introduction of a unitary Autonomic Nervous System Index (ANSI) may provide a way of further reducing information proxies (Sala et al., 2017). Notably this finding, as with all new findings, should be treated with caution.

From a clinical perspective, it is crucial to recall that HRV (particularly its time domain proxies) provides sensitive markers of prognosis in several conditions, particularly in coronary artery disease, predicting mortality in post-myocardial infarction (Huikuri and Stein, 2013).

Indeed the potential importance of assessing the short-term baroreflex control of heart rate/heart period as a means to describe clinical conditions was well established since several decades ago for hypertension (Bristow et al., 1969), heart failure (Eckberg et al., 1971), in addition to a strong predictive capacity for post-myocardial infarction mortality (La Rovere et al., 1998), even in animals (Billman et al., 1982). Implicitly these findings support the view of an integrated complex two-way (afferent/efferent) neural substratum of visceral regulation, at variance with the traditional efferent only view proposed by Langley (1921). It should also be considered that explicit acceptance of a mixed neural model of the autonomic (!) innervation could clear large fraction of the existing inconsistencies about HRV interpretation. This aspect is beyond the aim of the present study.

In the light of the above, here we aim to assess whether the application of advanced statistical tools, used in an integrated manner, might help unravel novel aspects of the (bivariate) relationships between the cardiac baroreflex and the autonomic indices (or proxies or measures) from RR V and arterial pressure variability, as initially exemplified by simple correlation. Data from a relatively large set of healthy subjects with a broad range of systolic arterial pressure (SAP, from normal to elevated) show that, in general, the frequency domain index α and the ANS proxies have significant (positive or negative) correlations. Accordingly, by a statistical data-driven approach, instead of model-based, we investigate, first, how cardiac baroreflex, as reflected by the α index, and ANS proxies [inclusive of ANSI (Sala et al., 2017)] match. We then assess how SAP levels affect these relationships, according to the study hypothesis that non-normotensive states could induce changes in the strength and significance of this kind of relationships.

We focus specifically on the role of SAP. Although arterial pressure values describe a continuum in the population, arterial hypertension definitions contemplate categories based on both systolic and diastolic thresholds, with slightly different values according to specific guidelines (Muntner et al., 2018). In this context, it is well recognized that SAP lowering (SPRINT Research Group, 2015) may be more important than diastolic blood pressure as an independent predictor of cardiovascular risk (Mourad, 2008). Systolic blood pressure also enjoys a specific role in hypertension treatment, whereby intensive lowering provides additional clinical benefit, as shown by the SPRINT Research Group (2015).

We express, from a statistical point of view, the effects of the three SAP categories (normotensive, pre-hypertensive, and hypertensive states) on the bivariate relationships between the α index and the ANS proxies as specific patterns of trends, i.e., increasing or decreasing trend as well as the so-called "umbrella" trend, which consists of concave- or convex-shape effects. To assess such effects and overcome several drawbacks inherent in the data under analysis (i.e., spurious age and gender effects, presence of subjects with outlying characteristics, improperness of the usual normality assumption), we carry out statistical analyses by combining a series of methods. Preliminarily, we set up so-called adjusted variables, i.e., the α index and the ANS proxies statistically transformed to be free of age and gender effects, in order to prevent results and conclusions of the study from potential biases caused by personal data not directly comparable (Lucini et al., 2018). On the other hand, ANSI being already free of age and gender effects by construction (Sala et al., 2017) requires no further transformation. Then, we use a robust measure of correlation computed with the Winsorizing method (Wilcox, 2012) in order to avoid potential influence of outlying subjects on the evaluation of the strength of the linear relationships under study. After that, we apply non-parametric statistical inference procedures (Hollander et al., 2014) on the Winsorized correlation (WINcorr) coefficients between the adjusted α index and adjusted ANS proxies plus ANSI to detect the presence of the hypothesized patterned effects without introducing any normality assumption. Finally, we perform all the statistical analyses in a resampling perspective according to the non-parametric bootstrap procedure (Davison and Hinkley, 1997) in order to give a more general value to the conclusions drawn. Results are displayed through convenient graphical tools that aim at providing valuable insights into the examined trends.

MATERIALS AND METHODS

Data for this observational, cross-sectional study, which is part of an ongoing series of investigations, focus on the use of autonomic indices in cardiovascular prevention. They refer to a population of 1154 ambulant subjects, who visited our outpatient Exercise Medicine Clinic for reasons varying from a health check-up to cardiovascular prevention (Lucini and Pagani, 2012) for chronic conditions, inclusive of hypertension (considering untreated, non-smokers individuals within the 17–86 years age range). The protocol of the study followed the principles of the Declaration of Helsinki and Title 45, US Code of Federal Regulations, Part 46, Protection of Human Subjects, Revised 13 November 2001, effective 13 December 2001. The project was approved by the Independent Ethics Committee of IRCCS Humanitas Clinical Institute (Rozzano, Italy). All subjects provided informed consent to participate.

Autonomic Evaluation

Our approach to the non-invasive evaluation of autonomic regulation has recently been summarized (Lucini et al., 2018). In brief, ECG, non-invasive (Finometer, TNO, Netherlands) arterial pressure and respiratory activity (piezoelectric belt, Marazza, Italy) are acquired on a PC. Beat-by-beat data series of 5 min rest followed by 5 min upright data are analyzed off-line with dedicated software (Badilini et al., 2005). As described previously (Pagani et al., 1986), from the autoregressive spectral analysis of RR interval and arterial pressure variability, a series of indices indirectly reflecting cardiovascular autonomic modulation is derived (**Table 1**). The software tool (Badilini et al., 2005) labels spectral components with a center frequency of 0.03–0.14 Hz as LF, and components within the range 0.15–0.35 Hz as HF, verifying the existence of an elevated coherence between RR variability and respiration. In addition, recordings of subjects with arrhythmias or LF breathing are discarded

TABLE 1 | Definition of the variables (ANS proxies plus ANSI) employed in the study[a].

Vars.[b]	Units	Definition
HR	beat/min	Heart rate
RR Mean	ms	Average of RR interval from tachogram
RR TP	ms^2	RR variance from tachogram
RR LFa	ms^2	Absolute power (a) of LF component of RR variability (V)
RR HFa	ms^2	Absolute power (a) of HF component of RRV
RR LFnu	nu	Normalized power (nu) of LF component of RRV
RR HFnu	nu	Normalized power (nu) of HF component of RRV
RR LF/HF	–	Ratio between absolute values of LF and HF
ΔRRLFnu	nu	Difference in LF power in nu between stand and rest
α index	ms/mmHg	Frequency domain measure of baroreflex gain
SAP	mmHg	SAP by sphygmomanometer
DAP	mmHg	Diastolic arterial pressure by sphygmomanometer
SAP Mean	mmHg	Average of systogram (i.e., SAP variability by Finometer)
SAP LFa	$mmHg^2$	Absolute power of LF component of systogram
ANSI[c]		Composite index of Autonomic Nervous System computed as a synthesis of RR Mean, RR TP, and ΔRR LFnu

*[a]Modified from Lucini et al. (2018). [b]LF components are comprised within the limits 0.03–0.14 Hz; HF components are comprised within the limits 0.14–0.45 Hz. Nu is obtained as P(f)nu = [P(f)/(RR TP−VLF)] * 100, where P is the component power, f corresponds to either LF or HF, and VLF indicates the power of the very LF (0–0.03 Hz) component. α index = average of the square root of the ratio between RR interval and SA pressure spectral powers of the LF and HF components. [c]More detailed definition in Sala et al. (2017). In brief, ANSI is computed in three stages: (1) to let the proxies be comparable in terms of magnitude, scale, and unit of measurement, and free them from age and gender effects, the percentile rank transformation is applied to RR Mean, RR TP, and ΔRRLFnu within each combination of gender and classes of age (**Table 3**); (2) an individual radar plot is built for each subject using the values of the transformed RR Mean, RR TP, and ΔRR LFnu. Each plot then contains a triangle with side lengths in the [0, 100] range; (3) the final ANS indicator is computed as the area of the triangles, which is subsequently transformed by percentile ranks over all the set of subjects. Ranging from 0 to 100 by construction, ANSI has an immediate clinical interpretation: the higher the value of ANSI, the better the individual autonomic condition, and vice versa, the lower the value, the worse the autonomic condition.*

(Lucini et al., 2017). The gain of cardiac baroreflex is also assessed by a bivariate method (α index = average of the square root of the ratio between RR interval and SA Pressure Spectral powers of the LF and HF components; Pagani et al., 1988). Finally, a unitary autonomic system index (ANSI) is derived from the three HRV most informative measures (RR, RR total power, and stand-rest difference of LF_{RR} in normalized units), as described in Sala et al. (2017). ANSI is treated as a percent ranked unitary proxy of cardiac autonomic regulation, by design free of age and gender bias. It should be pointed out that there is a still ongoing debate regarding the interpretation of individual autonomic indices, in particular LF/HF as markers of the sympathovagal balance (Billman, 2013). Of probably greater importance is the alternative view of the sympathetics and the vagi as functioning in a purely efferent system (Langley, 1921) or a sympatho-vagal dual feedback (negative and positive) organization. A summary of these aspects has recently been published (Pagani et al., 2018).

Statistics

Participants to the study, amounting to 1154 in all, were divided into the three SAP groups: normotensive (Nt), pre-hypertensive (preHt), and hypertensive (Ht), according to the definition reported in **Table 2** (second column). The majority of individuals fell into the Nt group (67.4%), while the others into the Ht (20.1%) and preHt (12.5%) groups, respectively. We introduced the further subdivision of the Nt and Ht groups in the SAP intervals indicated in the last column of **Table 2** in order to better meet the aims of statistical analyses, as will be described soon after.

We inspected potential links between baroreflex gain and HRV using the set of the 14 ANS measures listed in **Table 1**, which we treated as proxies of cardiovascular autonomic modulation and SAP variability. We included, as well, ANSI, which is a composite index of ANS set up such that it is free of age and gender effects (Sala et al., 2017, and legend below **Table 1**). Controlling for age and gender effects was one of the main problems with which we had to cope. Age and gender are biological parameters that inevitably affect the ANS proxies and the composition of the three SAP groups, this latter shown in **Table 3** within the combinations of gender and classes of age. For instance, almost 84% of Nt subjects are individuals with less than or equal to 49 years of age in both female (55.98% out of 1154) and male (44.02% out of 1154) groups. In the preHt group, this percentage reduces to 64.3% within females and 62.5% within males, while in the Ht group to 35.3% within females and 56.9% within males.

For the same arguments extensively discussed in Lucini et al. (2018), and with the same methodology therein presented, we accomplished the comparability among the SAP groups by statistically transforming the original ANS proxies in such a

TABLE 2 | Frequency and percentage distributions of the participants to the study within the three SAP groups and further subdivision in seven SAP intervals.

SAP groups	Definition[a]	Count	Percentage	Further subdivision in SAP intervals[b]
Normotensive (Nt)	Subjects with SAP $<$ 130 mmHg	778	67.4%	Nt1 [80,100): 84 subjs (7.3%) Nt2 [100,110): 158 subjs (13.7%) Nt3 [110,120): 282 subjs (24.4%) Nt4 [120,130): 254 subjs (22.0%)
Pre-hypertensive (preHt)	Subjects with 130 $\leq$ SAP $<$ 140 mmHg	144	12.5%	preHt [130,140): 144 subjs (12.5%)
Hypertensive (Ht)	Subjects with SAP $\geq$ 140 mmHg	232	20.1%	Ht1 [140,160): 167 subjs (14.5%) Ht2 [160,220]: 65 subjs (5.6%)
Total		1154	100.0%	

[a]Recalculated from Muntner et al. (2018). [b]For Nt and Ht groups only.

TABLE 3 | Distribution of the 1154 participants to the study by gender and classes of age within the three SAP groups.

Gender				SAP groups			Total
				Nt	preHt	Ht	
Female	Age in class	17–30	Count	204	8	4	216
			%	41.8	14.3	3.9	33.4
		31–49	Count	204	28	32	264
			%	41.8	50.0	31.4	40.9
		50–86	Count	80	20	66	166
			%	16.4	35.7	64.7	25.7
	Total		Count	488	56	102	646
			%	100.0	100.0	100.0	100.0
Male	Age in class	17–30	Count	124	17	14	155
			%	42.8	19.3	10.8	30.5
		31–49	Count	118	38	60	216
			%	40.7	43.2	46.1	42.5
		50–86	Count	48	33	56	137
			%	16.5	37.5	43.1	27.0
	Total		Count	290	88	130	508
			%	100.0	100.0	100.0	100.0

way they were free of age and gender effects. In short, we fitted a two-way full ANOVA model for each ANS proxy regarded as the dependent variable, and classes of age and gender as the independent variables through their main effects and interaction. Because not affected by age and gender, the resulting ANOVA residuals (given for each proxy by the difference between observed and predicted values) were referred to as *adjusted ANS proxies*, and accordingly used in place of the original ANS proxies in all the subsequent statistical analyses.

Following Lucini et al. (2002), our study hypothesis was that potential connections, observed over the total set of subjects, between the baroreflex gain (as measured by the α index) and the other ANS proxies could differ in strength, direction, or statistical significance depending on the SAP group. Focusing specifically on the linear relation (or correlation) between the α index and the other variables listed in **Table 1**, we were interested in assessing whether the preHt group could represent a sort of transition state from Nt to Ht group in which the correlations between the α index and the other ANS proxies plus ANSI could even strengthen. This research question mostly arose from our experience in analyzing this type data, where frequently we had observed non-monotonic (or curvilinear) effects of SAP groups on the correlations involving the α index.

As a preliminary analysis illustrating the main idea, **Figure 1** reports the scatter plots of the original ANS proxies and ANSI against the α index set up over the entire set of subjects, while these same graphs related to the three SAP groups are in the **Supplementary Material**. For each bivariate comparison involving the α index, Pearson correlation coefficients r and the p-values, obtained by the usual procedure based on the standardized normal distribution for testing the null hypothesis H_0: $\rho = 0$ against the alternative H_1: $\rho \neq 0$ (at the 0.05 nominal level), are reported above each panel. All the correlation coefficients result significantly different to zero; nevertheless, as expected, they have different magnitude and sign. For example, the correlation coefficients of α and RR TP ($r = 0.653$, $p < 0.001$), and α and ANSI ($r = 0.523$, $p < 0.001$), both denote at least medium positive linear relations, while a more moderate negative correlation is observed between α and SAP Mean ($r = -0.414$, $p < 0.001$) and a weaker negative correlation between α and RR LFHF ($r = -0.202$, $p < 0.001$). Nonetheless, by performing the same kind of analysis within each SAP group, we observed that the correlations involving α might strengthen or weaken depending on the SAP groups (**Supplementary Figures S1–S3** in **Supplementary Material**). For example, there is a medium correlation of α and ANSI overall ($r = 0.523$, $p < 0.001$) as well as in the Nt group ($r = 0.5$, $p < 0.001$), but the correlation tends to weaken in the Ht group ($r = 0.444$, $p < 0.001$) and strengthens in the preHt group ($r = 0.618$, $p < 0.001$). Again, the correlation of α and RR LFnu is weakly negative overall ($r = -0.281$, $p < 0.001$) and in the Nt group ($r = -0.261$, $p < 0.001$), but it is not significantly different from zero in the Ht group ($r = -0.033$, $p < 0.538$). All that seems then to evidence the presence of either monotonic- or curvilinear-type effects of the SAP groups on the correlations between the α index and the other variables.

The analyses performed such as in **Figure 1** also opened us a critical viewpoint concerning the choice of the statistical methodology to apply. Most importantly, that kind of inspection suffers from several weakness points. First, as already observed, the original ANS proxies are affected by age and gender effects, so that a more cautionary approach would require to deal with the adjusted ANS proxies (while ANSI is already free of such effects). Second, a few anomalous values appear as isolated points in the scatter plots. These correspond to subjects having outlying characteristics on several (but not all) measures. That is a typical situation that might occur with data collected from autoregressive spectral analysis of RR variability. As known in the statistical literature, the Pearson correlation coefficient is extremely sensitive to the presence of outliers. Accordingly, one recommendation is to carry out statistical analyses by using alternative strategies. We overcame this problem by relying on robust statistical measures (Wilcox, 2012) instead of removing outlying subjects from the set of data because in this second case the total amount of the available information would have been reduced. Third, to give a more general value to the conclusions drawn on the dataset at hand, it would have been more fitting to replicate the study on additional sets of data, or alternatively, on a much broader set of data suitable to be split, e.g., at random, into a series of subsets on which replicating the analyses separately. Since the whole available dataset was large enough to meet our analysis objectives, but not large enough to be split into subsets, we decided to turn to statistical resampling techniques, such as the bootstrap (Efron, 1982; Davison and Hinkley, 1997). Finally, we preferred not to apply the classical inferential procedures based on the normality assumption, which could have been too much restrictive in our case, and carry out, instead, the analyses by a purely non-parametric approach (Hollander et al., 2014).

In the light of the above issues, correlations between the α index and the other variables listed in **Table 1** were inspected both over the whole set of subjects and within the SAP groups by

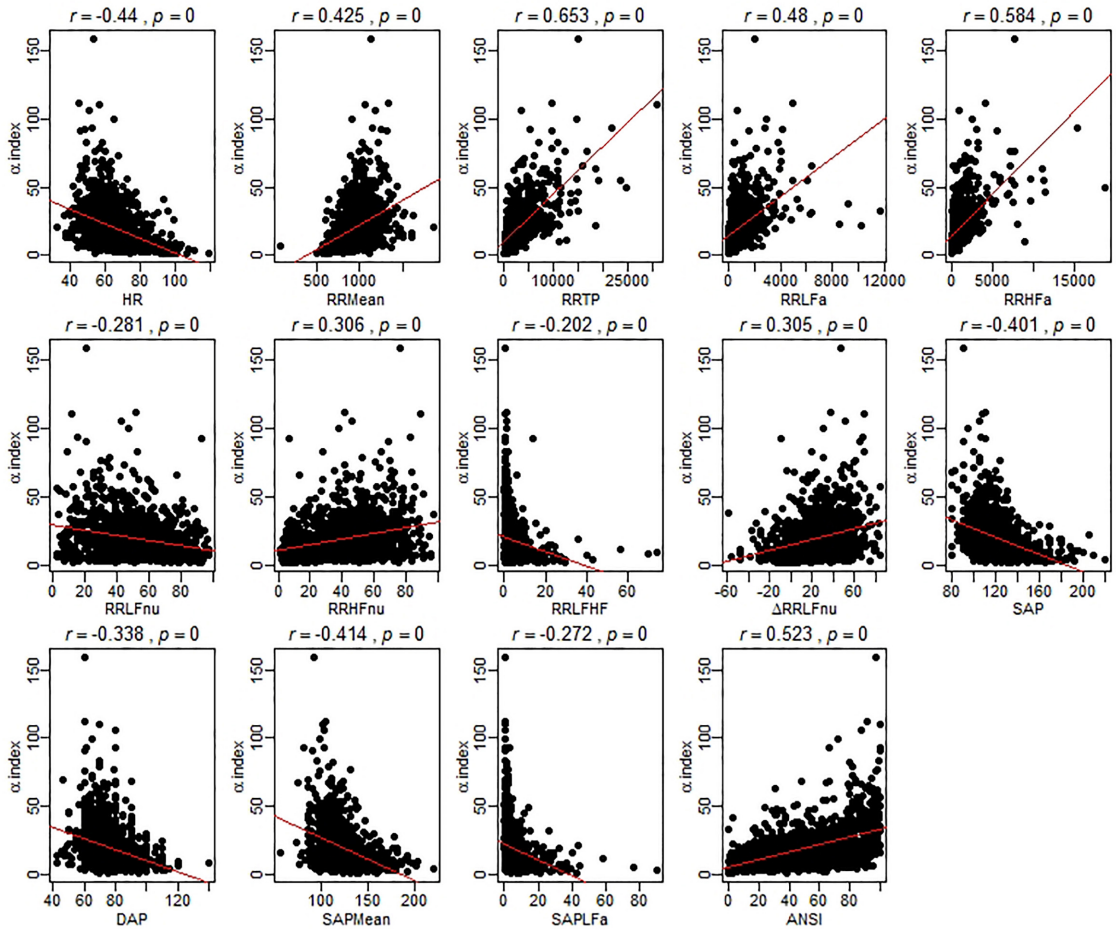

FIGURE 1 | Scatter plots of the α index against the ANS proxies and ANSI over the whole set of subjects. The Pearson correlation coefficient r between the α index and each of the other ANS proxies plus ANSI is written above each panel, together with the p-value of the standard procedure for testing: H_0: $\rho = 0$ against H_1: $\rho \neq 0$. In each panel, the regression line (with parameters estimated by the ordinary least-squares method) is depicted in red. It is worth stressing that these regression lines are used only as graphical references for better visualization of the spread of the point clouds, i.e., the α index is not regarded as the dependent variable of a regression model.

using the ANS proxies adjusted for age and gender effects and the following statistical methods (for which further methodological details are given in **Figure 2**):

(1) As a robust measure of correlation, we used the γ-WINcorr coefficient (Wilcox, 2012), with a proportion γ equal to 0.1. Winsorization consists of estimating the means, the variances, and the covariance involved in the Pearson correlation coefficient formula of two generic variables X_1 and X_2 by, first, computing their γ-th and (1 – γ)-th order quantiles and then replacing the first proportion γ and the last proportion 1 – γ of their values with these estimated quantiles. In such a way, two Winsorized distributions are obtained for X_1 and X_2 to which the Pearson correlation formula is applied (Wilcox, 2012);

(2) having decided to introduce no assumption for the data distribution, as a resampling technique we applied the non-parametric stratified balanced bootstrap to generate $B = 5000$ bootstrap replicates from the original data, i.e., 5000 new datasets each of size equal to $n = 1154$ subjects with $p = 16$ variables (the adjusted ANS proxies plus ANSI, and the classification variable given by the SAP group membership), which were set up such that:

(a) by balancing, over the whole set of the nB bootstrap observations generated, the same subject was randomly sampled (with repetition) for exactly B times, but he/she might not be present in each of the B bootstrap replicates or might be present twice or more in any bootstrap replicate. In such a way, simulation errors were reduced considerably in comparison with the ordinary bootstrap procedure (Davison et al., 1986);

(b) by stratification, in each of the B bootstrap replicates we reproduced the structure of the original data concerning the classification of subjects into the SAP groups. We had no reasonable indication for assuming a weighting schema different from the percentages computed on the original data (**Table 2**, fourth column). However, we had

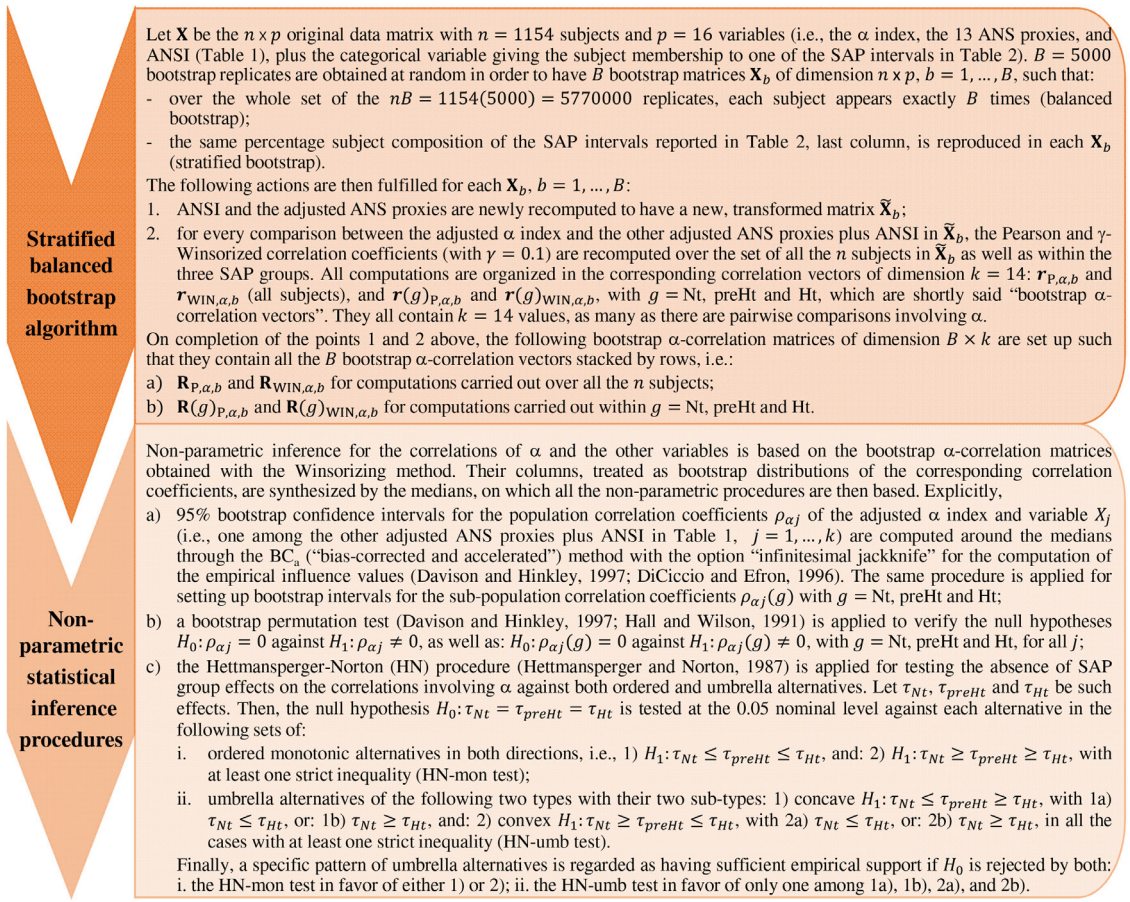

FIGURE 2 | The bootstrap algorithm and the statistical methodology for non-parametric inference.

to take into account that especially the Nt group had an internal considerably heterogeneous composition [i.e., SAP ranges from 80 to 130 mmHg (excl.)] as well as the size of the three SAP groups was strongly unbalanced. Accordingly, to prevent potential distortions caused by the heterogeneous within-groups compositions and the different size of the SAP groups, we applied the bootstrap by stratifying within the SAP intervals defined in the last column of **Table 2**. Such intervals represent a further subdivision of the Nt and Ht groups into sub-groups of a more similar (though not equal) size that are internally more SAP homogeneous. Each bootstrap replicate was therefore randomly generated to contain n = 1154 (not necessarily distinct) subjects falling into the SAP intervals in the same percentages as those reported in the last column of **Table 2**.

The adjusted ANS proxies and ANSI were recomputed on each of the B = 5000 bootstrap replicates obtained. In its turn, the WINcorr coefficient was computed on each replicate and for every comparison between the adjusted α index and the other ANS proxies plus ANSI, both over the whole set of subjects and within the SAP groups. In such a way, we obtained 5000 values of the WINcorr coefficient (i.e., a bootstrap distribution) for each type of examination and each pairwise comparison involving the α index. As a synthesis of the multitude of these bootstrap distributions, we used the median rather than the mean for reducing the influence of potential anomalous values on subsequent analysis results;

(3) non-parametric inference was drawn, both on the overall set of subjects and within the SAP groups, on the medians of the bootstrap WINcorr coefficients according to the following three approaches:

(a) with the aim of providing plausible ranges of variation for every correlation coefficient involving the α index, non-parametric 95% bootstrap confidence intervals were computed through the BC_a (i.e., "bias-corrected and accelerated" intervals, given as adjusted bootstrap percentiles) method (DiCiccio and Efron, 1996; Davison and Hinkley, 1997);

(b) to test the null hypothesis of zero correlation coefficients of the α index and the other variables, a bootstrap permutation test (Hall and Wilson, 1991; Davison

and Hinkley, 1997) was applied at the 0.05 nominal significance level;

(c) in line with the study hypothesis above described, we applied the Hettmansperger–Norton trend test (Hettmansperger and Norton, 1987) to verify the hypothesis, at the 0.05 nominal significance level, of no effect of the SAP groups on the correlation coefficients concerning the α index against the following two sets of patterned alternatives (explicitly presented in **Figure 2**):
   (i) the SAP groups have increasing/decreasing effects on the strength of the correlations (so-called monotonic ordered alternatives, similar to linear contrasts);
   (ii) the SAP groups have concave- or convex-shape effects on the strength of the correlations (so-called umbrella alternatives, similar to quadratic or curvilinear contrasts).

With the aim of simplifying the interpretations, we will present most of the findings obtained by the bootstrap procedure and the non-parametric inference through a synoptic figure and several graphs, such as the correlation plot and the ridgeline plot. In particular, this last graph turned out to be a powerful tool for visualization of the SAP group effects and their trend patterns, consistently with the Hettmansperger–Norton procedure.

All the statistical analyses and the pertaining routine codes were implemented in the R software, version 3.5.1 (R Core Team, 2018), along with the R libraries: "boot" for the bootstrap (Canty and Ripley, 2017); "corrplot" for the correlation plot in **Figure 4** (Wei and Simko, 2017); "ggplot2" (Wickham, 2016) and "ggridges" (Wilke, 2018) for the ridgeline plots in **Figure 6**; "pseudorank" for the Hettmansperger–Norton test (Happ et al., 2018); and "WRS2" for computation of the WINcorr coefficients (Mair and Wilcox, 2018).

RESULTS

Descriptive data concerning the original ANS proxies and ANSI are given in **Table 4** as means and standard deviations computed over the whole set of subjects and within the three SAP groups. A further inspection based on the box plots of the distributions of the (both original and adjusted) ANS proxies and ANSI within the SAP groups is reported in SM. As expected, RR Mean, RR TP, RR LFa, RR HFa, RR HFnu, ΔRR LFnu, and the α index present the highest mean values in the Nt group and the smallest ones in the Ht group. On the other hand, HR, SAP, DAP, SAP Mean, and SAP LFa have the highest mean values in the Ht group, and the smallest ones in the Nt group. The preHt group has the largest mean values for RR LFnu and RR LF/HF, and the Nt group the smallest ones. Regarding ANSI, it is worth observing that its mean values decrease from the Nt group to the Ht group, thus proving its sensitivity to the different ANS states observed under the various SAP conditions.

Regarding the bootstrap analysis, **Figure 3** displays panels of box plots of the within-groups bootstrap distributions of the WINcorr coefficients (with $\gamma = 0.1$) computed for every pairwise comparison involving the adjusted α index with the other adjusted ANS proxies along with ANSI (**Figure 2**). At a first insight, the umbrella pattern appears in its entire evidence in line with our study hypothesis, especially in some of the panels. For example, in the first panel concerning the WINcorr coefficient between the adjusted α and HR, it can be seen a convex effect of the SAP condition on the strength of the negative correlation, i.e., the negative linear relationship between α and HR (the higher the HR values, the smaller the α values) tends to strengthen in the preHt group. On the other hand, in the last panel concerning the WINcorr coefficient between the adjusted α and ANSI, a concave effect can be clearly seen, i.e., the positive linear relationship between α and ANSI (the higher the ANSI values, the higher the α values) tends to strengthen, once again, in the preHt group.

The bootstrap within-groups WINcorr distributions in **Figure 3** are used, through their medians, as empirical support to draw non-parametric inference. As a first result, **Table 5** shows plausible ranges of variations, set up for both the whole set of subjects and the SAP groups, of the correlation coefficients between the adjusted α index and the other variables. These ranges are given by the non-parametric 95% bootstrap confidence intervals computed using the medians of the WINcorr coefficients. Pearson correlation coefficients of the adjusted variables computed on the original dataset are as well reported (second column, **Table 5**). Moreover, the cells in the first three columns of **Table 5** are differently depicted according to the strength and sign of correlations (legend below **Table 5**). Several remarks are worth making. First, overall the medians of the WINcorr coefficients prove to be similar in both magnitude and sign to the Pearson correlation coefficients. No substantial change of interval of strength is then observed. However, winsorization has resulted in coefficients that are all, in the Nt group, or nearly all, in the whole set, slightly higher than the Pearson coefficients, while, on the other hand, in the preHt and Ht groups there is a mix of situations (i.e., some are higher, and some others are smaller than the Pearson coefficients). Moreover, by the figure reported in the legend of **Table 5**, it can be seen that winsorization has led, above all, to higher correlation coefficients (roughly +0.2) between α and RR LFa as well as RR HFa (in the preHt group especially), and to lower coefficients (nearly −0.1) between α and RR LF/HF as well as SAP LFa. Second, although the sign of both Pearson and WINcorr coefficients does not change across the groups, it is the magnitude that changes, especially moving from the Nt group to the Ht group. Regarding, in particular, the HRV measures RR LFnu, RR HFnu, RR LF/HF, ΔRR LFnu, along with SAP, DAP, SAP Mean, and SAP LFa, the strength of the linear relations with the α index reduces in the Ht group. Third, the bootstrap confidence intervals present fairly small widths in the whole set of subjects (0.096 on average) as well as in the Nt group (0.121 on average), thus suggesting that the strength of correlation in the various comparisons is appraised with high stability. On the other hand, the confidence intervals result wider in the preHt (0.270 on average) and Ht groups (0.240 on average), thus reflecting a greater internal heterogeneity of these two groups that is bolstered by their smaller sizes than the Nt group.

Figure 4 displays the correlation plot of the medians of the WINcorr coefficients, computed over the whole set of subjects and within the SAP groups, along with the results of the

TABLE 4 | Descriptive data (mean and standard deviation) of the ANS proxies and ANSI within the SAP groups and over the whole set of subjects.

	Nt		preHt		Ht		Total	
Vars.	**Mean**	***SD***	**Mean**	***SD***	**Mean**	***SD***	**Mean**	***SD***
HR	65.89	11.70	69.36	14.61	70.57	11.73	67.26	12.26
RR Mean	939.53	175.87	905.08	201.39	874.83	155.46	922.23	177.22
RR TP	3058.75	3233.55	2029.50	2944.21	1372.62	1271.78	2591.34	2988.47
RR LFa	895.37	1131.48	673.62	1173.97	423.88	523.82	777.87	1063.05
RR HFa	1016.94	1632.69	466.58	1744.07	262.98	495.39	805.99	1529.22
RR LFnu	50.08	21.08	57.75	22.28	56.73	21.90	52.37	21.63
RR HFnu	42.95	20.98	34.54	21.76	33.51	20.12	40.00	21.32
RR LF/HF	2.45	4.55	4.51	7.50	3.89	6.64	3.00	5.52
ΔRRLFnu	27.95	21.97	15.24	21.16	13.73	20.61	23.51	22.51
α index	23.23	16.96	13.36	10.20	10.19	6.36	19.38	15.69
SAP	111.78	10.27	132.22	2.71	152.81	15.02	122.58	19.78
DAP	70.86	8.61	82.31	8.32	92.07	11.62	76.55	12.65
SAP Mean	114.63	12.68	132.23	11.64	151.80	16.54	124.30	20.08
SAP LFa	4.14	5.40	6.49	9.14	7.11	10.09	5.03	7.22
ANSI	54.45	28.46	42.51	30.79	39.95	25.46	50.04	28.88

In every comparison among the within-groups means of each variable, a green cell denotes the largest computed mean, while a gray cell denotes the smallest computed mean.

bootstrap permutation procedure for testing the hypotheses of null correlation coefficients between the α index and each of the other variables, all adjusted for age and gender effects. Corresponding *p*-values are reported in the legend. In the graph, cells containing non-significant coefficients are marked with an X symbol. As can be seen, the hypothesis of the absence of a linear relation involving the α index is accepted at the 0.05 level: in the Nt group, with DAP; in the preHt group, with RR LFnu and RR HFnu; in the Ht group, with RR LFnu, RR HFnu, RR LF/HF, ΔRR LFnu, SAP, DAP, and SAP Mean. All this seems to support our starting conjecture about the existence of SAP group effects on the pairwise relationships between α and the other considered variables.

Regarding the trend analysis, **Figure 5** combines the results obtained with the bootstrap permutation test and the Hettmansperger–Norton (HN) trend test, this latter having as alternatives both monotonic ordered and umbrella effects of the SAP groups (**Figure 2**). Two aspects appear immediately. First, in all the considered pairwise comparisons, the HN test proves that there are at least either increasing or decreasing effects of the SAP condition on the strength of correlations between α and the other variables (**Figure 5**, second column). For instance, the positive correlation of α and RR TP tends to strengthen from Nt to preHt and Ht (a similar trend is observed for RR LFa and RR HFa). On the other hand, the positive correlation of α and RR HFnu tends to weaken and approach to zero from Nt to preHt and Ht. Second, in nearly all the pairwise comparisons, there is clear empirical evidence toward the presence of umbrella effects of either concave or convex shape (**Figure 5**, third column). For example, the negative correlation between the α index and HR, or also the positive correlation between the α index and ANSI, prove to be stronger in the preHt group than in the other two groups. The last two columns in **Figure 5** sum up all the main findings concerning the detection of the SAP groups in which the strongest linear relationships involving α are observed. It is worth pointing out that in just 10 out of the total 14 pairwise comparisons the preHt group turns out to be the one in which the linear relations involving α result as the strongest ones. Specifically, in preHt, there are the strongest positive correlations between α and RR Mean, RR TP, RR HFa, ΔRR LFnu, and ANSI, respectively, and the strongest negative correlations between α and HR, RR LF/HF, SAP, DAP, and SAP Mean. On the other hand, in Nt, there are the strongest positive correlation of α and RR HFnu, and the strongest negative correlations of α and RR LFnu and SAPLFa, while in Ht, there is the strongest positive correlation of α and RR LFa. Nonetheless, saying "the strongest correlation" does not necessarily intend a correlation of high magnitude, but only that is the highest estimated correlation (in absolute value) in the comparison among the three SAP groups. Accordingly, the cells in the last two columns of **Figure 5** are colored with different shades consistently with the interval of correlation strength (legend below **Table 5**) into which the pertaining 95% bootstrap confidence interval falls. Once again, the preHt group has a particular role because the α index proves to have a strong magnitude of positive correlation with RR HFa (95% CI: [0.610, 0.800]) and ANSI (95% CI: [0.599, 0.771]), respectively.

These interpretations can be visualized better through the ridgeline plots in **Figure 6**, in particular by observing, in each panel, the relative position of the smoothed density curves that interpolate the bootstrap distributions of the within-groups WINcorr coefficients.

DISCUSSION

By using non-parametric and robust statistical procedures, combined in the perspective of a multitude of simulated

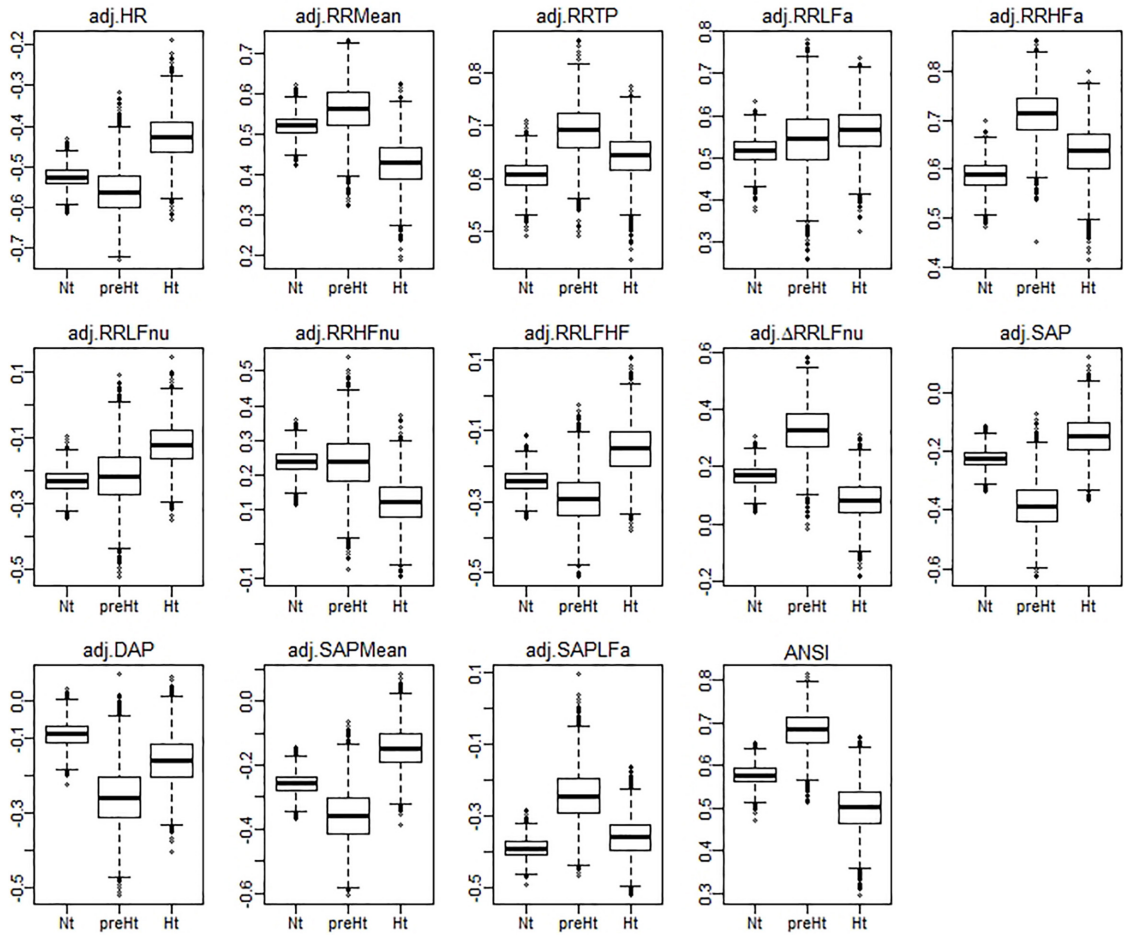

FIGURE 3 | Box plots of the bootstrap distributions of the WINcorr coefficients (with $\gamma = 0.1$) of the adjusted α index and the adjusted ANS proxies along with ANSI computed within the SAP groups over the $B = 5000$ bootstrap replicates.

replications of the study, we give empirical support to the conjecture, inspired by our empirical practice, that there exist specific pressure states in which the relationship between the cardiac baroreflex and ANS proxies can strengthen or weaken. We have turned this conjecture into practical terms by introducing the trend analysis of the SAP group effects on the correlations between the α index and each of the ANS proxies along with ANSI after adjustment for the potential biases by age and gender. We have focused on both ordered monotonic trends, i.e., increasing or decreasing effects moving from the Nt group to the Ht group, and umbrella trends, i.e., concave- or convex-shape effects concerning which the preHt group is regarded as an intermediate transition pressure condition.

Undoubtedly, a delicate issue that we had to face concerned the fact that the results found should not *strictly* depend on the adopted statistical methodology. All the more so because at present, we are not able yet to advance plausible explanations of such an observed phenomenon. In order to avoid potential straining caused by the applied statistical methods, although robust and non-parametric, we conducted an extensive preliminary study using alternative techniques to make the conclusions as far as possible untied from the specific analysis approach. In short, the results so obtained gave, in every case, empirical support to the existence of the patterned trends related to the SAP group memberships such as the ones presented.

Ultimately, the study and the statistical analyses we addressed should be more appropriately considered as a first exploratory phase toward a broader investigation that should also take into account the role of other individual characteristics (e.g., lifestyles), which we guess might affect the results found here to some extent.

Further Considerations Concerning the Statistical Approach

As already pointed out, the statistical approach we adopted to meet the objectives of the study was designed in order to overcome several drawbacks inherent in the type of data under analysis, namely:

(a) the different age-by-gender composition of the whole set of subjects, which led us to introduce the adjusted ANS

proxies (while ANSI is free of age and gender effects by construction);

(b) the presence of a small subset of outlying subjects concerning certain, but not all, variables, a problem that required us to use the WINcorr coefficient as a robust measure of the linear relationship between the α index and each of the other variables listed in **Table 1**;

(c) the necessity of providing a more general value to the statistical analyses without having the possibility of replicating the data collection on new sets of subjects, a fact that we overcame by turning to the bootstrap resampling technique;

(d) the improperness of the normality assumption for the bootstrap distributions of the WINcorr coefficients, for which reason we preferred to apply a non-parametric approach for both the bootstrap procedure and the inference.

Nevertheless, to ascertain which procedures or variants of the statistical methods could be the fittest ones to the data, at a preliminary stage we had to perform an extensive exploratory study and examine a range of alternative options. At the same time, this preliminary study allowed us to assess whether the main findings were as far as possible untied from the specific statistical approach used. One of the main problems was to assess the value of the proportion γ for the application of the Winsorizing method in the computation of correlation coefficients. We carried out the bootstrap procedure and all the subsequent analyses described in **Figure 2** in the presence of three tentative values of the quantile order, i.e., γ = 0.05, 0.1, 0.2. Given that there were no noteworthy difference in the results, we fixed γ equal to 0.1 as a sort of "compromise value," in order to avoid either still having a small number of outliers (γ = 0.05) or censoring the correlation coefficient distributions too much (γ = 0.2), especially in the preHt group, which is the SAP group with the smallest size (**Table 2**).

Another critical point was the choice of the non-parametric tests to employ against patterned alternatives. The typical distribution-free procedures adopted for testing, on the one hand, ordered monotonic and, on the other hand, umbrella alternatives are the Jonckheere–Terpstra (JT) test and the Mack–Wolfe (MW) test, respectively (Hollander et al., 2014). However, it is well-known that, in the presence of within-groups distributions with unequal variances, these tests are no

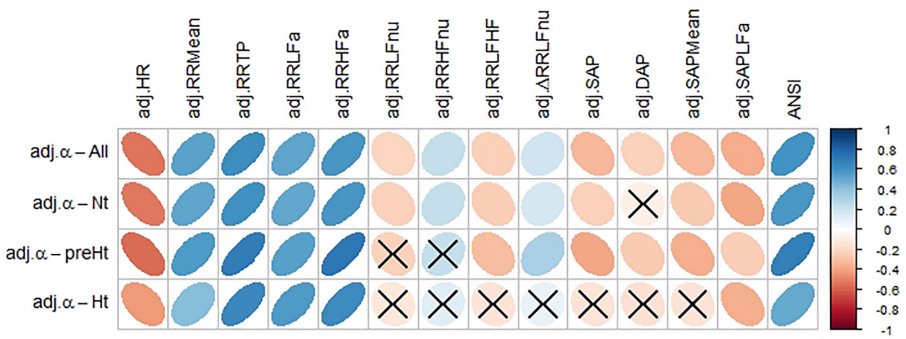

FIGURE 4 | Correlation plot of the WINcorr coefficients (with γ = 0.1) between the adjusted α index and ANS proxies plus ANSI over the whole set of subjects and within the SAP groups. A cross placed on an ellipse in the cells indicates a non-significant result at the 0.05 nominal significance level achieved by the bootstrap permutation test (*B* = 5000 replicates). The corresponding *p*-values are given in the following table:

Variables	adj.α - All	adj.α - Nt	adj.α - preHt	adj.α - Ht
adj.HR	0	0	0	0
adj.RRMean	0	0	0	0
adj.RRTP	0	0	0	0
adj.RRLFa	0	0	0	0
adj.RRHFa	0	0	0	0
adj.RRLFnu	0	0	0.071	0.170
adj.RRHFnu	0	0	0.051	0.185
adj.RRLFHF	0	0	0.010	0.108
adj.ΔRRLFnu	0	0.018	0.009	0.296
adj.SAP	0	0.001	0.003	0.118
adj.DAP	0	0.292	0.035	0.085
adj.SAPMean	0	0	0.005	0.104
adj.SAPLFa	0	0	0.041	0
ANSI	0	0	0	0

A cell is colored in light yellow in the presence of a non-significant result.

TABLE 5 | Non-parametric 95% bootstrap confidence intervals for the medians of the WINcorr coefficients (B = 5000 bootstrap replicates, γ = 0.1) between the adjusted α index and ANS proxies plus ANSI over the whole set of subjects and within the SAP groups.

Variables	Pearson corr coefficients	Median of WINcorr coefficients	95% Low confidence limit	95% Upper confidence limit
All subjects				
adj.HR	−0.499	**−0.531**	−0.573	−0.491
adj.RRMean	0.488	**0.531**	0.490	0.576
adj.RRTP	0.606	**0.619**	0.574	0.661
adj.RRLFa	0.442	**0.527**	0.477	0.583
adj.RRHFa	0.522	**0.589**	0.538	0.637
adj.RRLFnu	**−0.223**	−0.218	−0.276	−0.168
adj.RRHFnu	0.232	**0.237**	0.188	0.298
adj.RRLFHF	−0.153	**−0.230**	−0.285	−0.186
adj.ΔRRLFnu	0.198	0.198	0.145	0.262
adj.SAP	−0.279	**−0.325**	−0.372	−0.277
adj.DAP	−0.203	**−0.223**	−0.275	−0.172
adj.SAPMean	−0.305	**−0.331**	−0.380	−0.284
adj.SAPLFa	−0.267	**−0.368**	−0.412	−0.326
ANSI	0.571	**0.593**	0.558	0.634
Normotensive				
adj.HR	−0.496	**−0.527**	−0.579	−0.478
adj.RRMean	0.476	**0.521**	0.471	0.577
adj.RRTP	0.604	**0.607**	0.553	0.661
adj.RRLFa	0.438	**0.516**	0.456	0.581
adj.RRHFa	0.534	**0.588**	0.528	0.647
adj.RRLFnu	−0.211	**−0.230**	−0.301	−0.167
adj.RRHFnu	0.209	**0.238**	0.177	0.314
adj.RRLFHF	−0.161	**−0.240**	−0.314	−0.188
adj.ΔRRLFnu	0.156	**0.169**	0.106	0.247
adj.SAP	−0.208	**−0.223**	−0.292	−0.163
adj.DAP	−0.073	**−0.090**	−0.162	−0.024
adj.SAPMean	−0.255	**−0.258**	−0.325	−0.195
adj.SAPLFa	−0.302	**−0.390**	−0.441	−0.339
ANSI	0.550	**0.577**	0.531	0.625
Pre-hypertensive				
adj.HR	**−0.570**	−0.563	−0.673	−0.441
adj.RRMean	**0.569**	0.565	0.438	0.681
adj.RRTP	0.589	**0.692**	0.592	0.778
adj.RRLFa	0.397	**0.546**	0.402	0.691
adj.RRHFa	0.461	**0.713**	0.610	0.800
adj.RRLFnu	**−0.265**	−0.217	−0.417	−0.081
adj.RRHFnu	**0.291**	0.236	0.095	0.416
adj.RRLFHF	−0.186	**−0.293**	−0.469	−0.190
adj.ΔRRLFnu	**0.367**	0.330	0.175	0.494
adj.SAP	**−0.404**	−0.387	−0.531	−0.222
adj.DAP	**−0.306**	−0.259	−0.417	−0.111
adj.SAPMean	−0.327	**−0.358**	−0.532	−0.213
adj.SAPLFa	−0.207	**−0.245**	−0.400	−0.115
ANSI	**0.703**	0.684	0.599	0.771
Hypertensive				
adj.HR	**−0.483**	−0.428	−0.541	−0.320
adj.RRMean	**0.491**	0.429	0.318	0.543
adj.RRTP	0.640	**0.644**	0.563	0.724
adj.RRLFa	0.501	**0.567**	0.464	0.677
adj.RRHFa	0.525	**0.638**	0.512	0.720
adj.RRLFnu	**−0.135**	−0.123	−0.271	−0.014

(Continued)

TABLE 5 | Continued

Variables	Pearson corr coefficients	Median of WINcorr coefficients	95% Low confidence limit	95% Upper confidence limit
adj.RRHFnu	**0.149**	0.121	0.007	0.268
adj.RRLFHF	−0.102	**−0.151**	−0.299	−0.029
adj.ΔRRLFnu	**0.142**	0.083	−0.044	0.227
adj.SAP	−0.135	**−0.147**	−0.297	−0.023
adj.DAP	**−0.170**	−0.161	−0.322	−0.049
adj.SAPMean	**−0.158**	−0.147	−0.293	−0.032
adj.SAPLFa	−0.281	**−0.359**	−0.458	−0.260
ANSI	**0.558**	0.502	0.394	0.604

Pearson correlation coefficients of the adjusted variables (computed on the original dataset) are as well reported. Cells in the columns entitled "Pearson corr" and "Median of WINcorr" are colored differently according to the following intervals of correlation strength:

- Negative correlation coefficients:

strong	medium	moderate	weak / nearly null
(−0.8, −0.6]	(−0.6, −0.4]	(−0.4, −0.2]	(−0.2, 0)

- Positive correlation coefficients:

weak / nearly null	moderate	medium	strong
[0, +0.2)	[+0.2, +0.4)	[+0.4, +0.6)	[+0.6, +0.8)

The cells containing the variable names (first column) are colored in the same way as the cells in the WINcorr column. Bold values in the columns "Pearson corr" and "Median of WINcorr" refer to the pairwise comparisons between the two types of correlation coefficients, i.e., a coefficient in bold denotes that it is the largest (in absolute value) between the two types. The following graph depicts the differences: "Median of WINcorr – Pearson corr" as colored squares.

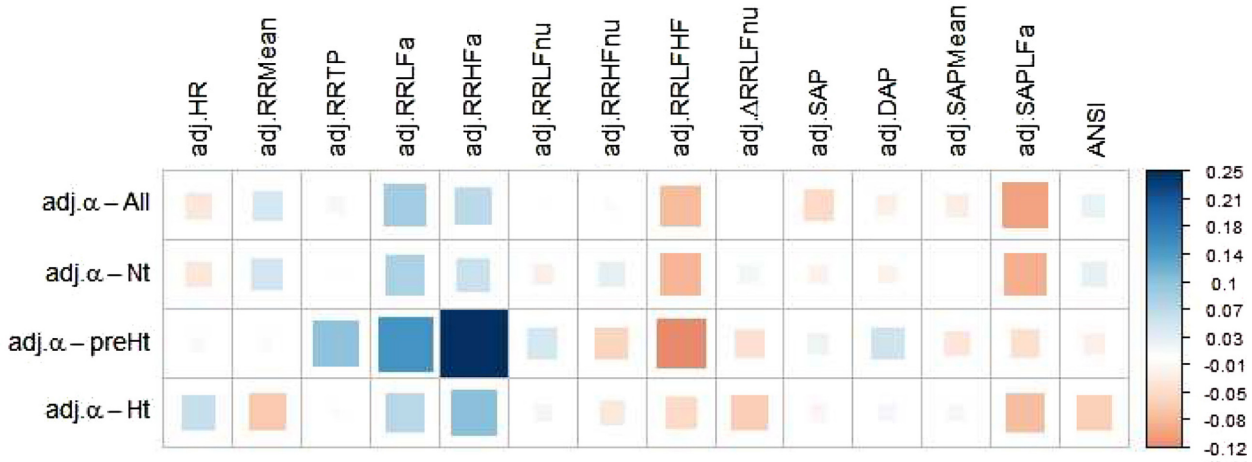

more distribution-free (Hollander et al., 2014). The bootstrap within-groups distributions of the WINcorr coefficients present this problem, as it was verified on the data through the opportune procedures (i.e., the usual tests for the homogeneity of variances, results omitted). Consequently, the JT and MW test results are not sufficiently trustworthy. Among all the possible alternative procedures (Hollander et al., 2014), the choice fell on the HN test, because it is less sensitive to the inequality of variances as well as it allows specifying various patterns of trends among the alternatives in a straightforward way (**Figure 2**).

As a final remark, we decided to carry out the analyses between the α index and the ANS proxies according to a bivariate, rather than a multivariate, approach. We are aware that the ANS proxies are, in their turn, pairwise correlated with different strength and sign, and that a multivariate approach could have taken into account these intertwined connections at best. Nonetheless, this would have required us to use methods of synthesis of the data having as disadvantages the facts of introducing additional margins of error in the analyses as well as making the reading of the findings less clear from a clinical point of view.

Clinical Implications and Limitations

We have shown that statistical manipulation of population data might suggest the existence of trends other than monotonic, i.e., umbrella-like, underlying the linear relationships between baroreflex gain and ANS proxies when SAP levels are taken

Variables	BPerm test and HN test – monotonic trend	HN test – umbrella trend	SAP group with the strongest (negative or positive) correlation between the adjusted α index and each adjusted variable	95% bootstrap confidence interval for the magnitude of the strongest estimated correlation in the detected SAP group
adj.HR	↗ 0	∪	preHt −	$[-0.673, -0.441]$
adj.RRMean	↘ 0	∩	preHt +	$[0.438, 0.681]$
adj.RRTP	↗ +	∩	preHt +	$[0.592, 0.778]$
adj.RRLFa	↗ +	---	Ht +	$[0.464, 0.677]$
adj.RRHFa	↗ +	∩	preHt +	$[0.610, 0.800]$
adj.RRLFnu	↗ 0	---	Nt −	$[-0.276, -0.168]$
adj.RRHFnu	↘ 0	---	Nt +	$[0.188, 0.298]$
adj.RRLFHF	↗ 0	∪	preHt −	$[-0.469, -0.190]$
adj.ΔRRLFnu	↘ 0	∩	preHt +	$[0.175, 0.494]$
adj.SAP	↗ 0	∪	preHt −	$[-0.531, -0.222]$
adj.DAP	↘ −	∪	preHt −	$[-0.417, -0.111]$
adj.SAPMean	↗ 0	∪	preHt −	$[-0.532, -0.213]$
adj.SAPLFa	↗ 0	∩	Nt −	$[-0.412, -0.326]$
ANSI	↘ 0	∩	preHt +	$[0.599, 0.771]$

FIGURE 5 | Synoptic figure summing up the results of both the bootstrap permutation (BPerm) test for null correlations and Hettmansperger–Norton (HN) test for ordered monotonic alternatives and umbrella alternatives. In all the cases in which the null hypothesis (i.e., absence of the SAP group effects) is rejected, the *p*-value is $p < 0.001$. The trend of the SAP group effects on the correlation coefficients involving the adjusted α index is connoted as "increasing" or "decreasing" on the basis of the sorting of the three SAP groups in the following order: Nt as first, preHt as second, and Ht as third (like in the box plots in **Figure 3**). Accordingly, the symbols in the second column "BPerm test and HN test – monotonic trend" have the following meaning: ↗ 0: increasing trend from negative correlations to a nearly null correlation. ↗ 0: increasing trend from negative correlations to a not significantly different from zero correlation. ↘ 0: decreasing trend from positive correlations to a nearly null correlation. ↘ 0: decreasing trend from positive correlations to a not significantly different from zero correlation. ↗ +: increasing trend from positive correlations to positive correlations. ↘ −: decreasing trend from a not significantly different from zero correlation to negative correlations. Moreover, the symbols in the third column "HN test – umbrella trend" have the following meaning: ∪: convex alternative. ∩: concave alternative. --- : absence of empirical support. Finally, in the fourth column, the SAP group with the strongest (negative or positive) correlation between the α index and each of the other variables is detected by the overall summary of all the main findings, and the pertaining 95% bootstrap confidence interval from **Table 5** is reported in the last column. In particular, a blue cell with a + symbol reports the group where there is the strongest estimated positive correlation involving α, while an orange cell with a − symbol reports the group with the strongest estimated negative correlation involving α. The different shades of colors (brighter/less bright) denote confidence intervals of stronger/weaker correlations, according to the intervals of correlation strength given in the legend below **Table 5**.

into account. The performed statistical analyses have disclosed a peculiar role of preHt, which is positioned at the apex/bottom of a curvilinear trend in most of the examined correlations, especially between the α index and ANSI (pertaining panel in **Figures 3**, **6**), where the correlation strengthen particularly in the preHt group (**Table 5** and **Figure 5**).

Overall, this investigation has highlighted the existence of at least medium-strong correlations (i.e., equal to or greater than 0.4 in absolute value, **Table 5**) between the α index and several ANS proxies that keep in magnitude over the SAP groups. That might bear potentially important implications in the clinic, in particular, keeping in mind that the HRV proxies are extracted from the simple (ECG derived) tachogram (even if to an extent mathematically implicit). In fact, the time and resources necessary to obtain the α index [more so if using invasive arterial pressure, as originally proposed (Bristow et al., 1969)] represent a strong barrier to its introduction in the clinic, even if the clinical information provided by this measure is definitively impressive (La Rovere et al., 1998). If, on the other hand, the same (or rather similar) information is provided by simpler methods, such as by indices like HRV (Task Force of the European Society of Cardiology and the North American Society of Pacing, and Electrophysiology, 1996; La Rovere et al., 1998), the barrier in a sense could evaporate. In addition, the growing availability of simple, wearable instruments, and related SW applications is providing potentially everybody with a means to measure HRV and derived indices throughout the day and night. This possibility justifies the study of specific combinations

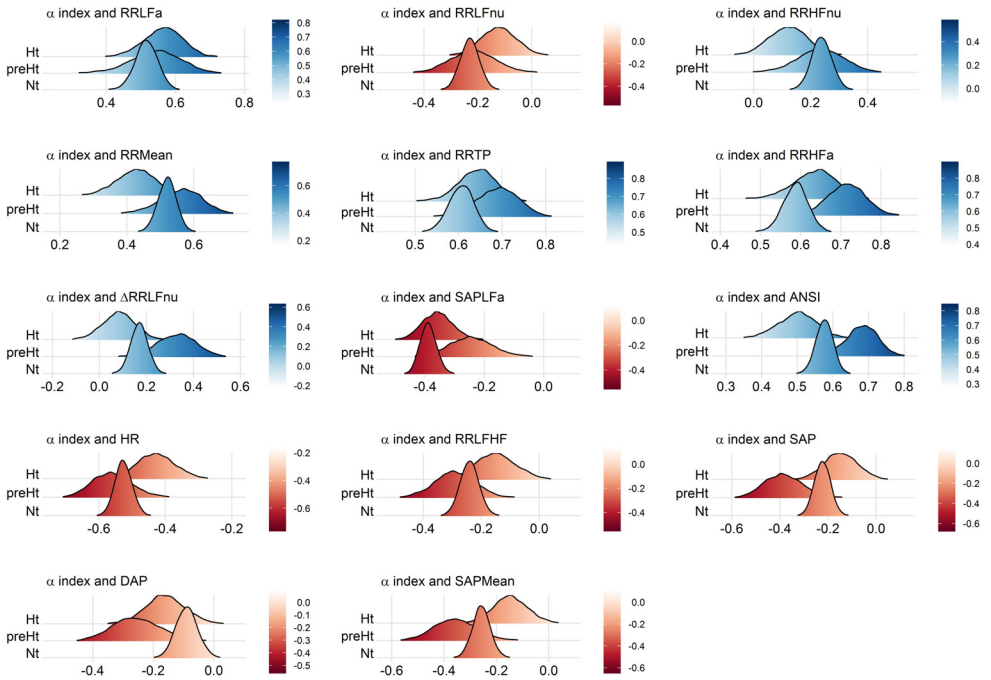

FIGURE 6 | Ridgeline plots of the bootstrap distributions of the WINcorr coefficients (with $\gamma = 0.1$) of the adjusted α index and the adjusted ANS proxies plus ANSI within the SAP groups. Blue density curves denote distributions of positive correlation values, while red density curves distributions of negative correlation values. First row of panels: presence of ordered monotonic effects (increasing or decreasing) of the SAP groups. Second–third rows of panels: presence of umbrella (concave-shape) effects of the SAP groups. Fourth–fifth rows of panels: presence of umbrella (convex-shape) effects of the SAP groups.

of instruments and SW applications, ideally in a supervised network, whereby preventive strategies might take advantage of personalized markers and indices, such as ANSI (Sala et al., 2017), that profit from the analogous power of information hidden in the baroreflex as predictive tool, ready to be incorporated, by proxy (i.e., HRV indices or ANSI), into clinical routines that need, however, to be more formally tested.

Among the limitations of the study, let us point out that our findings of significant correlations fall short of cause–effect relationship that would require different approaches to be tested [e.g., moving to causal inference analyses based on structural models for causality (Pearl, 2010)]. It should also be pointed out that although significant and with medium/strong magnitude (**Table 5** and **Figure 5**), within-groups correlation values between the α index and ANSI do not seem high enough to justify the use of ANSI to predict raw α-values. ANSI can only provide estimates of cardiac autonomic performance, as projected against a reference benchmark population (Sala et al., 2017).

CONCLUSION

In conclusions, we have shown that using a combination of robust and non-parametric statistical methods, along with the bootstrap, it is possible to overcome some of the major limitations ingrained into autonomic evaluation in a clinical setting. In particular, statistical manipulation of data based on adjusted variables frees the data structure from the inherent bias related to age and gender changes. In addition, information from relatively minor study groups can be improved in quality with statistical resampling techniques such as the bootstrap, which we implemented using a non-parametric procedure to avoid assuming conjectures about the distribution of the correlation coefficients of the α index and each of the other ANS proxies. It is also important to re-emphasize (Pagani and Malliani, 2000) that we are dealing with indirect data, hence variability proxies (e.g., LF component of RR variability) cannot provide detailed information of actual, raw electrophysiological figures of nerve activity but only suggest hypothesis about (Haken, 1983) general properties of autonomic regulation, within the overall model of a dual sympatho-vagal (Hess, 2014) contrasting balance (Malliani et al., 1991).

Finally, not choosing any *a priori* model for the data structure we were able to demonstrate the validity of non-monotonic effects of the SAP states on the relationships between the α index and the ANS proxies, disclosing an umbrella-like pattern, reminiscent of the cue function of arousal (Moruzzi and Magoun, 1949). That leaves us with a crucial indication that the α index (as a proxy of baroreflex gain) is medium-strongly correlated with several indices of ANS regulation (in particular, the composite indicator ANSI), further supporting the use in a clinical setting of the simpler HRV-derived proxies, thus reducing the economic and organizational bias and potential fostering a clinical use of ANS evaluation. There are potentially practical implications in clinical management, particularly of long-term conditions where autonomic impairment might be an important issue, such as in diabetic cardiac neuropathy

(Vinik and Ziegler, 2007), where traditional reflex-based models of examination have reached widespread standardization (Ewing et al., 1985). However, the introduction of novel diagnostic approaches, based on HRV and baroreflex gain, combined with advanced statistics, might facilitate the clinical assessment of graded autonomic impairment. A deeper assessment of the relationship between HRV and more complex autonomic indices, such as the baroreflex, might in addition provide a stronger and more rational basis for inferences supporting the widespread, sometimes aggressive, promotion of heart rate wearables. Furthermore, their use in a near future could also support distance-controlled, Internet-based, home-centered preventive behavioral (diet and exercise) therapies. The elevated computational power of modern wearables and smartphones, combined with the large bandwidth of Internet connections, permit to foresee applications providing personalized programs and regular support to individual patients (Wynter-Blyth and Moorthy, 2017) combining "soft" autonomic information with "hard" traditional clinical data (Editorial, 2004), avoiding to overload the health systems (Barnett, 2017).

ETHICS STATEMENT

This study was carried out in accordance with the recommendations of the Independent Ethics Committee of IRCCS Humanitas Clinical Institute (Rozzano, Italy) with written informed consent from all subjects. All subjects gave written informed consent in accordance with the Declaration of Helsinki. The general protocol was approved by the Independent Ethics Committee of IRCCS Humanitas Clinical Institute (Rozzano, Italy).

AUTHOR CONTRIBUTIONS

NS, MP, and DL contributed to conception and design of the study. MM contributed to data acquisition and database organization. NS designed the statistical methodological approach, implemented the R programming codes, and performed the statistical analyses. NS and MP wrote the first draft of the manuscript. All authors wrote sections of the manuscript and contributed to manuscript revision, read, and approved the submitted version.

SUPPLEMENTARY MATERIAL

The Supplementary Material for this article can be found online at: https://www.frontiersin.org/articles/10.3389/fphys.2019.00478/full#supplementary-material

REFERENCES

Akselrod, S., Gordon, D., Ubel, F. A., Shannon, D. C., Berger, A. C., and Cohen, R. J. (1981). Power spectrum analysis of heart rate fluctuation: a quantitative probe of beat-to-beat cardiovascular control. *Science* 213, 220–222. doi: 10.1126/science.6166045

Badilini, F., Pagani, M., and Porta, A. (2005). Heartscope: a software tool addressing autonomic nervous system regulation. *Comput. Cardiol.* 32, 259–262. doi: 10.1109/CIC.2005.1588086

Barnett, R. (2017). Case histories: hypertension. *Lancet* 389:2365.

Benarroch, E. E. (1993). The central autonomic network: functional organization, dysfunction, and perspective. *Mayo Clin. Proc.* 68, 988–1001. doi: 10.1016/S0025-6196(12)62272-1

Billman, G. E. (2013). The LF/HF ratio does not accurately measure cardiac sympatho-vagal balance. *Front. Physiol.* 4:26. doi: 10.3389/fphys.2013.00026

Billman, G. E., Schwartz, P. J., and Stone, H. L. (1982). Baroreceptor reflex control of heart rate: a predictor of sudden cardiac death. *Circulation* 66, 874–880. doi: 10.1161/01.CIR.66.4.874

Bristow, J. D., Honour, A. J., Pickering, G. W., Sleight, P., and Smyth, H. S. (1969). Diminished baroreflex sensitivity in high blood pressure. *Circulation* 39, 48–54. doi: 10.1161/01.CIR.39.1.48

Brown, D. (2017). *Origin: A Novel*. New York, NY: Random House Audio.

Canty, A., and Ripley, B. (2017). *Boot: Bootstrap R (S-Plus) Functions. R Package Version* 1.3-20. Available at: https://CRAN.R-project.org/package=boot

Davison, A. C., and Hinkley, D. V. (1997). *Bootstrap Methods and Their Application*. Cambridge: Cambridge University Press.

Davison, A. C., Hinkley, D. V., and Schechtman, E. (1986). Efficient bootstrap simulation. *Biometrika* 73, 555–566. doi: 10.1093/biomet/73.3.555

DiCiccio, T. J., and Efron, B. (1996). Bootstrap confidence intervals. *Stat. Sci.* 11, 189–212. doi: 10.1214/ss/1032280214

D'Souza, A., Bucchi, A., Johnsen, A. B., Logantha, S. J., Monfredi, O., Yanni, J., et al. (2014). Exercise training reduces resting heart rate via downregulation of the funny channel HCN4. *Nat. Commun.* 5:3775. doi: 10.1038/ncomms4775

Eckberg, D. L. (1997). Sympathovagal balance: a critical appraisal. *Circulation* 96, 3224–3232. doi: 10.1161/01.CIR.96.9.3224

Eckberg, D. L., Drabinsky, M., and Braunwald, E. (1971). Defective cardiac parasympathetic control in patients with heart disease. *N. Engl. J. Med.* 285, 877–883. doi: 10.1056/NEJM197110142851602

Editorial (2004). The soft science of medicine. *Lancet* 363:1247. doi: 10.1016/S0140-6736(04)16027-3

Efron, B. (1982). *The Jackknife, the Bootstrap and Other Resampling Plans*. Philadelphia, PA: SIAM, CBMS-NSF Regional Conference Series in Applied Mathematics, 38.

Ewing, D. J., Martyn, C. N., Young, R. J., and Clarke, B. F. (1985). The value of cardiovascular autonomic function tests: 10 years experience in diabetes. *Diab. Care* 8, 491–498. doi: 10.2337/diacare.8.5.491

Haken, H. (1983). *Synergetics: An Introduction*. Berlin: Springer–Verlag.

Hall, P., and Wilson, S. R. (1991). Two guidelines for bootstrap hypothesis testing. *Biometrics* 47, 757–762. doi: 10.2307/2532163

Happ, M., Zimmermann, G., Bathke, A. C., and Brunner, E. (2018). *Pseudorank: Pseudo-Ranks. R Package Version* 0.3.8. Available at: https://CRAN.R-project.org/package=pseudorank

Hess, W. R. (2014). *Nobel Lecture: The Central Control of the Activity of Internal Organs. Nobelprize.org.Nobel Media AB*. Available at: http://www.nobelprize.org/nobel_prizes/medicine/laureates/1949/hess-lecture.html

Hettmansperger, T. P., and Norton, R. M. (1987). Tests for patterned alternatives in k-sample problems. *J. Am. Stat. Assoc.* 82, 292–299. doi: 10.2307/2289166

Hollander, M., Wolfe, D. A., and Chicken, E. (2014). *Nonparametric Statistical Methods*, 3rd Edn. Hoboken, NJ: John Wiley & Sons.

Huikuri, H. V., and Stein, P. K. (2013). Heart rate variability in risk stratification of cardiac patients. *Prog. Cardiovasc. Dis.* 56, 153–159. doi: 10.1016/j.pcad.2013.07.003

Karemaker, J. M. (1997). Heart rate variability: why do spectral analysis? *Heart* 77, 99–101. doi: 10.1136/hrt.77.2.99

La Rovere, M. T., Bigger, J. T. Jr., Marcus, F. I., Mortara, A., and Schwartz, P. J. (1998). Baroreflex sensitivity and heart-rate variability in prediction of total cardiac mortality after myocardial infarction. ATRAMI (Autonomic Tone and Reflexes After Myocardial Infarction) Investigators. *Lancet* 351, 478–484. doi: 10.1016/S0140-6736(97)11144-8

Langley, J. N. (1921). *The Autonomic Nervous System (Pt. I)*. Cambridge: W. Heffer & Sons.

Lucini, D., Guzzetti, S., Casiraghi, S., and Pagani, M. (2002). Correlation between baroreflex gain and 24-h indices of heart rate variability. *J. Hypertens.* 20, 1625–1631. doi: 10.1097/00004872-200208000-00026

Lucini, D., Marchetti, I., Spataro, A., Malacarne, M., Benzi, M., Tamorri, S., et al. (2017). Heart rate variability to monitor performance in elite athletes: criticalities and avoidable pitfalls. *Int. J. Cardiol.* 240, 307–312. doi: 10.1016/j.ijcard.2017.05.001

Lucini, D., and Pagani, M. (2012). From stress to functional syndromes: an internist's point of view. *Eur. J. Intern. Med.* 23, 295–301. doi: 10.1016/j.ejim.2011.11.016

Lucini, D., Solaro, N., and Pagani, M. (2018). Autonomic differentiation map: a novel statistical tool for interpretation of heart rate variability. *Front. Physiol.* 9:401. doi: 10.3389/fphys.2018.00401

Mair, P., and Wilcox, R. (2018). *WRS2: Wilcox Robust Estimation and Testing. R Package Version* 0.10-0. Available at: https://CRAN.R-project.org/package=WRS2

Malliani, A., and Montano, N. (2002). Emerging excitatory role of cardiovascular sympathetic afferents in pathophysiological conditions. *Hypertension* 39, 63–68. doi: 10.1161/hy0102.099200

Malliani, A., Pagani, M., Lombardi, F., and Cerutti, S. (1991). Cardiovascular neural regulation explored in the frequency domain. *Circulation* 84, 482–492. doi: 10.1161/01.CIR.84.2.482

Malliani, A., Pagani, M., Montano, N., and Mela, G. S. (1998). Sympathovagal balance: a reappraisal. *Circulation* 98, 2640–2643. doi: 10.1161/circ.98.23.2640/a

Moruzzi, G., and Magoun, H. W. (1949). Brain stem reticular formation and activation of the EEG. *EEG Clin. Neurophysiol.* 1, 455–473. doi: 10.1016/0013-4694(49)90219-9

Mourad, J. J. (2008). The evolution of systolic blood pressure as a strong predictor of cardiovascular risk and the effectiveness of fixed-dose ARB/CCB combinations in lowering levels of this preferential target. *Vasc. Health Risk Manag.* 4, 1315–1325. doi: 10.2147/VHRM.S4073

Muntner, P., Carey, R. M., Gidding, S., Jones, D. W., Taler, S. J., Wright, J. T. Jr., et al. (2018). Potential US Population Impact of the 2017 ACC/AHA High Blood Pressure Guideline. *Circulation* 137, 109–118. doi: 10.1161/CIRCULATIONAHA.117.032582

Pagani, M., Lombardi, F., Guzzetti, S., Rimoldi, O., Furlan, R., Pizzinelli, P., et al. (1986). Power spectral analysis of heart rate and arterial pressure variabilities as a marker of sympatho-vagal interaction in man and conscious dog. *Circ. Res.* 59, 178–193. doi: 10.1161/01.RES.59.2.178

Pagani, M., and Malliani, A. (2000). Interpreting oscillations of muscle sympathetic nerve activity and heart rate variability. *J. Hypertens.* 18, 1709–1719. doi: 10.1097/00004872-200018120-00002

Pagani, M., Pizzinelli, P., Bergamaschi, M., and Malliani, A. (1982). A positive feedback sympathetic pressor reflex during stretch of the thoracic aorta in conscious dogs. *Circ. Res.* 50, 125–132. doi: 10.1161/01.RES.50.1.125

Pagani, M., Sala, R., Malacarne, M., and Lucini, D. (2018). Benchmarking heart rate variability to overcome sex-related bias. *Adv. Exp. Med. Biol.* 1065, 191–205. doi: 10.1007/978-3-319-77932-4_13

Pagani, M., Somers, V., Furlan, R., Dell'Orto, S., Conway, J., Baselli, G., et al. (1988). Changes in autonomic regulation induced by physical training in mild hypertension. *Hypertension* 12, 600–610. doi: 10.1161/01.HYP.12.6.600

Paton, J. F. R., Boscanc, P., Pickeringb, A. E., and Nalivaiko, E. (2005). The yin and yang of cardiac autonomic control: vago-sympathetic interactions revisited. *Brain Res Rev.* 49, 555–565. doi: 10.1016/j.brainresrev.2005.02.005

Pearl, J. (2010). An introduction to causal inference. *Int. J. Biostat.* 6, 1–59. doi: 10.2202/1557-4679.1203

R Core Team (2018). *R: A Language and Environment for Statistical Computing*. Vienna: R Foundation for Statistical Computing. Available at: https://www.R-project.org/

Sala, R., Malacarne, M., Solaro, N., Pagani, M., and Lucini, D. (2017). A composite autonomic index as unitary metric for heart rate variability: a proof of concept. *Eur. J. Clin. Invest.* 47, 241–249. doi: 10.1111/eci.12730

Sayers, B. M. (1973). Analysis of heart rate variability. *Ergonomics* 16, 17–32. doi: 10.1080/00140137308924479

Schwartz, P. J., Pagani, M., Lombardi, F., Malliani, A., and Brown, A. M. (1973). A cardiocardiac sympathovagal reflex in the cat. *Circ. Res.* 32, 215–220. doi: 10.1161/01.RES.32.2.215

Sprint Research Group (2015). A randomized trial of intensive versus standard blood-pressure control. *N. Engl. J. Med.* 373, 2103–2116. doi: 10.1056/NEJMoa1511939

Takahashi, M., Nakamoto, T., Matsukawa, K., Ishii, K., Watanabe, T., Sekikawa, K., et al. (2016). Cardiac parasympathetic outflow during dynamic exercise in humans estimated from power spectral analysis of P–P interval variability. *Exp. Physiol.* 101, 397–409. doi: 10.1113/EP085420

Task Force of the European Society of Cardiology and the North American Society of Pacing, and Electrophysiology (1996). Heart-rate variability: standards of measurements, physiological interpretation and clinical use. *Circulation* 93, 1043–1065. doi: 10.1161/01.CIR.93.5.1043

Vinik, A. I., and Ziegler, D. (2007). Diabetic cardiovascular autonomic neuropathy. *Circulation* 115, 387–397. doi: 10.1161/CIRCULATIONAHA.106.634949

Wei, T., and Simko, V. (2017). *R package "corrplot": Visualization of a Correlation Matrix (Version 0.84)*. Available at: https://CRAN.R-project.org/package=corrplot

White, D. W., and Raven, P. B. (2014). Autonomic neural control of heart rate during dynamic exercise: revisited. *J. Physiol.* 592, 2491–2500. doi: 10.1113/jphysiol.2014.271858

Wickham, H. (2016). *ggplot2: Elegant Graphics for Data Analysis*. New York, NY: Springer-Verlag.

Wilcox, R. R. (2012). *Introduction to Robust Estimation and Hypothesis Testing*, 3rd Edn. Amsterdam: Academic Press.

Wilke, C. O. (2018). *ggridges: Ridgeline Plots in "ggplot2". R Package Version* 0.5.1. Available at: https://CRAN.R-project.org/package=ggridges

Wynter-Blyth, V., and Moorthy, K. (2017). Prehabilitation: preparing patients for surgery. *BMJ* 358:j3702. doi: 10.1136/bmj.j3702

Conflict of Interest Statement: The authors declare that the research was conducted in the absence of any commercial or financial relationships that could be construed as a potential conflict of interest.

frontiers in Physiology

ORIGINAL RESEARCH
published: 07 May 2019
doi: 10.3389/fphys.2019.00477

Closed-Loop Cardiovascular Interactions and the Baroreflex Cardiac Arm: Modulations Over the 24 h and the Effect of Hypertension

Gianfranco Parati[1,2], Paolo Castiglioni[3], Andrea Faini[2], Marco Di Rienzo[3], Giuseppe Mancia[1], Riccardo Barbieri[4] and J. Philip Saul[5]*

[1] Department of Medicine and Surgery, University of Milano-Bicocca, Milan, Italy, [2] Istituto Auxologico Italiano, IRCCS, Department of Cardiovascular, Neural and Metabolic Sciences, S.Luca Hospital, Milan, Italy, [3] IRCCS Fondazione Don Carlo Gnocchi, Milan, Italy, [4] Politecnico di Milano, Milan, Italy, [5] West Virginia University School of Medicine, Morgantown, WV, United States

OPEN ACCESS

Edited by:
Maja Elstad,
University of Oslo, Norway

Reviewed by:
Helio Cesar Salgado,
University of São Paulo, Brazil
Vlasta Bari,
Policlinico San Donato (IRCCS), Italy

****Correspondence:***
Gianfranco Parati
gianfranco.parati@unimib.it

Specialty section:
This article was submitted to Autonomic Neuroscience, a section of the journal Frontiers in Physiology

Received: *15 January 2019*
Accepted: *05 April 2019*
Published: *07 May 2019*

Citation:
Parati G, Castiglioni P, Faini A, Di Rienzo M, Mancia G, Barbieri R and Saul JP (2019) Closed-Loop Cardiovascular Interactions and the Baroreflex Cardiac Arm: Modulations Over the 24 h and the Effect of Hypertension. Front. Physiol. 10:477. doi: 10.3389/fphys.2019.00477

Closed-loop models of the interactions between blood pressure (BP) and heart rate variations allow for estimation of baroreflex sensitivity (feedback effects of BP changes on heart rate) while also considering the feedforward effects of heart rate on BP. Our study is aimed at comparing modulations of feedback and feedforward couplings over 24 h in normotensive and hypertensive subjects, by assessing closed-loop baroreflex models in ambulatory conditions. Continuous intra-arterial BP recordings were performed for 24 h in eight normotensive and eight hypertensive subjects. Systolic BP (SBP) and pulse interval (PI) beat-by-beat series were analyzed by an autoregressive moving average model over consecutive 6-min running windows, estimating closed-loop feedback and feedforward gains in each window. The open-loop feedback gain was estimated for comparison. Normotensive and hypertensive patients were compared during wake (18:00–22:00) and sleep (23:00–5:00) periods by a mixed-effect linear model at $p < 0.05$. In both groups feedback (feedforward) gain averaged values were higher (lower) in sleep than in wake. Moreover, the closed-loop feedback gain was higher in normotensive subjects both in wake and sleep, whereas the closed-loop feedforward gain was higher in hypertensive subjects during sleep. By contrast, no significant differences were found between the normotensive and hypertensive groups for the open-loop feedback gain. Therefore, the closed-loop SBP-PI model can detect circadian alterations in the feedforward gain of PI on SBP and derangements of spontaneous baroreflex sensitivity in hypertension not detectable with the open-loop approach. These findings may help to obtain a more comprehensive assessment of the autonomic dysfunction underlying hypertension and for the in-depth evaluation of the benefits of rehabilitation procedures on autonomic cardiovascular modulation.

Keywords: ambulatory blood pressure monitoring, autonomic nervous system, arterial baroreflex, hypertension, blood pressure spectral analysis

INTRODUCTION

Animal and human studies have concordantly documented that the arterial baroreflex represents a fundamental mechanism to avoid excessive blood pressure (BP) oscillations and maintain its values within a range that preserves organ perfusion and avoids the risk associated with BP peaks (Mancia and Mark, 2011). Furthermore, data are available that in the clinical setting a baroreflex dysfunction may unveil the early occurrence of autonomic impairment in conditions such as arterial hypertension, diabetes, sleep apnea syndrome and aging, and predicts the risk of cardiovascular events in diseases like myocardial infarction, congestive heart failure or recurrent malignant arrhythmias (Parati et al., 2007, 2013).

Arterial baroreflex function can be assessed by delivering an external stimulus to baroreceptors and measuring the baroreflex-mediated response. Examples are the "Oxford" method, based on the intravenous injection of vasoactive drugs that induce reflex heart rate changes in response to drug-induced increases or reductions of systolic BP (SBP) (Smyth et al., 1969), and the "neck-chamber" method that stimulates or deactivates the carotid baroreceptors by respectively increasing or reducing carotid transmural pressure through changes in air pressure within a tight collar (Eckberg et al., 1975; Mancia et al., 1979). Other approaches are based on the analysis of baroreflex modulation of heart rate in response to the spontaneous fluctuations in BP which physiologically occur in daily life. At variance from the "Oxford" and "neck chamber" methods, such approaches avoid the inconveniences of the information obtained by delivery of external stimuli in the context of artificial laboratory settings and allow monitoring the baroreflex function in ambulant subjects for long periods (Mancia et al., 1983), without significantly interfering with their activities (Laude et al., 2004; Parati et al., 2004).

Both the laboratory and the "spontaneous" methods to study the arterial baroreflex estimate the feedback effects of SBP changes on pulse interval (PI), reciprocal of heart rate, neglecting the simultaneously occurring feedforward effects of PI on SBP, induced through changes in cardiac output. This can be acceptable under the "open-loop" assumption that these feedforward effects do not significantly influence the estimation of the gain of the feedback arc from SBP to PI. If the feedforward effects are not considered to be negligible, the open-loop assumption cannot be made and the feedforward effects of PI on SBP should be quantified simultaneously with the reflex feedback effects of SBP on PI. To date, "spontaneous" methods for evaluating the baroreflex function assessed feedback and feedforward effects simultaneously by mathematically modeling the beat-by-beat interactions among the cardiovascular variables through a closed-loop analysis of the time series (Barbieri et al., 1997, 2001). Simplified closed-loop models were based on bivariate autoregressive representations of the interactions between couples of cardiovascular time series (Barbieri et al., 1996), or on trivariate autoregressive models that also include respiratory signals (Baselli et al., 1988). Closed-loop auto-regressive moving average (ARMA) models of the SBP and PI beat-by-beat interactions were also proposed (Patton et al., 1996; Wyller et al., 2011). Applications of these models, however, have been limited to the laboratory environment only.

This work is focused on two primary aims. First, to characterize both the feedback and feedforward components of the SBP-PI coupling over 24 h in ambulatory subjects, which includes spontaneous variations of activity level during the day and night. Second, to compare the results between normotensive and hypertensive subjects to detect differences in their autonomic and vascular characteristics.

MATERIALS AND METHODS

Subjects

The study utilized 24-h ambulatory intra-arterial BP recordings performed at the University Hospital (Ospedale Maggiore Policlinico di Milano) of Milan, Italy. Invasive recordings were used to obtain an uninterrupted BP signal over the 24 h, an advantage not offered by discontinuous ambulatory BP recorders which have also lower accuracy. Invasive monitoring provides more accurate BP data also when compared to non-invasive continuous BP recordings from devices based on the volume clamp method at the finger artery level (Castiglioni et al., 1999), which require periodic interruptions for calibration and for switching the measuring cuff between two fingers (Imholz et al., 1993). Intra-arterial BP recordings were obtained in eight normotensive subjects (five males and three females of which one in the childbearing age) and eight subjects with moderate to severe essential hypertension (seven males and one female in the childbearing age). Normotensive subjects were referred to our hospital for a suspected hypertensive state which was excluded by the clinical evaluation. Exclusion criteria were: (1) clinical or laboratory evidence of cardiovascular disease in addition to hypertension, (2) other significant health abnormalities (e.g., diabetes), (3) smoking, (4) obesity, (5) prior drug treatment for hypertension, and (6) administration of cardiovascular drugs in the 4 weeks preceding the BP recording. To be included for analysis, the BP signal had to be of sufficiently high quality over the entire 24-h period.

Subjects were classified as normotensive or hypertensive by averaging three systolic and diastolic (D) BP values collected at 5 min intervals in the sitting position, after a 5 min rest, using a mercury sphygmomanometer in each of two visits, scheduled at 1-month intervals. The normotensive subjects had mean (SD) SBP and DBP values of 131 (6) and 84 (4) mmHg respectively, while the hypertensive subjects had corresponding values of 191 (19) and 104 (7) mmHg. Ages of the two groups were statistically similar: 43 (20) years (range: 19–70) for normotensive subjects vs. 50 (15) years (range: 28–67) for hypertensive subjects. No subject had any alteration in glucose metabolism or renal function. The study was carried out following the recommendations of the Ospedale Maggiore Policlinico di Milano (Milan, Italy) ethical committee with written informed consent from all subjects in accordance with the Declaration of Helsinki. The protocol was approved by the Ospedale Maggiore Policlinico di Milano (Milan, Italy).

Measurements Protocol

A catheter (11 cm long, 1.1 mm internal diameter) was percutaneously inserted into the radial artery of the non-dominant arm by the Seldinger technique after local anesthesia with 2% lidocaine. A rigid polyethylene tube connected the catheter to a transducing-perfusing unit contained in a plexiglass box secured to the patient's thorax at the heart level. The BP signal was stored on a magnetic tape cassette by an Oxford Medilog recorder bound to the subjects' waist. The method provides an accurate BP recording because of the stability of the zero signal, the transducer linearity between 50 and 250 mmHg, and the undistorted frequency-response up to 10 Hz (Stott et al., 1976).

Ambulatory recordings started around 6 pm and ended at 6–7 pm on the following day. Meal times, bed times and recreational times (T.V. watching, playing cards, visits from relatives) were standardized. Meals composition was also standardized and provided by the hospital canteen. Subjects were allowed to move within the hospital buildings and garden, but not outside the hospital area. They were asked to record their activities in a diary and were discouraged from performing any kind of vigorous physical exercise.

Data Analysis

The recorded BP signals were digitized (170 Hz, 12 bits), manually edited from movement artifacts, pulse pressure dampening, and premature beats. SBP was calculated for each pulse wave beat-by-beat and PI of a given beat "n" was computed as the interval between the times of occurrence of the systolic peak of the beat "n" and of the systolic peak of the successive beat, "n+1," as described previously (Di Rienzo et al., 2006). For the closed-loop analysis, the beat series were re-sampled at 3 Hz, high-pass filtered (corner frequency of 0.03 Hz) to remove very-low frequency components, and split into contiguous segments of 1024 samples (about 6 min). The SBP and PI variances in each 6-min segment were calculated and averaged over the entire recording as measures of SBP and PI short-term variability.

The feedback and feedforward components of the SBP-PI coupling were estimated using the following bivariate closed-loop autoregressive model in each segment:

$$\begin{bmatrix} PI(n) \\ SBP(n) \end{bmatrix} = \sum_{k=1}^{p} \begin{bmatrix} a_{11}(k) & a_{12}(k) \\ a_{21}(k) & a_{22}(k) \end{bmatrix} \times \begin{bmatrix} PI(n-k) \\ SBP(n-k) \end{bmatrix} + \begin{bmatrix} w_{PI}(n) \\ w_{SBP}(n) \end{bmatrix} \quad (1)$$

with $1 \leq n \leq 1024$, w_{PI} and w_{SBP} representing independent white Gaussian noises, and the model order p set equal to 14 to guarantee a model order higher than the minimum required by the Akaike criterion. The $a_{ji}(k)$ coefficients were estimated by the Levinson-Wiggins-Robinson algorithm (Wiggins and Robinson, 1967).

The feedback transfer function between SBP and PI, $G_{SBP\rightarrow PI}$, and the feedforward transfer function between PI and SBP, $G_{PI\rightarrow SBP}$, were estimated as:

$$G_{SBP\rightarrow PI}(f) = \frac{A_{12}(f)}{1 - A_{11}(f)} \quad (2)$$

$$G_{PI\rightarrow SBP}(f) = \frac{A_{21}(f)}{1 - A_{22}(f)} \quad (3)$$

$$\text{with } A_{ij}(f) = \sum_{k=1}^{p} a_{ij}(k) e^{-j2\pi fk} \quad (4)$$

The absolute values of feedback and feedforward transfer functions were computed in the low frequency (0.04–0.15 Hz, LF) and high frequency (0.15–0.5 Hz, HF) bands. The absolute value of closed-loop feedback gain, hereafter α_C, was taken as the measure of closed-loop baroreflex sensitivity on PI. The absolute value of the closed-loop feedforward gain, hereafter β_C, was taken as a measure of the sensitivity of the mechanical coupling between PI and SBP. Estimates of SBP-PI coupling were considered reliable only for data segments with SBP-PI squared coherence modulus greater than 0.5, which occurred almost exclusively in the LF band, leading to the exclusive use of the LF band for the SBP-PI relationships.

Since traditional methods for estimating the cardiac arm of the baroreflex with transfer function techniques do not consider the closed-loop nature of the baroreflex, the ratio between SBP-PI cross-spectrum and SBP spectrum

$$H_{SBP\rightarrow PI}(f) = \frac{P_{SBP-PI}(f)}{P_{SBP}(f)} \quad (5)$$

was also calculated over each 1024-point data segment, to evaluate how neglecting the closed-loop nature of the cardiac baroreflex influences the estimation of the feedback component. The open-loop feedback gain, α_O, was then estimated as the modulus of $H_{SBP\rightarrow PI}$ transfer function in the LF band. Values estimated over each 6-min running window (without overlapping) were averaged hour by hour to obtain hourly profiles over the 24 h. Moreover, spectral indices associated with autonomic cardiovascular control were computed. The LF power of SBP, both in absolute units and in normalized units, [LF/(LF+HF)], was calculated as an index of vasomotor sympathetic tone. The PI power in the HF band and the ratio between LF and HF powers of PI, LF/HF powers ratio, were calculated as indices of cardiac vagal modulation and of cardiac sympatho/vagal balance.

Statistical Analysis

Based on previous evidence (Castiglioni et al., 1999), spectral powers were log-transformed to reduce the skewness of their distribution. Gaussianity of log-transformed spectral powers and of feedback and feedforward baroreflex gains was verified by the Shapiro–Wilk's normality test. 24-h estimates were compared between normotensive and hypertensive subjects by the two-sided t-test. The two groups were also compared over shorter time periods selected as being more likely associated with higher and lower degrees of sympathetic activation, respectively. The segment between 6 and 10 pm was selected as the sub-period

with a higher sympathetic activation because it followed the stress related to the subject's invasive instrumentation. Subjects were awake and not lying in bed by their diaries, so this period was labeled "wake." The segment between 11 pm and 5 am was selected as the sub-period with lower sympathetic activation. Subjects were asleep according to their diaries, so this period is labeled "sleep." Normotensive and hypertensive groups were compared over the above "wake" and "sleep" subperiods considering one "between" factor (group factor) and one "within" factor (time factor). Significances of each of the two factors and of their interaction (time × group) were calculated by applying a mixed-effect linear model, with *post hoc* contrast analysis corrected for multiple comparisons by the Benjamini and Hochberg False Discovery Rate procedure.

Circadian/ultradian modulations were statistically described by hourly profiles of log-transformed feedback and feedforward gains. The relationship of either feedback and feedforward gains with BP and PI short-term variability was described by linear regression analysis with α_C or β_C calculated over the whole 24-h period as independent variables, and the average over the 24-h period of SBP or PI short-term variances (as assessed over the running window of 6 min employed for ARMA analysis) as dependent variables.

Analyses were performed with R Statistical package (The R Foundation for Statistical Computing, Vienna, Austria) setting the significance threshold at $p < 0.05$. The beat-by-beat series recorded in this study are available from the corresponding author on reasonable request.

RESULTS

Table 1 shows that compared to normotensive subjects, hypertensive subjects exhibited, over the 24 h, higher BP values, as well as a higher SBP variance. Furthermore, compared to normotensive subjects, hypertensive subjects had a lower baroreflex feedback gain (the difference, however, reaching the statistical significance when calculated by the closed-loop approach, α_C, and not by the open-loop approach, α_O) and a tendency ($p = 0.06$) toward a higher feedforward gain, β_C.

TABLE 1 | 24-h BP and heart rate mean, variance and spectral indices and 24-h feedback/feedforward baroreflex gains: mean (SD) with p significance of the difference between normotensive and hypertensive groups.

	Normotensive	Hypertensive	*p*-value
Mean			
SBP (mmHg)	120.8 (18.9)	170.9 (20.1)	**<0.001**
DBP (mmHg)	65.4 (11.2)	87.7 (16.2)	**<0.01**
Heart rate (bpm)	77.6 (5.4)	77.2 (12.8)	0.93
SBP variability			
Variance ($mmHg^2$)	229.4 (82.4)	395.6 (121.1)	**<0.01**
LF power ($mmHg^2$)	15.61 (6.69)	20.54 (8.85)	0.20
LF normalized power	0.50 (0.09)	0.45 (0.11)	0.38
PI variability			
Variance (ms^2)	19015 (10780)	13934 (7827)	0.38
HF power (ms^2)	426.9 (448.6)	171.6 (120.5)	0.28
LF/HF powers ratio	2.2 (1.7)	3.0 (2.3)	0.45
Baroreflex gains			
α_O (ms/mmHg)	7.19 (3.75)	4.13 (1.29)	0.0504
α_C (ms/mmHg)	3.33 (1.90)	1.75 (0.63)	**<0.05**
β_C (mmHg/ms)	0.12 (0.02)	0.17 (0.02)	0.06

p after two-sided t-test (the bold font highlights significances at $p < 0.05$); SBP, systolic blood pressure; DBP, diastolic blood pressure; LF, low frequency; HF, high frequency; α_O, feedback gain (open-loop model); α_C, feedback gain (closed-loop model); β_C, feedforward gain (closed-loop model). Variance, LF power, HF power, LF/HF powers ratio, and feedback/feedforward gains were log-transformed before the statistical test.

Closed-Loop Gains vs. Short-Term Variability

The regression analysis (**Figure 1**) shows that both feedback and feedforward gains were linearly related to short-term variability of both PI or SBP (i.e., the variance over a running window of 6 min). In particular, higher feedback gains were linearly associated with higher PI variances and lower SBP variances, while higher feedforward gains were linearly associated with lower PI variances and higher SBP variances. These observations were similar in the normotensive and hypertensive groups (**Figure 1**).

Wake vs. Sleep Subperiods

Table 2 shows that indices of vascular sympathetic modulation (LF power of SBP) and of cardiac sympatho/vagal balance (LF/HF powers ratio of PI) were higher in the *wake* than in the *sleep* subperiods, while the reverse was true for the index of cardiac vagal modulation (HF power of PI). Differences between wake and sleep subperiods in the PI spectral indices were more pronounced in the normotensive group, even if the "group" factor and the interaction between factors did not reach the statistical significance.

Wake and *sleep* sub-periods differed markedly also for closed-loop feedback and feedforward gains (**Figure 2**). The feedback gain was significantly higher and the feedforward gain was significantly lower during *sleep* ($p = 10^{-3}$ for factor "time" for both gains). The "group" factor reached statistical significance for both feedback ($p = 0.03$) and feedforward ($p = 0.04$) gains, and the hypertensive group had significantly lower feedback gains in *wake* and *sleep* conditions and significantly higher feedforward gains during *sleep*.

Also for the open-loop estimates of the feedback gain the factor "time" was significant ($p = 10^{-4}$), being α_O greater in *sleep* than in *wake* conditions both for normotensive (wake: 5.21 ± 3.25; sleep: 9.38 ± 5.44 ms/mmHg, $p < 0.05$) and hypertensive participants (wake: 3.11 ± 1.29; sleep: 5.26 ± 1.69 ms/mmHg, $p < 0.05$). However, differently from the results obtained for α_C, the factor "hypertension" fell short of statistical significance ($p = 0.06$).

24-h Profiles

Figure 3 describes the circadian/ultradian modulations of closed-loop gains in normotensive subjects and their alterations with hypertension. The feedback gain showed a clear night/day modulation with greater gains at night time. The 24-h closed-loop gain profile was higher in normotensive than in hypertensive

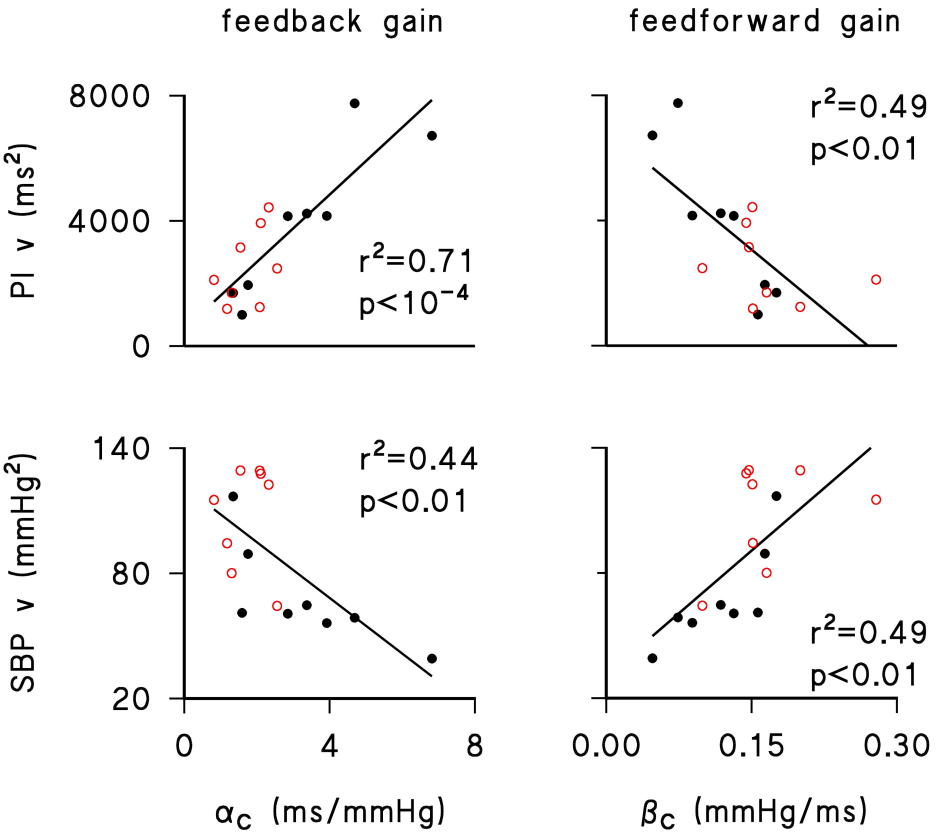

FIGURE 1 | Linear regression between feedback gain (α_C, *left panels*) or feedforward gain (β_C, *right panels*) and short-term variance of PI (PI v, *upper panels*) or SBP (SBP v, *lower panels*) for normotensive (black closed circles) and hypertensive (red open circles) individuals. Determination coefficients, r^2, and significance of linear trends, p, are reported in each panel. Short-term variances were calculated by averaging, over 24 h, the variance of SBP or PI values in each 6-min running window employed for assessing α_C and β_C.

subjects and the statistical significance between groups was achieved between early afternoon and midnight, progressively decreasing from midnight to noon.

The feedforward gain had a different profile. That is, it also showed a night/day modulation, but with lower values at night. Furthermore, it was greater in hypertensive subjects, with between-group differences that achieved the maximal statistical significance mainly at night. After 7 am, differences between groups decreased and almost vanished between 12 and 6 pm, in line with the mixed-effect linear model analysis that found a significant difference between hypertensive and normotensive subjects in *sleep* only (**Figure 2**). Significant differences between groups were also found around the awakening period. While the feedforward gain rose smoothly from 3 to 5 am in normotensive subjects, in hypertensive subjects it showed a rather constant "plateau" between 11 pm and 5 am, followed by a peak around the wake-up time, between 6 and 7 am.

Figure 4 compares the 24-h profiles of open- and closed-loop estimates. It shows similar circadian modulations with, however, closed-loop estimates always consistently lower than open-loop estimates, in both groups of participants.

TABLE 2 | Autonomic spectral indices in "wake" and "sleep" periods: mean (SD) and significance p of the factors time and group (abbreviations as in **Table 1**).

	Wake	Sleep	*p*-value		
			Time	Group	Time × group
SBP LF (mmHg²)					
Normotensive	21.2 (8.1)*	8.5 (6.1)	**<0.001**	0.434	0.991
Hypertensive	30.5 (21.9)*	9.2 (3.5)			
SBP normalized LF					
Normotensive	0.54 (0.08)*	0.39 (0.11)	**<0.001**	0.136	0.454
Hypertensive	0.48 (0.12)*	0.30 (0.10)			
PI HF (ms²)					
Normotensive	246 (240)*	768 (904)	**0.001**	0.255	0.247
Hypertensive	118 (67)°	235 (166)			
PI LF/HF					
Normotensive	2.7 (0.6)*	1.6 (1.1)	**0.002**	0.411	0.286
Hypertensive	3.7 (3.1)°	2.1 (1.0)			

Factors significance by mixed model analysis (the bold font highlights significances at $p < 0.05$): the "" and "°" symbols mark differences between "wake" and "sleep" periods significant at $p < 5\%$ and $p < 10\%$ after contrast analysis. LF powers, HF powers and the LF/HF powers ratio were log-transformed before statistical analysis.*

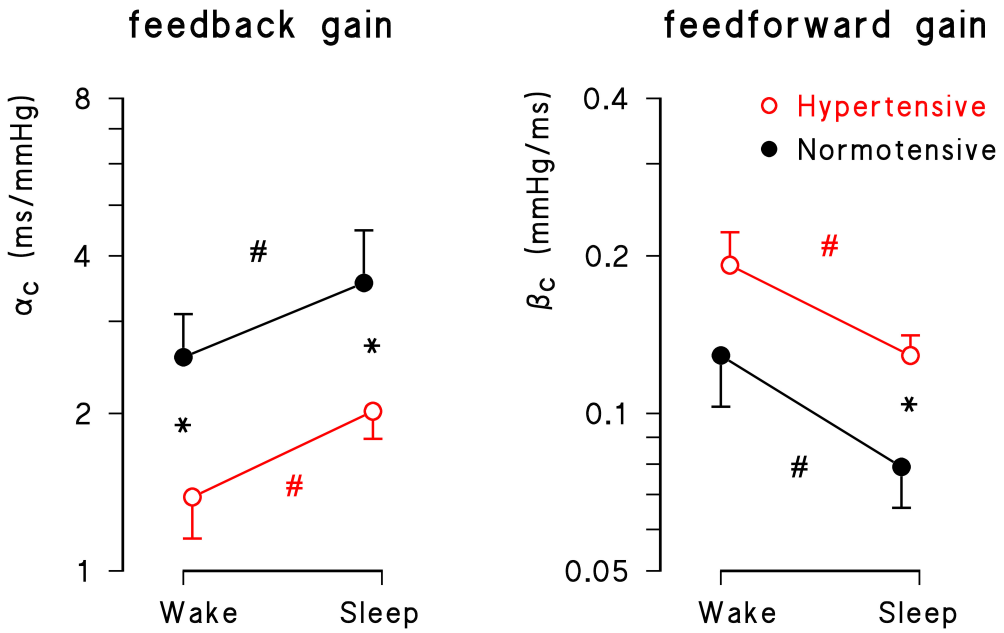

FIGURE 2 | Geometric mean ± geometric standard error for feedback (α_C) and feedforward (β_C) gains during *wake* and *sleep* periods in normotensive (solid black circle) and hypertensive (open red circle) groups. Asterisks indicate significant differences between groups; number signs, # indicate significant differences between conditions from the mixed-effect linear model analysis.

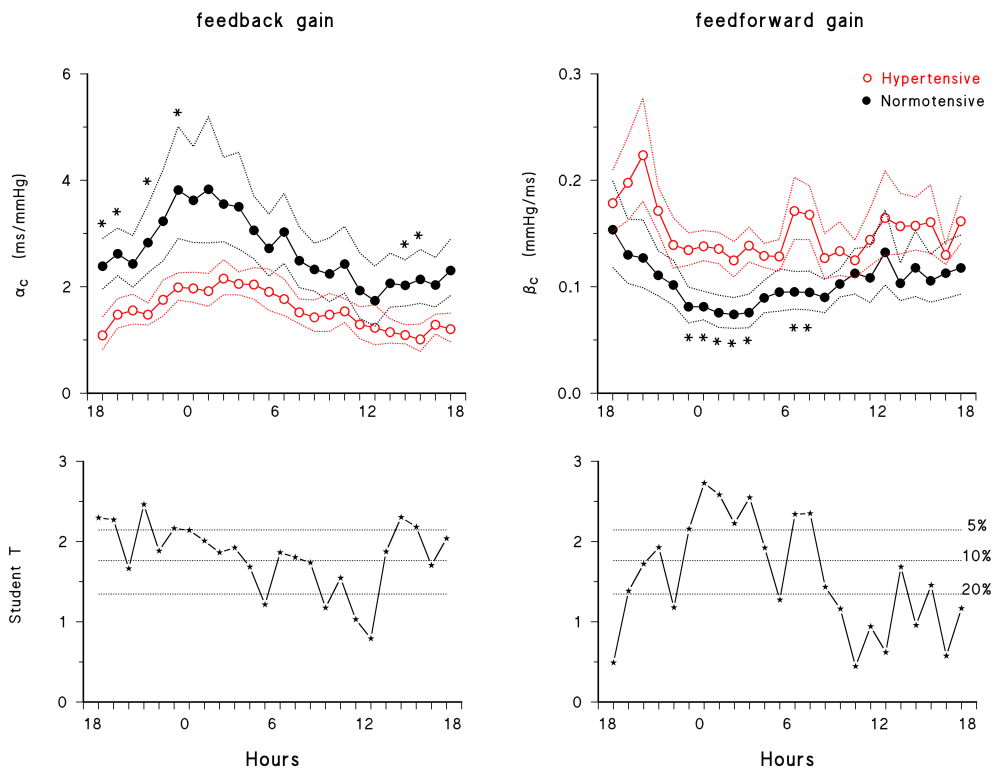

FIGURE 3 | 24-h closed-loop profiles. **(Upper)** Feedback and feedforward gains in normotensive (solid black circle) and hypertensive (open red circle) subjects: geometric mean ± geometric standard error, with * indicating significant differences ($p < 0.05$) between normotensive and hypertensive groups (unpaired *t*-test). **(Lower)** Student's *t*-test statistics for the difference between groups, with dotted horizontal lines representing the thresholds at 20, 10, and 5% significance.

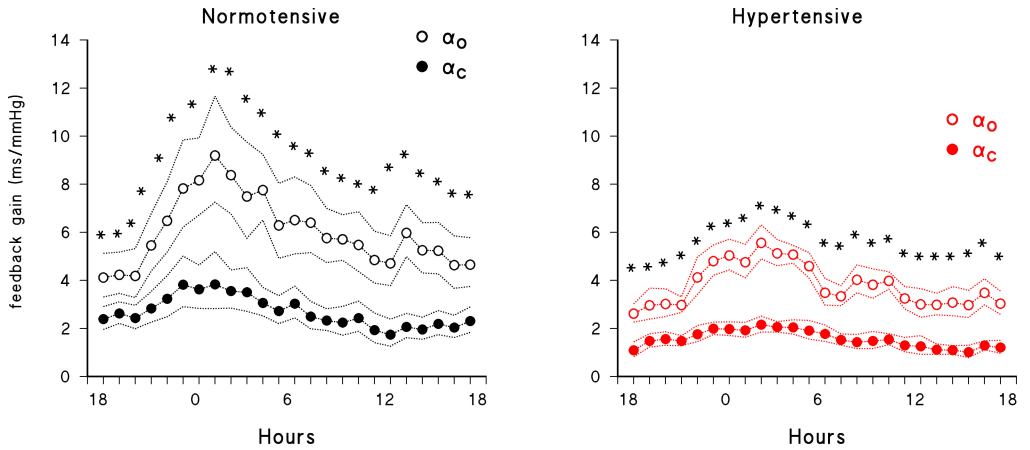

FIGURE 4 | Comparison of 24-h closed-loop (solid circles) and open-loop (open circles) feedback gains. Geometric mean ± geometric standard error in normotensive (black) and hypertensive (red) subjects; asterisks indicate significant ($p < 0.05$) differences between open- and closed-loop gains by paired *t*-test after log-transformation.

DISCUSSION

This study provides the first closed-loop quantitative characterization of the coupling between PI and SBP over the 24 h in ambulant subjects, separately for the feedback reflex component (heart rate modulations in response to BP changes) and for the feedforward mechanical component (BP variations in response to heart rate changes). It also compares, for the first time, closed-loop PI-SBP gains between normotensive and hypertensive subjects throughout the 24 h. Finally, it quantifies differences between closed- and open-loop estimates of baroreflex gain both at normal and high BPs. The following specific results deserve to be discussed.

Correlation of Feedback Gain With SBP and PI Variability

First, the sensitivity of the baroreflex-PI reflex, as quantified by the closed-loop feedback gain over the 24 h, correlated positively with PI variability and negatively with SBP variability. This is in line with similar correlations observed by assessing baroreflex sensitivity through injections of phenylephrine or nitroglycerin (Mancia et al., 1986).

Circadian Modulation of the Feedback Gain and Hypertension

Second, our participants exhibited a higher value of the closed-loop feedback gain during sleep than in the awake state, and the feedback gain was lower in hypertensive than in normotensive subjects over the entire 24-h period, with a difference that was more consistent during the day than during the night time. These findings extend to a closed-loop analysis of real-life observations previous reports on *wake*/*sleep* modulation and on the difference between normotensive and hypertensive subjects obtained in the laboratory from the PI responses to phenylephrine injections (Conway et al., 1983) and by a time-domain open-loop method, the "sequence technique" (Parati et al., 1988). Of note is the present observation that the awake-sleep modulation of the baroreflex gain, although reduced, is not suppressed in hypertension. Ultradian modulation of the baroreflex and its lower sensitivity during the day time have been attributed to central neural influences on the baroreflex arch (Di Rienzo et al., 2009). Changes of the baroreflex gain associated with the lying body position during sleep may also be involved, however, because higher baroreflex sensitivity in supine than in standing posture has been reported with different estimation methods (Laude et al., 2004).

Circadian Modulation of the Feedforward Gain

Third, this study provides novel information on the 24-h modulation of the feedforward gain. The mechanical coupling from PI to SBP had higher gain during *wake* than during *sleep* (**Figure 2**), probably because of a higher cardiac and vascular sympathetic activity in the awake period than at night, as suggested by previous studies (Di Rienzo et al., 1989; Furlan et al., 1990; Parati et al., 1990) but also by the present finding of greater LF power of SBP and LF/HF powers ratio of PI during the day time. A higher sympathetic activity may amplify, via changes in myocardial contractility, the effect of heart rate changes on cardiac output and vascular distensibility (Giannattasio et al., 2005), increasing the mechanical coupling between heart rate and BP. Interestingly, while the feedback gain correlated negatively with SBP variability (reflecting the baroreflex "buffering" action on BP fluctuations) the feedforward gain and SBP variability showed a positive relationship. This is consistent with the possibility that, as the feedforward gain increases, the same PI variations produce larger SBP variations.

Hypertension and Feedforward Gain

Fourth, our study provides novel information on alterations of the feedforward gain in hypertension. The gain of the PI-SBP

mechanical coupling tended to be higher in hypertensive subjects. Higher gain is consistent with the vascular alterations characterizing hypertension, such as decreased arterial distensibility and increased systemic vascular resistance (Mitchell et al., 2008), the presence of which may amplify the effect of changes in cardiac output (majorly dependent on heart rate) on BP. The differences between hypertensive and normotensive subjects were particularly significant during "sleep" (**Figures 2**, **3**), which might indicate an impaired capability of the hypertensive group to deactivate the mechanical PI-SBP coupling at night, an impairment which seems related to their known structural vascular changes responsible for an increased arterial stiffness, and to their lower capability to enhance vagal control and to reduce the cardiac sympatho/vagal balance at night (**Table 2**). It is worth noting that the profiles of the feedforward gains of normotensive and hypertensive subjects differed markedly in the hours immediately after awakening, between 6 and 8 am. The β_C peak visible in the hypertensive group only in this time window (**Figure 3**) suggests a faster rise of the feedforward gain in hypertensive subjects after wake-up. This finding might be related with the so-called morning BP surge and with the associated greater incidence of cardiovascular events after awakening reported in previous studies (Muller et al., 1989; Kario et al., 2003), an issue which deserves to be further investigated in future studies.

Open vs. Closed Loop Estimates

A last methodological point regards the influence of feedforward components when estimating the feedback gain. Feedback gains are substantially lower if estimated by closed-loop rather than by open-loop models. Open-loop techniques might disregard the influences of PI changes on changes in SBP and therefore ascribe all PI fluctuations in the frame of SBP-PI coupling to reflex influences triggered by changes in BP. For instance, the open loop approach does not take into account that, when PI lengthens due to the reflex effects of an elevation in SBP, it consequently leads to a reduction in SBP. Since also secondary changes in SBP may be linearly coupled to changes in PI, the mechanical gain from PI to SBP would reasonably lead to a bias toward higher feedback gains from SBP to PI. In our study, in spite of the relatively small number of subjects included, the more precise evaluation allowed by the closed-loop approach detected significant differences in baroreflex sensitivity between the normotensive and hypertensive groups which is in line with previous data obtained with vasoactive drugs (Conway et al., 1983). Conversely, the open-loop method, although showing a clear tendency toward a between groups difference, failed to cross the significance threshold.

Limitations

The use of invasive BP recordings more faithfully describes the beat-by-beat cardiovascular dynamics than non-invasive methods. Therefore, the methodology in this study needs to be adapted and validated in other settings where non-invasive recordings are considered. In fact, the use of an intra-arterial catheter for BP measurements is generally limited now to BP recordings in intensive care units, and non-invasive methods measuring BP at the digital artery level are preferred for monitoring free-moving subjects over the 24 h. Due to the peripheral measurement sites, the LF powers of SBP are amplified when measured at the finger artery level (Omboni et al., 1993; Castiglioni et al., 1999). Therefore, closed-loop estimates of the gains in the cardiac baroreflex loop obtained with these non-invasive methods might differ from those reported in the present work. A technical limitation to be mentioned is that we did not simultaneously record the electrocardiogram or any respiratory signal. Since the electrocardiogram was not measured, the baroreflex modulation of heart rate was quantified from PI measures, while R–R intervals are expected to more faithfully reflect the autonomic modulations of heart rate. However, discrepancies between PI and R–R intervals variability are negligible in comparison to the linear relationship between the two variables and BP, and mostly present in the frequency range occupied by the respiratory fluctuations only (Constant et al., 1999). We may therefore reasonably assume that our results, based on the slower oscillations in the LF band, are not substantially influenced by the choice between PI or R–R intervals. The lack of a respiratory signal means that our bivariate model cannot quantify how respiration influences the SBP and PI series. With a respiratory signal available, a trivariate ARMA model is likely to estimate the feedback and feedforward SBP-PI relations more precisely. However, a comparison of closed-loop baroreflex gains by a bivariate AR model of SBP and R–R intervals and by a trivariate AR model that also included a respiratory signal provided substantially similar results (Barbieri et al., 1997).

As a final methodological comment, it should be mentioned that, even if quantifying separately the feedforward and feedback components of the SBP-PI interactions, our closed-loop analysis does not measure the exact directional importance of the causality relation between the two series. Future closed-loop models including the concept of Granger causality within the assessment of the closed-loop relations might provide further details into the estimation of the feedforward and feedback transfer functions.

CONCLUSION

The removal of the open-loop assumption when modeling the interaction between BP and heart rate fluctuations offers a deeper insight into the mechanisms involved in daily life cardiovascular regulation. In particular, it allows the detection of specific patterns characterizing the altered cardiovascular regulation reported in essential hypertension separately for feedback and feedforward gains. Such closed-loop evaluation may improve the clinical relevance of SBP-PI coupling assessment over the 24 h, by separately quantifying the contribution of the baroreflex feedback gain and of the mechanical feedforward coupling between SBP and PI in relation to target organ damage, incidence of cardiovascular events and efficacy of treatments

in hypertension, a possibility which deserves to be specifically explored in future studies.

ETHICS STATEMENT

The study was carried out in accordance with the recommendations of the Ospedale Maggiore Policlinico di Milano (Milan, Italy) ethical committee with written informed consent from all subjects. All subjects gave written informed consent in accordance with the Declaration of Helsinki. The protocol was approved by the Ospedale Maggiore Policlinico di Milano (Milan, Italy).

AUTHOR CONTRIBUTIONS

GP and JS conceived the study. RB and PC performed the data analysis. AF performed the statistical analysis. GP and PC wrote the manuscript. All the authors fulfilled data interpretation and critically revised the manuscript.

REFERENCES

Barbieri, R., Bianchi, A. M., Triedman, J. K., Mainardi, L. T., Cerutti, S., and Saul, J. P. (1997). Model dependency of multivariate autoregressive spectral analysis. *IEEE Eng. Med. Biol. Mag.* 16, 74–85. doi: 10.1109/51.620498

Barbieri, R., Parati, G., and Saul, J. P. (2001). Closed- versus open-loop assessment of heart rate baroreflex. *IEEE Eng. Med. Biol. Mag.* 20, 33–42. doi: 10.1109/51.917722

Barbieri, R., Waldmann, R. A., Di Virgilio, V., Triedman, J. K., Bianchi, A. M., Cerutti, S., et al. (1996). Continuous quantification of baroreflex and respiratory control of heart rate by use of bivariate autoregressive techniques. *Ann. Noninvasive Electrocardiol.* 1, 264–277. doi: 10.1111/j.1542-474x.1996.tb00279.x

Baselli, G., Cerutti, S., Civardi, S., Malliani, A., and Pagani, M. (1988). Cardiovascular variability signals: towards the identification of a closed-loop model of the neural control mechanisms. *IEEE Trans. Biomed. Eng.* 35, 1033–1046. doi: 10.1109/10.8688

Castiglioni, P., Parati, G., Omboni, S., Mancia, G., Imholz, B. P., Wesseling, K. H., et al. (1999). Broad-band spectral analysis of 24 h continuous finger blood pressure: comparison with intra-arterial recordings. *Clin. Sci.* 97, 129–139. doi: 10.1042/cs0970129

Constant, I., Laude, D., Murat, I., and Elghozi, J. L. (1999). Pulse rate variability is not a surrogate for heart rate variability. *Clin. Sci.* 97, 391–397. doi: 10.1042/cs0970391

Conway, J., Boon, N., Jones, J. V., and Sleight, P. (1983). Involvement of the baroreceptor reflexes in the changes in blood pressure with sleep and mental arousal. *Hypertension* 5, 746–748. doi: 10.1161/01.hyp.5.5.746

Di Rienzo, M., Castiglioni, P., Mancia, G., Parati, G., and Pedotti, A. (1989). 24 h sequential spectral analysis of arterial blood pressure and pulse interval in free-moving subjects. *IEEE Trans. Biomed. Eng.* 36, 1066–1075. doi: 10.1109/10.40813

Di Rienzo, M., Castiglioni, P., and Parati, G. (2006). "Arterial blood pressure processing," in *Wiley Encyclopedia of Biomedical Engineering*, ed. M. Akay (Hoboken, NJ: John Wiley & Sons), 98–109.

Di Rienzo, M., Parati, G., Radaelli, A., and Castiglioni, P. (2009). Baroreflex contribution to blood pressure and heart rate oscillations: time scales, time-variant characteristics and nonlinearities. *Philos. Trans. A Math. Phys. Eng. Sci.* 367, 1301–1318. doi: 10.1098/rsta.2008.0274

Eckberg, D. L., Cavanaugh, M. S., Mark, A. L., and Abboud, F. M. (1975). A simplified neck suction device for activation of carotid baroreceptors. *J. Lab. Clin. Med.* 85, 167–173.

Furlan, R., Guzzetti, S., Crivellaro, W., Dassi, S., Tinelli, M., Baselli, G., et al. (1990). Continuous 24-hour assessment of the neural regulation of systemic arterial pressure and RR variabilities in ambulant subjects. *Circulation* 81, 537–547. doi: 10.1161/01.cir.81.2.537

Giannattasio, C., Failla, M., Lucchina, S., Zazzeron, C., Scotti, V., Capra, A., et al. (2005). Arterial stiffening influence of sympathetic nerve activity: evidence from hand transplantation in humans. *Hypertension* 45, 608–611. doi: 10.1161/01.hyp.0000157368.09939.88

Imholz, B. P., Langewouters, G. J., van Montfrans, G. A., Parati, G., van Goudoever, J., Wesseling, K. H., et al. (1993). Feasibility of ambulatory, continuous 24-hour finger arterial pressure recording. *Hypertension* 21, 65–73. doi: 10.1161/01.hyp.21.1.65

Kario, K., Pickering, T. G., Umeda, Y., Hoshide, S., Hoshide, Y., Morinari, M., et al. (2003). Morning surge in blood pressure as a predictor of silent and clinical cerebrovascular disease in elderly hypertensives: a prospective study. *Circulation* 107, 1401–1406. doi: 10.1161/01.cir.0000056521.67546.aa

Laude, D., Elghozi, J. L., Girard, A., Bellard, E., Bouhaddi, M., Castiglioni, P., et al. (2004). Comparison of various techniques used to estimate spontaneous baroreflex sensitivity (the EuroBaVar study). *Am. J. Physiol. Regul. Integr. Comp. Physiol.* 286, R226–R231.

Mancia, G., Ferrari, A., Gregorini, L., Parati, G., Ferrari, M. C., Pomidossi, G., et al. (1979). Control of blood pressure by carotid sinus baroreceptors in human beings. *Am. J. Cardiol.* 44, 895–902. doi: 10.1016/0002-9149(79)90220-0

Mancia, G., Ferrari, A., Gregorini, L., Parati, G., Pomidossi, G., Bertinieri, G., et al. (1983). Blood pressure and heart rate variabilities in normotensive and hypertensive human beings. *Circ. Res.* 53, 96–104. doi: 10.1161/01.res.53.1.96

Mancia, G., and Mark, A. L. (2011). "Arterial Baroreflexes in Humans," in *Supplement 8: Handbook of Physiology, The Cardiovascular System, Peripheral Circulation and Organ Blood Flow*, ed. American Physiological Society (Hoboken, NJ: Wiley-Blackwell), 755–793.

Mancia, G., Parati, G., Pomidossi, G., Casadei, R., Di Rienzo, M., and Zanchetti, A. (1986). Arterial baroreflexes and blood pressure and heart rate variabilities in humans. *Hypertension* 8, 147–153. doi: 10.1161/01.hyp.8.2.147

Mitchell, G. F., Conlin, P. R., Dunlap, M. E., Lacourciere, Y., Arnold, J. M., Ogilvie, R. I., et al. (2008). Aortic diameter, wall stiffness, and wave reflection in systolic hypertension. *Hypertension* 51, 105–111. doi: 10.1161/hypertensionaha.107.099721

Muller, J. E., Tofler, G. H., and Stone, P. H. (1989). Circadian variation and triggers of onset of acute cardiovascular disease. *Circulation* 79, 733–743. doi: 10.1161/01.cir.79.4.733

Omboni, S., Parati, G., Frattola, A., Mutti, E., Di Rienzo, M., Castiglioni, P., et al. (1993). Spectral and sequence analysis of finger blood pressure variability. Comparison with analysis of intra-arterial recordings. *Hypertension* 22, 26–33. doi: 10.1161/01.hyp.22.1.26

Parati, G., Castiglioni, P., Di Rienzo, M., and Mancia, G. (2007). "Arterial Baroreflex," in *Encyclopedia of Stress*, 2nd Edn, ed. G. Fink (Oxford: Academic Press), 248–257. doi: 10.1016/b978-012373947-6.00042-8

Parati, G., Castiglioni, P., Di Rienzo, M., Omboni, S., Pedotti, A., and Mancia, G. (1990). Sequential spectral analysis of 24-hour blood pressure and pulse interval in humans. *Hypertension* 16, 414–421. doi: 10.1161/01.hyp.16.4.414

Parati, G., Di Rienzo, M., Bertinieri, G., Pomidossi, G., Casadei, R., Groppelli, A., et al. (1988). Evaluation of the baroreceptor-heart rate reflex by 24-hour intra-arterial blood pressure monitoring in humans. *Hypertension* 12, 214–222. doi: 10.1161/01.hyp.12.2.214

Parati, G., Di Rienzo, M., Castiglioni, P., and Mancia, G. (2013). "Computer analysis of blood pressure and heart rate variability in subjects with normal and abnormal autonomic cardiovascular control," in *Autonomic Failure: A Textbook of Clinical Disorders of the Autonomic Nervous System*, 5th Edn, eds C. Mathias and R. Bannister (Oxford, MS: Oxford University Press), 307–322. doi: 10.1093/med/9780198566342.003.0026

Parati, G., Saul, J. P., and Castiglioni, P. (2004). Assessing arterial baroreflex control of heart rate: new perspectives. *J. Hypertens.* 22, 1259–1263. doi: 10.1097/01.hjh.0000125469.35523.32

Patton, D. J., Triedman, J. K., Perrott, M. H., Vidian, A. A., and Saul, J. P. (1996). Baroreflex gain: characterization using autoregressive moving average analysis. *Am. J. Physiol.* 270, H1240–H1249.

Smyth, H. S., Sleight, P., and Pickering, G. W. (1969). Reflex regulation of arterial pressure during sleep in man. A quantitative method of assessing baroreflex sensitivity. *Circ. Res.* 24, 109–121. doi: 10.1161/01.res.24.1.109

Stott, F. D., Terry, V. G., and Honour, A. J. (1976). Factors determining the design and construction of a portable pressure transducer system. *Postgrad. Med. J.* 52(Suppl. 7), 97–99.

Wiggins, R. A., and Robinson, E. A. (1967). Recursive solution to the multi-channel filtering problem. *J. Geophys. Res.* 70, 1885–1891. doi: 10.1029/jz070i008p01885

Wyller, V. B., Barbieri, R., and Saul, J. P. (2011). Blood pressure variability and closed-loop baroreflex assessment in adolescent chronic fatigue syndrome during supine rest and orthostatic stress. *Eur. J. Appl. Physiol.* 111, 497–507. doi: 10.1007/s00421-010-1670-9

Conflict of Interest Statement: The authors declare that the research was conducted in the absence of any commercial or financial relationships that could be construed as a potential conflict of interest.

frontiers in Neuroscience

ORIGINAL RESEARCH
published: 09 July 2019
doi: 10.3389/fnins.2019.00694

Cross-Wavelet Time-Frequency Analysis Reveals Sympathetic Contribution to Baroreflex Sensitivity as Cause of Variable Phase Delay Between Blood Pressure and Heart Rate

Roel W. de Boer† *and John M. Karemaker**

Department of Medical Biology, Section Systems Physiology, Amsterdam University Medical Centers, Location AMC, Amsterdam, Netherlands

OPEN ACCESS

Edited by:
Maja Elstad,
University of Oslo, Norway

Reviewed by:
Michal Javorka,
Comenius University in Bratislava, Slovakia
André Diedrich,
Vanderbilt University, United States
Jens Tank,
Helmholtz Association of German Research Centers (HZ), Germany

***Correspondence:**
John M. Karemaker
j.m.karemaker@amsterdamumc.nl
orcid.org/0000-0003-0142-5425
†*orcid.org/0000-0002-6749-8419*

Specialty section:
This article was submitted to Autonomic Neuroscience, a section of the journal Frontiers in Neuroscience

Received: *13 January 2019*
Accepted: *19 June 2019*
Published: *09 July 2019*

Citation:
de Boer RW and Karemaker JM (2019) Cross-Wavelet Time-Frequency Analysis Reveals Sympathetic Contribution to Baroreflex Sensitivity as Cause of Variable Phase Delay Between Blood Pressure and Heart Rate. Front. Neurosci. 13:694. doi: 10.3389/fnins.2019.00694

Introduction: Baroreflex sensitivity (BRS) is often presented as a single number, but it is actually a frequency-dependent phenomenon whose value changes constantly due to internal and external stimuli. The standing posture, for instance, necessitates a changeover from vagal to sympathetic predominance for cardiovascular control. We present a wavelet cross-spectral analysis of blood pressure (BP) and interbeat interval (IBI) recordings in the search for variations in gain and phase between these signals. Additionally, we show how the lag in sympathetic response dictates BP-to-IBI phase relations.

Methods: Recordings in supine and head-up tilted (HUT) position, obtained earlier in 10 healthy subjects (4f/6m, aged 27–47 years) were used. BP and IBI were measured from the continuous finger pressure (by Finometer). The cross-wavelet analysis produced time- and frequency dependent gain (wBRS, wavelet derived BRS) and phase, using the MATLAB® wavelet toolbox. We also applied the wBRS method to model-generated BP- and IBI-data with known interrelations to test the results of this analysis technique. Finally, wBRS values were compared with the xBRS-approach, which is a time domain method for continuous BRS estimation in a sliding 10-s window.

Results: In resting supine conditions, wBRS fluctuates; more at respiratory frequencies than in the 0.1 Hz band. After HUT, wBRS at the respiratory frequency decreases from average 22.7 to 8.5 ms/mmHg, phase between BP and IBI increases from −30° to −54°; in the sympathetic 0.1 Hz range these numbers are 13.3→6.3 ms/mmHg and −54°→−59°. The values found by xBRS are intermediate between wBRS-resp and wBRS-0.1 Hz. The **Appendix** shows that for the simulated data the BRS and phase values as found by the wavelet technique can be explained from vector additions of vagal and sympathetic BRS contributions.

Discussion: During supine rest parasympathetic control of heart rate dominates BRS; after HUT this is diminished and less effective. Due to the reaction times of the autonomic effectors, the phase relations between the signals depend on the relative contribution of the sympathetics, which explains the larger phase shift.

Conclusion: Cross wavelet analysis allows to follow fast BRS changes in time and frequency, while the computed phase relations help understand sympathetic participation.

Keywords: baroreflex sensitivity, cross-wavelet analysis, xBRS, phase delay, cardiovascular variability, finger blood pressure, heart rate, blood pressure

INTRODUCTION

Baroreflex sensitivity (BRS) is commonly defined as the ratio of a change in inter beat-interval (IBI) and the change in systolic arterial blood pressure (SAP) that caused it: BRS = ΔIBI/ΔSAP. Several techniques have been proposed for the determination of the BRS, e.g., by studying the resulting IBI-increase after an angiotensin-provoked rise of blood pressure (Smyth et al., 1969), or following neck suction or a Valsalva maneuver (Goldstein et al., 1982). Later, investigators derived BRS estimators from spontaneous fluctuations in pressure and heart-rate for subjects in resting conditions, either using time-domain techniques such as sequential methods (Bertinieri et al., 1985; Parati et al., 1988), or applying spectral approaches (De Boer et al., 1986; Robbe et al., 1987; Parati et al., 1995).

Most of these techniques return a single BRS-value over a period of time, although time-varying BRS-values have been considered, both for time-domain (Westerhof et al., 2004; Eckberg and Kuusela, 2005; Wesseling et al., 2017) and frequency domain (e.g., Li et al., 2018) approaches. Several authors used transfer function analysis to obtain frequency-dependent BRS values, mainly in animal models; a review is given by Kawada and Sugimachi (2016).

In real life, the value of the BRS will change continuously, due to internal and external stimuli, of which a change of posture is a very strong one, as it necessitates activation of the sympathetic nervous outflow to the vasculature and concomitantly to the heart, thereby increasing heart rate and contractility, although that effect is not strictly necessary as is proven in patients who have a cardiac transplant (Rudas et al., 1993).

Figure 1 presents a schematic diagram of presumed baroreflex-mediated delays between blood pressure (BP) variations and IBI variations. A change in BP affects the heart rate first of all by fast vagal influence, which may affect the very interval during which the systolic pressure happens, or the next one (Pickering and Davies, 1973). In addition, the slower sympathetic effect of BP variations on IBI is observed only after a delay of some 2–3 s (Borst and Karemaker, 1983) and so the length of the present IBI is affected both by the value of the present BP and by the combined effect of a number of previous BP values. Hence, for a slowly varying pressure this delay in the sympathetic contribution to the BRS may counteract the expected effect. A simple example, considering an open-loop situation: if the sympathetic influence would have a fixed time to peak effect of 4 s, then its action on 8-s variations in blood-pressure (0.125 Hz) would be counter-intuitive: during an increase in BP the sympathetic effect would tend to increase the heart rate. The vagal action would still work to lower the heart rate under these conditions and so an apparent *negative* sympathetic contribution to the total BRS-value appears. It follows that the observed BRS is a combination of vagal and sympathetic effects, which leads to a frequency-dependent phase-difference between pressure- and interval variations, as shown previously (De Boer et al., 1987). In the present study we will stress that BRS should not be considered as one number, but as a variable, frequency-dependent phenomenon.

To study simultaneously the variation in time and the spectral properties of the BRS, we applied a cross wavelet analysis technique. We tested its use on a set of experimental data which were available from earlier experiments in our laboratory (JMK). Data from 10 healthy subjects were analyzed; they were relaxed, supine (supposedly in a vagus-dominated state), then had three periods of paced breathing, followed by a head-up tilt, which would lead to a sympathetically dominated state. We applied wavelet cross-spectral analysis, which revealed variable gain and phase in the computed BRS during the experimental protocol. Similar techniques have been used by Kashihara et al. (2009) for data from anesthetized rabbits and by Keissar et al. (2010), both for normal subjects and for patients with cardiovascular issues. For comparison, we also show an analysis of the variability of the BRS as found by the xBRS technique for the considered data (Westerhof et al., 2004; Wesseling et al., 2017).

In addition, we performed the same spectral analysis for a set of simulated BP and IBI data. The simulated BP values are varying with both 0.1 Hz and a respiratory frequency (0.25 Hz). The BP data generate IBI values, using a simple model for the vagal and sympathetic influence on heart rate. The analysis of the simulated data both corroborates the validity of the applied analysis technique, and clarifies the differences in computed wavelet-derived BRS values (wBRS) under different circumstances.

MATERIALS AND METHODS

Subjects, Experimental Conditions

We used a subset of 25-min recordings from an experimental study into orthostatic tolerance performed in our Institute in the period 2001–2002 under auspices of the European Space

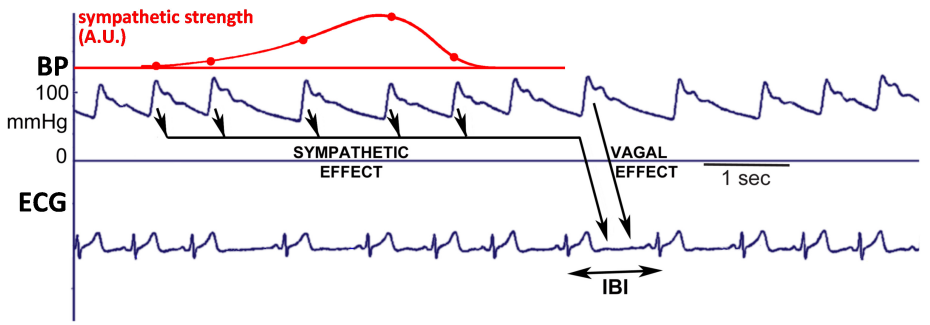

FIGURE 1 | Schematic diagram to explain how the simulated IBI-data were generated. The systolic pressure is considered to rapidly affect the length of the ongoing IBI, due to the vagal effect. In addition, the values of diastoles/systoles activate the sympathetics: lower pressure values cause more activity, inducing a shorter IBI. After a pressure change, the effect on IBI starts slowly, but lasts for some seconds, and so the considered IBI is affected by several past pressure-values, as depicted by the arrows. The dots on the red line indicate the relative contributions of each of these previous pressure values to the ongoing beat duration, in addition to the vagal effect.

Agency (ESA). The study had been authorized by the appropriate Ethical Boards and subjects had given written informed consent in accordance with the Declaration of Helsinki. The anonymized data from 10 subjects (4f/6m) were used, average age 35 years (range 27–47), BMI 21.9 kg/m^2 (19.3–26.0). The subjects were resting supine on a tilt table for 10 min, followed by three frequencies of paced breathing (audio cue, 10, 6, 15/min, respectively, each for 1.2 min, 1 min recovery); rate and hyper- or hypoventilation were checked by continuous measurement of expired CO_2 level. Then subjects were head-up tilted (HUT) in 1 s to a 70°, relaxed standing position, remained leaning against the table for 5 min and finally they were tilted back and 2 min of relaxed supine recording followed (Gisolf et al., 2004). In this study we used the IBI data and the derived systolic pressures from the continuous finger blood pressure data (Finometer, BMI-TNO, Netherlands; sample frequency 200 Hz, start of an IBI is set by the firmware at a point that corresponds to the very start of the systolic upslope as determined by a proprietary algorithm).

The data were analyzed using the beat-to-beat formalism, in which the nth systolic pressure (SAP_n) gets the same index as the IBI in which it occurs (IBI_n), and for spectral analysis purposes the time between items of the series (i.e., the sample frequency) is set to equal the mean IBI (De Boer et al., 1984, 1985). This is the most unambiguous way to study time- and phase-relationships between blood-pressure and IBI data (Karemaker and De Boer, 2017).

Simulated Data

Simulated data were constructed that are similar to observed data from our experimental protocol. A series of 2000 SAP-IBI pairs ("heart beats") was prepared. The pressure values consisted of a mean value of 120 mmHg plus the sum of two time-dependent sinusoidal contributions with frequencies of 0.1 and 0.25 Hz and amplitude 5 mmHg each. In addition, Gaussian noise (sigma = 2 mmHg) was added. The baroreflex control of IBI by the systolic pressures is modeled by vagal and sympathetic contributions (**Figure 1**). To relate the simulated data to the experimental protocol, the mean IBI and the vagal strength were set at different values during the simulated "supine" period (the first 1500 and final 200 beats) than during the "head up tilt" period (beats 1500–1800). Mean IBI was set at 1000 ms (supine) and 700 ms (HUT). Fast ("vagal") and slower ("sympathetic") baroreflex contributions transformed the fluctuations in pressure values into IBI-variations. The vagal BRS, affecting the length of the very interval in which the systolic pressure occurred, was set at 9 ms/mmHg in the supine period and at 3 ms/mmHg during HUT. The sympathetic contribution consisted of a time-varying contribution of previous pressures, linearly increasing from zero to 3 ms/mmHg between 5.6 and 3.2 s before the considered IBI, and next decreasing to zero again at 0.8 s. Gaussian noise (sigma = 5 ms) was added. The parameters we used are taken from our 1987 paper (De Boer et al., 1987), where a justification for their values is given.

Analysis Technique

Wavelets are short oscillatory signals with an amplitude that goes from zero to a maximum and back to zero; wavelets are characterized by their shape, frequency and duration (Torrence and Compo, 1998). To apply wavelet analysis to a signal, e.g., a cardiovascular signal, the wavelet is convolved with the signal. A high correlation value at a certain point in time implies that the signal at that moment contains information at the frequency of the wavelet. By applying a series of wavelets with different frequencies to the signal, its frequency content at each moment in time can be determined. This is in contrast to standard Fourier-analysis techniques, which compute the frequency content of the signal over a period in time.

Cross wavelet analysis is a technique that was developed in the 1980s for the simultaneous analysis of two signals in the frequency domain and in the time domain. It is mainly used in fields such as oceanography (Jevrejeva et al., 2003), meteorology (Torrence and Compo, 1998), and econometrics (Rua and Nunes, 2009). The technique has also been applied

for studies in circulation physiology (Kashihara et al., 2009; Keissar et al., 2010). The great strength of cross analysis is that it enables one to study how spectral features evolve over time. Hence values for magnitude, BRS, phase and coherence can be determined as a function of time. Using classical cross spectral analysis, one obtains only a single value for these parameters for each considered time period. In this paper, we consider the BP-IBI interaction as an open-loop system, i.e., the variation of IBI is due to BP fluctuations by means of the baroreflex control system.

We utilized the continuous wavelet transform from the MATLAB® Wavelet Toolbox (MATLAB® R2018b), which is both powerful and very user-friendly. We kept most MATLAB® default settings, using Morse wavelets and four octaves with 12 steps each for the logarithmically distributed frequency values (49 frequencies). For our purpose, mainly the MATLAB® cwt-function and the wcoherence-function were needed, for the one-dimensional wavelet transform and for the wavelet coherence and cross-spectrum, respectively. The wcoherence function was slightly modified to obtain non-normalized values for the wavelet cross spectrum.

The wBRS and the phase angle ϕ between systolic pressure and IBI were computed as follows:

wcsSS, wcsII, and wcsSI are the cross spectra of SAP vs. SAP, IBI vs. IBI, and SAP vs. IBI, respectively. For a registration with N beats, the dimension of these complex matrices is $N \times 49$. Next, in matrix-notation:

$$\text{wBRS} = \frac{\text{abs (wcsSI)}}{\text{abs (wcsSS)}}$$

$$\phi = \text{angle (wcsSI)}$$

$$r^2 = \frac{\text{abs (wcsSI)}^2}{\text{abs (wcsSS)} \times \text{abs (wcsII)}}$$

This results in three matrices for wBRS, ϕ and r^2, each with size $N \times 49$. Values were discarded where $r^2 < 0.5$, because for low coherence the wBRS and phase angle ϕ cannot be reliably estimated (De Boer et al., 1985; p. 353). For N beats, $N \times 2$ values of intervals and pressure are given. Hence, the resulting data in the $N \times 49$ matrices contain much dependency. For smoothing purposes, we used a moving average filter with width $\sqrt{N/2}$, i.e., 32 for a recording of 2000 beats. The apparent frequency in the wavelet spectra is derived from the global sample rate, which is one over the averaged IBI. Because the *local* sample rate is one over the *local* IBI, this apparent frequency will vary with the *local* IBI (as will be visible in **Figures 7A,B**).

In order to study separately the low frequency 0.1 Hz-range and the higher frequency respiratory frequency range, wBRS-values and phase angle values were averaged in two octave-sized frequency-ranges: 0.07–0.15 Hz (LF) and 0.15–0.3 Hz (HF). Hence for the averaging over the frequencies, adjusted frequency ranges were used, with $f_{adj} = f \times (\text{IBI}_{local}/\text{IBI}_{total})$, where IBI_{local} is computed with a moving average filter with width $\sqrt{N/2}$.

xBRS-Computation

We computed the instantaneous baroreflex sensitivity (xBRS) by the cross-correlation of blood pressure and interbeat interval (IBI) in a 10-s sliding window as described by Westerhof et al. (2004). In short: a 10 s window moves in 1-s steps over the SAP and IBI signals, and values are resampled at a 1 s rate after application of a cubic spline. Then, cross-correlations of SAP and IBI are computed in this window with 0, 1, 2, and 5 s delay. The delay with the highest cross-correlation value is taken as optimal delay τ. If this value is positive and significant at $p < 0.05$, the quotient of the standard deviations of IBI and of SAP is taken as the local xBRS value. For details see also Wesseling et al. (2017).

RESULTS

Example for Subject A

We present the analysis of the data for the first subject in our protocol. **Figures 2A,B** are the recordings of the IBI and SAP during the experimental procedure. The two vertical lines indicate the moments of the tilt up and the tilt down procedure, respectively. During the HUT-period, both the value and the variability of the IBI decrease, while little change is seen in the blood pressure values.

Figures 3A,B present the wavelet-power of the IBI- and SAP-data over the same period; vertical is the frequency in mHz, and the color in each point indicates the amount of spectral power at this frequency at this moment in time. The vertical color bar indicates the numeric values. A horizontal dotted line is drawn at frequency 0.1 Hz. In **Figure 3A** mainly respiratory influence is seen for the IBI-spectrum around the 0.18 Hz range, which disappears during the HUT period. The effect of a short episode of forced 0.1 Hz breathing at around 12 min is visible in the figure. The respiratory influence in the spectrum of SAP values (**Figure 3B**) is less clear, while some spectral contributions in the very low-frequency (<0.07 Hz) range may exist, but we focus in this paper on the higher frequencies. For this subject, a short burst of power is visible in the SAP spectrum around 23 min due to the tilt-down activity [Of note: this is not a movement artifact in the recording, but due to the cardiovascular dynamics during and after a fast tilt-down maneuver (Van Heusden et al., 2006)].

Next, **Figure 3C** presents the wavelet cross-spectrum of IBI and SAP, where the color indicates the value of the squared coherence r^2. The arrows indicate the phase ϕ between IBI and SAP variations, but arrows are only drawn in time-frequency positions where $r^2 > 0.5$. A horizontal arrow ("3 o'clock") indicates no phase difference between IBI and SAP ($\phi = 0°$), and an arrow pointing downward in the 6 o'clock direction implies SAP-variations to lead IBI-variations by 90° ($\phi = -90°$), **Figure 3C** suggests during the supine period – until 18 min – mainly a $\phi = 0°$ value in the HF range, but during the HUT period (18–23 min), the phase is approximately $\phi = -60°$. The same value of approximately $\phi = -60°$ is seen around 0.1 Hz under both experimental conditions, except in the case of paced breathing at that frequency (around 12 min, **Figure 2**). Note that a phase delay of −60° at a frequency of 0.1 Hz amounts to a delay of 1.7 s, or one and a half beat in the supine period, or almost three beats during HUT.

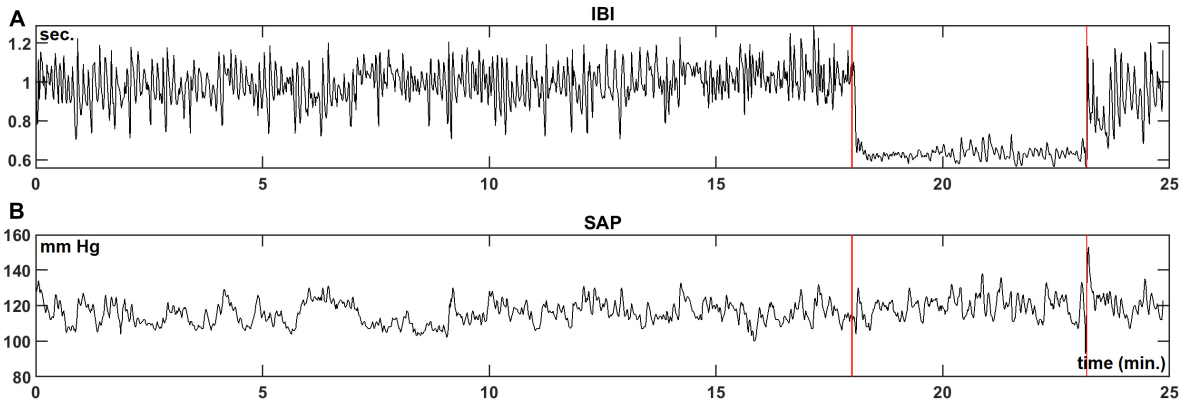

FIGURE 2 | Example registration of IBI **(A)** and SAP **(B)** data for a resting supine subject, who is passively moved to a 70° head-up-tilt position and back (between the vertical lines). In this case, a large increase in heart-rate during HUT is observed, while the blood pressure level is hardly affected.

Figure 3D presents the computed wBRS for the various frequencies, where the values are indicated by the color bar. The wBRS values are shown only when $r^2 > 0.5$. During the supine intervals the wBRS is seen to be in the 30–50 ms/mmHg range, while during HUT the wBRS is much lower and is more clearly defined at lower frequencies.

To differentiate between LF and HF variability, we present in **Figures 3E–H** plots of the various variables over time, averaged over the LF range (red line) and over the HF range (black line). In **Figure 3E**, the spectral powers of IBI for both frequency ranges are not too different, but large fluctuations are seen during the supine period. The power becomes much less during HUT. For the spectral values of SAP (**Figure 3F**), the power tends to increase during HUT. The spike at the end of the HUT period was discussed above.

During the supine period the phase between variations in IBI and SAP is around 0° for the HF band; its value fluctuates between 0° and around −60° for the LF band (**Figure 3G**). During HUT the phase is approximately −60° for both frequency bands. The wBRS-values (**Figure 3H**) show considerable variability during the supine period, with larger values of 30–45 ms/mmHg in the HF band than in the LF band (15–35 ms/mmHg). During HUT, the wBRS diminishes to values below 10 ms/mmHg.

All Subjects

The same analysis was performed for the experimental recordings from all ten subjects. The relevant data are summarized in **Table 1**, where the subjects are ordered according to their supine IBI. Although variability exists between the results of the different subjects, supine, and HUT conditions are seen to produce highly different results. The paired two-tailed Student's *t*-Test was applied to the results for the supine and HUT periods. As shown in **Table 1**, the differences between $wBRS_{supine}$ and $wBRS_{HUT}$ were found to be highly significant, both for the low and the high frequency range. Phase differences between the supine and HUT period were not significant for the LF, but highly significant for the HF.

wBRS-Variability

For comparison purposes, the data of **Figure 2** were also analyzed by the sequential xBRS-method (Westerhof et al., 2004; Wesseling et al., 2017). **Figure 4** shows the xBRS values together with the wBRS values for LF and HF from **Figure 3H**. The peaks and troughs in the signals of the xBRS-curve and the HF wBRS curve are rather similar, and the low BRS value during the HUT-maneuver is evident in all three curves. **Figures 5A,B** are scatterplots of xBRS vs. the LF and HF wBRS, respectively. Data are shown from the supine (black) and HUT (red) periods. A clear correlation between the values is seen between the xBRS and wBRS datasets, which have been computed using rather different methods.

Simulated Data

For the simulated IBI and SAP data (see section "Materials and Methods"), the same analysis was performed. **Figures 6A,B** show the IBI and SAP values, and **Figures 7A,B** present the wavelet spectral values as a function of time. The vertical axis shows the frequency as derived from a constant sample rate equal to one over the global mean of IBI (0.96 s in this simulation). However, with the wavelet technique results are obtained for frequencies related to the *local* sample rate, which is one over the *local* IBI (see **Figure 6A**): 1.0 s for beats 1–1500 and 1801–2000 ("supine") and 0.7 s for beats 1501–1800 ("HUT"). Hence the *apparent* frequency in the wavelet spectra varies with the *local* IBI: the imposed 0.1 and 0.25 Hz frequencies appear at somewhat higher values during the supine period, and at lower values during HUT.

The wavelet cross spectrum in **Figure 7C** shows a high coherence, except at the moments of transition from supine to HUT and vice versa. **Figures 7D–H** show for the simulated data similar information as **Figures 3D–H**. Especially **Figures 7G,H** demonstrate that the wavelet analysis is well able to derive specific information from the SAP- and IBI-data. The various conditions (simulated supine vs. HUT) lead to quite different phase angles (**Figure 7G**) and wBRS-values (**Figure 7H**) in the two frequency-ranges. In the **Appendix** we show that these wavelet-derived

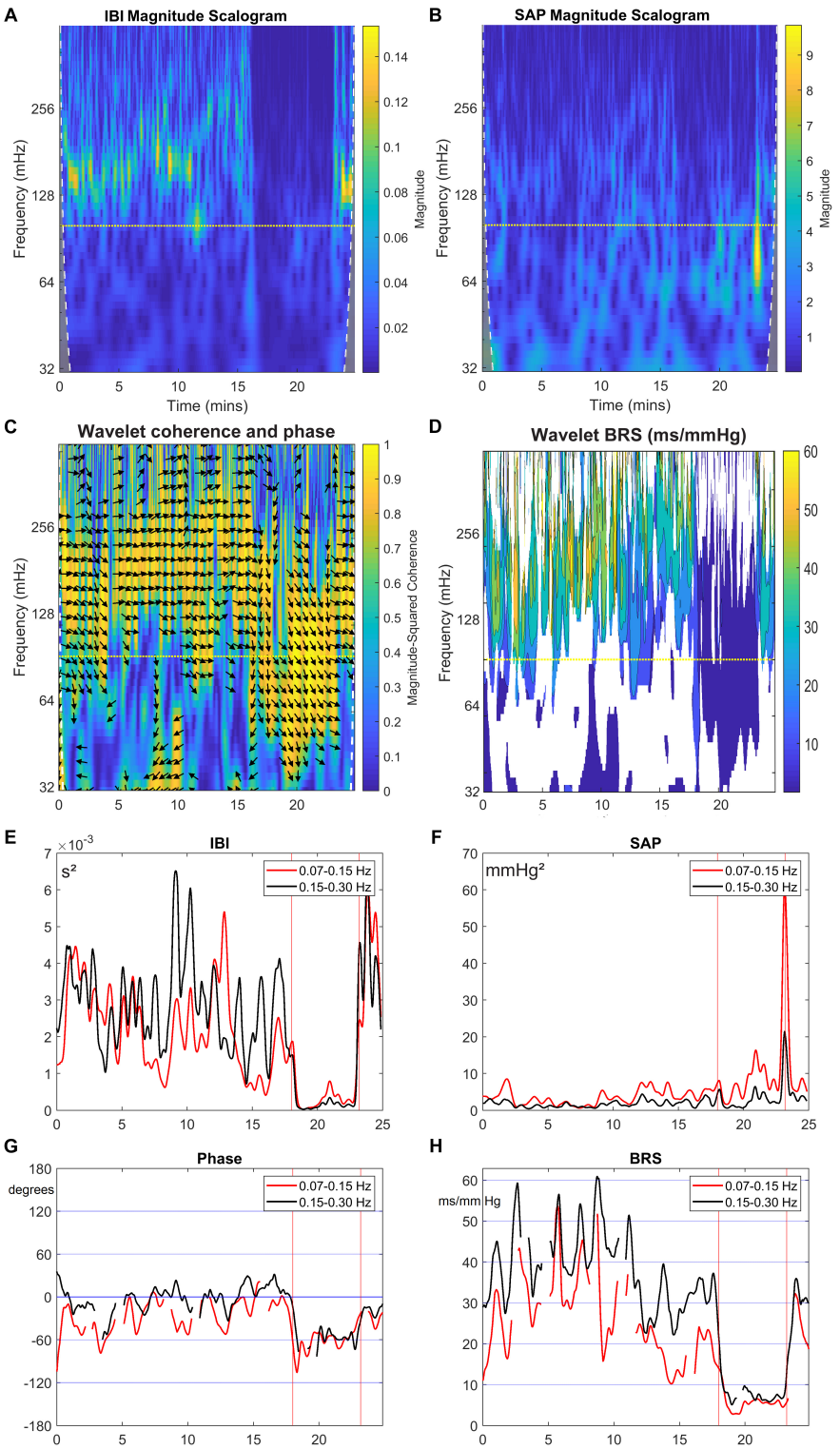

FIGURE 3 | Wavelet analysis of IBI and SAP variability, and resulting BRS and phase between SAP and IBI for the data from **Figure 2**. The colors in the upper panels show the spectral power for each frequency and for each point of time, **(A)** for IBI and **(B)** for SAP. The 0.1 Hz frequency is indicated by a dotted line. **(C)** shows the wavelet coherence r^2 (color) and phase (arrows) between SAP and IBI. Arrows pointing in the 3 o'clock indicate zero phase difference. Phase is shown only where $r^2 > 0.5$. In **(D)**, the BRS is calculated from the data in the first two panels (only where $r^2 > 0.5$). In **(E,F),** the mean spectral power in the LF band (red line) and in HF band (black line) is shown for IBI and SAP variability. **(G,H)** show the mean phase between SAP and IBI and the mean BRS for both frequency bands. A negative phase implies SAP-variations leading IBI-variations.

TABLE 1 | Summary of the results for the 10 subjects, ordered according to supine IBI.

Subject	IBI ± SD (s)		SAP (mmHg)		wBRS LF (ms/mmHg)		wBRS HF (ms/mmHg)		Phase LF (degrees)		Phase HF (degrees)		wBRS supine – HUT (ms/mmHg)		Phase supine – HUT (degrees)	
	Supine	HUT	Supine	HUT	Supine	HUT	Supine	HUT	Supine	HUT	Supine	HUT	LF	HF	LF	HF
J	0.64 ± 0.04	0.59 ± 0.04	129 ± 4	147 ± 7	8.1 ± 2.7	4.7 ± 1.2	12.3 ± 3.0	5.7 ± 1.4	−86 ± 18	−77 ± 26	−70 ± 13	−76 ± 12	3.4	6.6	−10	6
C	0.65 ± 0.04	0.58 ± 0.02	114 ± 6	115 ± 7	6.2 ± 1.7	4.7 ± 1.5	8.2 ± 2.8	5.1 ± 1.2	−59 ± 18	−57 ± 15	−58 ± 19	−52 ± 22	1.5	3.1	−3	−5
F	0.76 ± 0.06	0.64 ± 0.05	112 ± 7	111 ± 9	11.0 ± 4.3	4.2 ± 0.8	18.5 ± 5.7	5.3 ± 1.0	−41 ± 20	−54 ± 14	−32 ± 30	−63 ± 8	6.8	13.2	13	31
A	0.98 ± 0.10	0.63 ± 0.03	115 ± 6	119 ± 6	24.1 ± 12.1	5.0 ± 1.4	38.6 ± 12.1	7.2 ± 1.4	−35 ± 38	−61 ± 17	−4 ± 23	−61 ± 15	19.1	31.4	26	57
E	0.94 ± 0.08	0.73 ± 0.06	111 ± 6	122 ± 7	12.5 ± 3.7	7.5 ± 2.7	26.6 ± 7.7	11.5 ± 4.8	−83 ± 21	−67 ± 45	−46 ± 15	−63 ± 17	5.0	15.1	−15	17
G	0.99 ± 0.08	0.75 ± 0.06	102 ± 6	106 ± 7	14.6 ± 4.9	7.3 ± 1.6	19.8 ± 5.6	7.9 ± 1.7	−50 ± 14	−62 ± 12	−25 ± 18	−70 ± 10	7.3	11.9	12	45
H	1.04 ± 0.03	0.82 ± 0.03	102 ± 4	118 ± 8	8.0 ± 3.2	4.2 ± 1.1	11.9 ± 3.7	4.3 ± 1.1	−48 ± 26	−65 ± 16	−21 ± 21	−71 ± 16	3.8	7.6	17	50
I	1.02 ± 0.07	0.87 ± 0.06	117 ± 7	117 ± 6	13.0 ± 5.6	8.8 ± 3.7	24.9 ± 7.7	14.7 ± 4.1	−63 ± 31	−74 ± 18	−18 ± 21	−18 ± 15	4.2	10.2	11	−1
D	1.03 ± 0.06	0.87 ± 0.07	104 ± 5	110 ± 6	11.4 ± 4.2	6.8 ± 1.8	18.5 ± 6.5	9.5 ± 2.0	−46 ± 38	−41 ± 64	−33 ± 20	−44 ± 15	4.6	9.0	−5	11
B	1.31 ± 0.10	0.95 ± 0.08	113 ± 5	113 ± 6	24.4 ± 12.8	9.5 ± 2.3	47.4 ± 13.6	14.1 ± 4.2	−30 ± 44	−34 ± 12	4 ± 20	−18 ± 17	14.9	33.3	4	22
Mean ± SEM	0.94 ± 0.06	0.74 ± 0.04	112 ± 3	118 ± 4	13.3 ± 2.0	6.3 ± 0.6	22.7 ± 3.9	8.5 ± 1.2	−54 ± 6	−59 ± 4	−30 ± 7	−54 ± 7	7.1 ± 1.8	14.1 ± 3.2	5 ± 4	23 ± 7
												p-value:	0.003	0.002	0.250	0.008
													*	*	–	*

For each subject, separate supine and HUT values (mean and standard deviation) are given for IBI, SAP, and wBRS and phase (SAP vs. IBI) for both frequency ranges. The last columns give the difference between mean wBRS and mean phase for supine and HUT conditions. The row indicated "Mean" shows the mean and standard error of the variables. The p-values for the paired two-tailed Student's t-test are given.

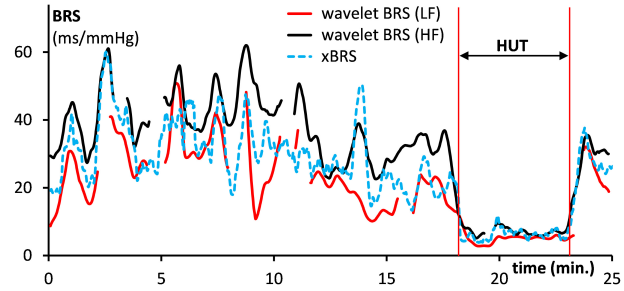

FIGURE 4 | Comparison of the computed xBRS (dotted line) with the wavelet BRS in the LF range (drawn red line) and the HF range (black). Data are for the subject of **Figure 2**. The HUT period is indicated.

values correspond well with the theoretical values as derived from the simulation parameters.

DISCUSSION

In this paper we apply a wavelet technique to analyze the cardiovascular regulation by the baroreflex during varying physiological conditions (supine and head-up-tilt). Using data from healthy subjects, we show that both the magnitude and the phase of the wBRS – being the wavelet derived BRS in open loop representation – differ between the supine condition and during a head-up-tilt maneuver. Analysis of simulated data demonstrates that the applied technique retrieves the correct parameters from the simulation (see **Appendix**). The main purpose of this paper is to describe the analysis technique and to demonstrate how the results can be applied to better understand the relations between cardiovascular signals. Therefore, we do not emphasize the interindividual differences between subjects nor the statistical characteristics of the method. This also applies to possible time patterns in the variability of the instantaneous wavelet results: in an earlier publication the 20–50 s variations in xBRS were attributed to the interaction of respiratory and cardiovascular control in the resting state. The present study was not designed to investigate this issue further.

Although several authors have used wavelet techniques in the study of cardiovascular regulation (e.g., Brychta et al., 2006; Stankovski et al., 2013; Singh et al., 2018), only few papers are known to us which applied cross wavelet techniques for the analysis of blood-pressure and heart-rate variability (Keissar et al., 2006, 2008, 2010; Kashihara et al., 2009). The first papers of Keissar et al. (2006, 2008) show principally the usefulness of this technique in the study of the ANS. In their 2010 paper these authors present the fluctuations of computed BRS values for supine subjects and during active standing up. In their registration the BRS values vary less rapidly compared to our results. We assume this to be due to the differences in analysis techniques. Kashihara et al. (2009) used wavelet techniques to identify the dynamic baroreflex properties from transient changes of step pressure inputs in anesthetized rabbits. Both Orini et al. (2010, 2012), Carrasco-Sosa and Guillen-Mandujano (2012) and Carrasco-Sosa and Guillén-Mandujano, 2013 used a

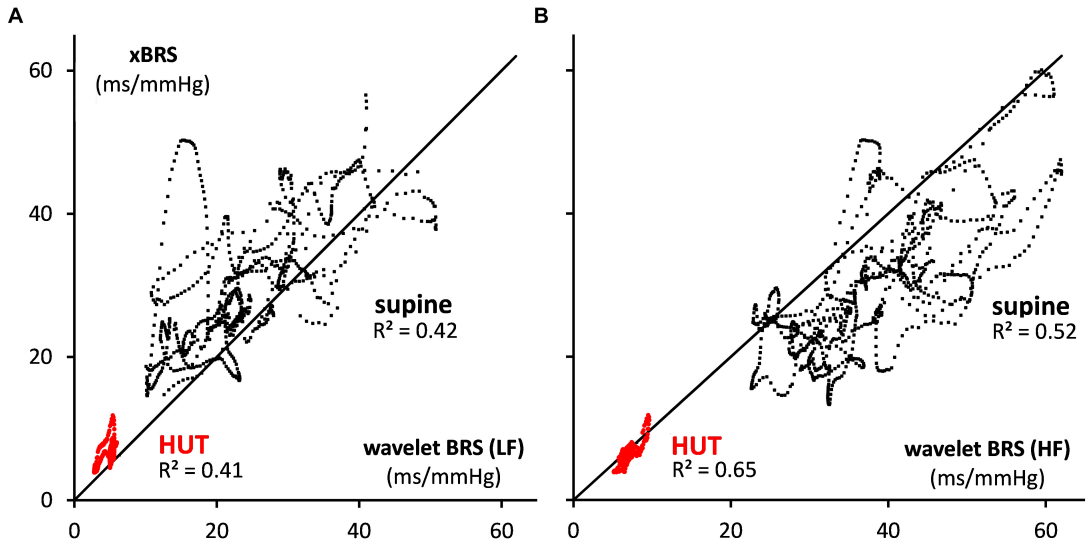

FIGURE 5 | Scatterplots of xBRS vs. the wavelet BRS in the **(A)** LF and **(B)** HF range. The black dots indicate data points in supine position, and red dots are for HUT. The black line of identity is shown.

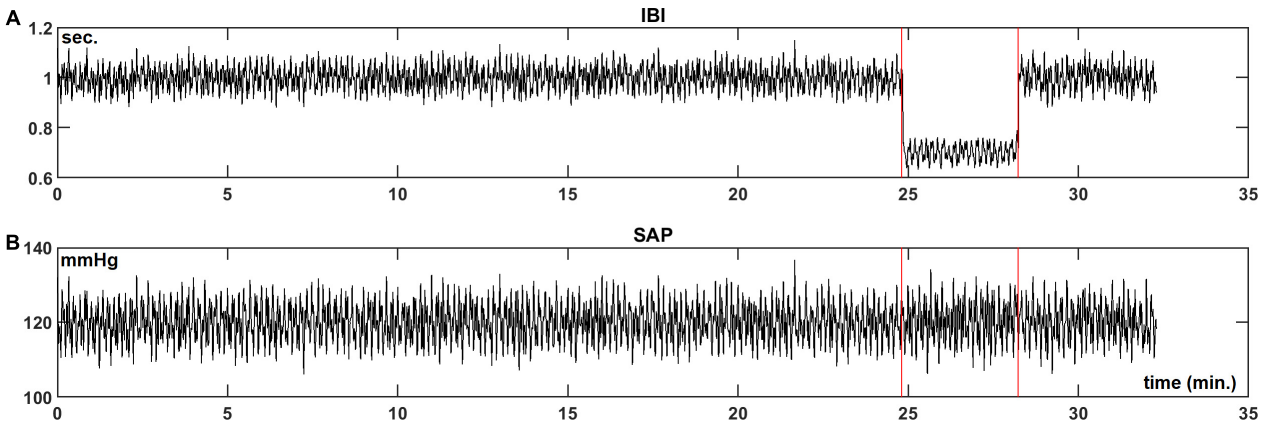

FIGURE 6 | Simulated IBI **(A)** and SAP **(B)** data as described in section "Materials and Methods." In the simulation, during the "HUT"-period (25 to 28.5 min) the mean IBI is decreased from 1.0 to 0.7 s and the vagal influence is reduced.

different time-frequency analysis method [SPWVD: smoothed pseudo Wigner–Ville distribution (Xiang and Hu, 2012)] to dynamically assess the spontaneous BRS under varying physiological conditions. In our opinion, the wavelet approach has similar power as the SPWVD approach and is conceptually more straightforward. In addition, the wavelet computation is now readily available in the powerful MATLAB® toolbox.

The summary of data presented in **Table 1** indicates that BRS under supine conditions is higher than during the HUT period, both for the low and high frequency parts of the signals (Cooke et al., 1999). In the LF range, the mean phase difference between SAP to IBI was similar at −54° and −59° for the supine and HUT conditions, respectively. This corresponds well with the phase angle of around 70° as suggested by the 1987-model from De Boer et al. (1987). In accordance with this model, the phase for the HF variations was much lower (mean: −30°) for the data from the supine period; however, during HUT again a value of −54° was found, indicating a departure from the simple model.

We put the wBRS-technique to the test in two different ways. First, we compared the wBRS-results, separately for LF and HF, to the xBRS-method, which is a completely different technique to obtain a high rate of BRS-estimates in time (cf. **Figures 4**, **5**). xBRS was shown to take a mid-position between LF-wBRS and HF-wBRS, which can be understood because xBRS is estimated in a sliding 10-s window and therefore both respiratory and 10-s variations will affect the resulting regression coefficient between BP and IBI. **Figure 5B** shows a good correlation between xBRS and HF-wBRS, with, as to be expected, consistently lower values for xBRS (Frederiks et al., 2000).

As a second test, we constructed a set of simulated SAP data, which controlled the IBI data through simulated sympathetic

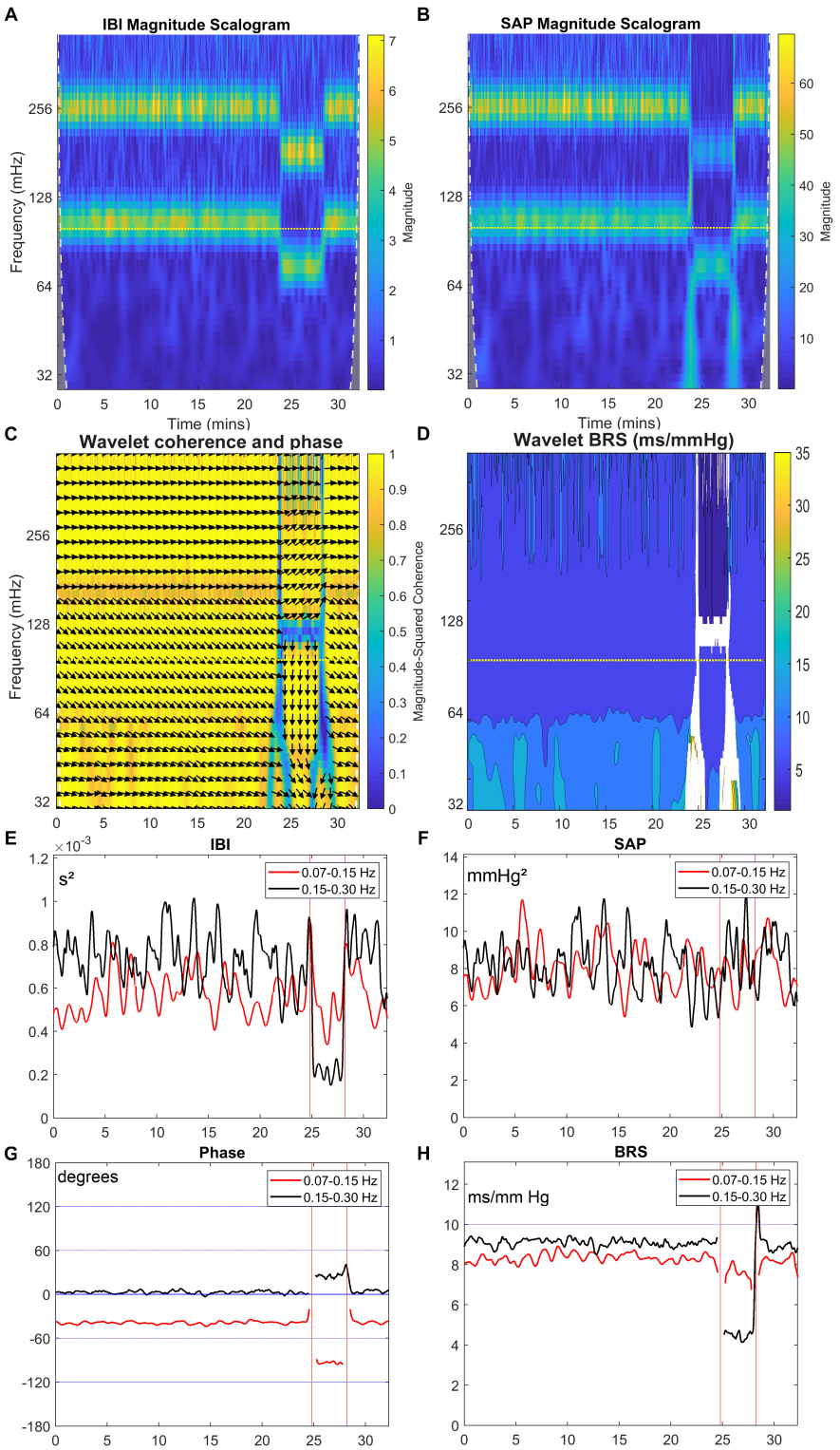

FIGURE 7 | Wavelet analysis of IBI and SAP variability and resulting BRS for simulated data. The layout of this figure is identical to **Figure 3**. The colors in the upper panels show the spectral power for each frequency and for each point of time, **(A)** for IBI and **(B)** for SAP. **(C)** shows the wavelet coherence r^2 (color) and phase (arrows) between SAP and IBI. In **(D)**, the BRS is calculated from the data in **(A,B)**. In **(E,F)**, the mean spectral power in the LF band (red line) and in HF band (black line) is shown for IBI and SAP variability. **(G,H)** show the mean phase between SAP and IBI and the mean BRS for both frequency bands. A negative phase implies SAP-variations leading IBI-variations. The imposed frequencies are 0.1 and 0.25 Hz but due to our beat-to-beat approach the *apparent* frequencies are slightly higher during the supine period, and lower during the (shorter) HUT period.

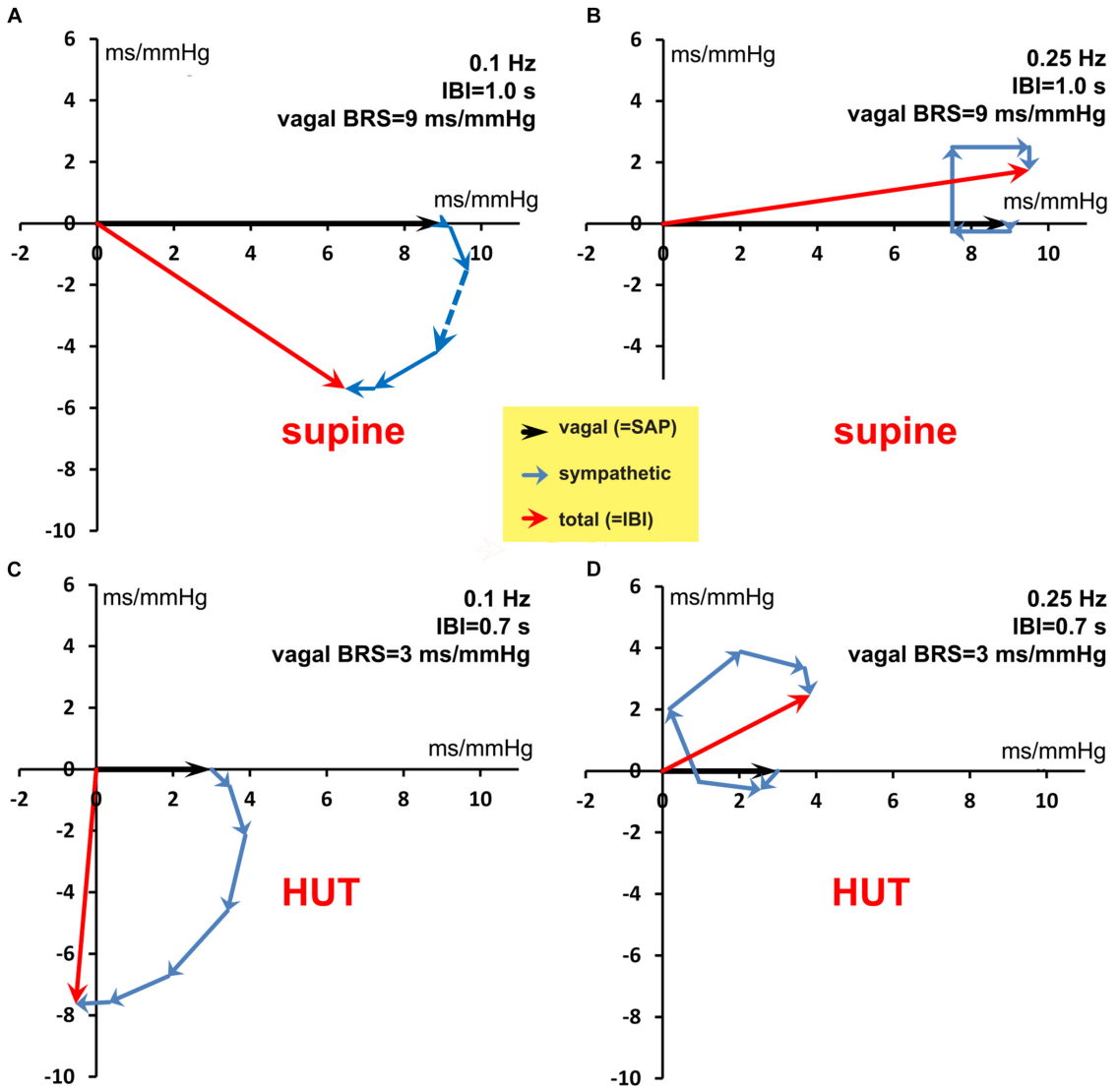

FIGURE 8 | Vector addition of the frequency-dependent vagal and sympathetic BRS contributions for simulated data. The black vector indicates the vagal BRS contribution, coinciding in phase with the SAP variation. The blue vectors are the sympathetic BRS contributions, varying in size and direction, as suggested by **Figure 1**. The sum of vagal and sympathetic contributions determines the total BRS-vector (red), which controls the IBI-variations, the phase of which differs in general from the SAP phase. **(A,B)** are for the simulated supine conditions, with frequency 0.1 and 0.25 Hz, respectively. The orientation and size of the dashed vector in **(A)** is explained in detail in the text. **(C,D)** are for the HUT condition, with faster IBI and less vagal contribution. The figure shows that a variety of phase angles and BRS magnitudes can result from the combination of vagal and sympathetic effects.

and parasympathetic involvement. The **Appendix** shows how the computed wBRS values and the phase angles between variations in SAP and IBI can be well explained by the vector-addition of the vagal and sympathetic BRS-contributions (**Figure 8** and **Table 2**). The **Appendix** also demonstrates that in the case of interaction of parasympathetic and sympathetic drive the apparent BRS-value can be quite different from expectation.

We did not specifically analyze the short periods of paced breathing in the protocol; in particular the period of 6 breaths per minute is, generally, well-recognizable in IBI, not so much in BP (cf. **Figure 2** at 12 min), therefore, it also appears clearly in the IBI spectrum (e.g., **Figure 3A**).

The large fluctuations in observed values, both for wBRS and xBRS, are notable. In earlier publications it has been argued that the blood pressure controlling system is working by noisy parameters, and hence large intrinsic variability results, even when time-averaged values are determined (Westerhof et al., 2004; Eckberg and Kuusela, 2005; Karemaker and Wesseling, 2008; Wesseling et al., 2017). Since our data come from resting, healthy subjects, the variability observed in this paper might be pointing directly at the inner working of what also is found by more abstract approaches such as entropy of the observed beat-to-beat values of IBI and BP (Richman and Moorman, 2000). The disappearance of variability after induction of anesthesia

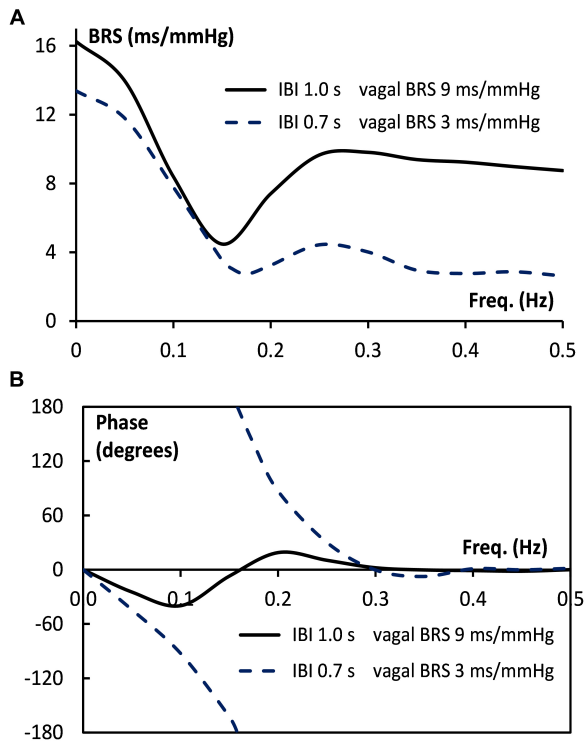

FIGURE 9 | Bode plot of BRS for simulated supine and HUT data. The size **(A)** and the phase angle **(B)** of the BRS vector are given as a function of frequency, both for the supine (drawn line) and the HUT conditions (dotted line).

TABLE 2 | Calculated length (BRS) and phase angle of the BRS-vectors, relating the IBI and SAP variations in our simulated data.

	Vector-summation				
	IBI (s)	**Vagal BRS (ms/mmHg)**	**Freq. (Hz)**	**BRS (ms/mmHg)**	**Phase angle**
Supine	1.0	9	0.10	8.4	−40°
Supine	1.0	9	0.25	9.7	10°
HUT	0.7	3	0.10	7.6	−94°
HUT	0.7	3	0.25	4.6	33°
Supine	1.0	9	0.16	4.7	4°
HUT	0.7	3	0.16	3.2	172°

*The first two rows are with the simulation parameters for the "supine" period (**Figures 8A,B**) for the two imposed frequencies (0.1 and 0.25 Hz). The next two rows are for the "HUT" simulation (**Figures 8C,D**). In addition, values are given for an imposed frequency of 0.16 Hz (**Figures 10A,B**). In the latter case, under simulated HUT conditions the sympathetic influence dominates, leading to antiphase between IBI and SAP values.*

(Scheffer et al., 1993) is another argument why we consider the variability of wBRS and phase relations between BP and IBI to be real phenomena rather than the result of intricate calculations applied to inherently poor-quality, noisy data.

The system that regulates blood pressure and heart rate is a closed loop feedback system: blood pressure controls heart rate through the baroreflex, and the heart rate controls the blood pressure - to some extent - through diastolic runoff (Windkessel effect) and Starling's law (De Boer et al., 1987; Faes et al., 2011; Porta et al., 2011). In ambulatory conditions, the separate determination of open- and closed loop gains is complex (Parati et al., 2019) and therefore often pharmacological methods are used for this purpose, applying Granger causality tests (Porta et al., 2013). A different approach to the study of causal couplings between the various cardiovascular parameters is in the information domain studies, often applying entropy measures (Faes et al., 2011; Javorka et al., 2017a,b, 2018). The technique we present in this paper only considers the baroreflex control of heart rate, which amounts to an open-loop analysis. This is justified if the feedforward gain of the baroreflex control is much larger than the feedback gain, each gain being scaled according to the noise entering the system at both ends of the loop (De Boer, 1985, p. 154). Although the observed phase-relationship between SAP- and IBI-variability that we present in this paper can be explained by a high baroreflex gain including sympathetic contributions, this result certainly does not yet prove that the baroreflex is the dominant factor in the cardiovascular loop.

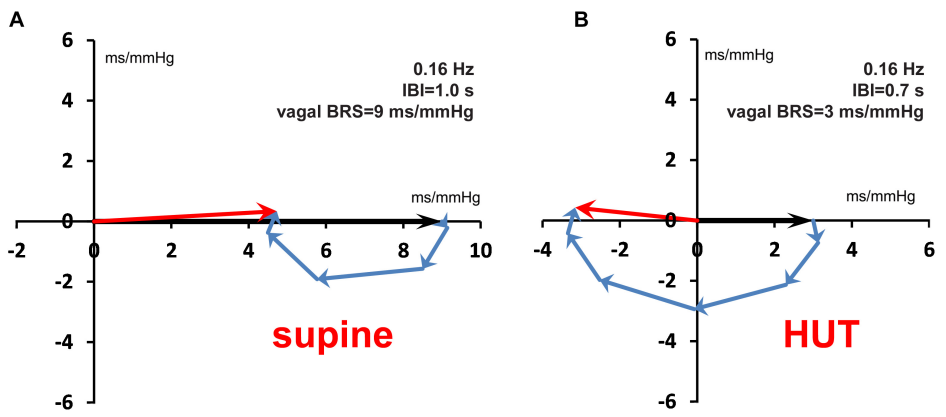

FIGURE 10 | Vector addition of vagal and sympathetic BRS contributions for the 0.16 Hz frequency, both for the supine **(A)** and the HUT condition **(B)**. Around this frequency the Bode plot (**Figure 9B**) shows for the HUT condition a phase angle of ±180°. Note the antiphase between SAP and IBI variations in **(B)**.

In this paper we extended these earlier studies into the moment-to-moment variability of the condition of the autonomic nervous system (ANS). Heart rate- and blood pressure variability are considered to be reflections of the ANS, but most techniques to catch its condition in a number require extended periods of time. For instance, the recommendation of the "Task Force" (Malik et al., 1996) prescribes a period of at least 5 min to obtain stable measures. This shows the clash of requirements: on the one hand the cardiologist/clinician who needs a set number to describe a patient's condition, a number that can show health or disease, and on the other hand the investigator/clinician who wants to look into the ANS and see how it changes and adapts to instantaneous stimuli, external or internal. In the latter case heart rate and blood pressure variability, and also the computed BRS, are only substitutes for what really is going on inside the central nervous system.

CONCLUSION

The wavelet approach is an elegant way for time-frequency analysis of cardiovascular data. It enables the estimation of (cross)spectra and derived quantities such as wBRS during time-varying conditions without the need of arbitrary cut-offs. From the cross spectra, one obtains both the coherence and the phase between two signals, which can be used as a strict test for model-based studies. This gives a new way to manage, for instance, the data streams that are collected in intensive care clinical settings, but it may also point the way to a more appropriate use and interpretation of the multitude of e-health data which more and more people are collecting.

ETHICS STATEMENT

The study used anonymized data from previous studies. These studies had been carried out in accordance with the recommendations of ESA's Medical Review Board and the Medical Ethics Committee of the Academic Medical Center, Amsterdam. All subjects had given written informed consent in accordance with the Declaration of Helsinki. The protocol was approved by both Ethics Committees.

AUTHOR CONTRIBUTIONS

Both authors conceived and designed the study, analyzed and interpreted the data, and drafted the manuscript. JK acquired the data.

ACKNOWLEDGMENTS

The authors gratefully acknowledge the help of Wim J. Stok, M.Sc., in all matters concerning ICT-support.

REFERENCES

Bertinieri, G., di Rienzo, M., Cavallazzi, A., Ferrari, A. U., Pedotti, A., and Mancia, G. (1985). A new approach to analysis of the arterial baroreflex. *J. Hypertens Suool.* 3, S79–S81.

Borst, C., and Karemaker, J. M. (1983). Time delays in the human baroreceptor reflex. *J. Auton. Nerv. Syst.* 9, 399–409. doi: 10.1016/0165-1838(83)90004-8

Brychta, R. J., Shiavi, R., Robertson, D., Biaggioni, I., and Diedrich, A. (2006). A simplified two-component model of blood pressure fluctuation. *Am. J. Physiol. Heart Circ. Physiol.* 292, H1193–H1203. doi: 10.1152/ajpheart.00645.2006

Carrasco-Sosa, S., and Guillen-Mandujano, A. (2012). "Correlation between spectral measures of systolic blood pressure variability and heart rate variability during paced breathing, standing and exercise," in *Proceedings of the Computing in Cardiology*, (Krakow: IEEE), 169–172.

Carrasco-Sosa, S., and Guillén-Mandujano, A. (2013). "Correlations between spectral measures of baroreflex sensitivity variability and hrv during supine position, paced breathing, standing and exercise," in *Proceedings of the Computing in Cardiology*, (Zaragoza: IEEE),

Cooke, W. H., Hoag, J. B., Crossman, A. A., Kuusela, T. A., Tahvanainen, K. U. O., and Eckberg, D. L. (1999). Human responses to upright tilt: a window on central autonomic integration. *J. Physiol.* 517, 617–628. doi: 10.1111/j.1469-7793.1999.0617t.x

De Boer, R. W. (1985). *Beat-to-beat blood-Pressure Fluctuations and Heart-Rate Variability in Man: Physiological Relationships, Analysis Techniques and a Simple Model*. Amsterdam: University of Amsterdam.

De Boer, R. W., Karemaker, J. M., and Strackee, J. (1984). Comparing spectra of a series of point events particularly for heart rate variability data. *IEEE Trans. Biomed. Eng.* 31, 384–387. doi: 10.1109/TBME.1984.325351

De Boer, R. W., Karemaker, J. M., and Strackee, J. (1985). Relationships between short-term blood-pressure fluctuations and heart-rate variability in resting subjects I: a spectral analysis approach. *Med. Biol. Eng. Comput.* 23, 352–358. doi: 10.1007/BF02441589

De Boer, R. W., Karemaker, J. M., and Strackee, J. (1987). Hemodynamic fluctuations and baroreflex sensitivity in humans: a beat-to-beat model. *Am. J. Physiol.* 253, H680–H689.

De Boer, R. W., Karemaker, J. M., and Van Montfrans, G. A. (1986). "Determination of baroreflex sensitivity by spectral analysis of spontaneous blood pressure and heart rate fluctuations in man," in *Neural Mechanisms and Cardiovascular Disease*, 3rd Edn, eds B. Lown, A. Malliani, and M. Prosdocimi (Berlin: Springer-Verlag).

Eckberg, D. L., and Kuusela, T. A. (2005). Human vagal baroreflex sensitivity fluctuates widely and rhythmically at very low frequencies. *J. Physiol.* 567, 1011–1019. doi: 10.1113/jphysiol.2005.091090

Faes, L., Nollo, G., and Porta, A. (2011). Information domain approach to the investigation of cardio-vascular, cardio-pulmonary, and vasculo-pulmonary causal couplings. *Front. Physiol.* 2:80. doi: 10.3389/fphys.2011.00080

Frederiks, J., Swenne, C. A., TenVoorde, B. J., Honzíkovaá, N., Levert, J. V., Maan, A. C., et al. (2000). The importance of high-frequency paced breathing in spectral baroreflex sensitivity assessment. *J. Hypertens.* 18, 1635–1644. doi: 10.1097/00004872-200018110-00015

Gisolf, J., Akkerman, E. M., Schreurs, A. W., Strackee, J., Stok, W. J., and Karemaker, J. M. (2004). Tilt table design for rapid and sinusoidal posture change with minimal vestibular stimulation. *Aviat. Space Environ. Med.* 75, 1086–1091.

Goldstein, D. S., Horwitz, D., and Keiser, H. R. (1982). Comparison of techniques for measuring baroreflex sensitivity in man. *Circulation* 66, 432–439. doi: 10.1161/01.CIR.66.2.432

Javorka, M., Czippelova, B., Turianikova, Z., Lazarova, Z., Tonhajzerova, I., and Faes, L. (2017a). Causal analysis of short-term cardiovascular variability: state-dependent contribution of feedback and feedforward mechanisms. *Med. Biol. Eng. Comput.* 55, 179–190. doi: 10.1007/s11517-016-1492-y

Javorka, M., Krohova, J., Czippelova, B., Turianikova, Z., Lazarova, Z., Javorka, K., et al. (2017b). Basic cardiovascular variability signals: mutual directed interactions explored in the information domain. *Physiol. Meas.* 38, 877–894. doi: 10.1088/1361-6579/aa5b77

Javorka, M., Krohova, J., Czippelova, B., Turianikova, Z., Lazarova, Z., Wiszt, R., et al. (2018). Towards understanding the complexity of cardiovascular oscillations: insights from information theory. *Comput. Biol. Med.* 98, 48–57. doi: 10.1016/j.compbiomed.2018.05.007

Jevrejeva, S., Moore, J. C., and Grinsted, A. (2003). Influence of the arctic oscillation and el niño-southern oscillation (enso) on ice conditions in the baltic sea: the wavelet approach. *J. Geophys. Res.* 108:4677. doi: 10.1029/2003JD003417

Karemaker, J. M., and De Boer, R. W. (2017). Vagal baroreflex latency in circulatory control. *J. Physiol.* 595, 2197–2198. doi: 10.1113/JP273766

Karemaker, J. M., and Wesseling, K. H. (2008). Variability in cardiovascular control: the baroreflex reconsidered. *Cardiovasc. Eng.* 8, 23–29. doi: 10.1007/s10558-007-9046-4

Kashihara, K., Kawada, T., Sugimachi, M., and Sunagawa, K. (2009). Wavelet-based system identification of short-term dynamic characteristics of arterial baroreflex. *Ann. Biomed. Eng.* 37, 112–128. doi: 10.1007/s10439-008-9599-4

Kawada, T., and Sugimachi, M. (2016). Open-loop static and dynamic characteristics of the arterial baroreflex system in rabbits and rats. *J. Physiol. Sci.* 66, 15–41. doi: 10.1007/s12576-015-0412-5

Keissar, K., Davrath, L. R., and Akselrod, S. (2006). Time-frequency wavelet transform coherence of cardio-respiratory signals during exercise. *Comput. Cardiol.* 33, 733–736.

Keissar, K., Davrath, L. R., and Akselrod, S. (2008). Wavelet transform coherence estimates in cardiovascular analysis: error analysis and feasibility study. *Comput. Cardiol.* 35, 461–464. doi: 10.1109/CIC.2008.4749078

Keissar, K., Maestri, R., Pinna, G. D., La Rovere, M. T., and Gilad, O. (2010). Non-invasive baroreflex sensitivity assessment using wavelet transfer function-based time-frequency analysis. *Physiol. Meas.* 31, 1021–1036. doi: 10.1088/0967-3334/31/7/011

Li, K., Rüdiger, H., Haase, R., and Ziemssen, T. (2018). An innovative technique to assess spontaneous baroreflex sensitivity with short data segments: multiple trigonometric regressive spectral analysis. *Front. Physiol.* 9:10. doi: 10.3389/fphys.2018.00010

Malik, M., Bigger, J. T., Camm, A. J., Kleiger, R. E., Malliani, A., Moss, A. J., et al. (1996). guidelines heart rate variability: standards of measurement, physiological interpretation, and clinical use. *Eur. Heart J.* 17, 354–381. doi: 10.1093/oxfordjournals.eurheartj.a014868

Orini, M., Laguna, P., Mainardi, L. T., and Bailón, R. (2012). Assessment of the dynamic interactions between heart rate and arterial pressure by the cross time–frequency analysis. *Physiol. Meas.* 33, 315–331. doi: 10.1088/0967-3334/33/3/315

Orini, M., Mainardi, L. T., Gil, E., Laguna, P., and Bailón, R. (2010). "Dynamic assessment of spontaneous baroreflex sensitivity by means of time-frequency analysis using either RR or pulse interval variability," in *Proceedings of the2010 Annual International Conference of the IEEE Engineering in Medicine and Biology Society*, Buenos Aires,

Parati, G., Castiglioni, P., Faini, A., Di Rienzo, M., Mancia, G., Barbieri, R., et al. (2019). Closed-Loop cardiovascular interactions and the baroreflex cardiac arm: modulations over the 24 h and the effect of hypertension. *Front. Physiol.* 10:1–10. doi: 10.3389/fphys.2019.00477

Parati, G., Di Rienzo, M., Bertinieri, G., Pomidossi, G., Casadei, R., Groppelli, A., et al. (1988). Evaluation of the baroreceptor-heart rate reflex by 24-hour intra-arterial blood pressure monitoring in humans. *Hypertension* 12, 214–222. doi: 10.1161/01.HYP.12.2.214

Parati, G., Saul, J. P., Di Rienzo, M., and Mancia, G. (1995). Spectral analysis of blood pressure and heart rate variability in evaluating cardiovascular regulation: a critical appraisal. *Hypertension* 25, 1276–1286. doi: 10.1161/01.hyp.25.6.1276

Pickering, T. G., and Davies, J. (1973). Estimation of the conduction time of the baroreceptor-cardiac reflex in man. *Cardiovasc. Res.* 7, 213–219. doi: 10.1093/cvr/7.2.213

Porta, A., Bari, V., Bassani, T., Marchi, A., Pistuddi, V., and Ranucci, M. (2013). Model-based causal closed-loop approach to the estimate of baroreflex sensitivity during propofol anesthesia in patients undergoing coronary artery bypass graft. *J. Appl. Physiol.* 115, 1032–1042. doi: 10.1152/japplphysiol.00537.2013

Porta, A., Catai, A. M., Takahashi, A. C. M., Magagnin, V., Bassani, T., Tobaldini, E., et al. (2011). Causal relationships between heart period and systolic arterial pressure during graded head-up tilt. *Am. J. Physiol. Regul. Integr. Comp. Physiol.* 300, R378–R386. doi: 10.1152/ajpregu.00553.2010

Richman, J. S., and Moorman, J. R. (2000). Physiological time-series analysis using approximate entropy and sample entropy. *Am. J. Physiol. Heart Circ. Physiol.* 278, H2039–H2049.

Robbe, H. W. J., Mulder, L. J. M., Ruddel, H., Langewitz, W. A., Veldman, J. B. P., and Mulder, G. (1987). Assessment of baroreceptor reflex sensitivity by means of spectral analysis. *Hypertension* 10, 538–543. doi: 10.1161/01.hyp.10.5.538

Rua, A., and Nunes, L. C. (2009). International comovement of stock market returns: a wavelet analysis. *J. Empir. Finance* 16, 632–639. doi: 10.1016/J.JEMPFIN.2009.02.002

Rudas, L., Pflugfelder, P. W., and Kostuk, W. J. (1993). Immediate cardiovascular responses to orthostasis in the early and late months after cardiac transplantation. *Int. J. Cardiol.* 38, 141–150. doi: 10.1016/0167-5273(93)90173-E

Scheffer, G. J., TenVoorde, B. J., Karemaker, J. M., Ros, H. H., and De Lange, J. J. (1993). Effects of thiopentone, etomidate and propofol on beat-to-beat cardiovascular signals in man. *Anaesthesia* 48, 849–855. doi: 10.1111/j.1365-2044.1993.tb07412.x

Singh, R. S., Saini, B. S., and Sunkaria, R. K. (2018). Times varying spectral coherence investigation of cardiovascular signals based on energy concentration in healthy young and elderly subjects by the adaptive continuous morlet wavelet transform. *IRBM* 39, 54–68. doi: 10.1016/j.irbm.2017.12.004

Smyth, H. S., Sleight, P., and Pickering, G. W. (1969). Reflex regulation of arterial pressure during sleep in man: a quantitative method of assessing baroreflex sensitivity. *Circ. Res.* 24, 109–121. doi: 10.1161/01.RES.24.1.109

Stankovski, T., Cooke, W. H., Rudas, L., Stefanovska, A., and Eckberg, D. L. (2013). Time-frequency methods and voluntary ramped-frequency breathing: a powerful combination for exploration of human neurophysiological mechanisms. *J. Appl. Physiol.* 115, 1806–1821. doi: 10.1152/japplphysiol.00802.2013

Torrence, C., and Compo, G. P. (1998). A practical guide to wavelet analysis. *Bull. Am. Meteorol. Soc.* 79, 61–78.

Van Heusden, K., Gisolf, J., Stok, W. J., Dijkstra, S., and Karemaker, J. M. (2006). Mathematical modeling of gravitational effects on the circulation: importance of the time course of venous pooling and blood volume changes in the lungs. *Am. J. Physiol. Heart Circ. Physiol.* 291, H2152–H2165. doi: 10.1152/ajpheart.01268.2004

Wesseling, K. H., Karemaker, J. M., Castiglioni, P., Toader, E., Cividjian, A., Settels, J. J., et al. (2017). Validity and variability of xBRS: instantaneous cardiac baroreflex sensitivity. *Physiol. Rep.* 5:e135091. doi: 10.14814/phy2.13509

Westerhof, B. E., Gisolf, J., Stok, W. J., Wesseling, K. H., and Karemaker, J. M. (2004). Time-domain cross-correlation baroreflex sensitivity: performance on the EUROBAVAR data set. *J. Hypertens.* 22, 1371–1380. doi: 10.1097/01.hjh.0000125439.28861.ed

Xiang, L., and Hu, A. (2012). Comparison of methods for different timefrequency analysis of vibration signal. *J. Softw.* 7, 68–74. doi: 10.4304/jsw.7.1.68-74

Conflict of Interest Statement: The authors declare that the research was conducted in the absence of any commercial or financial relationships that could be construed as a potential conflict of interest.

APPENDIX

Explanation of the Cross Spectral Results for the Simulated Data

This appendix shows how the amplitudes and phase angles of the wBRS values as presented in **Figures 7G,H** can be derived from the time-course of the BRS as assumed in the simulations.

In our open-loop simulation, the varying SAP values affect the length of the successive intervals by the vagal contribution – acting on IBI without delay – and by the slower sympathetic contributions (**Figure 1**). The vagal BRS is taken as 9 and 3 ms/mmHg in the supine and HUT condition, respectively, and the strength of the sympathetic BRS is taken as increasing from zero to 3 ms/mmHg in the time span of 5.6–3.2 s before the considered IBI, and then decreasing to zero again at 0.8 s before the IBI. In the following calculation only small deviations of the mean values are considered and so the SAP and IBI values may be considered to be equally spaced at distances 1000 ("supine") and 700 ms ("HUT").

The wavelet analysis decomposes the fluctuations in SAP and IBI into their constituent frequencies, where the phase-angles between the SAP- and IBI-components may vary. Then, for every frequency the quotient of the IBI- and SAP-components results in a BRS-vector, which has a magnitude and phase angle [see also De Boer (1985, pp. 157–159)].

An example to manually compute the BRS from simulated data: consider **Figure 8A**, which represents 0.1 Hz fluctuations during the "supine" period, i.e., the mean IBI is taken as 1000 ms and the vagal contribution to the BRS is 9 ms/mmHg. Both the 0.1 Hz SAP-variation and the 0.1 Hz IBI-variation are presented as rotating vectors in this diagram. The phase of the 0.1 Hz SAP-variation is defined as 0° (direction of 3 o'clock in the figure) and rotation in this figure is anticlockwise. The variation in IBI is determined by a number of previous SAP values through the action of the baroreflex. In our simulation the vagal BRS contribution (no delay!) has also a phase of 0° and a strength of 9 ms/mmHg (heavy black arrow in **Figure 8A**). As to the sympathetic influence: the preceding SAP values have different weights and lags in their contribution to the total BRS (**Figure 1**). The sympathetic contribution of each SAP-value to the total BRS appears in **Figure 8A** as a vector (blue arrow).

For example: the dashed arrow indicates the baroreflex contribution of $SAP_{n\ -\ 3}$ to IBI_n. This SAP value leads the considered IBI by three beats or 3 s, which implies a phase angle of $3/10 \times 360° = 108°$ for the considered 0.1 Hz contribution. The length of the dashed vector is given by the strength of the BRS-contribution at each instant, 2.75 ms/mmHg in this case. In a similar way the other sympathetic vectors are calculated. For a mean IBI value of 1.0 s, five previous SAP-values contribute to the sympathetic effect, with strengths 0.25, 1.5, 2.75, 2.0, and 0.75 ms/mmHg., and phase angles −36°, −72°, −108°, −144°, and −180°, respectively. These vectors are added to the vagal BRS (9 ms/mmHg) and the vector summation results in a total BRS (red arrow) of magnitude 8.4 ms/mmHg and a phase angle of −39.8°, which also represents the relative size and phase angle of the IBI-variation at this frequency.

The figure shows that interval variations lag behind pressure variations, as expected for a baroreflex-effect. The computed magnitude and phase angle values correspond with the wBRS results as shown in **Figures 7G,H** for the 0.1 Hz variations in the "supine" period.

In an identical manner, the resulting BRS-vectors for the HF band (**Figure 8B**) and for the "HUT" data (**Figures 8C,D**) are calculated (**Table 2**, top four lines). The results are always in agreement with the wavelet results from **Figures 7G,H**, although minor differences exist due to the presence of the added random noise in the simulated data.

The vector plots show that the delayed action of the sympathetic influence results in a frequency dependent BRS value, which needs not be in phase with the pressure variations. This is illustrated in **Figure 9**, which shows the Bode plot (magnitude and phase) for the frequency dependence of the BRS for our simulated data, both for the supine conditions (drawn line) and for the HUT period (dashed line). **Figure 9A** shows that under supine conditions (drawn line) a slightly different frequency of the "10-second rhythm," for example 0.08 Hz or 0.12 Hz, results in quite different apparent BRS-values, 11 and 6 ms/mmHg, respectively. For the simulated HUT conditions, the phase plot (**Figure 9B**, dotted line) shows around 0.16 Hz a phase angle of ±180°, implying that for this frequency the interval variations are in antiphase with the pressure variations. **Figure 10** shows the vector-plots of the BRS for this 0.16 Hz frequency: both for the supine and for the low-vagal-BRS HUT condition the sympathetic BRS-contribution is seen to counteract the vagal BRS action. Although this might be a questionable effect which exaggerates physiologically realistic conditions, the lag in the sympathetic effect can be expected to influence observed BRS values to a great extent.

frontiers in Physiology

ORIGINAL RESEARCH
published: 23 August 2019
doi: 10.3389/fphys.2019.01061

Effects of Prolonged Head-Down Bed Rest on Cardiac and Vascular Baroreceptor Modulation and Orthostatic Tolerance in Healthy Individuals

Franca Barbic[1†], Karsten Heusser[2†], Maura Minonzio[1], Dana Shiffer[1], Beatrice Cairo[3], Jens Tank[2], Jens Jordan[2], André Diedrich[4], Peter Gauger[2], Roberto Antonio Zamuner[5], Alberto Porta[3,6] and Raffaello Furlan[1]*

[1]Humanitas Clinical and Research Center, Department of Internal Medicine, Istituto di Ricovero e Cura a Carattere Scientifico (IRCCS), Humanitas University, Rozzano, Italy, [2]German Aerospace Center (DLR), Institute of Aerospace Medicine, Cologne, Germany, [3]Department of Biomedical Sciences for Health, University of Milan, Milan, Italy, [4]Autonomic Dysfunction Center, Clinical Research Center (CRC), Department of Medicine, Vanderbilt University, Nashville, TN, United States, [5]Departamento de Kinesiología, Universidad Católica del Maule, Talca, Chile, [6]Department of Cardiothoracic, Vascular Anesthesia and Intensive Care, Istituto di Ricovero e Cura a Carattere Scientifico (IRCCS) Policlinico di San Donato, San Donato Milanese, Italy

OPEN ACCESS

Edited by:
Tijana Bojić,
University of Belgrade, Serbia

Reviewed by:
Philip J. Millar,
University of Guelph, Canada
Paola Sandroni,
Mayo Clinic, United States

***Correspondence:**
Franca Barbic
franca.barbic@humanitas.it

†These authors have contributed equally to this work

Specialty section:
This article was submitted to Autonomic Neuroscience, a section of the journal Frontiers in Physiology

Received: *21 January 2019*
Accepted: *02 August 2019*
Published: *23 August 2019*

Citation:
Barbic F, Heusser K, Minonzio M, Shiffer D, Cairo B, Tank J, Jordan J, Diedrich A, Gauger P, Zamuner RA, Porta A and Furlan R (2019) Effects of Prolonged Head-Down Bed Rest on Cardiac and Vascular Baroreceptor Modulation and Orthostatic Tolerance in Healthy Individuals. Front. Physiol. 10:1061. doi: 10.3389/fphys.2019.01061

Orthostatic intolerance commonly occurs after prolonged bed rest, thus increasing the risk of syncope and falls. Baroreflex-mediated adjustments of heart rate and sympathetic vasomotor activity (muscle sympathetic nerve activity – MSNA) are crucial for orthostatic tolerance. We hypothesized that prolonged bed rest deconditioning alters overall baroreceptor functioning, thereby reducing orthostatic tolerance in healthy volunteers. As part of the European Space Agency Medium-term Bed Rest protocol, 10 volunteers were studied before and after 21 days of –6° head down bed rest (HDBR). In both conditions, subjects underwent ECG, beat-by-beat blood pressure, respiratory activity, and MSNA recordings while supine (REST) and during a 15-min 80° head-up tilt (TILT) followed by a 3-min –10 mmHg stepwise increase of lower body negative pressure to pre-syncope. Cardiac baroreflex sensitivity (cBRS) was obtained in the time (sequence method) and frequency domain (spectrum and cross-spectrum analyses of RR interval and systolic arterial pressure – SAP, variability). Baroreceptor modulation of sympathetic discharge activity to the vessels (sBRS) was estimated by the slope of the regression line between the percentage of MSNA burst occurrence and diastolic arterial pressure. Orthostatic tolerance significantly decreased after HDBR (12 ± 0.6 min) compared to before (21 ± 0.6 min). While supine, heart rate, SAP, and cBRS were unchanged before and after HDBR, sBRS gain was slightly depressed after than before HDBR (sBRS: –6.0 ± 1.1 versus –2.9 ± 1.5 burst% × mmHg^{-1}, respectively). During TILT, HR was higher after than before HDBR (116 ± 4 b/min versus 100 ± 4 b/min, respectively), SAP was unmodified in both conditions, and cBRS indexes were lower after HDBR (α index: 3.4 ± 0.7 ms/mmHg; BRS_{SEQ} 4.0 ± 1.0) than before (α index: 6.4 ± 1.0 ms/mmHg; BRS_{SEQ} 6.8 ± 1.2). sBRS gain was significantly more depressed after HDBR than before (sBRS: –2.3 ± 0.7 versus –4.4 ± 0.4 burst% × mmHg^{-1}, respectively). Our findings suggest that

baroreflex-mediated adjustments in heart rate and MSNA are impaired after prolonged bed rest. The mechanism likely contributes to the decrease in orthostatic tolerance.

Keywords: orthostatic intolerance, bed rest, baroreflex sensitivity, muscle sympathetic nerve activity, spectrum analysis

INTRODUCTION

In 1944, Dock pointed out that "The physician must always consider complete bed rest as a highly un-physiologic and definitely hazardous form of therapy, to be ordered only for specific indications and discontinued as early as possible" (Dock, 1944). The statement, which challenged medical beliefs of that period, is now supported by numerous physiological investigations and clinical observations. For example, bed rest is associated with reductions in both effective circulating blood volume and cardiac output. Moreover, muscular atrophy particularly of lower limbs, thromboembolism, and infections may occur (Allen et al., 1999; McIntyre, 2013). In addition, prolonged bed rest predisposes to the common hospitalization-associated disability syndrome (Allen et al., 1999; Covinsky et al., 2011; Ettinger, 2011). Orthostatic intolerance and syncope have been observed after prolonged bed rest in various clinical settings (Feldstein and Weder, 2012; Guerin et al., 2016; Tzur et al., 2018). The condition negatively impacts patients' quality of life and increases the risk of falls (Shibao et al., 2007; Juraschek et al., 2017). Sometimes dramatic impairments in orthostatic tolerance have also been observed in astronauts returning to Earth (Ertl et al., 2002; Levine et al., 2002; Diedrich et al., 2007, 2015), which led to the discovery of novel mechanisms affecting orthostatic tolerance (Levine et al., 1997; Diedrich et al., 2007). For example, weightlessness elicited changes in muscle sympathetic nerve activity (MSNA) (Ertl et al., 2002) and in baroreflex heart rate regulation (Cox et al., 2002; Eckberg et al., 2010).

In healthy humans, venous pooling below the heart upon standing tends to reduce cardiac output and blood pressure (Mosqueda-Garcia et al., 1997; Furlan et al., 2001; Diedrich and Biaggioni, 2004). These changes unload cardiopulmonary and arterial baroreceptors eliciting compensatory changes in heart rate (HR) and in muscle sympathetic nerve activity (MSNA) (Mosqueda-Garcia et al., 1997; Furlan et al., 2000; Barbic et al., 2015). In healthy subjects, HR, plasma norepinephrine, and MSNA markedly increase with standing. Thus, systolic blood pressure is maintained while diastolic blood pressure slightly increases (Furlan et al., 2000). Conversely, an impaired baroreflex function as observed in patients with baroreflex failure (Robertson et al., 1993; Furlan et al., 2001; Heusser et al., 2005) promotes orthostatic intolerance. In addition, a proper baroreceptor function plays a crucial role in synchronizing the neural sympathetic discharge activity and the cardiovascular spontaneous fluctuations at 0.1 Hz (LF) in the upright position (Furlan et al., 2000). The synchronization appears to be important for orthostatic tolerance (Furlan et al., 2000, 2015; Barbic et al., 2007).

We tested the hypothesis that a controlled long-lasting bed rest may induce changes in baroreceptor response while supine and during up-right position, eventually resulting in reduced orthostatic tolerance in healthy volunteers.

MATERIALS AND METHODS

Experimental Protocol

As part of the European Space Agency Medium-Term-Bed Rest Study (ClinicalTrials.gov Identifier: NCT01655979; Buehlmeier et al., 2014), 10 healthy men (33 ± 1 years, BMI 23.4 ± 0.2 kg/m^2) were studied before and after 21 days of −6° head down bed rest (HDBR). The study was conducted at the DLR facilities of the Institute of Aerospace Medicine (Colonie, Germany).

Before starting with the study protocol, the subjects were confined to the metabolic ward of the German Aerospace Center for 7 days for environmental, routine, and diet adaptation. During the intervention period (HDBR), all the activities of daily routine such as eating and hygienic procedures took place in bed. The subjects were allowed to change their horizontal position by maintaining at least one shoulder in contact with the mattress. Muscular activity of the legs was not allowed. A passive physical therapy was included regularly every 3–4 days to reduce the psychological tension. The adherence to the study rules was controlled by study nurses in charge and by a continuous 24-h video monitoring (Buehlmeier et al., 2014).

During the HDBR, volunteers were encouraged to keep a constant day and night routine, characterized by 16–17 h of wakefulness and 7–8 h of night sleep. Ward lights were turned off from 11 pm to 6 am. Temperature and humidity inside the metabolic ward were controlled during the study (21.5 ± 1°C, 40 ± 6.3%) (Buehlmeier et al., 2014).

An independent medical doctor monitored the subjects' health status during daily ward rounds. No adverse events according to good clinical practice were reported, and no drugs potentially affecting cardiovascular autonomic system were prescribed during HDBR (Buehlmeier et al., 2014).

Diet composition followed the requirements given by a standardization document of ESA ("Standardization of bed rest study conditions," Version 1.5) based on 120% of resting metabolic rate (RMR) to account for the low physical activity associated with the bed rest period (Buehlmeier et al., 2014). Methyl-xanthine derivatives (e.g., caffeine), alcohol, and flavor enhancers were prohibited.

During the HDBR, the volunteers were supplemented with 1,000 IU vitamin D3 per day in order to overcome the sunlight exclusion (Buehlmeier et al., 2014).

Before and after 21 days of −6° head down bed rest (HDBR), all subjects underwent to continuous ECG,

beat-by-beat blood pressure (BP; Finapres Medical Systems, Ohmeda), respiratory rate (Electrobioimpedance Amplifier, Biopac System, Inc.), and MSNA (Nerve Traffic Analyzer; model 662C-3; University of Iowa Bioengineering, Iowa City, IA, USA) recordings. Measurements were obtained in the supine position (REST) and during 15 min of 80° head-up tilt (TILT) followed by a 3-min −10 mmHg stepwise increase of lower body negative pressure (LBNP) up to pre-syncope. Pre-syncope was defined as progressive hypotension, tachycardia/bradycardia, pallor, yawning, and symptoms including sweating, nausea, and lightheadedness (el-Bedawi and Hainsworth, 1994; Protheroe et al., 2013). Tilt termination criteria were as follows: sudden onset of pallor, blurred vision, lightheadedness, sweating, nausea, an increase or a decrease in HR greater than 40% and/or a decrease in systolic arterial pressure (SAP) greater than 40% compared to what observed during the first 5 min of asymptomatic TILT.

The time of TILT to pre-syncope was computed to quantify the orthostatic tolerance.

MSNA was recorded from the peroneal nerve of the right leg as detailed elsewhere (Mosqueda-Garcia, 1996). Briefly, multiunit recordings of postganglionic sympathetic activity were obtained by placing a tungsten electrode in the right peroneal nerve, posterior to the fibular head. A reference electrode was inserted subcutaneously, close by the recording needle.

This study was carried out in accordance with the recommendations of the Aerztekammer Nordrhein (Dusseldorf, Germany) with written informed consent from all subjects. The protocol was approved by the ethic committee of the Aerztekammer Nordrhein (Dusseldorf, Germany).

Data Analysis

ECG, BP, respiratory activity, and MSNA were digitized at 500 Hz by an analog-to-digital converter (AT-MIO 16E2; National Instruments) and recorded with BNC-2110 data acquisition system and LabVIEW 7.0 software (National Instruments, Austin, TX, USA) for off-line analysis.

MSNA raw signal was filtered (700–2,000 Hz), amplified (1,000 × 99.9), rectified, and integrated with a time constant of 0.1 s *via* a nerve traffic analysis system (662C-3, University of Iowa). The sympathetic bursts were detected by an adaptive thresholding methodology accounting for the baseline wandering and different MSNA burst amplitudes as previously described (Diedrich et al., 2009). Specifically, the burst detection threshold was updated on a beat-to-beat basis to follow baseline wandering and changes of MSNA burst amplitude (Diedrich et al., 2009). The threshold was then assessed by calculating the minimum value of the sympathetic burst and the difference between the maximum and minimum values in each cardiac cycle. The running threshold was provided by the minimum value plus 30% of the difference between the maximum and minimum values of the burst.

The MSNA burst was searched in a temporal window ranging from 0.9 to 1.7 s starting from the R-wave peak of the first R-wave peak delimiting the current cardiac cycle to account for the latency from aortic and carotid baroreceptor stimulation to the potential vascular sympathetic response (Macefield et al., 1994; Wallin et al., 1994; Diedrich et al., 2009). SAP was computed as the maximum BP in a given heart period approximated as the temporal distance between two successive R-wave peaks detected in the ECG. Diastolic arterial pressure (DAP) was computed as the minimum arterial pressure following SAP. The temporal occurrences of the MSNA burst and DAP were also stored.

Autoregressive spectrum and cross-spectrum analysis of RR interval, SAP, and respiratory activity variability have been described in detail elsewhere (Pagani et al., 1986; Furlan et al., 2000; Barbic et al., 2007). For RR interval spontaneous variability, there are two major spectral components, the amplitude of which is affected by changes in cardiac neural autonomic control (Pagani et al., 1986; Furlan et al., 2000; Barbic et al., 2007). One is the high frequency, HF component (HF_{RR}, 0.25 Hz), synchronous with the respiration, an accepted index of vagal modulation to the sinoatrial node (Task Force of the European Society of Cardiology and the North American Society of Pacing and Electrophysiology, 1996; Furlan et al., 2000; Barbic et al., 2007). The other is the low frequency, LF (LF_{RR}, 0.1 Hz), that when expressed in normalized units has been proposed to primarily reflect the sympathetic efferent modulation to the sinoatrial node and its changes (Pagani et al., 1986; Task Force of the European Society of Cardiology and the North American Society of Pacing and Electrophysiology, 1996; Furlan et al., 2000; Barbic et al., 2007). Spectral components of RR variability in the high frequency (HF) and in the low frequency (LF) range are provided in absolute (ms^2) and in normalized units (n.u.). Absolute values of each component were computed as the integral of the oscillatory components LF_{RR} and HF_{RR}. Normalization was achieved by dividing the absolute power of each component by total variance minus the power of the very-low frequency component (0.03 Hz) and subsequently multiplying by 100 (Task Force of the European Society of Cardiology and the North American Society of Pacing and Electrophysiology, 1996). The LF/HF is a dimensionless index of the instantaneous reciprocal changes of cardiac sympathetic and vagal modulation (Pagani et al., 1986; Task Force of the European Society of Cardiology and the North American Society of Pacing and Electrophysiology, 1996). The LF oscillatory component of SAP variability (LF_{SAP}, 0.1 Hz), expressed in absolute values, is a marker of the sympathetic vascular modulation (Furlan et al., 2000; Barbic et al., 2007).

The time series length of REST, and TILT comprised of 300 consecutive beats, recorded 3 min before tilt interruption because of pre-syncope. The stationarity of the identified sequence was tested according to Magagnin and colleagues (Magagnin et al. 2011) over the original series after linear de-trending. If the test for the steadiness of mean and variance was not satisfied, a new selection was identified to have all the prerequisites for guaranteed restricted weak stationarity (Magagnin et al., 2011). Indeed, the stationarity of the mean is necessary even after linear de-trending because the cardiovascular variability trends are complex and not completely addressed by a simple linear approach.

All the analyses were performed on signals recorded in supine position (REST) and after 3 min of head-up tilt when all the volunteers were asymptomatic (TILT) before and after HDBR.

Baroreflex Control of Heart Rate

The cardiac baroreflex sensitivity (cBRS) was obtained in the frequency domain by the alpha index (α); Pagani et al., 1986; Furlan et al., 2000) and in the time domain according to the baroreflex sequence analysis approach (Bertinieri et al., 1988; Parati et al., 1988) as previously implemented by Porta et al. (2013).

The frequency domain approach is based on cross-spectral analysis of RR and SAP variability. After having obtained a squared coherence function (K^2) >0.5, the α index was computed as the square root of the ratio between the powers of the LF (0.1 Hz) spectral components of RR interval and SAP variability (Pagani et al., 1988).

The sequence analysis approach is based on the search for sequences characterized by the contemporaneous increase (positive sequence) or decrease (negative sequence) of RR and SAP values. Both positive and negative sequences are referred to as baroreflex sequences as previously described (Bertinieri et al., 1988). They were identified according to the following prerequisites: (1) the length of the sequences was four beats (three increases or decreases); (2) the lag between RR and SAP values was set to 0; (3) the total SAP variation was larger than 1 mmHg; (4) the total RR variation was larger than 5 ms; and (5) the correlation coefficient in the plane [SAP(i), RR(i)], where (i) is the cardiac beat number, was larger than 0.85. When a baroreflex sequence matched those prerequisites, the slope of the regression line in the plane [SAP(i), RR(i)] was calculated and averaged over all baroreflex sequences. This average was indicated as BRS and expressed as ms/mmHg. The percentage of baroreflex sequences found in the analyzed signals was also quantified.

Baroreflex Control of Sympathetic Activity to the Vessels

The assessment of sBRS considers how the DAP value relates to the occurrence of a MSNA burst accounting for the baroreflex latency (Hart et al., 2010). As previously described (Hart et al., 2010; Barbic et al., 2015; Marchi et al., 2015), DAP values were grouped into bins of 1 mmHg; the percentage of times that a MSNA burst was detected as associated with the considered values of DAP was counted. A weighted linear regression between nerve activity and DAP was performed. In the plane reporting MSNA burst incidence values (%) on the y axis and DAP values on the x axis, a linear regression analysis was performed. The slope of the regression line (a) furnished the index of sBRS gain provided that the correlation coefficient (r_{sBRS}) was significant ($p < 0.05$). The slope of the regression line is a negative value. Therefore, the steeper the sBRS gain, the more negative is the slope (**Figure 1**). Conversely, when the slope tends to 0, the regression line is flatter and the sBRS gain is less negative. More negative values correspond to a more efficient sympathetic baroreflex, while less negative value to a more depressed sympathetic baroreflex. Indeed, flattening of the DAP-MSNA relationship implies a decrease in the sympathetic modulation to the vessels in response to a unit change of DAP (Barbic et al., 2015).

Statistical Analysis

Continuous variables are expressed as mean ± standard error. The normality of data was tested *via* Kolmogorov-Smirnov test. Paired t test was used to assess differences in orthostatic tolerance time before and after HDBR. Repeated measure two-way analysis of variance followed by Holm-Sidak *post hoc* test was used to assess differences in hemodynamics, respiration cardiovascular autonomic parameters, baroreflex control indexes, and MSNA between REST and TILT before and after HDBR. The level of significance was set at 5%. SigmaPlot 11 (Systat Software Inc., Chicago, IL, USA) was used for statistical analysis.

RESULTS

The time to pre-syncope during orthostatic testing before and after HDBR is shown in **Figure 2**. The mean time to pre-syncope was 21.5 ± 0.8 min before and 12.5 ± 1.1 min after HDBR ($p < 0.05$). Before HDBR, all subjects required additional LBNP application to induce pre-syncope. Three subjects experienced pre-syncope with −10 mmHg, one with −20 mmHg, five with −30 mmHg, and one with −40 mmHg of LBNP. Conversely, after HDBR only in three of 10 volunteers, a −10 mmHg of LBNP was necessary to induce pre-syncope.

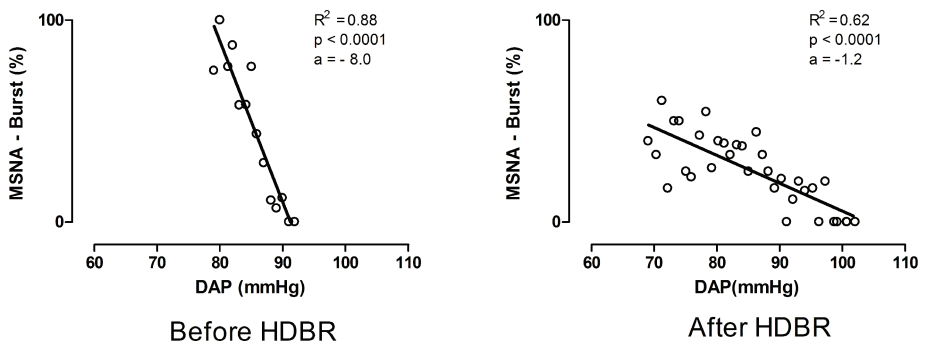

FIGURE 1 | Representative example of the values of sBRS during 80° head-up tilt before and after bed rest. Notice that after bed rest the gain of sBRS indicated by the slope (*a*) of the regression line between MSNA burst % occurrence and DAP values was lower as reflected by a flatter regression line than pre HDBR.

The mean values of the hemodynamics and respiratory activity while supine (REST) and during TILT before and after HDBR are reported in **Table 1**.

Before HDBR, HR and DAP values were higher during TILT than during REST, whereas no differences were observed in the SAP and respiration. After HDBR, HR and DAP were greater during TILT than during REST, without modifications in both SAP and respiratory activity (**Table 1**). Notably, HR during tilt after HDBR was greater than before HDBR (**Table 1**).

Cardiovascular autonomic as well as cardiac and sympathetic baroreflex indexes while supine (REST) and during TILT before and after HDBR are shown in **Table 2**.

At REST, cardiac baroreceptor control indices α and cBRS were unchanged after HDBR. The spectral indices of cardiac sympathetic and vagal modulation were only slightly modified, namely an increase in the $LF_{n.u.}$ component of sympathetic modulation of the sino-atrial node and a mild increase in the LF/HF ratio were observed. The gain of the sympathetic baroreflex modulation sBRS was significantly depressed after HDBR (sBRS: −2.9 ± 1.5 burst%/mmHg) compared to before (sBRS: −6.0 ± 1.1 burst%/mmHg). An adequate MSNA signal to noise ratio for burst activity automatic analysis was obtained in 8 of 10 individuals. MSNA was greater after HDBR. The spectral marker of sympathetic vasomotor control, LF_{SAP}, was unchanged (**Table 2**).

During TILT, RR interval, RR variance, and LF_{RR} values were lower after HDBR than before, as well as was the cardiac baroreceptor indices α. The $cBRS_{seq}$ index was slightly, but not significantly, lower after HDBR (**Table 2**).

The gain of sBRS, as indicated by the slope (a) (**Figure 1**) of the regression line between MSNA-burst % and DAP values, was significantly more depressed after HDBR (sBRS: −2.3 ± 0.7 burst%/mmHg) than before HDBR (sBRS: −4.4 ± 0.4 burst%/mmHg) indicating a less efficient sympathetic baroreflex control after HDBR (**Table 2**). This pattern was associated with only a slight, although non-significant, increase in MSNA values and a mild decrease in LF_{SAP} during HDBR compared to before HDBR (**Table 2**). Finally, after HDBR, the effect of orthostatic stimulus on MSNA discharge seems to be blunted, although not significantly, compared to before.

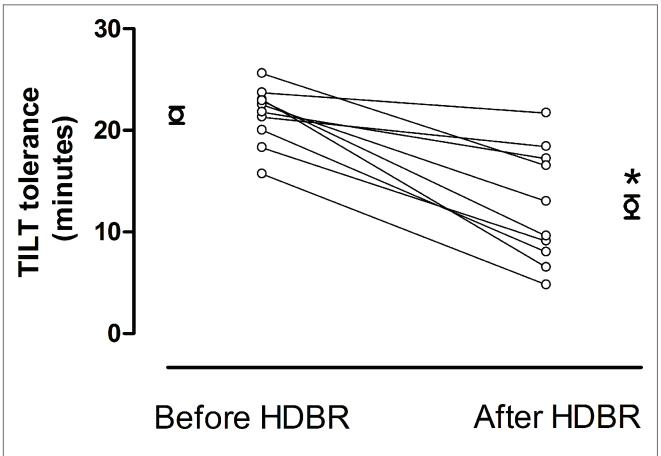

FIGURE 2 | Individual and mean values ± standard error of the 80° head-up tilt tolerance before and after HDBR. After HDBR orthostatic tolerance was significantly reduced compared to before HDBR.

TABLE 1 | Hemodynamics and respiratory activity while supine (REST) and during 80° head-up tilt (TILT) before and after HDBR.

	Before HDBR		After HDBR	
Parameters	**REST**	**TILT**	**REST**	**TILT**
HR, b/min	71.8 ± 3.0	99.7 ± 4.1*	70.7 ± 2.2	116.1 ± 4.1*,#
SAP, mmHg	130 ± 4	129 ± 4	130 ± 3	129 ± 6
DAP, mmHg	76 ± 2	88 ± 3*	74 ± 2	87 ± 3*
RESP, breaths/min	16.5 ± 1.9	16.2 ± 0.9	14.6 ± 0.5	15.4 ± 1.3

**REST vs. TILT $p < 0.05$.*

#Before HDBR vs. after HDBR $p < 0.05$.

HR, heart rate; SAP, systolic arterial pressure; DAP, diastolic arterial pressure; RESP, respiratory frequency; MSNA, muscle sympathetic nerve activity. Values are expressed as mean ± standard error.

DISCUSSION

The important finding of our study is that a 3-week lasting HDBR significantly reduced orthostatic tolerance in healthy young men. The response was associated with impaired baroreceptor control of vascular sympathetic drive, both, while supine and during orthostatic testing.

To quantify the potential changes in the orthostatic tolerance induced by HDBR, every volunteer underwent a 80° head-up tilt followed by LBNP (el-Bedawi and Hainsworth, 1994; Protheroe et al., 2013). The approach enabled us to quantify orthostatic tolerance in each individual, although it made MSNA recording procedure more complex. Following HDBR, time to pre-syncope decreased substantially as much less orthostatic stress was tolerated. This observation further indicates that HDBR remarkably impairs orthostatic tolerance.

Chronic bed-confinement is still a common condition in several clinical settings, particularly in patients hospitalized after major trauma and surgery as well as in the elderly (Feldstein and Weder, 2012; Guerin et al., 2016; Tzur et al., 2018). In this context, reduced gravity tolerance, induced by the gravitational and physical deconditioning associated with bed rest, was found to promote an increased risk of loss of consciousness and falls (Shibao et al., 2007; Juraschek et al., 2017).

Several studies addressed the pathophysiological mechanisms potentially underlying the impaired orthostatic tolerance induced by bed rest or after weightlessness (Blomqvist et al., 1980; Pawelczyk et al., 2001; Waters et al., 2005), a condition that is known to mimic the hemodynamic and autonomic effects of the prolonged lying down position. Pathophysiological mechanisms of orthostatic intolerance include hypovolemia induced by central plasma volume redistribution leading to secondary diuresis increase (Iwasaki et al., 2004; Waters et al., 2005), endothelial dysfunction (Coupe et al., 2009), and vascular sympathetic withdrawal (Kamiya et al., 2003). In addition, a proper baroreflex function controlling the cardiovascular system has been highlighted as mandatory for adequate orthostatic tolerance (Robertson et al., 1993; Mosqueda-Garcia et al., 1997;

TABLE 2 | Autonomic parameters, cardiac and sympathetic baroreceptor indexes, and MSNA assessed while supine (REST) and during 80° head-up tilt (TILT), before and after HDBR.

	Before HDBR		After HDBR	
Parameters	**REST**	**TILT**	**REST**	**TILT**
RR, ms	848 ± 35	634 ± 25*	856 ± 26	522 ± 19*,#
RR var., ms^2	2,288 ± 279	1,632 ± 412	2,270 ± 497	465 ± 176*,#
SAP var., $mmHg^2$	11.9 ± 2.1	40.5 ± 6.6*	11.8 ± 1.8	39.3 ± 10.7*
LF_{RR}, ms^2	805 ± 177	1,167 ± 298	649 ± 145	235 ± 82#
n.u.	58.7 ± 6.6	87.6 ± 3.4*	67.8 ± 6.1	83.5 ± 3.5*
HF_{RR}, ms^2	390 ± 85	154 ± 65*	347 ± 121	28 ± 12*
n.u.	36.7 ± 7.4	11.0 ± 3.2*	31.0 ± 6.1	14.7 ± 3.4*
LF/HF	2.7 ± 0.4	19.2 ± 2.1	3.1 ± 0.2	17.1 ± 3.1
LF_{SAP}, $mmHg^2$	5.4 ± 1.0	32.3 ± 6.6*	4.1 ± 1.1	23.9 ± 7.7*
α, ms/mmHg	12.4 ± 0.9	6.4 ± 1.0*	14.5 ± 1.9	3.4 ± 0.7*#
$cBRS_{SEQ}$	18.1 ± 1.9	6.8 ± 1.2*	15.3 ± 2.7	4.0 ± 1.0*
sBRS§, burst% × $mmHg^{-1}$	–6.0 ± 1.1	–4.4 ± 0.4	–2.9 ± 1.5#	–2.3 ± 0.7#
MSNA§, burst/min	18.0 ± 1.5	29.1 ± 1.7*	25.3 ± 1.8#	32.2 ± 2.3
MSNA§, burst/100 beats	26.9 ± 2.5	30.4 ± 2.4	35.0 ± 2.7	27.8 ± 2.7

§MSNA, n = 8 subjects.

**REST vs. TILT p < 0.05.*

#Before HDBR vs. after HDBR, p < 0.05.

RR, RR interval; var., variance; SAP, systolic arterial pressure; LF, low frequency; n.u., normalized units; HF, high frequency; α, cardiac baroreflex index assessed in the frequency domain; $cBRS_{SEQ}$, cardiac baroreflex index assessed in the time domain; sBRS, sympathetic baroreflex gain; MSNA, muscle sympathetic nerve activity.

Furlan et al., 2000; Kamiya et al., 2000a,b, 2003; Iwasaki et al., 2004; Heusser et al., 2005; Tank et al., 2012; Marchi et al., 2015). In addition, this study stresses further the relevance to separately assess both cardiac and sympathetic branches of the baroreflex regulatory activity in humans as already reported by previous studies while supine (Dutoit et al., 2010; Taylor et al., 2015) and during incremental head-up tilt (Marchi et al., 2016).

In our study, sympathetic baroreflex control of MSNA in the supine position was substantially attenuated following HDBR. The response was associated with increased MSNA, a finding already described after bed rest (Tanaka et al., 2013) and during (Ertl et al., 2002) and after weightlessness (Levine et al., 2002). Conversely, other authors found a reduced MSNA burst frequency after 14-day HDBR (Shoemaker et al., 1998). Remarkably, SAP and LF_{SAP} were unaffected by HDBR. This observation suggests that an increase in sympathetic activity after HDBR was not sufficient to produce tonic and phasic vasomotor responses.

With regard to the baroreflex control of heart rate, no changes were induced by HDBR when the subjects were supine, in keeping with a previous bed rest study performed under controlled plasma volume conditions (Iwasaki et al., 2004). Conversely, Kamiya and colleagues reported that after 60 and 120 days of HDBR, the gain of the baroreflex control of heart rate was flatter than at baseline (Kamiya et al., 2000a,b). The longer duration of HDBR stimulus compared to the present study may account for the differences on cardiac baroreflex control results. Not surprisingly, in the present study, HR and the spectral indices of RR variability were unmodified after HDBR.

With orthostatic stress, the gain of sympathetic baroreceptor modulation was remarkably depressed, in the presence of only a slight increase in MSNA. This unexpected finding might be accounted for by few possibilities. The statistical power of our study may have been too low to detect MSNA changes. Alternatively, HDBR may have primarily acted on the pre- and/or post-ganglionic sympathetic neurons by blunting their spontaneous discharge activity. If so, reduced baroreceptor inhibition observed after HDBR may not increase post-ganglionic sympathetic firing. Accordingly, SAP and LF_{SAP} were unmodified after HDBR. As expected, the cardiac baroreceptor indexes were lower after HDBR in the presence of a proper HR increase during the gravitational stimulus.

Of interest, Kamiya and colleagues (Kamiya et al., 2000a,b) found that sBRS slopes increased while supine and during 60°HUT, differently from what we observed in the present study. We do believe that a longer duration of HDBR stimulus (60 and 120 compared to our 21 days of HDBR) may account for the differences on both cardiac and sympathetic baroreflex control between our and Kamiya's results. Indeed, baroreceptor changes following HDBR are likely to be characterized by a time course that could partially explain the observed discrepancies.

In addition, in the present paper, the sBRS was obtained as the relationship between the percentage of times that a MSNA burst was detected as associated with the considered diastolic arterial pressure bin to quantify the sympathetic baroreflex control of the vessels. Such an approach proved to be effective in assessing sympathetic baroreceptor modulation in supine position during a modified Oxford trial (Hart et al., 2010) and during the orthostatic challenge (Barbic et al., 2015; Marchi et al., 2015). Of importance, this index is based on a probabilistic approach that is independent of a normalization procedure. By contrast, other methods enabling the assessment of baroreceptor modulation of sympathetic activity are based on the evaluation of burst amplitude (Kamiya et al., 2000a,b) or area (Doherty et al., 2018) and on their relationship with diastolic arterial pressure changes. Notably, all these approaches

require a normalization procedure that in most of the cases is represented by the highest burst observed during baseline condition or during controlled respiration (Diedrich et al., 2009). These normalization procedures are highly dependent on the specific situations occurring during the experimental condition utilized as a reference period and on mathematical procedure utilized to normalize the actual values and specific experimental conditions (Salmanpour and Shoemaker, 2012). As a consequence, any normalization procedure features some degree of arbitrariness.

Our data confirm the usefulness to extend the separate assessment of both cardiac and sympathetic branches of the reflex also when exploring the effects of prolonged physical deconditioning such as after HDBR.

Taken together, our findings suggest that HDBR exerted different changes on cardiac and sympathetic baroreceptor modulation both while supine and during the orthostatic stimulus. In the supine position, cardiac baroreflex gain and HR did not change, whereas a remarkable decrease in sympathetic baroreceptor control with a proper increase of MSNA discharge was evident. During the tilt maneuver, while a proper cardiac baroreceptor gain decrease and tachycardia were found, a concomitant reduction of baroreceptor modulation of sympathetic discharge to the vessels was observed in the absence of appropriate MSNA increase. Therefore, HDBR seems to act mostly on the sympathetic baroreceptor control of vasomotion. Accordingly, our healthy volunteers were unable to tolerate the orthostatic position as much as observed before HDBR.

CONCLUSIONS

Our study confirms the need to separately assess cardiac and sympathetic branches of baroreceptor cardiovascular control. This methodological approach seems to be useful also when exploring the effects of physical deconditioning as mimicked by the medium-term bed rest. Our data bear important implication in clinical setting characterized by a prolonged period of bed confinement and inactivity such as after fractures and major surgery in hospitalized patients and in the elderly. Finally, we hypothesize that baroreceptor assessment might be helpful to identify patients at increased risk of orthostatic intolerance that is more likely to suffer from syncope, falls, and consequent global disability syndrome.

ETHICS STATEMENT

This study was carried out in accordance with the recommendations of the Aerztekammer Nordrhein (Dusseldorf, Germany) with written informed consent from all subjects. All subjects gave written informed consent in accordance with the Declaration of Helsinki. The protocol was approved by the ethic commission of the Aerztekammer Nordrhein (Dusseldorf, Germany).

AUTHOR CONTRIBUTIONS

FB and RF were responsible for the conception and design of the study. FB, KH, RF, and PG were responsible for the acquisition of data. FB, BC, MM, DS, and RZ were involved in data analysis. FB, KH, RF, AP, AD, JJ, and JT were involved in data interpretation. FB, RF, KH, JJ, JT, AD, and AP contributed to the drafting of the article. All authors critically revised the draft and approved the final version of the manuscript.

FUNDING

This research project was supported by the European Space Agency grant AO-06-BR-18 and by the Ecker Technology SAGL, Lugano, Switzerland.

ACKNOWLEDGMENTS

We thank Wolfram Sies for the technical support and Dr. Judith Buehlmeier for the organization and constructive criticisms.

REFERENCES

Allen, C., Glasziou, P., and Del Mar, C. (1999). Bed rest: a potentially harmful treatment needing more careful evaluation. *Lancet* 354, 1229–1233. doi: 10.1016/S0140-6736(98)10063-6

Barbic, F., Perego, F., Canesi, M., Gianni, M., Biagiotti, S., Costantino, G., et al. (2007). Early abnormalities of vascular and cardiac autonomic control in Parkinson's disease without orthostatic hypotension. *Hypertension* 49, 120–126. doi: 10.1161/01.HYP.0000250939.71343.7c

Barbic, F., Heusser, K., Marchi, A., Zamuner, A. R., Gauger, P., Tank, J., et al. (2015). Cardiovascular parameters and neural sympathetic discharge variability before orthostatic syncope: role of sympathetic baroreflex control to the vessels. *Physiol. Meas.* 36, 633–641. doi: 10.1088/0967-3334/36/4/633

Bertinieri, G., Di Rienzo, M., Cavallazzi, A., Ferrari, A. U., Pedotti, A., and Mancia, G. (1988). Evaluation of baroreceptor reflex by blood pressure monitoring in unanesthetized cats. *Am. J. Phys.* 254, H377–H383. doi: 10.1152/ajpheart.1988.254.2.H377

Blomqvist, C. G., Nixon, J. V., Johnson, R. L. Jr., and Mitchell, J. H. (1980). Early cardiovascular adaptation to zero gravity simulated by head-down tilt. *Acta Astronaut.* 7, 543–553. doi: 10.1016/0094-5765(80)90043-0

Buehlmeier, J., Mulder, E., Noppe, A., Frings-Meuthen, P., Angerer, O., Rudwill, F., et al. (2014). A combination of whey protein and potassium bicarbonate supplements during head-down-tilt bed rest: presentation of a multidisciplinary randomized controlled trial (MEP study). *Acta Astronaut.* 95, 82–91. doi: 10.1016/j.actaastro.2013.11.001

Coupe, M., Fortrat, J. O., Larina, I., Gauquelin-Koch, G., Gharib, C., and Custaud, M. A. (2009). Cardiovascular deconditioning: from autonomic nervous system to microvascular dysfunctions. *Respir. Physiol. Neurobiol.* 169, S10–S12. doi: 10.1016/j.resp.2009.04.009

Covinsky, K. E., Pierluissi, E., and Johnston, C. B. (2011). Hospitalization-associated disability "she was probably able to ambulate, but I'm not sure". *JAMA* 306, 1782–1793. doi: 10.1001/jama.2011.1556

Cox, J. F., Tahvanainen, K. U., Kuusela, T. A., Levine, B. D., Cooke, W. H., Mano, T., et al. (2002). Influence of microgravity on astronauts' sympathetic

and vagal responses to Valsalva's manoeuvre. *J. Physiol.* 538, 309–320. doi: 10.1113/jphysiol.2001.012574

Diedrich, A., and Biaggioni, I. (2004). Segmental orthostatic fluid shifts. *Clin. Auton. Res.* 14, 146–147. doi: 10.1007/s10286-004-0188-9

Diedrich, A., Paranjape, S. Y., and Robertson, D. (2007). Plasma and blood volume in space. *Am. J Med Sci* 334, 80–85. doi: 10.1097/MAJ.0b013e318065b89b

Diedrich, A., Porta, A., Barbic, F., Brychta, R. J., Bonizzi, P., Diedrich, L., et al. (2009). Lateralization of expression of neural sympathetic activity to the vessels and effects of carotid baroreceptor stimulation. *Am. J. Physiol. Heart Circ. Physiol.* 296, H1758–H1765. doi: 10.1152/ajpheart.01045.2008

Diedrich, A., Mandsager, K. T., and Robertson, D. (2015). *Orthostatic intolerance and vasovagal syncope after spaceflight*. Switzerland: Springer.

Dock, W. (1944). The evil sequelae of complete bed rest. *JAMA* 125, 1083–1085. doi: 10.1001/jama.1944.02850340009004

Doherty, C. J., Incognito, A. V., Notay, K., Burns, M. J., Slysz, J. T., Seed, J. D., et al. (2018). Muscle sympathetic nerve responses to passive and active one-legged cycling: insights into the contributions of central command. *Am. J. Physiol. Heart Circ. Physiol.* 314, H3–H10. doi: 10.1152/ajpheart.00494.2017

Dutoit, A. P., Hart, E. C., Charkoudian, N., Wallin, B. G., Curry, T. B., and Joyner, M. J. (2010). Cardiac baroreflex sensitivity is not correlated to sympathetic baroreflex sensitivity within healthy, young humans. *Hypertension* 56, 1118–1123. doi: 10.1161/HYPERTENSIONAHA.110.158329

Eckberg, D. L., Halliwill, J. R., Beightol, L. A., Brown, T. E., Taylor, J. A., and Goble, R. (2010). Human vagal baroreflex mechanisms in space. *J. Physiol.* 588, 1129–1138. doi: 10.1113/jphysiol.2009.186650

el-Bedawi, K. M., and Hainsworth, R. (1994). Combined head-up tilt and lower body suction: a test of orthostatic tolerance. *Clin. Auton. Res.* 4, 41–47. doi: 10.1007/BF01828837

Ertl, A. C., Diedrich, A., Biaggioni, I., Levine, B. D., Robertson, R. M., Cox, J. F., et al. (2002). Human muscle sympathetic nerve activity and plasma noradrenaline kinetics in space. *J. Physiol.* 538, 321–329. doi: 10.1113/jphysiol.2001.012576

Ettinger, W. H. (2011). Can hospitalization-associated disability be prevented? *JAMA* 306, 1800–1801. doi: 10.1001/jama.2011.1563

Feldstein, C., and Weder, A. B. (2012). Orthostatic hypotension: a common, serious and underrecognized problem in hospitalized patients. *J. Am. Soc. Hypertens.* 6, 27–39. doi: 10.1016/j.jash.2011.08.008

Furlan, R., Porta, A., Costa, F., Tank, J., Baker, L., Schiavi, R., et al. (2000). Oscillatory patterns in sympathetic neural discharge and cardiovascular variables during orthostatic stimulus. *Circulation* 101, 886–892. doi: 10.1161/01.CIR.101.8.886

Furlan, R., Magatelli, R., Palazzolo, L., Rimoldi, A., Colombo, S., and Porta, A. (2001). Orthostatic intolerance: different abnormalities in the neural sympathetic response to a gravitational stimulus. *Auton. Neurosci.* 90, 83–88. doi: 10.1016/S1566-0702(01)00271-5

Furlan, R., Montano, N., and Porta, A. (2015). *Cardiovascular rhythms in vasovagal Syncope*. Switzerland: Springer.

Guerin, A., Bureau, M. L., Ghazali, N., Gervais, R., Liuu, E., Seite, F., et al. (2016). Factors associated with orthostatic hypotension in hospitalized elderly patients. *Aging Clin. Exp. Res.* 28, 513–517. doi: 10.1007/s40520-015-0451-z

Hart, E. C., Joyner, M. J., Wallin, B. G., Karlsson, T., Curry, T. B., and Charkoudian, N. (2010). Baroreflex control of muscle sympathetic nerve activity: a nonpharmacological measure of baroreflex sensitivity. *Am. J. Physiol. Heart Circ. Physiol.* 298, H816–H822. doi: 10.1152/ajpheart.00924.2009

Heusser, K., Tank, J., Luft, F. C., and Jordan, J. (2005). Baroreflex failure. *Hypertension* 45, 834–839. doi: 10.1161/01.HYP.0000160355.93303.72

Iwasaki, K., Zhang, R., Perhonen, M. A., Zuckerman, J. H., and Levine, B. D. (2004). Reduced baroreflex control of heart period after bed rest is normalized by acute plasma volume restoration. *Am. J. Phys. Regul. Integr. Comp. Phys.* 287, R1256–R1262. doi: 10.1152/ajpregu.00613.2002

Juraschek, S. P., Daya, N., Appel, L. J., Miller, E. R. 3rd, Windham, B. G., Pompeii, L., et al. (2017). Orthostatic hypotension in middle-age and risk of falls. *Am. J. Hypertens.* 30, 188–195. doi: 10.1093/ajh/hpw108

Kamiya, A., Iwase, S., Kitazawa, H., Mano, T., Vinogradova, O. L., and Kharchenko, I. B. (2000a). Baroreflex control of muscle sympathetic nerve activity after 120 days of 6 degrees head-down bed rest. *Am. J. Phys. Regul. Integr. Comp. Phys.* 278, R445–R452. doi: 10.1152/ajpregu.2000.278.2.R445

Kamiya, A., Michikami, D., Fu, Q., Niimi, Y., Iwase, S., and Mano, T. (2000b). Arterial baroreflex control of sympathetic vasoconstrictor traffic and orthostatic intolerance after head-down bed rest. *J. Gravit. Physiol.* 7, P177–P178.

Kamiya, A., Michikami, D., Fu, Q., Iwase, S., Hayano, J., Kawada, T., et al. (2003). Pathophysiology of orthostatic hypotension after bed rest: paradoxical sympathetic withdrawal. *Am. J. Phys. Heart Circ. Phys.* 285, H1158–H1167. doi: 10.1152/ajpheart.00965.2002

Levine, B. D., Zuckerman, J. H., and Pawelczyk, J. A. (1997). Cardiac atrophy after bed-rest deconditioning: a nonneural mechanism for orthostatic intolerance. *Circulation* 96, 517–525. doi: 10.1161/01.CIR.96.2.517

Levine, B. D., Pawelczyk, J. A., Ertl, A. C., Cox, J. F., Zuckerman, J. H., Diedrich, A., et al. (2002). Human muscle sympathetic neural and haemodynamic responses to tilt following spaceflight. *J. Physiol.* 538, 331–340. doi: 10.1113/jphysiol.2001.012575

Macefield, V. G., Wallin, B. G., and Vallbo, A. B. (1994). The discharge behaviour of single vasoconstrictor motoneurones in human muscle nerves. *J. Physiol.* 481, 799–809.

Magagnin, V., Bassani, T., Bari, V., Turiel, M., Maestri, R., Pinna, G. D., et al. (2011). Non-stationarities significantly distort short-term spectral, symbolic and entropy heart rate variability indices. *Physiol. Meas.* 32, 1775–1786. doi: 10.1088/0967-3334/32/11/S05

Marchi, A., Bari, V., De Maria, B., Cerutti, S., Heusser, K., Tank, J., et al. (2015). Evaluation of the correlation between cardiac and sympathetic baroreflex sensitivity before orthostatic syncope. *Conf. Proc. IEEE Eng. Med. Biol. Soc.* 2015, 2063–2066. doi: 10.1109/EMBC.2015.7318793

Marchi, A., Bari, V., De Maria, B., Esler, M., Lambert, E., Baumert, M., et al. (2016). Simultaneous characterization of sympathetic and cardiac arms of the baroreflex through sequence techniques during incremental head-up tilt. *Front. Physiol.* 7:438. doi: 10.3389/fphys.2016.00438

McIntyre, H. (2013). Admission to hospital could be considered a disease. *BMJ* 346, f3242–f3243. doi: 10.1136/bmj.f3242

Mosqueda-Garcia, R. (1996). Microneurography in neurological research. *Am. Acad. Neurol.* 2, 4–5.

Mosqueda-Garcia, R., Furlan, R., Fernandez-Violante, R., Desai, T., Snell, M., Jarai, Z., et al. (1997). Sympathetic and baroreceptor reflex function in neurally mediated syncope evoked by tilt. *J. Clin. Invest.* 99, 2736–2744. doi: 10.1172/JCI119463

Pagani, M., Lombardi, F., Guzzetti, S., Rimoldi, O., Furlan, R., Pizzinelli, P., et al. (1986). Power spectral analysis of heart rate and arterial pressure variabilities as a marker of sympatho-vagal interaction in man and conscious dog. *Circ. Res.* 59, 178–193. doi: 10.1161/01.RES.59.2.178

Pagani, M., Somers, V., Furlan, R., Dell'Orto, S., Conway, J., Baselli, G., et al. (1988). Changes in autonomic regulation induced by physical training in mild hypertension. *Hypertension* 12, 600–610. doi: 10.1161/01.HYP.12.6.600

Parati, G., Di Rienzo, M., Bertinieri, G., Pomidossi, G., Casadei, R., Groppelli, A., et al. (1988). Evaluation of the baroreceptor-heart rate reflex by 24-hour intra-arterial blood pressure monitoring in humans. *Hypertension* 12, 214–222. doi: 10.1161/01.HYP.12.2.214

Pawelczyk, J. A., Zuckerman, J. H., Blomqvist, C. G., and Levine, B. D. (2001). Regulation of muscle sympathetic nerve activity after bed rest deconditioning. *Am. J. Physiol. Heart Circ. Physiol.* 280, H2230–H2239. doi: 10.1152/ajpheart.2001.280.5.H2230

Porta, A., Bari, V., Bassani, T., Marchi, A., Pistuddi, V., and Ranucci, M. (2013). Model-based causal closed-loop approach to the estimate of baroreflex sensitivity during propofol anesthesia in patients undergoing coronary artery bypass graft. *J. Appl. Physiol.* 115, 1032–1042. doi: 10.1152/japplphysiol.00537.2013

Protheroe, C. L., Ravensbergen, H. R., Inskip, J. A., and Claydon, V. E. (2013). Tilt testing with combined lower body negative pressure: a "gold standard" for measuring orthostatic tolerance. *J. Vis. Exp.* 73:e4315. doi: 10.3791/4315

Robertson, D., Hollister, A. S., Biaggioni, I., Netterville, J. L., Mosqueda-Garcia, R., and Robertson, R. M. (1993). The diagnosis and treatment of baroreflex failure. *N. Engl. J. Med.* 329, 1449–1455. doi: 10.1056/NEJM199311113292003

Salmanpour, A., and Shoemaker, J. K. (2012). Baroreflex mechanisms regulating the occurrence of neural spikes in human muscle sympathetic nerve activity. *J. Neurophysiol.* 107, 3409–3416. doi: 10.1152/jn.00925.2011

Shibao, C., Grijalva, C. G., Raj, S. R., Biaggioni, I., and Griffin, M. R. (2007). Orthostatic hypotension-related hospitalizations in the United States. *Am. J. Med.* 120, 975–980. doi: 10.1016/j.amjmed.2007.05.009

Shoemaker, J. K., Hogeman, C. S., Leuenberger, U. A., Herr, M. D., Gray, K., Silber, D. H., et al. (1998). Sympathetic discharge and vascular resistance

after bed rest. *J. Appl. Physiol.* 84, 612–617. doi: 10.1152/jappl.1998.84.2.612

Tanaka, K., Nishimura, N., Sato, M., Kanikowska, D., Shimizu, Y., Inukai, Y., et al. (2013). Arterial pressure oscillation and muscle sympathetic nerve activity after 20 days of head-down bed rest. *Auton. Neurosci.* 177, 266–270. doi: 10.1016/j.autneu.2013.02.025

Tank, J., Heusser, K., Malehsa, D., Hegemann, K., Haufe, S., Brinkmann, J., et al. (2012). Patients with continuous-flow left ventricular assist devices provide insight in human Baroreflex physiology. *Hypertension* 60, 849–855. doi: 10.1161/HYPERTENSIONAHA.112.198630

Task Force of the European Society of Cardiology and the North American Society of Pacing and Electrophysiology (1996). Heart rate variability: standards of measurement, physiological interpretation and clinical use. *Circulation* 93, 1043–1065.

Taylor, C. E., Witter, T., El Sayed, K., Hissen, S. L., Johnson, A. W., and Macefield, V. G. (2015). Relationship between spontaneous sympathetic baroreflex sensitivity and cardiac baroreflex sensitivity in healthy young individuals. *Physiol. Rep.* 3:e12536. doi: 10.14814/phy2.12536

Tzur, I., Izhakian, S., and Gorelik, O. (2018). Orthostatic hypotension in internal medicine wards. *Curr. Med. Res. Opin.* 35, 1–27. doi: 10.1080/03007995.2018.1546679

Wallin, B. G., Burke, D., and Gandevia, S. (1994). Coupling between variations in strength and baroreflex latency of sympathetic discharges in human muscle nerves. *J. Physiol.* 474, 331–338. doi: 10.1113/jphysiol.1994.sp020025

Waters, W. W., Platts, S. H., Mitchell, B. M., Whitson, P. A., and Meck, J. V. (2005). Plasma volume restoration with salt tablets and water after bed rest prevents orthostatic hypotension and changes in supine hemodynamic and endocrine variables. *Am. J. Phys. Heart Circ. Phys.* 288, H839–H847. doi: 10.1152/ajpheart.00220.2004

Conflict of Interest Statement: The authors declare that the research was conducted in the absence of any commercial or financial relationships that could be construed as a potential conflict of interest.

frontiers in Physiology

ORIGINAL RESEARCH
published: 27 August 2019
doi: 10.3389/fphys.2019.01104

Autonomic Abnormalities in Patients With Primary Sjogren's Syndrome – Preliminary Results

*Enrico Brunetta[1], Dana Shiffer[1], Pietro Mandelli[2], Sara Achenza[3], Marco Folci[1], Aurora Zumbo[1], Maura Minonzio[1], Beatrice Cairo[4], Giris Jacob[5], Laura Boccassini[6], Piercarlo Sarzi Puttini[6], Alberto Porta[4,7] and Raffaello Furlan[1,8]**

[1] Department of Internal Medicine, Humanitas Clinical and Research Center – IRCCS, Milan University, Milan, Italy, [2] Department of Pathophysiology and Transplantation, Faculty of Medicine and Surgery, University of Milan, Milan, Italy, [3] Department of Nephrology, Humanitas Clinical and Research Center – IRCCS, Milan University, Milan, Italy, [4] Department of Biomedical Sciences for Health, Faculty of Medicine and Surgery, University of Milan, Milan, Italy, [5] Department of Internal Medicine F, J. Recanati Autonomic Dysfunction Center, Tel Aviv Sourasky Medical Center and Sackler School of Medicine, Tel Aviv University, Tel Aviv, Israel, [6] Reumathology Unit, Luigi Sacco University Hospital, ASST Fatebenefratelli Sacco, Milan, Italy, [7] Department of Cardiothoracic, Vascular Anesthesia and Intensive Care, IRCCS Policlinico San Donato, Milan, Italy, [8] Department of Biomedical Sciences, Humanitas University, Milan, Italy

Primary Sjögren's syndrome (pSS) is an autoimmune disease affecting exocrine glands and extra-glandular organs. There are conflicting reports on the presence of autonomic dysfunction in pSS and no data are available on the functional status of sympathetic outflow to the vessels and baroreceptor [baroreflex sensitivity (BRS)] control mechanisms. We investigated the cardiac (cBRS) and sympathetic (sBRS) baroreceptor modulation in both time and frequency domains and the cardiovascular autonomic profile in pSS patients compared to healthy controls. Autonomic symptoms were quantified by the Composite Autonomic Symptom Scale (COMPASS31) three-item questionnaire. The EULAR Sjogren's syndrome patient reported index (ESSPRI) questionnaire evaluated the magnitude of pSS clinical symptoms, i.e., fatigue, pain, and sicca symptoms. Electrocardiogram, beat-by-beat arterial pressure (AP) and respiratory activity were continuously recorded in 17 pSS patients and 16 healthy controls, while supine and during 75° head-up tilt. In seven patients and seven controls, muscle sympathetic nerve activity (MSNA) was measured. Spectrum analysis of RR variability provided markers of cardiac vagal modulation (HF_{RR} nu) and sympatho-vagal balance [low frequency (LF)/high frequency (HF)]. The power of LF (0.1 Hz) oscillations of systolic arterial pressure (SAP) variability (LF_{SAP}) evaluated the vasomotor response to sympathetic stimulation. Compared to controls, pSS patients scored higher in total COMPASS31 ($p < 0.0001$) and all ESSPRI subdomains (fatigue, $p = 0.005$; pain, $p = 0.0057$; dryness, $p < 0.0001$). Abnormal scialometry (<1.5 ml/15 min) and Schirmer tests (<5 mm/5 min) were found in pSS patients and salivary flow rate was negatively associated with ESSPRI dryness ($p = 0.0014$). While supine, pSS patients had lower SEQ_{cBRS} index of cardiac baroreceptor sensitivity, higher HF_{RRnu} ($p = 0.021$), lower LF/HF ($p = 0.007$), and greater MSNA ($p = 0.038$) than controls. No differences were observed in LF_{SAP} between groups. During orthostatic challenge, although LF_{SAP} increased similarly in both groups, MSNA was greater in pSS patients ($p = 0.003$). At

OPEN ACCESS

Edited by:
Tijana Bojić,
University of Belgrade, Serbia

Reviewed by:
Paola Sandroni,
Mayo Clinic, United States
Flavia Ravelli,
University of Trento, Italy

***Correspondence:**
Raffaello Furlan
raffaello.furlan@hunimed.eu

Specialty section:
This article was submitted to Autonomic Neuroscience, a section of the journal Frontiers in Physiology

Received: *10 January 2019*
Accepted: *08 August 2019*
Published: *27 August 2019*

Citation:
Brunetta E, Shiffer D, Mandelli P, Achenza S, Folci M, Zumbo A, Minonzio M, Cairo B, Jacob G, Boccassini L, Puttini PS, Porta A and Furlan R (2019) Autonomic Abnormalities in Patients With Primary Sjogren's Syndrome – Preliminary Results. Front. Physiol. 10:1104. doi: 10.3389/fphys.2019.01104

rest pSS patients showed lower cBR control and greater parasympathetic modulation. Furthermore, greater sympathetic nerve activity was observed in pSS patients while supine and in response to gravitational challenge. We hypothesized that such enhanced sympathetic vasoconstrictor activity might reflect an attempt to maintain blood pressure in a setting of likely reduced vascular responsiveness.

Keywords: primary Sjogren's syndrome, baroreceptor activity, power spectrum analysis, heart rate variability, muscle sympathetic nerve activity

INTRODUCTION

Primary Sjogren syndrome (pSS) is a chronic systemic autoimmune disease which primarily affects the exocrine glands, most commonly the salivary and lacrimal glands, leading to xerostomia and xerophthalmia (Fox, 2005). Its prevalence is estimated to be about 7 per 100,000 person-years (Qin et al., 2015). It is characterized by a high female-to-male ratio of 9:1 and the mean age of onset is around the 4th to 5th decade of life (Qin et al., 2015). At least a third of patients develop extraglandular manifestations (Vitali et al., 2002). These may involve the skin (Ramos-Casals et al., 2004), vessels (Scofield, 2011), joints (Pease et al., 1993), and muscles (Lindvall et al., 2002). Among the visceral organs affected are the lungs (Quismorio, 1996), heart (Gyongyosi et al., 1996), kidneys (Gamron et al., 2000), and the gastrointestinal tract (Ebert, 2012).

The pathogenesis of pSS involves an abnormal immunological response to an inflammatory insult in predisposed individuals which ultimately results in a perpetuated inflammatory response (Fox, 2005). However, an analysis on sialadenitis progression in patients with pSS showed no correlation between the degree of salivary gland destruction and salivary secretions (Jonsson et al., 1993). Thus, it seems that the severity of clinical manifestation does not correspond to the degree of organ inflammation, and therefore symptoms might not be completely attributed to the inflammatory process alone (Humphreys-Beher et al., 1999).

With exocrine glandular dysfunction being the hallmark of the disease and as its function is highly regulated by the autonomic nervous system (ANS) (Proctor and Carpenter, 2007), several studies aimed to evaluate neural autonomic involvement in the disease process. Moreover, a range of autonomic symptoms have been described in pSS patients such as orthostatic hypotension, urinary retention, and gastroparesis (Mandl et al., 2008; Newton et al., 2012; Goodman et al., 2017).

Several studies have performed objective autonomic function assessment in patients with pSS, however, evidence remain inconclusive. While some investigation, via cardiovascular autonomic reflex testing, inferred alterations in both parasympathetic and sympathetic function others observed parasympathetic dysfunction only or no alteration at all (Andonopoulos et al., 1998; Barendregt et al., 1999; Mandl et al., 2001, 2007; Niemela et al., 2003; Kovacs et al., 2004). Furthermore, conflicting data have also been produced by studies using spectral analysis of heart rate (HR) variability, a sensitive non-invasive method to detect early and subtle abnormalities in cardiovascular autonomic function (Niemela et al., 2000; Tumiati et al., 2000; Barendregt et al., 2002; Cai et al., 2008; Ng et al., 2012; Koh et al., 2017). Finally, no data are available on the baroreceptor control in these patients. As a reminder, baroreflex sensitivity (BRS) can be used to evaluate autonomic dysfunction by assessing the efficiency of the baroreflex response to variations of arterial pressure (AP). The characterization of baroreflex function is usually carried out via the evaluation of cardiac baroreflex (cBR) (Smyth et al., 1969; Pickering et al., 1972) and sympathetic baroreflex (sBR) (Sundlof and Wallin, 1978; Kienbaum et al., 2001) through the estimation of BRS as the variation of the target variable in correspondence to a unit change of AP. Consequently, cBR sensitivity (cBRS) is calculated as the variation of heart period (HP) in response to modification of systolic AP (SAP) (Smyth et al., 1969; Pickering et al., 1972). sBR sensitivity (sBRS) is evaluated by measuring the variation in probability of occurrence of the muscle sympathetic nerve activity (MSNA) burst per unit change of diastolic AP (DAP).

Presently, in patients with pSS there is no data on the functional status of the sympathetic outflow activity to the vessels, as assessed by microneurography. This technique allows to directly measure the MSNA, reflecting neural vasoconstriction activity to intramuscular vessels. We reasoned that given the possible subclinical vasculitis which has been hypothesized to be present in these patients (Scofield, 2011), MSNA assessment would be particularly suitable to add valuable information about the pathophysiological mechanisms occurring in pSS.

The aim of the current study was therefore to investigate the characteristics of the BRS, the cardiovascular autonomic profile, and the sympathetic vasomotor function in patients affected by pSS compared to healthy controls. The relationship between the autonomic profile, sympathetic vasomotor function, and clinical feature in pSS patients was also explored.

MATERIALS AND METHODS

Study Population

Nineteen patients with pSS (18 females and 1 male) and 17 age- and gender-matched healthy controls (15 females and 2 males) were enrolled in the study which was performed at the Humanitas Clinical and Research Center, Rozzano, Italy. The pSS patients were referred from the immunological outpatient clinic of the Humanitas Clinical and Research Center and the Rheumatology outpatient clinic of L. Sacco Hospital, Milan, Italy. The patients were previously diagnosed with pSS according to the revised American European Consensus Group (AECG) criteria (Vitali et al., 2002).

At enrollment, the participants underwent a comprehensive medical history assessment and physical exam and got acquainted with the clinical laboratory environment to ensure maximal reproducibility of the results.

Exclusion criteria were applied to both groups as follows: current human immunodeficiency virus (HIV) and/or hepatitis C virus (HCV) infection; previous history of cancer or any lymphoproliferative disease; active pregnancy; substance/alcohol abuse; presence of comorbidities such as diabetes mellitus, Parkinson's disease, chronic kidney disease (stages 4 or 5), other known systemic autoimmune diseases, sarcoidosis, amyloidosis, IgG4 disease, ischemic and/or valve heart disease, heart failure, atrial fibrillation, hypertension, the presence of a pacemaker, and a previously diagnosed primary dysautonomia.

Following a detailed explanation of the aims and procedures involved in the study, all study participants provided a signed informed consent. Because of fear of the microneurography procedure, seven patients and seven controls selectively did not give consent to undergo the MSNA recording procedure, but agreed to undergo the remaining variables recording. The protocol adhered to the principles of the Helsinki declaration and was approved by the Humanitas Clinical and Research Center ethics committee (authorization no. 1395).

Recorded Variables and Experimental Protocol

The experimental procedures were performed on all participants during the morning hours (8.30 a.m.–12 p.m.) in a quiet and dim lighted room, with comfortable temperature. The subjects were instructed to avoid intense physical activity in the 24 h preceding the study and to consume a light breakfast and avoid caffeine, smoking, and alcohol on the day of the investigation. pSS patients were instructed to suspend the use of pilocarpine 3 days prior to the study and none of the participants were on other medications that may affect the ANS function.

For each subject, an electrocardiogram (ECG), non-invasive AP (Nexfin monitor, BMEYE B.V., Amsterdam, Netherlands), and respiratory movements by a thoracic belt positioned at mid-chest level (Respibelt, Francesco Marazza) were continuously recorded for a period of 15 min while supine.

To allow for cross calibration of the non-invasive beat-to-beat blood pressure (BP) signal, BP was measured every 3 min by an automated device (Phillips Comfort Care Adult, cuff size 27.0–35.0 cm, United States).

A direct recording of the MSNA by microneurographic technique was performed on 12 pSS patients and 9 controls, both in the supine position and during head up tilt, a stimulus which enhances the overall cardiovascular sympathetic activity (Furlan et al., 2000). MSNA was recorded from the peroneal nerve of the left leg (Tank et al., 2003; Diedrich et al., 2009). Briefly, multiunit recordings of postganglionic sympathetic discharge activity were obtained by a tungsten electrode inserted through unanesthetized skin into a left peroneal nerve fascicle, posterior to the fibular head. A reference electrode was inserted subcutaneously, close by the recording needle. Adjustments in the electrode's position were performed until the characteristic signal of sympathetic origin was detected (Wallin and Fagius, 1988). The raw neural signal was amplified (1000-fold), band-pass filtered (bandwidth between 700 and 2000 Hz), and rectified and integrated (time constant of 0.1 s) by a nerve traffic analyzer (model 662C-3; University of Iowa Bioengineering Department, Iowa City, IA, United States).

Following instrumentation and a preliminary 5-min adjustment period, supine data acquisition was initiated. Recordings were continued while the subject underwent a progressive head up tilt challenge (15° increments, up to 75° head-up elevation), each level maintained for 3 min. This was followed by a 5-min recovery period.

The Valsalva maneuver and the sinus arrhythmia (SA) test were also performed during the 15-min supine recording. Valsalva ratio, a global index of baroreflex mediated control of HR and SA ratios, an index of efferent parasympathetic cardiac modulation, were computed dividing the highest HR value by the lowest HR value recorded during each of those tests. Details of the procedure are described elsewhere (Hilz and Dutsch, 2005).

Extraction of the Beat-to-Beat Variability Series

Electrocardiogram, continuous AP, respiratory activity, and MSNA were digitized at 400 Hz/channel (ADInstruments, Powerlab, PL3516/P, Oxford, United Kingdom). The signals were stored on a personal computer hard disk for offline analysis.

The R-wave peaks were detected using the traditional first-derivative thresholding method. The temporal distance between two consecutive identified R-wave peaks was taken as the HP approximated as RR interval. The maximum value of AP inside the *i*th RR interval was defined as the *i*th SAP value, while the minimum value before the *i*th SAP value was taken as the *i*th DAP. The identified R-wave peaks and the positions of the corresponding SAP and DAP values were then manually checked to avoid erroneous detections or missed beats.

Muscle sympathetic nerve activity bursts were automatically detected from the integrated MSNA, using an adaptive thresholding method to account for baseline wandering (Diedrich et al., 2009). Bursts were searched for in a temporal window ranging from 0.9 to 1.7 s after each R-wave peak, based on the known sBR latency, i.e., the conduction time from the aortic and carotid baroreceptors to the peroneal nerve, which correspond to approximately 1.3 s (Wallin et al., 1994; Hamner and Taylor, 2001; Diedrich et al., 2009).

This application was made possible by the exploitation of the calibrated MSNA series (cMSNA) detailed in a study by Marchi et al. (2016a) expressing the MSNA variability in bursts/s. Briefly, the cMSNA signal was obtained from the integrated MSNA signal by counting the number of MSNA bursts inside a moving time window of 5 s. The resulting step-wise count MSNA signal was then low-pass filtered with a finite impulse response filter with a cutoff frequency of 0.5 Hz, in order to retain exclusively the frequency range of cardiovascular variability. Finally, the low-pass count MSNA signal was down-sampled in correspondence with the first R-wave peak delimiting each *i*th RR interval. The resulting time series was expressed in burst/s by dividing the count cMSNA values by the length of the time window. As

a result, the beat-to-beat variability of cMSNA = {cMSNA(i), i = 1,…, N} was synchronous with the beat-to-beat variability series of HR, SAP, and DAP.

Variability Power Spectral Analysis

Analysis was performed in the supine position and during head up tilt test. The time series length was fixed at 300 consecutive beats in both conditions. The stationarity of the selected sequence was tested over the original series after linear detrending (Magagnin et al., 2011). If the test for the steadiness of mean and variance was not fulfilled, a new selection was carried out until the prerequisites for restricted weak stationarity were obtained (Magagnin et al., 2011). Test for the stationarity of the mean was carried out even after linear detrending.

Power spectral analysis was performed over RR, SAP, and respiratory series (Pagani et al., 1986; Task Force of the European Society of Cardiology and the North American Society of Pacing and Electrophysiology, 1996). The Levinson–Durbin recursion was used to assess the autoregressive model coefficients and the variance of the white noise. The number of coefficients was automatically chosen, based on the Akaike's figure of merit, ranging between 8 and 14.

From RR and SAP series we derived the markers of autonomic control. The high frequency (HF_{RR}) component (0.15–0.4 Hz) is taken as an index of the vagal efferent modulation directed to the sinoatrial node and the low frequency (LF_{RR}) component (0.04–0.15 Hz), which when expressed in normalized units (nu), is thought to primarily reflect the sympathetic modulation of the sinoatrial node activity and of its changes (Furlan et al., 2000), although its functional meaning is still debated (Pomeranz et al., 1985; Parati et al., 1995). The LF_{RR}/HF_{RR} ratio, a dimensionless index, assesses the sympatho–vagal relationship modulating the cardiac sinoatrial node (Pagani et al., 1986; Furlan et al., 2000), although, recently, a review questioned its interpretation and use, particularly in psychological research (Heathers and Goodwin, 2017). The LF component of SAP variability, indicated as LF_{SAP}, is considered an indirect marker of the sympathetic vasomotor control (Furlan et al., 2000; Barbic et al., 2007). Finally, the sympathetic drive directed to the vessels was evaluated directly through the burst rate of the integrated MSNA, expressed as bursts/min.

Cardiac and Sympathetic Baroreflex Estimation

A spectral approach applied to RR and SAP variability was used to assess cBRS computed as the squared root of the ratio between LF_{RR} and LF_{SAP}, termed as αLF_{cBRS}, and expressed in ms $mmHg^{-1}$ (Pagani et al., 1988; Barbic et al., 2007; Porta et al., 2013).

Additionally, another approach used for cBRS estimation was based on the cBR sequence method (Bertinieri et al., 1985) as implemented by Porta et al. (2000) and is indicated as SEQ_{cBRS} hereafter. Briefly, the methodology is based on the analysis of sequences of simultaneous increases (positive +/+ sequences) or decreases (negative −/− sequences) of RR and SAP values. The sequences in both time series were chosen with a length equal to four consecutive values and the time lag between SAP and RR (τ_{RR-SAP}) was 0 beats to take into account the fast vagal arm of the baroreflex (Porta et al., 2013). A spontaneous cBR sequence was selected only if the following prerequisites were satisfied (Laude et al., 2004): (1) the absolute value of the total RR variation was >5 ms; (2) the absolute value of the total SAP variation was >1 mmHg; (3) the linear correlation coefficient computed over a given cBR sequence, r_{RR-SAP}, was >0.85. The percentage of sequences that satisfied the selection prerequisites with respect to all sequences was calculated and indicated as $SEQ\%_{cBR}$. Over each sequence the slope of the linear regression in the plane [SAP(i), RR($i + \tau_{RR-SAP}$)] was calculated. The obtained regression slope values were subsequently averaged over all baroreflex sequences and the resulting value was taken as an estimate of SEQ_{cBRS}, expressed in ms $mmHg^{-1}$. While SEQ_{cBRS} is taken as a measure of the effectiveness of the cBR, $SEQ\%_{cBR}$ is taken as a measure of the degree of involvement of cBR (Marchi et al., 2016b).

Regarding sBR, in agreement with the spectral approach proposed by Pagani et al. (1986), sBRS was estimated using LF_{sBRS} which was calculated as the squared root of the ratio between LF_{cMSNA} and LF_{DAP} and expressed in burst s^{-1} $mmHg^{-1}$.

Additionally, SEQ_{sBRS} was estimated over the cMSNA and DAP beat-to-beat variability series, with an approach similar to SEQ_{cBRS}. Specifically, sBR sequences were defined with length equal to four consecutive beats and the lag between the paired MSNA burst rate and DAP values expressed in beats, termed as $\tau_{MSNA-DAP}$, was set to 1 to account for the sBR latency. The sequences were then selected to have opposite sign variations over the two series, i.e., the simultaneous increase of cMSNA and decrease of DAP values (±sequences) or *vice versa* (−/+ sequences). The prerequisites necessary for the selection of a sequence were: (1) the absolute value of cMSNA change >0; (2) the absolute value of the total DAP variation was >1 mmHg; (3) the absolute value of the linear correlation coefficient computed in the [DAP(i), cMSNA($i + \tau_{MSNA-DAP}$)] plane over a given sBR sequence, $r_{cMSNA-DAP}$ was >0.85 (Marchi et al., 2016b). The slope of the regression line of each selected cMSNA−DAP sequence was calculated and subsequently the average of all slopes (defined as SEQ_{sBRS}) was taken as an estimate of sBRS and expressed in bursts s^{-1} $mmHg^{-1}$. The percentage of sBR sequences with respect to all sequences was computed as well and indicated as $SEQ\%_{sBR}$. Both indexes were considered with analogous physiological meaning to the corresponding cBR ones but with relevance to the sBR arm.

Symptoms and Diseases Activity Assessment

The assessment of the intensity of clinical symptoms was obtained by the following questionnaires, filled out by all subjects:

- The EULAR Sjogren's syndrome patient reported index (ESSPRI) was used for assessing the overall burden of disease associated symptoms. Specifically, about levels of fatigue, overall pain, and sicca symptoms (numerical scale 0–10, with 0 being the absence of symptom and 10 the greatest symptom intensity) (Seror et al., 2011).

- The Composite Autonomic Symptom Scale (COMPASS 31) was used to quantify the following autonomic symptoms: orthostatic intolerance and vasomotor, secretomotor, gastrointestinal, and urinary and pupillomotor dysfunction symptoms (31 items; score range 0–100, with 0 being the absence of symptom and 100 the greatest symptom intensity) (Sletten et al., 2012).

Objective markers of disease's secretory impairment were assessed only in pSS patients. Salivary gland function was evaluated by a non-stimulated total salivary flow scialometry test (positive if ≤1.5 ml/15 min) (Vitali et al., 2002). Signs of ocular involvement were assessed by the Schirmer test I (positive if ≤5 mm/5 min) and serum was analyzed for the presence of ANA, RF, anti-SSA, and anti-SSB autoantibodies.

Statistical Analysis

For sample size calculation we focused on the LF/HF ratio because it was the only variable of interest available in literature. Sample size calculation was based on the results from Tumiati et al. (2000) concerning HR variability analysis in patients with pSS compared with healthy controls. We computed the LF/HF ratio difference between Sjogren patients and controls at rest reported in figure 2 of the above mentioned paper. Based on a power of 0.8 and a significance level of 0.01 because of potential multiple comparisons, we estimated the necessary sample size for our current study to be 11 patients per group. In spite of this number, we recruited additional patients and controls (i.e., 17 and 19, respectively) to account for potential drop out or for non-optimal signal to noise ratio in the case of microneurography.

The normality of the data was established by Kolmogorov–Smirnov test. An unpaired *t*-student test was used to assess for differences in mean values between patients and controls.

The Spearman rank correlation test was used for associations between subjective symptoms, objective markers of disease activity, and objective autonomic function assessment. Continuous variables are expressed as mean ± standard error (SEM). Significance level was set at 5%. GraphPad Prism™ was used for statistical analysis.

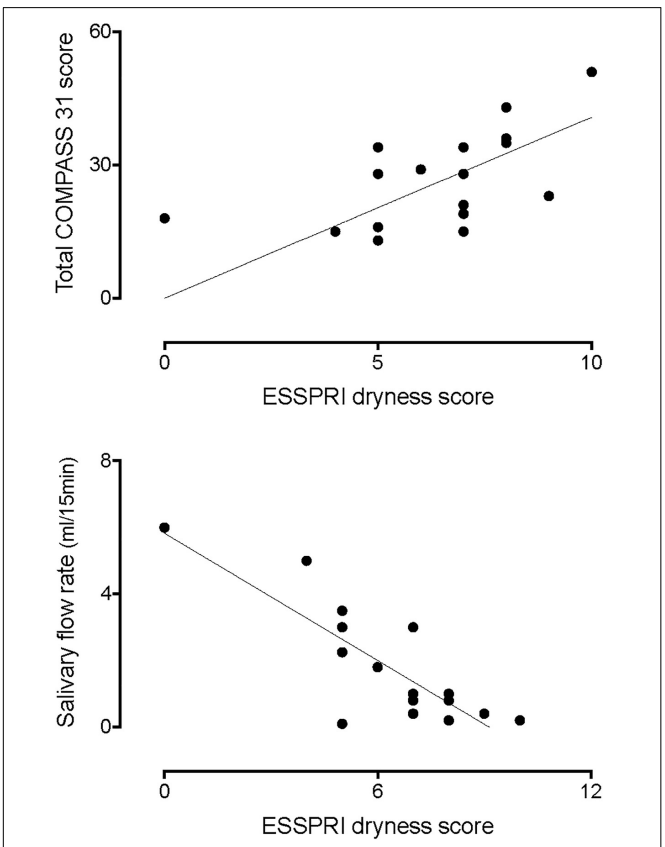

FIGURE 1 | Correlation between the ESSPRI dryness score and the total COMPASS 31 score **(top graph)**. Please notice that the higher the dryness score the greater the autonomic symptoms score ($r = 0.6359$, $p = 0.0036$). In addition, there was an inverse correlation between the dryness score and the amount of salivary flow (**bottom graph**, $r = -0.6577$, $p = 0.0061$).

RESULTS

The demographic, hemodynamic, respiratory, and immunologic characteristics of the pSS patient and control groups are displayed in **Table 1**. Due to excessive atrial and ventricular premature beat activity in the recorded variables, spectral analysis was not performed on two patients and one control. Thus, final data analysis was performed on 17 pSS (16 females and 1 male, BMI 20.2 ± 2.8) and 16 age-matched healthy controls (14 females and 2 males, BMI 21.3 ± 2.1). From this final study population, because of the absence of written consent and presence of sub-optimal signal/noise ratio, a MSNA signal adequate for automatic analysis was obtained for seven pSS patients and seven controls.

Abnormal scialometry (<1.5 ml/15 min) and Schirmer tests (< 5 mm/5 min) were found in pSS patients and salivary flow rate was negatively associated with ESSPRI dryness ($p = 0.0014$).

Disease Activity Indices and Autonomic Profile

Assessment of autonomic symptom presence and burden of disease activity showed, as expected, a significantly greater mean score in pSS group compared to the control group in the total ESSPRI (18.0 ± 5.2 vs. 5.3 ± 1.7; $p < 0.0001$), fatigue (6.6 ± 2.2 vs. 3.2 ± 0.8; $p = 0.0051$), pain (5.1 ± 2.7 vs. 1.8 ± 1.1; $p = 0.0057$), and dryness (6.4 ± 2.3 vs. 0.3 ± 0.5; $p < 0.0001$) ESSPRI domains.

With regards to the COMPASS31, a significantly higher mean score was obtained for the pSS group in the total score (27.0 ± 10.9 vs. 9.0 ± 5.7; $p < 0.0001$), secretomotor (3.2 ± 1.5 vs. 0.0 ± 0.0; $p < 0.0001$), and pupillomotor impairment scores (7.9 ± 2.9 vs. 2.4 ± 2.9; $p = 0.0003$). No significant differences were found in the domains of orthostatic intolerance (3.4 ± 2.5 vs. 0.9 ± 1.3; $p = 0.058$); vasomotor (2.0 ± 2.9 vs. 0.0 ± 0.0, $p = 0.059$); gastrointestinal (8.3 ± 3.9 vs. 5.0 ± 3.3; $p = 0.236$); and bladder function (2.2 ± 2.7 vs. 0.7 ± 0.9; $p = 0.353$) between the two groups.

Figure 1, upper panel, shows the correlation between the ESSPRI dryness score and the total COMPASS 31 score. Please notice that the higher the dryness score the greater the autonomic

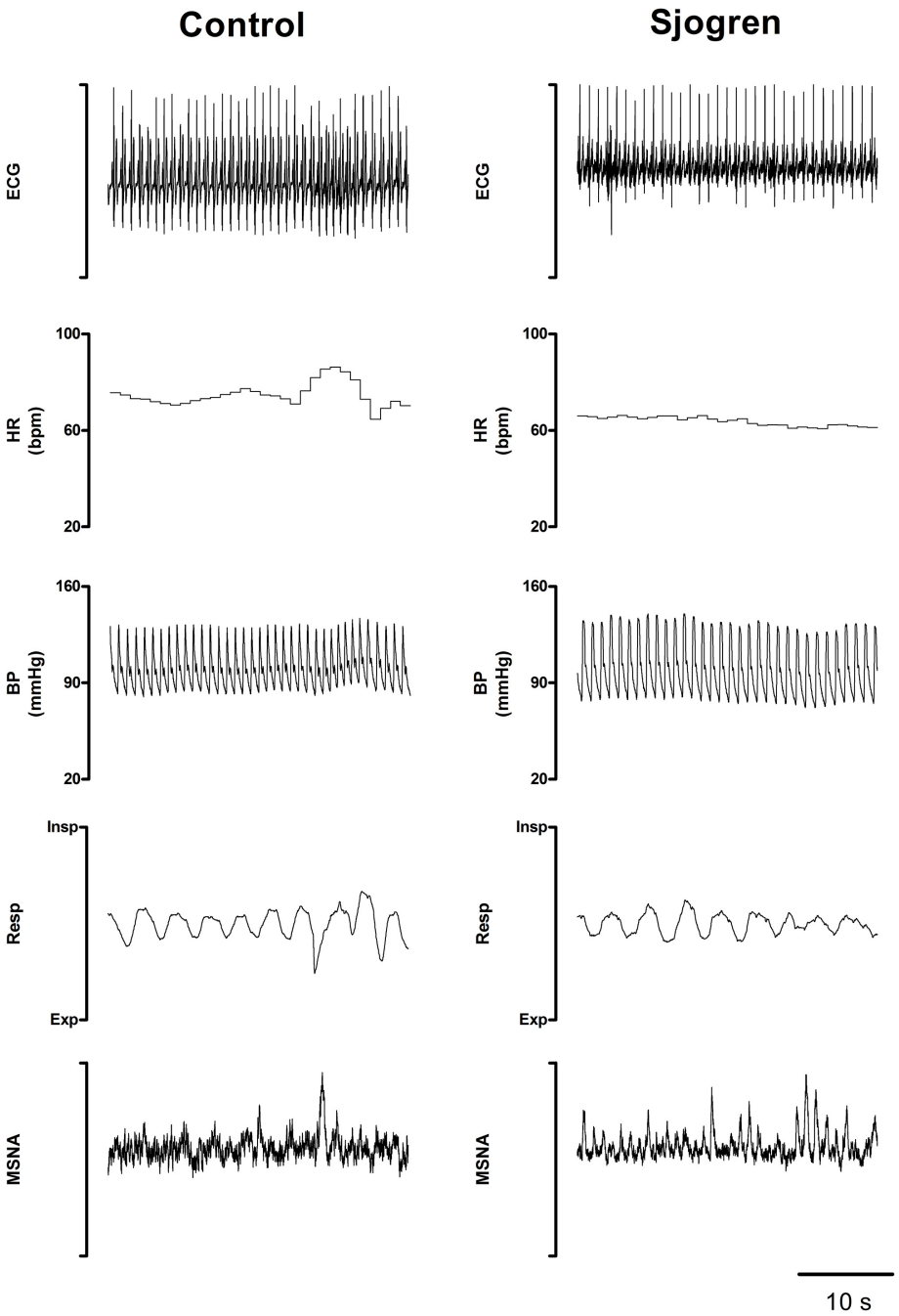

FIGURE 2 | Recorded variables in a representative Sjogren patient and in a control subject while recumbent. Notice the greater burst activity characterizing the patient's MSNA compared to the control.

symptoms score (r = 0.6359, 95% CI 0.2088–0.8593, p = 0.0036). In addition, there was a linear, inverse, relationship between the dryness score and the amount of salivary flow (lower panel, r = −0.6577, 95% CI −0.8847 to −0.1784, p = 0.0061).

Baroreflex Sensitivity

Table 2 displays the results both for the cardiac and the sympathetic arms of the BRS at rest. Regarding the cardiac arm, SEQ_{cBRS} was significantly lower in pSS patients than in controls whereas the αLF_{cBRS} index was only slightly smaller. αLF_{cBRS} was significantly decreased (**Table 3**) during the tilt maneuver with respect to the resting state in both populations (p = 0.009 in pSS patients and p = 0.030 in healthy controls), as expected (Furlan et al., 2000).

SEQ_{sBR} and αLF_{sBRS} were similar between the two groups at rest and during tilt (**Table 2**). In addition, no significant variations

TABLE 1 | Characteristics of the study population.

Characteristics	Patients (n = 17)	Controls (n = 16)
Age (years)	57.2 ± 13.7	51.0 ± 13.9
BMI (kg/cm^2)	20.2 ± 2.8	21.3 ± 2.1
HR (beats/min)	66.4 ± 3.4	66.3 ± 2.3
SAP (mmHg)	125.3 ± 5.9	116.8 ± 3.6
Resp (cycles/min)	18.7 ± 1.7	16.1 ± 1.0
ANA seropositives *n*, (%)	15, (88)	NA
RF seropositives *n*, (%)	6, (35)	NA
Anti-SSA abs seropositives *n*, (%)	12, (70)	NA
Anti-SSB abs seropositives *n*, (%)	6, (35)	NA
Positive scialometry test *n*, (%)	11, (65)	NA
Positive Schirmer's test *n*, (%)	15, (88)	NA

BMI, body mass index; HR, heart rate; SAP, systolic arterial pressure; Resp, respiratory activity; ANA, antinuclear antibodies; RF, rheumatoid factor autoantibodies; SSA, Sjogren syndrome-related antigen A; SSB, Sjogren syndrome-related antigen B; NA, not applicable. Data are expressed as mean ± SEM.

TABLE 2 | Cardiac and sympathetic baroreflex sensitivity (BRS) evaluation by sequence and spectral methods during supine rest.

	Patients	Controls
SEQ_{cBRS} (ms mmHg^{-1})	5.58 ± 0.61[§]	9.51 ± 0.50
αLF_{cBRS} (ms mmHg^{-1})	15.9 ± 4.6	18.1 ± 3.2
SEQ_{sBRS} (bursts s^{-1} mmHg^{-1})	−0.11 ± 0.03	−0.10 ± 0.03
αLF_{sBRS} (bursts s^{-1} mmHg^{-1})	6.21 ± 1.62	5.03 ± 5.98

SEQ_{cBRS} indicates cardiac baroreflex sensitivity calculated over the SAP-RR spontaneous sequences of cBR origin, by the sequence method, i.e., SAP changes with same sign of RR variations; αLF_{cBRS}, spectral index of cBR sensitivity, computed as the square root of the ratio between LF_{RR} and LF_{SAP}; SEQ_{sBRS}, sympathetic baroreflex sensitivity calculated over the DAP-MSNA sequences of sBR origin, by the sequence method, i.e., DAP changes with opposite sign of the MSNA burst rate variations; αLF_{sBRS}, spectral index of sBR sensitivity, computed as the square root of the ratio between LF_{MSNA} and LF_{DAP}. Results are expressed as mean ± SEM. [§] $p < 0.005$ patients vs. controls.

TABLE 3 | Cardiac and sympathetic baroreflex sensitivity (BRS) evaluation by sequence and spectral methods during 75° head-up tilt.

	Patients	Controls
SEQ_{cBRS} (ms mmHg^{-1})	6.23 ± 1.66	6.77 ± 1.40
αLF_{cBRS} (ms mmHg^{-1})	6.54 ± 1.83	7.65 ± 1.51
SEQ_{sBRS} (bursts s^{-1} mmHg^{-1})	−0.11 ± 0.01	−0.10 ± 0.03
αLF_{sBRS} (bursts s^{-1} mmHg^{-1})	9.43 ± 2.35	9.49 ± 3.24

*Remaining abbreviations as in **Table 2**. Results are expressed as mean ± SEM.*

were observed in both indices during tilt in either pSS patients and healthy controls (**Table 3**).

Cardiovascular Autonomic Assessment

As to the cardiovascular reflex tests performed in the supine position, no significant differences were seen between the pSS group and control group in mean Valsalva ratio values (1.43 ± 0.1 vs. 1.64 ± 0.09; p = 0.09) and mean SA ratio (1.20 ± 0.03 vs. 1.24 ± 0.04; p = 0.49).

Figure 2 shows representative examples of the variables that were recorded while supine in a patient with pSS and in a healthy control. Notice that MSNA burst rate was greater in the pSS patient than in the control subject at rest whereas BP and HR were similar in both individuals.

Tables 4, **5** summarize the mean spectral indices and MSNA burst activity of sympathetic vasomotor control in the pSS and control group, both in the supine position and in response to tilt.

In the supine position, the pSS group had significantly lower LF_{RR} (nu) and higher HF_{RR} (nu) values compared to the control group. The LF/HF ratio was significantly lower in the patient group. **Figure 3** depicts the differences in the values of the spectral index of cardiac vagal modulation HF_{RR} in nu and of arterial BRS SEQ_{cBRS}, as observed in Sjogren patients and controls, both at rest and during the tilt maneuver. At rest HF_{RR} in nu was greater in patients than in controls. This was associated with lower arterial BRS. During tilt, SEQ_{cBRS} decreased in both patients and controls, but still HF_{RR} was higher in patients.

No significant differences were observed between the groups in LF_{SAP}, and in αLF, an index of arterial baroreflex function. In contrast, neural post-ganglionic sympathetic discharge activity (MSNA) was significantly greater in pSS patients compared to controls (**Figure 2**).

In response to the head up tilt challenge patients and controls had similar HR (85.8 ± 5.4 and 83.2 ± 3.4 beats/min, respectively), SAP (126.5 ± 6.5 and 119.1 ± 1 mmHg, respectively), and respiratory rate (16.1 ± 1.0 and

TABLE 4 | Indices of autonomic function and MSNA in pSS patients and healthy controls during the supine position.

	Supine	
	Patients	Controls
VM ratio	1.43 ± 0.09	1.64 ± 0.09
SA ratio	1.20 ± 0.03	1.24 ± 0.04
R–R interval (ms)	951.1 ± 41.1	907.5 ± 26.9
σ^2_{RR} (ms^2)	1725 ± 537	1356 ± 285.4
HF_{RR} (ms^2)	593.9 ± 283	237.9 ± 61.7
HF_{RR} (nu)	54.6 ± 5.7*	32.8 ± 3.2
LF_{RR} (ms^2)	338.4 ± 109	460.8 ± 110
LF_{RR} (nu)	43.2 ± 5.5*	63.2 ± 3.6
LF/HF	1.87 ± 0.98*	2.48 ± 0.42
SAP (mmHg)	121.6 ± 5.9	114.2 ± 2.9
σ^2_{SAP} (mmHg^2)	20.7 ± 4.1	14.4 ± 4.7
LF_{SAP} (mmHg^2)	1.83 ± 0.52	1.80 ± 0.41
MSNA (bursts/min)	30.57 ± 2.75*	20.71 ± 3.29
MSNA (bursts/100 beats)	49.08 ± 2.68*	29.55 ± 2.81

*VM ratio indicates the ratio between the highest and the lowest heart rate values during the Valsalva maneuver; SA ratio, sinus arrhythmia ratio between the highest and the lowest heart rate values during a 2-min long controlled respiration at 6 breaths per minute; σ^2_{RR}, variance of R–R interval; HF, high frequency component; LF, low frequency component; LF/HF, ratio between the low frequency and the high frequency components of RR variability; nu, normalized units; SAP, systolic arterial pressure; σ^2_{SAP}, variance of systolic arterial pressure; MSNA, muscle sympathetic nerve activity. Data are expressed as mean ± SEM. *$p < 0.05$ patients vs. controls (Kolmogorov–Smirnov test).*

TABLE 5 | Indices of autonomic function and MSNA in pSS patients and healthy controls during 75° head-up tilt.

	75° head-up tilt	
	Patients	**Controls**
R–R interval (ms)	743.1 ± 46.0	727.3 ± 23.8
σ^2_{RR} (ms^2)	880.2 ± 203.5	1115.0 ± 212.6
HF_{RR} (ms^2)	70.7 ± 18.4	60.0 ± 17.1
HF_{RR} (nu)	33.2 ± 6.8*	11.1 ± 1.6
LF_{RR} (ms^2)	403.3 ± 113.2	550.8 ± 146.9
LF_{RR} (nu)	56.5 ± 8.8	79.8 ± 4.2
LF/HF	5.48 ± 1.70*	10.38 ± 1.82
SAP (mmHg)	117.6 ± 5.43	119.3 ± 3.24
σ^2_{SAP} ($mmHg^2$)	27.67 ± 7.1	15.39 ± 1.4
LF_{SAP} ($mmHg^2$)	10.54 ± 2.97	7.10 ± 1.38
MSNA (bursts/min)	51.14 ± 3.81§	32.14 ± 3.32
MSNA (bursts/100 beats)	60.33 ± 3.02*	38.47 ± 2.31

*Abbreviations as in **Table 4**. Data are expressed as mean ± SEM. *$p < 0.05$ patients vs. controls (Kolmogorov–Smirnov test). §$p < 0.005$ patients vs. controls (Kolmogorov–Smirnov test).*

18.6 ± 1.6 breaths/min, respectively). MSNA burst rate was greater in patients (**Table 3**). The two groups were characterized by a similar increase in mean LF/HF ratio and LF_{SAP} values whereas the increase of MSNA was greater in patients compared to controls (**Figure 4**).

Post hoc power calculations yielded a statistical power of 56% with an effect size of 0.87 (medium to large effect, considering the suggestions from Quintana, 2017). This was calculated on the variable LF/HF, after a multiple comparison correction of the significance level.

DISCUSSION

The results of the present study indicate that pSS patients suffer more from global symptom burden and autonomic dysfunction symptoms compared to healthy controls, in agreement with a previous study (Newton et al., 2012). In particular, they scored markedly higher in the secretomotor and pupillomotor domains, a finding which is not surprising since sicca symptoms are considered hallmarks of the disease. Furthermore, in pSS patients secretomotor dysfunction was strongly associated with decreased measured salivary production.

It has to be pointed out that spectral analysis of RR variability revealed subtle abnormalities in the cardiac autonomic control that would have remained hidden when considering the simple hemodynamic profile of the two groups in the supine position. Indeed, while HR, SAP, and respiratory rate mean values were

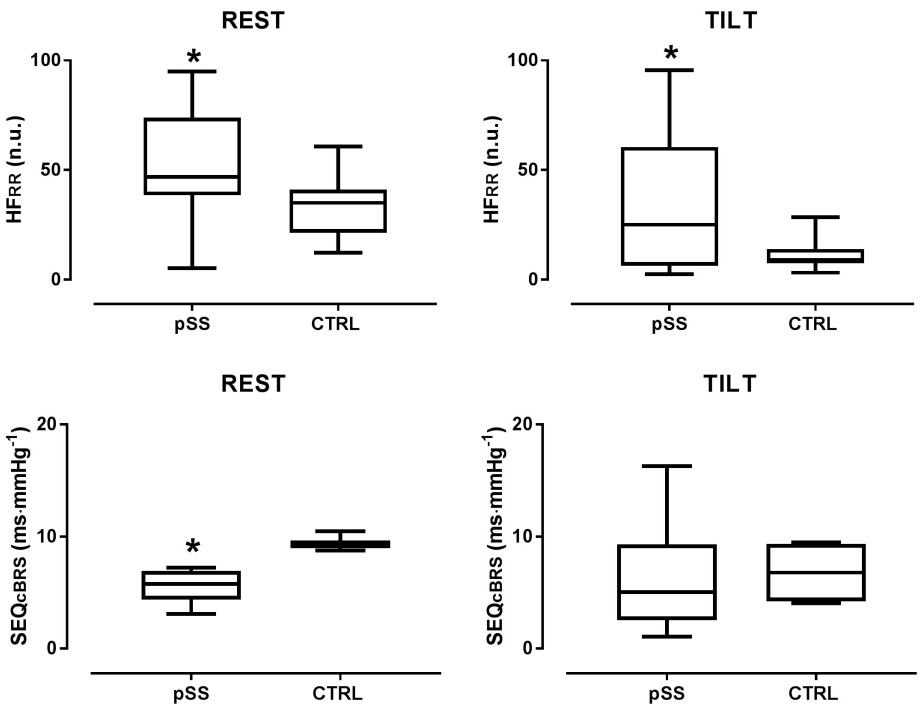

FIGURE 3 | Box plots showing the differences in the values of the spectral index of cardiac parasympathetic modulation HF_{RR} in nu and of arterial baroreflex sensitivity SEQ_{cBRS}, as observed in Sjogren patients and controls both at rest and during the tilt maneuver. Notice that at rest HF_{RR} was greater in patients suggesting a prevailing cardiac vagal modulation compared with controls. This was associated with a lower arterial baroreflex control of HR, a finding which points to the independence of the cardiac vagal modulation from arterial baroreceptor modulation in Sjogren patients at rest. During tilt, SEQ_{cBRS} decreased in both patients and controls but still HF_{RR} was higher in patients than in healthy controls further highlighting its independence from baroreceptor modulation. HF_{RR} indicates the high frequency oscillatory component of RR interval variability; SEQ_{cBRS} is the index of arterial baroreflex sensitivity obtained by the spontaneous sequences method. *$p < 0.05$.

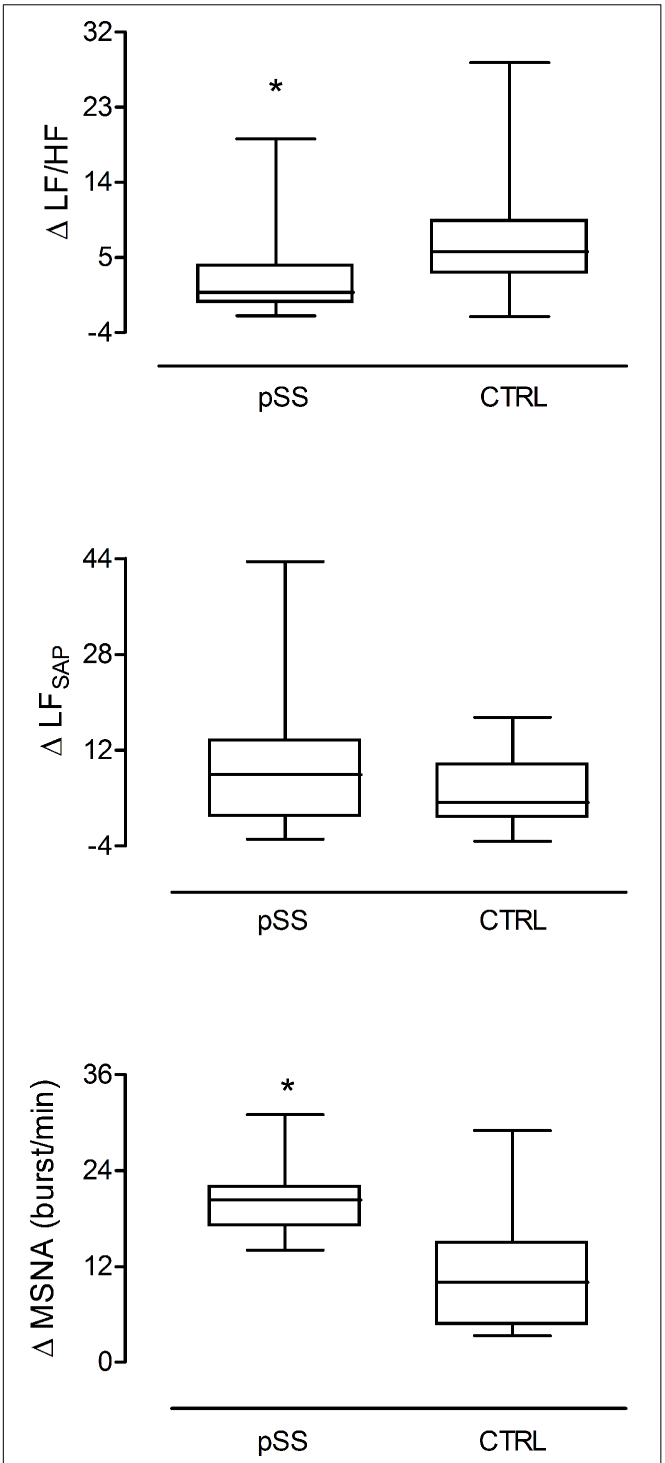

FIGURE 4 | Changes induced by the gravitational stimulus (75° head-up tilt) on the spectral index of cardiac sympatho-vagal balance LF/HF, sympathetic vasomotor control LF_{SAP}, and on the neural post-ganglionic sympathetic (MSNA) burst activity in patients (left box plot) and in healthy controls (right box plot). In response to tilt, patients were characterized by a greater increase in the sympathetic discharge activity to the vessels compared to controls in the presence of similar enhancement of the spectral index, LF_{SAP}. This latter assesses both the sympathetic vasomotor control and the arteries smooth muscle responsiveness. *$p = 0.03$.

similar in pSS patients and controls, patients were characterized by markedly higher HF_{RR} (nu), an index of vagal efferent modulation directed to the sinoatrial node. In addition, the LF/HF ratio was lower in pSS, reflecting a shift of the sympatho–vagal instantaneous modulation toward vagal predominance compared to controls. These findings are in keeping with previous observations (Tumiati et al., 2000). In addition, such cardiac parasympathetic prevalence might reflect an autonomic compensatory mechanism in a setting of a potentially reduced local exocrine glands cholinergic sensitivity (Imrich et al., 2015), in turn accounting for the sicca symptoms such as xerostomia and xerophthalmia.

In response to head up tilt, even though both groups demonstrated an increase in cardiac sympathetic modulation, an expected response to orthostatic challenge (Furlan et al., 2000), the increase in both the LF_{RR} (nu) and LF/HF ratio was milder in pSS patients, indicating a relative impairment in sympathetic function or insufficient withdrawal of cardiac vagal modulation, which is in keeping with previously reported data (Cai et al., 2008; Ng et al., 2012). Although the functional meaning of the LF component of RR variability is still controversial (Pomeranz et al., 1985; Parati et al., 1995) altogether, the changes in HF_{RR} nu and in the LF/HF ratio suggest that pSS patients were characterized by predominant cardiovagal modulatory activity at rest and possibly an attenuated capability to properly decrease their cardiac vagal modulation in response to the orthostatic stimulus, compared to healthy controls.

In the current investigation arterial baroreflex sensitivity was lower in pSS patients than in controls, as assessed in the time domain by the sequences technique. A similar pattern, although not statistically significant, was observed when arterial baroreceptor function was evaluated in the frequency domain by the αLF_{cBRS} index. The presence of an enhanced cardiac parasympathetic modulation in a setting of reduced arterial baroreflex sensitivity as observed in our Sjogren patients is surprising, since it diverges from most of the physiological (Furlan et al., 2000; Laude et al., 2004; Marchi et al., 2016b) and pathophysiological (Pagani et al., 1988; Barbic et al., 2007) conditions where a decreased baroreceptor sensitivity was found to be associated with a reduced, rather than enhanced, cardiac parasympathetic activity. These patterns may suggest the independence of the cardiac autonomic profile from arterial baroreceptor activity in Sjogren patients while supine, highlighting the potential role of a centrally mediated enhanced cardiac vagal modulation (**Figure 3**). During tilt, both SEQ_{cBRS} and αLF_{cBRS} index decreased in patients similarly to healthy controls, thus suggesting a normal arterial baroreceptor unloading during the gravitational stimulus. However, still HF_{RR} was greater in patients than in controls (**Figure 3**) further highlighting its independence from the baroreceptor modulation.

Although the presence of both autonomic symptoms and cardiac sympatho–vagal control disturbances were observed, no association was found between spectral indices of cardiac neural control and symptoms, as was also reported by others (Mandl et al., 2007, 2008).This might be due to differences in the underlying pathological mechanisms leading to the symptoms

and objective signs in pSS (Waterman et al., 2000; Dawson et al., 2006; Mandl et al., 2010).

The pathogenesis responsible for the sicca symptoms in pSS is still under investigation. Symptoms may result from end organ damage with decreased responsiveness to autonomic modulatory activity or from a dysfunction of the ANS itself or from both. Notably, although autoimmune and inflammatory processes are involved in the destruction of exocrine glands in pSS, there seems to be no association between the degree of damage and glands functional status (Imrich et al., 2015). However, there is some evidence pointing to a cholinergic dysfunction affecting those glands, which seems to take place independently of the damage produced by inflammation (Imrich et al., 2015). This is also supported by the fact that, Pilocarpine, a parasympathomimetic drug and a mainstay treatment for pSS, improves salivary secretions (Ramos-Casals et al., 2010). Furthermore, a previous study suggested that central regulation of cholinergic activity seemed unaffected in pSS and it was therefore proposed that cholinergic dysfunction occurs at the peripheral or exocrine gland level (Imrich et al., 2015). This lends further support, although indirect, to the role of autonomic abnormalities as possible etiopathogenetic mechanism in pSS.

In the present study, the fact that pSS patients showed an overactive cardiac parasympathetic modulation might reflect the attempt to regulate and overcome a cholinergic dysfunction possibly originating at the glandular level, in the effort to maintain some secretory capability. This parasympathetic overactivity was however reflected by HR variability changes and not by mean HR modifications, a divergent pattern which can be observed in other pathophysiological condition such as vasovagal syncope (Furlan et al., 1998b).

The combined use of power spectral analysis of SAP variability and the direct post-ganglionic sympathetic neural discharge recordings enabled the detection of additional alterations in the vascular autonomic control in pSS. At rest the spectral index LF_{SAP}, a non-invasive marker of the sympathetic vasomotor control, was similar in both groups and in keeping with previous findings (Cai et al., 2008), whereas MSNA burst rate was greater in pSS. The discrepancy in the MSNA activity compared to LF_{SAP} at rest is unusual in a setting of normal sympathetic baroreceptor modulatory activity. Indeed, conditions leading to an increase of the MSNA, such as the presence of an hyper adrenergic state like that observed in POTS (Furlan et al., 1998a) or in response to upright position in healthy individuals (Furlan et al., 2000), were found to be paraleled by similar changes of LF_{SAP} (Furlan et al., 2000).

Despite the limited number of patients in the current study, taken together these findings indicate that in the supine position pSS patients exhibit discordant cardiac and vascular sympathetic control characterized by predominant vagal cardiac modulation and greater sympathetic nerve activity targeting the vessels.

There might be several possible explanations accounting for this possible discrepancy. It could potentially be the result of a peripheral compensatory response in the attempt to balance the excessive parasympathetic cardiac activity. Alternatively, the sympathetic post-ganglionic discharge activity could have been enhanced in response to peripheral vascular damage due to subclinical vasculitis. This might reduce the capability of the arterial smooth muscle of adequately contracting under the sympathetic firing, similarly to what was observed in the healthy subjects of the current study. Notably, it has been shown that peripheral and visceral vasculitis in pSS patients were strongly associated with the presence of anti-SSA/-SSB autoantibodies (Scofield, 2011), a finding that was as high as 80% in our pSS population. The observation of a mismatch between an enhanced MSNA and a concomitant "normal" LF_{SAP} at rest in pSS compared to controls mimics what was previously observed after atenolol administration in healthy subjects (Cogliati et al., 2004) and points to a possible similar underlying mechanism. This latter may be a potential mismatch between the neural sympathetic vasomotor modulation and the target vascular response. In addition, LF_{SAP} is a comprehensive index of the sympathetic control of the vessels. It reflects both neural vasomotor control as well as arterial smooth muscle responsiveness (Furlan et al., 1990; Diedrich et al., 2003). Conversely, MSNA is a direct measure of the sympathetic post-ganglionic neural discharge to the arteries (Delius et al., 1972a,b; Sanders et al., 1988). Therefore, although MSNA burst rate and LF_{SAP} are both related to the sympathetic vascular control, they are not equal, such that to some extent the latter also reflects the integrity of the target organ, i.e., the vascular smooth muscle functioning.

The fact that sympathetic baroreceptor modulation of MSNA was similar in patients and controls in the presence of greater sympathetic firing must be pointed out. It suggests the presence of primary central sympathetic overactivity in our pSS patients, independently of baroreceptor sympathetic inhibitory modulation which was comparable to that of healthy controls. Therefore, the existence of peripheral vascular damage induced by possible chronic subclinical inflammation, previously described in pSS (Fox, 2005; Scofield, 2011), could potentially cause a blunted vessel response to sympathetic vasoconstrictor stimuli. Consequently, in order to produce proper vasoconstriction and maintain adequate BP values similar to healthy age-matched individuals, a greater amount of sympathetic firing might be necessary in pSS patients. The greater increase of MSNA observed in pSS during tilt compared to controls, in the presence of similar SAP and LF_{SAP} values in the two groups, seems to lend further support to the present hypothesis.

Limitations

The current investigation is a preliminary study with a small number of participants. This is partially due to the presence in the protocol of an invasive procedure, i.e., the direct recording of the neural sympathetic discharge activity. Thus, results and conclusions should be carefully considered.

In our interpretation of the results, we are proposing still unconfirmed hypotheses rather than drawing definite conclusions. Future studies based on larger pSS populations might help to confirm the present etiopathogenic hypotheses.

Finally, the *post hoc* power calculations regarding LF/HF ratio was found to be 56%. One may argue that such a value is low especially when compared to the original value of the power set *a priori* to calculate the sample size of our study based on Tumiati et al. (2000), namely 0.8. This discrepancy is likely to be related to a larger variability in our group. It has to be pointed out that a low statistical power raises the possibility of a type II error, i.e., the presence of false negative results that, however, should not affect our interpretation of the findings mainly based on discussing positive results (i.e., significant differences).

CONCLUSION

The results of the current study revealed the presence of subtle disturbances in the cardiac autonomic control in pSS patients, namely a dominant cardiac parasympathetic modulation at rest with reduced cBR control of HR. Furthermore, direct recording of the sympathetic post-ganglionic neural discharge to vessels by microneurography technique detected the presence of a greater sympathetic nerve activity in patients, both while supine and in response to gravitational challenge. In a setting of preserved sympathetic baroreceptor control, we hypothesized that a primary enhanced sympathetic vasoconstrictor activity would be required to keep BP values stables, if a possible chronic subclinical vasculitis were present.

ETHICS STATEMENT

This study was carried out in accordance with the recommendations of the Italian National Bioethics Committee with written informed consent from all subjects. All subjects gave written informed consent in accordance with the Declaration of Helsinki. The protocol was approved by the local IRB (no. 1395\2015).

AUTHOR CONTRIBUTIONS

EB, SA, GJ, PP, AP, and RF: conception and design of the research. PM, MF, AZ, and LB: performing studies. BC and DS: data analysis. EB, DS, BC, GJ, PP, AP, and RF: interpretation of study results. DS and MM: figure drawing. DS: preparation of the first draft of the manuscript. DS, BC, AP, and RF: manuscript editing and revision. EB, DS, PM, SA, MF, AZ, MM, BC, GJ, LB, PP, AP, and RF: final version approval of the manuscript.

REFERENCES

Andonopoulos, A. P., Christodoulou, J., Ballas, C., Bounas, A., and Alexopoulos, D. (1998). Autonomic cardiovascular neuropathy in Sjogren's syndrome. A controlled study. *J. Rheumatol.* 25, 2385–2388.

Barbic, F., Perego, F., Canesi, M., Gianni, M., Biagiotti, S., Costantino, G., et al. (2007). Early abnormalities of vascular and cardiac autonomic control in Parkinson's disease without orthostatic hypotension. *Hypertension* 49, 120–126. doi: 10.1161/01.hyp.0000250939.71343.7c

Barendregt, P. J., Tulen, J. H., van den Meiracker, A. H., and Markusse, H. M. (2002). Spectral analysis of heart rate and blood pressure variability in primary Sjogren's syndrome. *Ann. Rheum. Dis.* 61, 232–236. doi: 10.1136/ard.61.3.232

Barendregt, P. J., van Den Meiracker, A. H., Markusse, H. M., Tulen, J. H., Boomsma, F., van Der Heijde, G. L., et al. (1999). Parasympathetic failure does not contribute to ocular dryness in primary Sjogren's syndrome. *Ann. Rheum. Dis.* 58, 746–750. doi: 10.1136/ard.58.12.746

Bertinieri, G., di Rienzo, M., Cavallazzi, A., Ferrari, A. U., Pedotti, A., and Mancia, G. (1985). A new approach to analysis of the arterial baroreflex. *J. Hypertens. Suppl.* 3, S79–S81.

Cai, F. Z., Lester, S., Lu, T., Keen, H., Boundy, K., Proudman, S. M., et al. (2008). Mild autonomic dysfunction in primary Sjogren's syndrome: a controlled study. *Arthritis Res. Ther.* 10:R31. doi: 10.1186/ar2385

Cogliati, C., Colombo, S., Ruscone, T. G., Gruosso, D., Porta, A., Montano, N., et al. (2004). Acute beta-blockade increases muscle sympathetic activity and modifies its frequency distribution. *Circulation* 110, 2786–2791. doi: 10.1161/01.cir.0000146335.69413.f9

Dawson, L. J., Stanbury, J., Venn, N., Hasdimir, B., Rogers, S. N., and Smith, P. M. (2006). Antimuscarinic antibodies in primary Sjogren's syndrome reversibly inhibit the mechanism of fluid secretion by human submandibular salivary acinar cells. *Arthritis Rheum* 54, 1165–1173. doi: 10.1002/art.21764

Delius, W., Hagbarth, K. E., Hongell, A., and Wallin, B. G. (1972a). General characteristics of sympathetic activity in human muscle nerves. *Acta Physiol. Scand.* 84, 65–81. doi: 10.1111/j.1748-1716.1972.tb05157.x

Delius, W., Hagbarth, K. E., Hongell, A., and Wallin, B. G. (1972b). Manoeuvres affecting sympathetic outflow in human muscle nerves. *Acta Physiol. Scand.* 84, 82–94. doi: 10.1111/j.1748-1716.1972.tb05158.x

Diedrich, A., Jordan, J., Tank, J., Shannon, J. R., Robertson, R., Luft, F. C., et al. (2003). The sympathetic nervous system in hypertension: assessment by blood pressure variability and ganglionic blockade. *J. Hypertens.* 21, 1677–1686. doi: 10.1097/00004872-200309000-00017

Diedrich, A., Porta, A., Barbic, F., Brychta, R. J., Bonizzi, P., Diedrich, L., et al. (2009). Lateralization of expression of neural sympathetic activity to the vessels and effects of carotid baroreceptor stimulation. *Am. J. Physiol. Heart Circ. Physiol.* 296, H1758–H1765. doi: 10.1152/ajpheart.01045.2008

Ebert, E. C. (2012). Gastrointestinal and hepatic manifestations of Sjogren syndrome. *J. Clin. Gastroenterol.* 46, 25–30. doi: 10.1097/MCG.0b013e3182329d9c

Fox, R. I. (2005). Sjogren's syndrome. *Lancet* 366, 321–331.

Furlan, R., Guzzetti, S., Crivellaro, W., Dassi, S., Tinelli, M., Baselli, G., et al. (1990). Continuous 24-hour assessment of the neural regulation of systemic arterial pressure and RR variabilities in ambulant subjects. *Circulation* 81, 537–547. doi: 10.1161/01.cir.81.2.537

Furlan, R., Jacob, G., Snell, M., Robertson, D., Porta, A., Harris, P., et al. (1998a). Chronic orthostatic intolerance: a disorder with discordant cardiac and vascular sympathetic control. *Circulation* 98, 2154–2159. doi: 10.1161/01.cir.98.20.2154

Furlan, R., Piazza, S., Dell'Orto, S., Barbic, F., Bianchi, A., Mainardi, L., et al. (1998b). Cardiac autonomic patterns preceding occasional vasovagal reactions in healthy humans. *Circulation* 98, 1756–1761. doi: 10.1161/01.cir.98.17.1756

Furlan, R., Porta, A., Costa, F., Tank, J., Baker, L., Schiavi, R., et al. (2000). Oscillatory patterns in sympathetic neural discharge and cardiovascular variables during orthostatic stimulus. *Circulation* 101, 886–892. doi: 10.1161/01.cir.101.8.886

Gamron, S., Barberis, G., Onetti, C. M., Strusberg, I., Hliba, E., Martellotto, G., et al. (2000). Mesangial nephropathy in Sjogren's syndrome. *Scand. J. Rheumatol.* 29, 65–67.

Goodman, B. P., Crepeau, A., Dhawan, P. S., Khoury, J. A., and Harris, L. A. (2017). Spectrum of autonomic nervous system impairment in sjogren syndrome. *Neurologist* 22, 127–130. doi: 10.1097/NRL.0000000000000134

Gyongyosi, M., Pokorny, G., Jambrik, Z., Kovacs, L., Kovacs, A., Makula, E., et al. (1996). Cardiac manifestations in primary Sjogren's syndrome. *Ann. Rheum. Dis.* 55, 450–454.

Hamner, J. W., and Taylor, J. A. (2001). Automated quantification of sympathetic beat-by-beat activity, independent of signal quality. *J. Appl. Physiol.* 91, 1199–1206. doi: 10.1152/jappl.2001.91.3.1199

Heathers, J. A. J., and Goodwin, M. S. (2017). Dead Science in Live Psychology: a Case Study from Heart Rate Variability (HRV). *PsyArXiv* [Preprint]. doi: 10.31234/osf.io/637ym

Hilz, M. J., and Dutsch, M. (2005). Methods of quantitative evaluation of the autonomic nerve system. *Nervenarzt* 76:767.

Humphreys-Beher, M. G., Brayer, J., Yamachika, S., Peck, A. B., and Jonsson, R. (1999). An alternative perspective to the immune response in autoimmune exocrinopathy: induction of functional quiescence rather than destructive autoaggression. *Scand. J. Immunol.* 49, 7–10.

Imrich, R., Alevizos, I., Bebris, L., Goldstein, D. S., Holmes, C. S., Illei, G. G., et al. (2015). Predominant glandular cholinergic dysautonomia in patients with primary sjogren's syndrome. *Arthritis Rheumatol.* 67, 1345–1352. doi: 10.1002/art.39044

Jonsson, R., Kroneld, U., Backman, K., Magnusson, B., and Tarkowski, A. (1993). Progression of sialadenitis in Sjogren's syndrome. *Br. J. Rheumatol.* 32, 578–581. doi: 10.1093/rheumatology/32.7.578

Kienbaum, P., Karlssonn, T., Sverrisdottir, Y. B., Elam, M., and Wallin, B. G. (2001). Two sites for modulation of human sympathetic activity by arterial baroreceptors? *J. Physiol.* 531, 861–869. doi: 10.1111/j.1469-7793.2001.0861h.x

Koh, J. H., Kwok, S. K., Lee, J., and Park, S. H. (2017). Autonomic dysfunction in primary Sjogren's syndrome: a prospective cohort analysis of 154 korean patients. *Korean J. Intern. Med.* 32, 165–173. doi: 10.3904/kjim.2015.219

Kovacs, L., Paprika, D., Takacs, R., Kardos, A., Varkonyi, T. T., Lengyel, C., et al. (2004). Cardiovascular autonomic dysfunction in primary Sjogren's syndrome. *Rheumatology* 43, 95–99. doi: 10.1093/rheumatology/keg468

Laude, D., Elghozi, J. L., Girard, A., Bellard, E., Bouhaddi, M., Castiglioni, P., et al. (2004). Comparison of various techniques used to estimate spontaneous baroreflex sensitivity (the EuroBaVar study). *Am. J. Physiol. Regul. Integr. Comp. Physiol.* 286, R226–R231.

Lindvall, B., Bengtsson, A., Ernerudh, J., and Eriksson, P. (2002). Subclinical myositis is common in primary Sjogren's syndrome and is not related to muscle pain. *J. Rheumatol.* 29, 717–725.

Magagnin, V., Bassani, T., Bari, V., Turiel, M., Maestri, R., Pinna, G. D., et al. (2011). Non-stationarities significantly distort short-term spectral, symbolic and entropy heart rate variability indices. *Physiol. Meas.* 32, 1775–1786. doi: 10.1088/0967-3334/32/11/S05

Mandl, T., Bornmyr, S. V., Castenfors, J., Jacobsson, L. T., Manthorpe, R., and Wollmer, P. (2001). Sympathetic dysfunction in patients with primary Sjogren's syndrome. *J. Rheumatol.* 28, 296–301.

Mandl, T., Granberg, V., Apelqvist, J., Wollmer, P., Manthorpe, R., and Jacobsson, L. T. (2008). Autonomic nervous symptoms in primary Sjogren's syndrome. *Rheumatology* 47, 914–919. doi: 10.1093/rheumatology/ken107

Mandl, T., Hammar, O., Theander, E., Wollmer, P., and Ohlsson, B. (2010). Autonomic nervous dysfunction development in patients with primary Sjogren's syndrome: a follow-up study. *Rheumatology* 49, 1101–1106. doi: 10.1093/rheumatology/keq042

Mandl, T., Wollmer, P., Manthorpe, R., and Jacobsson, L. T. (2007). Autonomic and orthostatic dysfunction in primary Sjogren's syndrome. *J. Rheumatol.* 34, 1869–1874.

Marchi, A., Bari, V., De Maria, B., Esler, M., Lambert, E., Baumert, M., et al. (2016a). Calibrated variability of muscle sympathetic nerve activity during graded head-up tilt in humans and its link with noradrenaline data and cardiovascular rhythms. *Am. J. Physiol. Regul. Integr. Comp. Physiol.* 310, R1134–R1143. doi: 10.1152/ajpregu.00541.2015

Marchi, A., Bari, V., De Maria, B., Esler, M., Lambert, E., Baumert, M., et al. (2016b). Simultaneous characterization of sympathetic and cardiac arms of the baroreflex through sequence techniques during incremental head-up tilt. *Front. Physiol.* 7:438. doi: 10.3389/fphys.2016.00438

Newton, J. L., Frith, J., Powell, D., Hackett, K., Wilton, K., Bowman, S., et al. (2012). Autonomic symptoms are common and are associated with overall symptom burden and disease activity in primary Sjogren's syndrome. *Ann. Rheum. Dis.* 71, 1973–1979. doi: 10.1136/annrheumdis-2011-201009

Ng, W. F., Stangroom, A. J., Davidson, A., Wilton, K., Mitchell, S., and Newton, J. L. (2012). Primary Sjogrens syndrome is associated with impaired autonomic response to orthostasis and sympathetic failure. *QJM* 105, 1191–1199. doi: 10.1093/qjmed/hcs172

Niemela, R. K., Hakala, M., Huikuri, H. V., and Airaksinen, K. E. (2003). Comprehensive study of autonomic function in a population with primary Sjogren's syndrome. No evidence of autonomic involvement. *J Rheumatol.* 30, 74–79.

Niemela, R. K., Pikkujamsa, S. M., Hakala, M., Huikuri, H. V., and Airaksinen, K. E. (2000). No signs of autonomic nervous system dysfunction in primary Sjorgen's syndrome evaluated by 24 hour heart rate variability. *J. Rheumatol.* 27, 2605–2610.

Pagani, M., Lombardi, F., Guzzetti, S., Rimoldi, O., Furlan, R., Pizzinelli, P., et al. (1986). Power spectral analysis of heart rate and arterial pressure variabilities as a marker of sympatho-vagal interaction in man and conscious dog. *Circ. Res.* 59, 178–193. doi: 10.1161/01.res.59.2.178

Pagani, M., Somers, V., Furlan, R., Dell'Orto, S., Conway, J., Baselli, G., et al. (1988). Changes in autonomic regulation induced by physical training in mild hypertension. *Hypertension* 12, 600–610. doi: 10.1161/01.hyp.12.6.600

Parati, G., Saul, J. P., Di Rienzo, M., and Mancia, G. (1995). Spectral analysis of blood pressure and heart rate variability in evaluating cardiovascular regulation. A critical appraisal. *Hypertension* 25, 1276–1286. doi: 10.1161/01.hyp.25.6.1276

Pease, C. T., Shattles, W., Barrett, N. K., and Maini, R. N. (1993). The arthropathy of Sjogren's syndrome. *Br. J. Rheumatol.* 32, 609–613.

Pickering, T. G., Gribbin, B., and Sleight, P. (1972). Comparison of the reflex heart rate response to rising and falling arterial pressure in man. *Cardiovasc. Res.* 6, 277–283. doi: 10.1093/cvr/6.3.277

Pomeranz, B., Macaulay, R. J., Caudill, M. A., Kutz, I., Adam, D., Gordon, D., et al. (1985). Assessment of autonomic function in humans by heart rate spectral analysis. *Am. J. Physiol.* 248, H151–H153.

Porta, A., Bari, V., Bassani, T., Marchi, A., Pistuddi, V., and Ranucci, M. (2013). Model-based causal closed-loop approach to the estimate of baroreflex sensitivity during propofol anesthesia in patients undergoing coronary artery bypass graft. *J. Appl. Physiol.* 115, 1032–1042. doi: 10.1152/japplphysiol.00537.2013

Porta, A., Baselli, G., Rimoldi, O., Malliani, A., and Pagani, M. (2000). Assessing baroreflex gain from spontaneous variability in conscious dogs: role of causality and respiration. *Am. J. Physiol. Heart Circ. Physiol.* 279, H2558–H2567.

Proctor, G. B., and Carpenter, G. H. (2007). Regulation of salivary gland function by autonomic nerves. *Auton. Neurosci.* 133, 3–18. doi: 10.1016/j.autneu.2006.10.006

Qin, B., Wang, J., Yang, Z., Yang, M., Ma, N., Huang, F., et al. (2015). Epidemiology of primary Sjogren's syndrome: a systematic review and meta-analysis. *Ann. Rheum. Dis.* 74, 1983–1989.

Quintana, D. S. (2017). Statistical considerations for reporting and planning heart rate variability case-control studies. *Psychophysiology* 54, 344–349. doi: 10.1111/psyp.12798

Quismorio, F. P. Jr. (1996). Pulmonary involvement in primary Sjogren's syndrome. *Curr. Opin. Pulm. Med.* 2, 424–428. doi: 10.1097/00063198-199609000-00013

Ramos-Casals, M., Anaya, J. M., Garcia-Carrasco, M., Rosas, J., Bove, A., Claver, G., et al. (2004). Cutaneous vasculitis in primary Sjogren syndrome: classification and clinical significance of 52 patients. *Medicine* 83, 96–106. doi: 10.1097/01.md.0000119465.24818.98

Ramos-Casals, M., Tzioufas, A. G., Stone, J. H., Siso, A., and Bosch, X. (2010). Treatment of primary Sjogren syndrome: a systematic review. *JAMA* 304, 452–460. doi: 10.1001/jama.2010.1014

Sanders, J. S., Ferguson, D. W., and Mark, A. L. (1988). Arterial baroreflex control of sympathetic nerve activity during elevation of blood pressure in normal man: dominance of aortic baroreflexes. *Circulation* 77, 279–288. doi: 10.1161/01.cir.77.2.279

Scofield, R. H. (2011). Vasculitis in Sjogren's Syndrome. *Curr. Rheumatol. Rep.* 13, 482–488. doi: 10.1007/s11926-011-0207-5

Seror, R., Ravaud, P., Mariette, X., Bootsma, H., Theander, E., Hansen, A., et al. (2011). EULAR Sjogren's Syndrome patient reported index (ESSPRI): development of a consensus patient index for primary Sjogren's syndrome. *Ann. Rheum. Dis.* 70, 968–972. doi: 10.1136/ard.2010.143743

Sletten, D. M., Suarez, G. A., Low, P. A., Mandrekar, J., and Singer, W. (2012). COMPASS 31: a refined and abbreviated composite autonomic symptom score. *Mayo. Clin. Proc.* 87, 1196–1201. doi: 10.1016/j.mayocp.2012.10.013

Smyth, H. S., Sleight, P., and Pickering, G. W. (1969). Reflex regulation of arterial pressure during sleep in man. *Circ. Res.* 24, 109–121. doi: 10.1161/01.res.24.1.109

Sundlof, G., and Wallin, B. G. (1978). Human muscle nerve sympathetic activity at rest. Relationship to blood pressure and age. *J. Physiol.* 274, 621–637. doi: 10.1113/jphysiol.1978.sp012170

Tank, J., Schroeder, C., Diedrich, A., Szczech, E., Haertter, S., Sharma, A. M., et al. (2003). Selective impairment in sympathetic vasomotor control with norepinephrine transporter inhibition. *Circulation* 107, 2949–2954. doi: 10.1161/01.cir.0000072786.99163.fe

Task Force of the European Society of Cardiology and the North American Society of Pacing and Electrophysiology, (1996). Heart rate variability: standards of measurement, physiological interpretation and clinical use. *Circulation* 93, 1043–1065. doi: 10.1161/01.cir.93.5.1043

Tumiati, B., Perazzoli, F., Negro, A., Pantaleoni, M., and Regolisti, G. (2000). Heart rate variability in patients with Sjogren's syndrome. *Clin. Rheumatol.* 19, 477–480.

Vitali, C., Bombardieri, S., Jonsson, R., Moutsopoulos, H. M., Alexander, E. L., Carsons, S. E., et al. (2002). Classification criteria for Sjögren's syndrome: a revised version of the European criteria proposed by the American-European Consensus Group. *Ann. Rheum. Dis.* 61, 554–558. doi: 10.1136/ard.61.6.554

Wallin, B. G., Burke, D., and Gandevia, S. (1994). Coupling between variations in strength and baroreflex latency of sympathetic discharges in human muscle nerves. *J. Physiol.* 474, 331–338. doi: 10.1113/jphysiol.1994.sp020025

Wallin, B. G., and Fagius, J. (1988). Peripheral sympathetic neural activity in conscious humans. *Annu. Rev. Physiol.* 50, 565–576. doi: 10.1146/annurev.physiol.50.1.565

Waterman, S. A., Gordon, T. P., and Rischmueller, M. (2000). Inhibitory effects of muscarinic receptor autoantibodies on parasympathetic neurotransmission in Sjogren's syndrome. *Arthritis Rheum* 43, 1647–1654. doi: 10.1002/1529-0131(200007)43:7<1647::aid-anr31>3.0.co;2-p

Conflict of Interest Statement: The authors declare that the research was conducted in the absence of any commercial or financial relationships that could be construed as a potential conflict of interest.

frontiers in Physiology

ORIGINAL RESEARCH
published: 18 October 2019
doi: 10.3389/fphys.2019.01319

Comparison of Causal and Non-causal Strategies for the Assessment of Baroreflex Sensitivity in Predicting Acute Kidney Dysfunction After Coronary Artery Bypass Grafting

*Vlasta Bari[1], Emanuele Vaini[1], Valeria Pistuddi[1], Angela Fantinato[1], Beatrice Cairo[2], Beatrice De Maria[3], Laura Adelaide Dalla Vecchia[3], Marco Ranucci[1] and Alberto Porta[1,2]**

[1] Department of Cardiothoracic, Vascular Anesthesia and Intensive Care, IRCCS Policlinico San Donato, Milan, Italy, [2] Department of Biomedical Sciences for Health, University of Milan, Milan, Italy, [3] IRCCS Istituti Clinici Scientifici Maugeri, Milan, Italy

OPEN ACCESS

Edited by:
Tijana Bojić, University of Belgrade, Serbia

Reviewed by:
Flavia Ravelli, University of Trento, Italy
Michal Javorka, Comenius University, Slovakia

***Correspondence:**
Alberto Porta
alberto.porta@unimi.it

Specialty section:
This article was submitted to Autonomic Neuroscience, a section of the journal Frontiers in Physiology

Received: *30 March 2019*
Accepted: *30 September 2019*
Published: *18 October 2019*

Citation:
Bari V, Vaini E, Pistuddi V, Fantinato A, Cairo B, De Maria B, Dalla Vecchia LA, Ranucci M and Porta A (2019) Comparison of Causal and Non-causal Strategies for the Assessment of Baroreflex Sensitivity in Predicting Acute Kidney Dysfunction After Coronary Artery Bypass Grafting. Front. Physiol. 10:1319. doi: 10.3389/fphys.2019.01319

Coronary artery bypass graft (CABG) surgery may lead to postoperative complications such as the acute kidney dysfunction (AKD), identified as any post-intervention increase of serum creatinine level. Cardiovascular control reflexes like the baroreflex can play a role in the AKD development. The aim of this study is to test whether baroreflex sensitivity (BRS) estimates derived from non-causal and causal approaches applied to spontaneous systolic arterial pressure (SAP) and heart period (HP) fluctuations can help in identifying subjects at risk of developing AKD after CABG and which BRS estimates provide the best performance. Electrocardiogram and invasive arterial pressure were acquired from 129 subjects (67 ± 10 years, 112 males) before (PRE) and after (POST) general anesthesia induction with propofol and remifentanil. Subjects were divided into AKDs (n = 29) or no AKDs (noAKDs, n = 100) according to the AKD development after CABG. The non-causal approach assesses the transfer function from the HP-SAP cross-spectrum in the low frequency (LF, 0.04–0.15 Hz) band. BRS was estimated according to three strategies: (i) sampling of the transfer function gain at the maximum of the HP-SAP squared coherence in the LF band; (ii) averaging of the transfer function gain in the LF band; (iii) sampling of the transfer function gain at the weighted central frequency of the spectral components of the SAP series dropping in the LF band. The causal approach separated the two arms of cardiovascular control (i.e., from SAP to HP and *vice versa*) and accounted for the confounding influences of respiration via system identification and modeling techniques. The causal approach provided a direct estimate of the gain from SAP to HP by observing the HP response to a simulated SAP rise from the identified model structure. Results show that BRS was significantly lower in AKDs than noAKDs during POST regardless of the strategy adopted for its computation. Moreover, all the BRS estimates during POST remained associated with

AKD even after correction for demographic and clinical factors. Non-causal and causal BRS estimates exhibited similar performances. Baroreflex impairment is associated with post-CABG AKD and both non-causal and causal methods can be exploited to improve risk stratification of AKD after CABG.

Keywords: heart rate variability, arterial pressure, autonomic nervous system, cardiovascular control, adverse outcome, intensive care unit, cardiac surgery, propofol anesthesia

INTRODUCTION

Cardiac baroreflex (BR) is a regulatory mechanism aiming at maintaining the physiological homeostasis by adjusting heart period (HP) in response to arterial pressure (AP) variations (Smyth et al., 1969; Laude et al., 2004). The efficiency of this reflex is generally assessed by computing the baroreflex sensitivity (BRS), quantifying the magnitude of HP changes following a unit variation of AP (Vanoli and Adamson, 1994; Pinna et al., 2015).

The gold standard strategy to characterize BR is the invasive pharmacological method (Smyth et al., 1969) that evaluates the slope of the response of HP to a pharmacologically induced increase or decrease in systolic AP (SAP), referred to as BR sensitivity (BRS). Non-invasive strategies to assess BRS exist and are based on the analysis of the spontaneous variability of HP and SAP in time domain (Bertinieri et al., 1985; Westerhof et al., 2004; Bauer et al., 2010; Muller et al., 2012; De Maria et al., 2018), or frequency domain (Robbe et al., 1987; Pagani et al., 1988; Saul et al., 1991; Porta et al., 2000, 2013; Faes et al., 2004; Pinna et al., 2017) or using identification procedures estimating parameters of mathematical models (Baselli et al., 1994; Patton et al., 1995; Porta et al., 2000; Nollo et al., 2001; Xiao et al., 2005; Porta et al., 2013).

Among the different methodologies to assess BRS, the non-causal method in the frequency domain has been the most frequently exploited one (Robbe et al., 1987; Pagani et al., 1988; Saul et al., 1991; Porta et al., 2000, 2013; Faes et al., 2004; Pinna et al., 2017). The non-causal approach in the frequency domain is grounded on the computation of the cross-spectrum between the HP and SAP variability series and on the estimation of the transfer function directly from it. Then, once obtained the HP-SAP transfer function, a strategy is needed to convert the gain function into a single number representing the BRS. Non-causal frequency domain BRS markers are mostly assessed in the low frequency (LF, from 0.04 to 0.15 Hz) because in this band the prerequisites for their safe computation, namely the high HP-SAP association and HP variations lagging behind SAP ones are more likely to be fulfilled (de Boer et al., 1985). Moreover, the baroreflex origin of the LF oscillations detected in HP series has been repeatedly suggested as a consequence of resonance properties of baroreflex control loop and/or the latency of the baroreflex circuit (De Boer et al., 1987; Baselli et al., 1994; Goldstein et al., 2011).

Baroreflex sensitivity estimates derived from the causal closed loop approach (Baselli et al., 1994; Xiao et al., 2005; Porta et al., 2013) have recently gained attention. The main features of this class of BRS markers is that directionality of the HP-SAP dynamical interactions and their closed loop nature are explicitly accounted by the model structure underlying their computation. Since the two characteristics are neglected by more traditional non-causal frequency domain approaches, causal closed loop BRS markers might have additional advantage in clinical applications. Moreover, the additional advantage of the causal closed loop BRS estimates is the possibility of accounting for the presence of confounding factors, such as respiration (RESP) (Porta et al., 2012), contaminating both HP and SAP variability.

The impairment of BR has a clinical value given that low BRS values are associated to adverse outcome in several pathological conditions. As a matter of fact, low BRS has a remarkable predictive power of adverse events in chronic heart failure (Gouveia et al., 2015; Pinna et al., 2017), myocardial infarction (Landolina et al., 1997; La Rovere et al., 1998; De Ferrari et al., 2007), diabetes (Gerritsen et al., 2001) and hypertension (Collier et al., 2001; Gerritsen et al., 2001). More recently, BRS estimates have been found to be useful in stratifying the risk of adverse events and morbidity after major surgery (Toner et al., 2016; Ranucci et al., 2017) and the inability to cope with increased SAP variability has been correlated with a greater risk in critical care unit (ICU) (Porta et al., 2018). Acute kidney dysfunction (AKD) is one of the major complications after coronary artery bypass graft (CABG) surgery (Ranucci et al., 2017). Since AKD increases early and long-term mortality (Liotta et al., 2014) and it is associated to cardiovascular complications such as heart failure (Holzmann et al., 2013), the prevention of AKD after CABG would improve the patient's prognosis. Moreover, it would reduce patient's ICU stay and, consequently, hospitalization costs.

The use of BRS markers in predicting AKD after CABG requires the optimization of the technique for the computation of BRS. Indeed, the perioperative evaluation of BRS in patients undergoing CABG is a challenging issue because they usually feature an impaired BR regulation and the concomitant presence of pharmacological therapy (Porta et al., 2013; Bari et al., 2018). Therefore, the aim of this work is to check the performance of non-causal and causal strategies for the BRS quantification in differentiating patients who developed AKD after CABG from the ones who did not (noAKD). We consider three non-causal strategies to compute BRS based on cross-spectrum estimation from spontaneous HP and SAP variability: (i) sampling the transfer function gain at the maximum of the squared coherence function (K^2) in the LF band (Bari et al., 2018); (ii) averaging the transfer function gain in the LF band (Pinna et al., 2017); (iii) sampling the transfer function gain at the weighted central frequency of the SAP spectral components dropping in the LF band (Porta et al., 2000, 2013). These three non-causal markers were compared to a causal BRS estimate accounting for the closed loop HP-SAP dynamical interactions and RESP influences (Baselli et al., 1994; Porta et al., 2013). Each technique was tested

in patients scheduled for CABG before and after the induction of propofol general anesthesia.

MATERIALS AND METHODS

Non-causal Open Loop Assessment of BRS in the Frequency Domain

The non-causal approach is based on the estimation of the traditional input-output relation via the cross-spectrum between two series (Saul et al., 1991; Pinna et al., 2002). Being based on the cross-spectrum, this is an open loop approach that hides the closed loop structure of the interactions (Porta et al., 2002). Cross-spectrum was estimated through a parametric approach based on the computation of the coefficients of the bivariate autoregressive model assessed over HP and SAP (Porta et al., 2000). The model order was fixed to 10. The coefficients of the model were identified through least squares approach (Baselli et al., 1997). The transfer function was estimated as the ratio of the cross-spectrum computed from SAP to HP to the power spectrum of SAP. The BRS function was computed in the frequency domain as the modulus of the transfer function in the LF band, namely from 0.04 to 0.15 Hz (Task Force of the European Society of Cardiology, and the North American Society of Pacing and Electrophysiology, 1996). The squared HP-SAP coherence K^2 was computed as the ratio between the squared modulus of the HP-SAP cross-spectrum divided by the product of the two spectra of HP and SAP. This function was labeled as K^2 and ranged between 0 and 1, with 0 indicates null correlation and 1 maximum correlation.

Strategies to Derive the BRS Marker From the BRS Function

A single BRS value was derived from the BRS function according to three different strategies. The first strategy (**Figures 1A,D**), denoted as the MAX strategy, computed the BRS marker as the sampling of the BRS function at the maximum of the K^2 in LF band (Bari et al., 2018). The index was indicated as BRS_{MAX}. The correspondent peak of the K^2 was also stored and labeled as ${K^2}_{MAX}$. The second approach took the average of the BRS function in the LF band (**Figures 1B,E**) (Pinna et al., 2017). This approach will be referred to as the AVG strategy. The index was indicated as BRS_{AVG}. Similarly, K^2 was averaged in the LF band and this average was indicated as ${K^2}_{AVG}$. The third strategy assessed BRS (**Figures 1C,F**) as the sampling of the BRS function at the weighted central frequency (WCF) of SAP, namely at the average central frequency of spectral components of SAP series dropping in the LF band computed using their power as weights (Porta et al., 2000, 2013). The spectral decomposition technique was applied to obtain SAP spectral components, their central frequency and power (Baselli et al., 1997). This approach will be referred to as the WCF strategy. The BRS marker was indicated as BRS_{WCF}. K^2 was sampled at WCF as well and the value was indicated as ${K^2}_{WCF}$. K^2 markers were dimensionless, while BRS indexes were expressed in $ms{\cdot}mmHg^{-1}$. It is worth noting that, while MAX and AVG approaches can be applied in the 100% of the subjects in any experimental condition, the WCF one can be performed only whether at least one spectral component with central frequency dropping in the LF band was detected in the power spectrum of SAP variability series. By definition, BRS_{MAX}, BRS_{AVG} and BRS_{WCF} were larger than 0.

Causal Closed Loop Assessment of BRS

The gains along the two arms of the HP-SAP closed loop control (i.e., the baroreflex feedback pathway from SAP to HP and the mechanical feedforward arm from HP to SAP) were estimated according to a causal linear trivariate model describing the HP-SAP dynamical interactions and considering RESP as an exogenous input acting on both series (Baselli et al., 1994; Porta et al., 2000). In particular, the current HP and SAP were described according to an autoregressive model with exogenous input that combines previous samples of the same series with previous, and eventually present, values of the other series present in the set formed by HP, SAP, RESP with a sample of a white random noise. Being the model structure fully exploited to disentangle the baroreflex feedback pathway from the mechanical feedforward one and considering the directional structure of the model blocks (i.e., the output depends on past, and eventually present, values of the input), the approach is in closed loop and causal. Since RESP was considered exogenous to both HP and SAP time series, RESP dynamic was modeled via the linear combination of its past values plus a sample of a random white noise. All regressions had the same order optimized in the range from 4 to 14 via the Akaike information criterion for multivariate processes. Further details on the procedures followed to estimate the coefficients of the linear regressions and optimization of the model order can be found in Baselli et al. (1997), Porta et al. (2013). The BR gain was computed by feeding the block representing the dynamical relation from SAP to HP with an artificial SAP ramp of unit slope simulating a SAP rise. The slope of the corresponding HP response computed over the first 15 samples was then taken as an estimate of BRS, labeled as $BRS_{SAP \rightarrow HP}$, and expressed in $ms{\cdot}mmHg^{-1}$. The gain of the mechanical feedforward pathway was estimated as the first coefficient of the dynamical relation from HP to SAP. It was labeled as $a_{HP \rightarrow SAP}(1)$ and expressed in $mmHg{\cdot}s^{-1}$. Both $BRS_{SAP \rightarrow HP}$ and $a_{HP \rightarrow SAP}(1)$ can be smaller than 0.

Experimental Protocol

One-hundred twenty-nine patients (67 $\pm$ 10 years, age from 43 to 86 years, 112 males) scheduled for elective, or urgent, CABG surgery at the Department of Cardiothoracic and Vascular Anesthesia and Intensive Care of the IRCCS Policlinico San Donato, San Donato Milanese, Milan, Italy, were enrolled for this study. The study was performed in keeping with the Declaration of Helsinki for research studies involving humans and, before participating, subjects signed a written informed consent. The study was approved by the ethical committee in charge at the IRCCS Policlinico San Donato.

Inclusion criteria were sinus rhythm, age over 18 years, absence of previous kidney dysfunction and of autonomic nervous system pathology. Electrocardiogram (ECG) and invasive AP, measured at the radial artery, were acquired directly

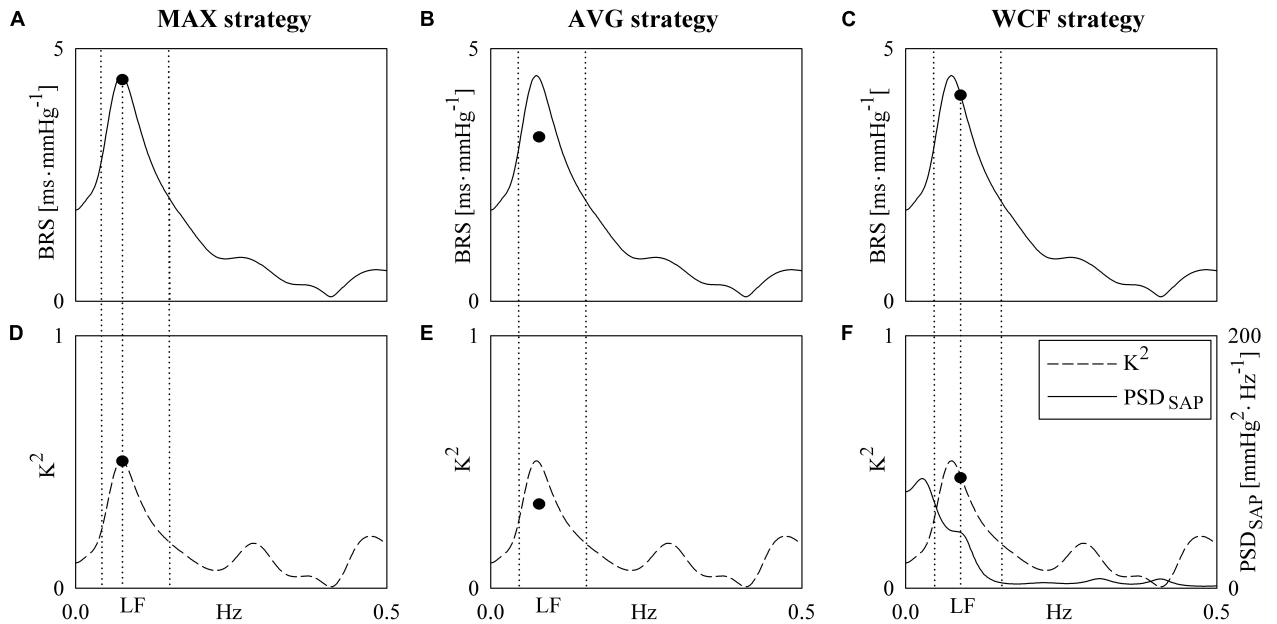

FIGURE 1 | The line graphs show examples of computation of the BRS markers. They are derived from HP and SAP series recorded from the same subject during PRE. The first strategy samples the BRS function **(A)** in the LF band at the maximum of K^2 **(D)**. The sampling of the BRS function and K^2 is marked with a solid circle in both **(A)** and **(D)**. The second strategy averages the BRS function in the LF band. The average of the BRS and the average of K^2 is indicated with a solid circle in **(B)** and **(E)**. The third strategy samples the BRS function **(C)** at the WCF of the spectral components of SAP power spectral density PSD_{SAP} (**F**, solid line) detected in LF band. The sampling of the BRS function **(C)** and K^2 (**F**, dashed line) is marked with a solid circle. The frequency in correspondence of the sampling was indicated as vertical dotted lines as well as the inferior and superior limits of the LF band.

from patient's monitor with an analog-to-digital board (National Instruments, Austin, TX, United States) connected to a laptop for 10 min before (PRE) and after (POST) the induction of general anesthesia performed with propofol and remifentanil. About 1 h before the first acquisition, patients were treated with an intramuscular injection of 0.5 mg of atropine and 100 μg of fentanyl. Anesthesia was induced with an intravenous bolus of 1.5 mg·kg^{-1} of propofol and 0.2 μg·kg^{-1}·min^{-1} of remifentanil according to the standard practice of our institute and was then maintained by infusion at a rate of 3 mg·kg^{-1}·h^{-1} and from 0.05 to 0.5 μg·kg^{-1}·min^{-1} respectively. Subjects breathed spontaneously during PRE and were mechanically ventilated at a rate from 12 to 16 breaths per minute during POST, inhaling a mixture of 1:1 of oxygen and air. Patients were followed during their stay in ICU after CABG surgery and their serum creatinine level was monitored. AKD was defined as any postoperative increase of serum creatinine level from preoperative values in the first 48 h after surgery (Ranucci et al., 2017). Patients were then divided in two groups, defined as AKD (n = 29, age 68.7 ± 10.6, 24 males) and noAKD (n = 100, age 66.0 ± 9.4, 88 males), according to whether the occurrence of AKD after CABG surgery was observed or not.

Beat-to-Beat Series Extraction and Time Domain Indexes

From ECG and AP signals, beat-to-beat variability series were extracted. HP was measured as the temporal distance between two R-wave peaks on the ECG. SAP was taken as the maximum of AP inside the HP and diastolic AP (DAP) as the minimum of AP following SAP. The amplitude of the first QRS complex (from baseline to apex) was utilized as an ECG-derived RESP series (Porta et al., 1998). Series lasting 250 beats were extracted during PRE and POST and they were manually inspected and corrected in case of missing beats or misdetections. The effect of ectopic beats was limited via linear interpolation using the most adjacent values of HP, SAP and DAP unaffected by ectopies. Corrections never exceeded 5% of total beats utilized for the analysis. Time domain indexes as mean and variance of HP, SAP and DAP were calculated. They were labeled as μ_{HP}, σ^2_{HP}, μ_{SAP}, σ^2_{SAP}, μ_{DAP} and σ^2_{DAP}, and expressed respectively in ms, ms^2, mmHg, mmHg^2, mmHg, mmHg^2.

Statistical Analysis

Unpaired t-test, or Mann–Whitney rank sum test when appropriate, was applied over demographic and clinical variables to test their difference between noAKD and AKD groups. χ^2 test was used in case of dichotomous variables. Two-way repeated measures analysis of variance (one factor repetition, Holm–Sidak test for multiple comparisons) was performed over cardiovascular control parameters to assess differences between groups (i.e., noAKD and AKD) assigned the experimental condition (i.e., PRE or POST) and between conditions assigned the group of individuals.

In the multivariate logistic regression model built over demographic and clinical factors capable of discriminating the two groups with $p < 0.1$ the cardiovascular variability

markers were introduced one by one. Regression coefficient, odds ratio, 95% confidence interval and type I error probability p of the multivariate logistic regression model were evaluated to assess the degree of association of cardiovascular variability markers with the outcome accounting for the demographic and clinical factors. For the variability markers that remained associated with the outcome with $p < 0.05$, a receiver operating characteristic (ROC) curve was calculated at the univariate level and the area under the ROC curve (AUC) was assessed. The best combination of sensitivity and specificity was found according to the Youden index for each variability parameter remaining significantly associated with the outcome and the negative predictive value (NPV) and positive predictive value (PPV) were consequently assessed. Then, a ROC curve was built using all the clinical parameters that remained associated with the outcome with $p < 0.05$ alone or in combination with every single cardiovascular variability marker that remained associated with the outcome. The performance of the discrimination between AKD and noAKD group of the multivariate logistic regression models was evaluated via the AUC. Statistical analyses were carried out using commercial statistical software (Sigmaplot version 14.0, Systat, Inc., Chicago, IL, United States and IBM SPSS Statistics version 22.0, IBM, Armonk, NY, United States). A $p < 0.05$ was deemed as significant for all the analyses.

RESULTS

Table 1 summarizes clinical and demographic parameters of noAKD and AKD subjects. Only hematocrit (HTC) was lower in patients developing AKD post-surgery. The preoperative serum creatinine level was not different between groups but the type I error probability p was below the value set to include this parameter in the multivariate logistic regression model (i.e., 0.1). As a consequence of the outcome, patients developing AKD had a longer mechanical ventilation time and stay in intensive care unit.

Table 2 shows results of time domain parameters assessed in noAKD and AKD subjects during PRE and POST. The cardiovascular control depression induced by general anesthesia was evident. In fact, an increase of μ_{HP} during POST could be observed in both noAKD and AKD groups as well as a concomitant reduction of μ_{SAP}, μ_{DAP} and σ^2_{HP}. σ^2_{SAP} was significantly reduced in POST only in noAKDs. Only σ^2_{HP} and σ^2_{SAP} were able to separate AKD from noAKD group: indeed, during PRE σ^2_{HP} and σ^2_{SAP} were lower in AKDs than noAKDs. σ^2_{DAP} was similar in both groups irrespective of the experimental condition.

As expected, K^2 and BRS markers were computed in 100% of the subjects via AVG and MAX strategies. Conversely, it was possible to compute K^2 and BRS markers with the WCF strategy in the 96% of noAKD subjects during PRE, 99% of noAKDs during POST, 93.1% of AKDs during PRE and 100% of AKDs during POST. $BRS_{SAP\rightarrow HP}$ and $a_{HP\rightarrow SAP}(1)$ were computed in 100% of the subjects irrespective of the group.

Table 3 shows the results of K^2 assessed between HP and SAP according to the different strategies (i.e., MAX, AVG, and WCF). All K^2 markers were reduced during POST compared to PRE. Reduction was significant regardless of the group with the notable exception of K^2_{AVG} that diminished significantly only in noAKDs. None of the K^2 markers was able to differentiate the two groups.

Box-and-whisker plots of **Figure 2** show the BRS values as a function of the experimental condition (i.e., PRE and POST) in noAKDs (white boxes) and AKDs (gray boxes). The BRS estimates are computed via the MAX (**Figure 2A**), AVG (**Figure 2B**), and WCF (**Figure 2C**) strategies. BRS_{MAX}, BRS_{AVG} and BRS_{WCF} were significantly reduced during POST in AKD subjects compared to noAKD ones, while no between-group differences were observed during PRE. BRS_{MAX} and BRS_{AVG} were not affected by propofol anesthesia regardless of the group (i.e., noAKD or AKD). Conversely, BRS_{WCF} decreased during POST in AKD group, while it was not influenced by propofol anesthesia in noAKDs.

Figure 3 has the same structure of **Figure 2** but it shows results of $BRS_{SAP\rightarrow HP}$ (**Figure 3A**) and $a_{HP\rightarrow SAP}(1)$ (**Figure 3B**).

TABLE 1 | Clinical and demographic markers in noAKD and AKD subjects.

Marker	noAKD (n = 100)	AKD (n = 29)	p
Age [years]	66.0 ± 9.4	68.7 ± 10.6	0.21
Gender [male]	88 (88)	24 (83)	0.32
Weight [kg]	78.6 ± 14.9	78.1 ± 17.4	0.88
BMI [kg·m^{-2}]	28.2 ± 14.7	27.2 ± 4.94	0.70
Congestive heart failure	3 (3)	2 (7)	0.31
Recent myocardial infarction	14 (14)	4 (14)	0.55
LVEF [%]	52.8 ± 11.9	52 ± 10.3	0.75
Diabetes	29 (29)	11 (38)	0.24
COPD	7 (7)	3 (10)	0.40
Serum creatinine [mg·dl^{-1}]	1.0 ± 0.3	1.2 ± 0.87	0.08
Hypertension	62 (62)	22 (76)	0.12
Previous cerebrovascular accident	7 (7)	2 (7)	0.67
HCT [%]	39.6 ± 3.8	36.4 ± 4.6	<0.001
Catecholamine administration	14 (14)	3 (33)	0.15
ACE inhibitors	29 (29)	11 (38)	0.24
Beta-blockers	57 (57)	17 (59)	0.53
Calcium antagonists	7 (7)	0 (0)	0.16
Amiodarone	8 (8)	4 (14)	0.27
Combined intervention	6 (6)	2 (7)	0.57
Logistic EuroSCORE	1.8 ± 1.8	2.3 ± 1.2	0.12
CPB time [minutes]	63.3 ± 20.7	66.8 ± 26.8	0.45
Nadir temperature on CPB [°C]	32.9 ± 0.8	32.9 ± 0.9	0.98
Mechanical ventilation time [hours]	12.1 ± 1.6	17.8 ± 11.5	<0.001
ICU stay [days]	2.0 ± 1.6	3.0 ± 2.2	0.001
Hospital stay [days]	7.7 ± 2.5	8.0 ± 3.2	0.61

BMI, body mass index; LVEF, left ventricular ejection fraction; COPD, chronic obstructive pulmonary disease; HCT, hematocrit; ACE, angiotensin converting enzyme; EuroSCORE, European System for Cardiac Operative Risk Evaluation; CPB, cardiopulmonary bypass; ICU, intensive care unit; p, type I error probability. Continuous data are presented as mean ± standard deviation and categorical data as number (percentage).

TABLE 2 | Time domain parameters in noAKD and AKD patients during PRE and POST.

Marker	PRE		POST	
	noAKD	AKD	noAKD	AKD
μ_{HP} [ms]	936.7 ± 147.0	922 ± 124.0	1112.2 ± 152.7*	1091.0 ± 216.9*
σ^2_{HP} [ms^2]	1709.9 ± 1473.4	1016.8 ± 1110.7§	714.9 ± 996.4*	333.5 ± 289.8*
μ_{SAP} [mmHg]	160.2 ± 27.7	170.4 ± 30.5	108.1 ± 18.6*	109.0 ± 25.7*
σ^2_{SAP} [mmHg^2]	34.5 ± 49.3	20.5 ± 12.4§	17.3 ± 19.3*	12.1 ± 7.4
μ_{DAP} [mmHg]	78.0 ± 17.6	72.6 ± 10.4	61.5 ± 9.9*	59.7 ± 10.5*
σ^2_{DAP} [mmHg^2]	64.7 ± 181.9	25.6 ± 80.7	67.8 ± 251.7	8.5 ± 9.4

*HP, heart period; AP, arterial pressure; SAP, systolic AP; DAP, diastolic AP; μ_{HP}, HP mean; σ^2_{HP}, HP variance; μ_{SAP}, SAP mean; σ^2_{SAP}, SAP variance; μ_{DAP}, DAP mean; σ^2_{DAP}, DAP variance. The symbol * indicates $p < 0.05$ versus PRE within the same group (i.e., noAKD or AKD). The symbol § indicates $p < 0.05$ versus noAKD within the same experimental condition (i.e., PRE or POST).*

TABLE 3 | K^2 values computed according to the three different strategies.

Marker	PRE		POST	
	noAKD	AKD	noAKD	AKD
K^2_{MAX}	0.56 ± 0.22	0.56 ± 0.23	0.33 ± 0.19*	0.28 ± 0.16*
K^2_{WCF}	0.36 ± 0.39	0.30 ± 0.42	0.17 ± 0.16*	0.12 ± 0.10*
K^2_{AVG}	0.35 ± 0.20	0.36 ± 0.19	0.16 ± 0.11*	0.12 ± 0.08

*HP, heart period; SAP, systolic arterial pressure; LF, low frequency; K^2, squared coherence between HP and SAP; K^2_{MAX}, maximum K^2 in the LF band; K^2_{AVG}, averaged K^2 in the LF band; K^2_{WCF}, K^2 sampled at the weighted central frequency of the SAP spectral components in the LF band. The symbol * indicates $p < 0.05$ versus PRE.*

$BRS_{SAP\rightarrow HP}$ was reduced during POST with respect to PRE regardless of the group (i.e., noAKD or AKD). Moreover, after the induction of anesthesia $BRS_{SAP\rightarrow HP}$ in AKDs was lower than in noAKDs. The effect of the anesthesia was evident over $a_{HP\rightarrow SAP}(1)$: indeed, it became less negative during POST in both groups. However, $a_{HP\rightarrow SAP}(1)$ was not able to differentiate noAKDs from AKDs regardless of the experimental condition (i.e., PRE or POST).

All the indexes exhibiting between-group differences at a univariate level (i.e., σ^2_{HP} and σ^2_{SAP} during PRE, BRS_{MAX}, BRS_{AVG}, BRS_{WCF}, and $BRS_{SAP\rightarrow HP}$ during POST) entered a multivariate logistic regression model accounting for clinical and demographic factors resulting different between noAKD and AKD groups with a $p < 0.1$ (i.e., HTC and preoperative serum creatinine level). Only BRS indexes, regardless of the strategy used to calculate them, remained significantly associated with the outcome while time domain indexes did not. Moreover, when BRS markers were examined in combination with HTC and preoperative serum creatinine level, only HTC remained associated to the outcome. Regression coefficient, odds ratio, 95% confidence interval and type I error probability p of the multivariate logistic regression models are shown in **Table 4** as well as AUCs of the ROC curves. It can be observed that the combination of clinical parameters (i.e., HTC) with the BRS improves the predictive power of AKD as stressed by the increase of AUC compared to the model accounting for the sole HTC. However, the difference between the AUC computed over HTC and that computed by combining HTC with BRS markers is limited. It is worth noting that the model combining HTC with BRS_{AVG} during POST achieved the highest AUC at multivariate level. **Figure 4** shows the superposition of the ROC curves assessed from the multivariate logistic regression models built using only HTC (blue line) and by combining HTC with $BRS_{SAP\rightarrow HP}$ during POST (yellow line), HTC and BRS_{WCF} during POST (green line), HTC with BRS_{AVG} during POST (red line), and HTC with BRS_{MAX} during POST (black line).

Receiver operating characteristic curves were also calculated using solely BRS markers able to distinguish AKD and noAKD groups (i.e., BRS_{MAX}, BRS_{AVG}, BRS_{WCF}, and $BRS_{SAP\rightarrow HP}$). The AUC of ROC curves relevant to BRS_{MAX}, BRS_{AVG}, BRS_{WCF}, and $BRS_{SAP\rightarrow HP}$ during POST were 0.641, 0.662, 0.658, and 0.671 respectively. The cutoff value for each BRS marker was calculated according to the Youden's index, and the corresponding sensitivity, specificity, PPV and NPV were computed and reported in **Table 5**. It can be observed that $BRS_{SAP\rightarrow HP}$ reported the highest AUC assessed at the univariate level with the highest specificity (i.e., 79%) and PPV (i.e., 41.7%) compared to BRS_{MAX}, BRS_{AVG}, and BRS_{WCF}. The improved specificity and PPV of $BRS_{SAP\rightarrow HP}$ were reached at the cost of a reduced sensitivity (i.e., 51.7%) and NPV (i.e., 84.9%) with respect to BRS_{MAX}, BRS_{AVG}, and BRS_{WCF}.

DISCUSSION

The main findings of this work can be summarized as follows: (i) propofol general anesthesia depresses autonomic function and cardiovascular control; (ii) the reduction of BRS during propofol general anesthesia is more evidently detected using causal than non-causal BRS estimates; (iii) time domain markers are weakly associated with AKD; (iv) BRS markers can separate AKD from noAKD individuals regardless of the computational strategy; (v) BRS assessed after propofol general anesthesia induction is reduced in subjects developing AKD; (vi) both non-causal and causal BRS markers remain associated to AKD even after accounting for clinical and demographic confounding factors;

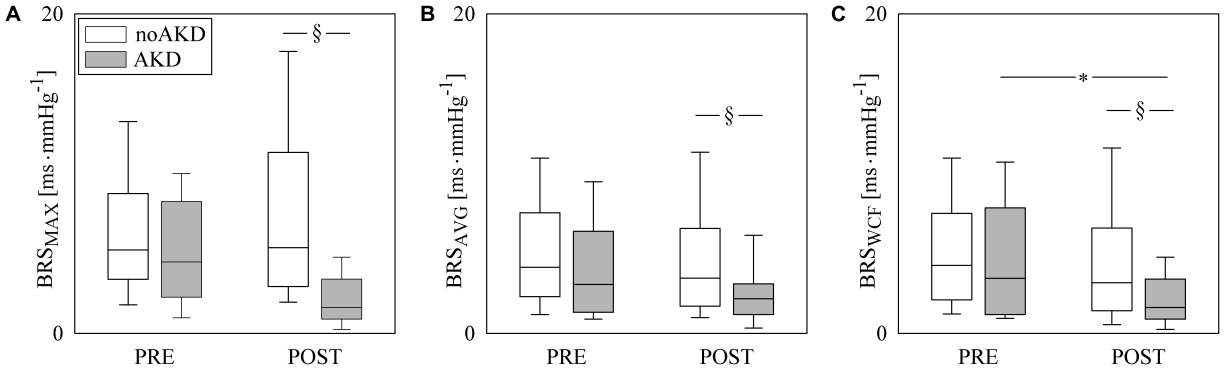

FIGURE 2 | The box-and-whisker graphs show BRS_{MAX} **(A)**, BRS_{AVG} **(B)**, and BRS_{WCF} **(C)** as a function of the experimental condition (i.e., PRE and POST) in noAKD (white boxes) and AKD (gray boxes) individuals. Box height represents the interquartile range, median is marked with a solid line and whiskers denote the 5th and 95th percentile. The symbol * indicates a significant change between experimental conditions (i.e., PRE and POST) within the same group (i.e., noAKD or AKD), while the symbol § indicates a significant difference between groups within the same experimental condition with $p < 0.05$.

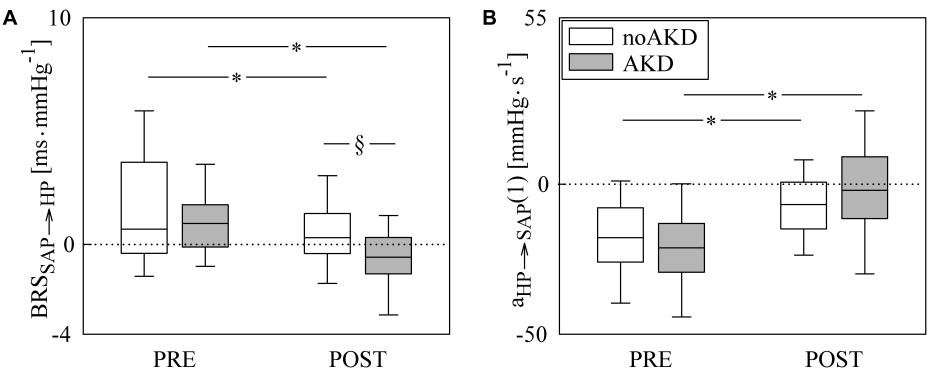

FIGURE 3 | The box-and-whisker graphs show $BRS_{SAP \rightarrow HP}$ **(A)** and $a_{HP \rightarrow SAP}(1)$ **(B)** as a function of the experimental condition (i.e., PRE and POST) in noAKD (white boxes) and AKD (gray boxes) individuals. Box height represents the interquartile range, median is marked with a solid line and whiskers denote the 5th and 95th percentile. The dotted lines mark the zero value. The symbol * indicates a significant change between experimental conditions (i.e., PRE and POST) within the same group (i.e., noAKD or AKD), while the symbol § indicates a significant difference between groups within the same experimental condition with $p < 0.05$.

(vii) performances of non-causal and causal BRS indexes in stratifying the risk of AKD after CABG were similar.

Autonomic Function and Cardiovascular Control Are Depressed During Propofol General Anesthesia

Propofol-based general anesthesia is known to depress autonomic function and cardiovascular control (Boer et al., 1990; Ebert et al., 1992; Sellgren et al., 1994; Hidaka et al., 2005; Sato et al., 2005; El Beheiry and Mak, 2013; Porta et al., 2013) leading to bradycardia (Tramer et al., 1997) and hypotension (Au et al., 2016). This result is confirmed in this study. Indeed, the mean of HP increased and mean of both SAP and DAP decreased. Moreover, the decrease of HP variance suggests a depression of autonomic control (Pomeranz et al., 1985). The effect of propofol general anesthesia was less strong on variance of SAP than HP and that on DAP variance was even weaker. The effect of propofol anesthesia was more evident over causal than non-causal BRS markers: indeed, the causal BRS marker was the sole index able to indicate the decrease of BRS in both AKDs and noAKDs during POST. The better performance of the causal closed loop BRS estimate compared to non-causal BRS markers in detecting the impairment of the BR control during propofol anesthesia was first suggested over a smaller group of CABG patients in Porta et al. (2013). The improved performance is likely to be due to the ability of the causal closed loop approach to account for the non-baroreflex-mediated origin of part of the HP variability in the LF band (Preiss and Polosa, 1974; Baselli et al., 1994) and for the anticausal effects related to the active presence of mechanical feedforward pathway (Porta et al., 2013). Also the migration of the gain of the mechanical feedforward arm toward 0 during propofol anesthesia, originally observed in Porta et al. (2013) and interpreted along with the BRS decrease as an indication of the depression of the overall HP-SAP control loop, was confirmed in the present study. The reduction of the impact of HP variability on SAP changes along the mechanical feedforward pathway is the likely consequence of vasodilatation and reduced left ventricular contractility induced by propofol anesthesia (Porta et al., 2013). The overall depression

of the cardiovascular control in response to propofol anesthesia was suggested even by the significant decrease of K^2 during POST regardless of the method utilized for the computation of K^2 marker.

Time Domain Markers Separate AKDs From noAKDs but They Are Not Associated With AKD After Accounting for Clinical and Demographic Factors

Few markers in the time domain were able to separate AKD and noAKD groups during PRE (i.e., σ^2_{HP} and σ^2_{SAP}). Since σ^2_{HP} is directly linked to the amplitude of both vagal and sympathetic outflow modulations directed to the heart (Pomeranz et al., 1985; Montano et al., 1994), while σ^2_{SAP} raises with the relevance of sympathetic outflow modulations directed to the vessels (Pagani et al., 1997; Cooke et al., 1999; Marchi et al., 2016a), it can be hypothesized that autonomic regulation could play a role in AKD development. Conversely, none of the time domain parameters during POST was able to differentiate AKD from noAKD group and this limited ability can be taken again a hallmark of the autonomic function depression following propofol general anesthesia. However, when σ^2_{HP} and σ^2_{SAP} during PRE were added one by one to clinical and demographic markers featuring the best performance in separating AKDs from noAKDs (i.e., HTC and serum creatinine level), time domain markers did not provide complementary information, thus supporting the concept that AKD is weakly linked to the magnitude of autonomic activity and/or modulation. This disappointing finding could be the consequence of the unspecific characteristic of these two markers, thus prompting for the exploitation of cardiovascular control indexes that are much more specifically linked to regulatory reflexes such as the BR.

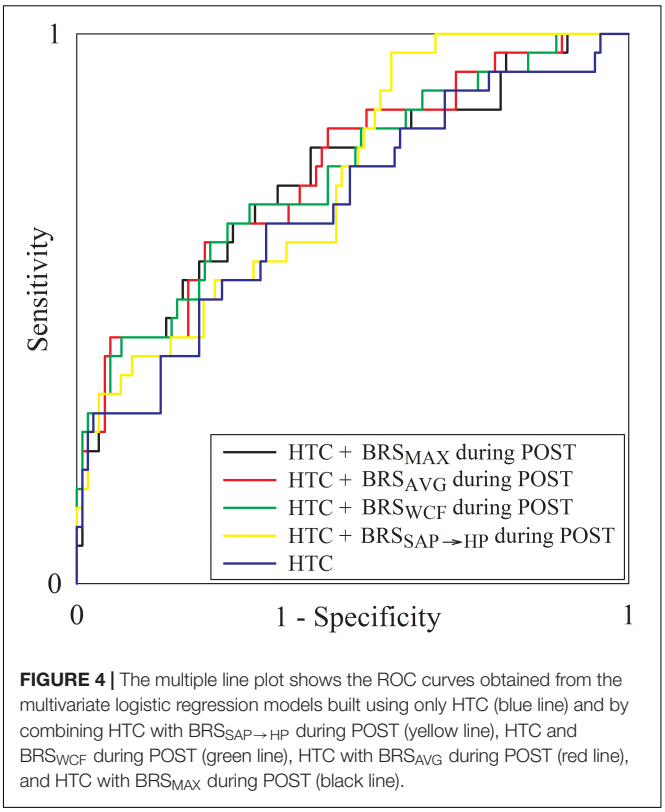

FIGURE 4 | The multiple line plot shows the ROC curves obtained from the multivariate logistic regression models built using only HTC (blue line) and by combining HTC with $BRS_{SAP\rightarrow HP}$ during POST (yellow line), HTC and BRS_{WCF} during POST (green line), HTC with BRS_{AVG} during POST (red line), and HTC with BRS_{MAX} during POST (black line).

TABLE 4 | Results of multivariate logistic regression analysis for AKD prediction.

Parameter	Regression coefficient	Odds ratio	95% confidence interval	*p*	AUC
BRS_{MAX} during POST	−0.118	0.889	0.798–0.991	0.034	0.741
HCT	−0.196	0.822	0.731–0.925	0.001	
Constant	6.870	963.067		0.002	
BRS_{AVG} during POST	−0.188	0.829	0.697–0.984	0.032	0.747
HCT	−0.194	0.823	0.732–0.926	0.001	
Constant	6.823	918.982		0.003	
BRS_{WCF} during POST	−0.154	0.857	0.736–0.998	0.048	0.742
HCT	−0.203	0.817	0.725–0.920	0.001	
Constant	7.017	531.34		0.002	
$BRS_{SAP\rightarrow HP}$ during POST	−0.345	0.708	0.529–0.948	0.020	0.731
HCT	−0.184	0.832	0.741–0.934	0.002	
Constant	5.687	295.054		0.010	
HCT	−0.200	0.819	0.731–0.918	0.001	0.690
Constant	6.344	568.82		0.004	

BRS, baroreflex sensitivity; HP, heart period; SAP, systolic arterial pressure; LF, low frequency; BRS_{MAX}, BRS obtained by sampling the transfer function gain between HP and SAP at the maximum of HP-SAP squared coherence in LF band; BRS_{AVG}, BRS obtained as the average of the transfer function gain between HP and SAP in LF band; BRS_{WCF}, BRS obtained by sampling the transfer function gain between HP and SAP at the weighted central frequency of the SAP spectral components in LF band; $BRS_{SAP\rightarrow HP}$, causal closed loop BRS; POST, after anesthesia induction; HCT, hematocrit; AUC, area under the receiver operating characteristic curve.

BRS Is Lower in AKDs During POST and the BRS Association With AKD Remains After Accounting for Clinical and Demographic Factors

Both non-causal and causal BRS estimates were able to distinguish AKD and noAKD groups while markers measuring the mere association between HP and SAP variability series (i.e., K^2 indexes) and the gain of the mechanical feedforward pathway were useless. Remarkably, all BRS indexes remained associated to the adverse outcome even when combined with clinical and demographic parameters that were detected to be significantly associated to AKD, thus confirming the relevance of the association between BRS and AKD (Ranucci et al., 2017). Remarkably, this association was confirmed in this study using an additional class of methods for BRS estimation, namely the causal closed loop method. More specifically, we found that BRS was lower in patients who developed AKD after CABG, thus suggesting that a more active BR control is protective against AKD, while a depressed BR regulation

TABLE 5 | Results of logistic regression analysis for AKD prediction.

Parameter	cutoff [ms·mmHg^{-1}]	sensitivity	specificity	PPV	NPV	AUC
BRS_{MAX} during POST	7.73	93.1%	36.4%	29.8%	94.8%	0.641
BRS_{AVG} during POST	3.17	82.8%	53.5%	34.1%	91.5%	0.662
BRS_{WCF} during POST	4.82	93.1%	28.5%	29.5%	94.6%	0.658
$BRS_{SAP\rightarrow HP}$ during POST	−0.59	51.7%	79.0%	41.7%	84.9%	0.671

BRS, baroreflex sensitivity; HP, heart period; SAP, systolic arterial pressure; LF, low frequency; BRS_{MAX}, BRS obtained by sampling the transfer function gain between HP and SAP at the maximum of HP-SAP squared coherence in LF band; BRS_{AVG}, BRS obtained as the average of the transfer function gain between HP and SAP in LF band; BRS_{WCF}, BRS obtained by sampling the transfer function gain between HP and SAP at the weighted central frequency of the SAP spectral components in LF band; $BRS_{SAP\rightarrow HP}$, causal closed loop BRS; POST, after anesthesia induction; PPV, positive predictive value; NPV, negative predictive value; AUC, area under the receiver operating characteristic curve.

should be considered a risk factor for the development of AKD. The association between low BRS values and AKD could be the consequence of an insufficient BR response to hypotension and hypoperfusion situations that might be occurred during CABG surgery (Mangano et al., 1998; Provenchere et al., 2003; Pavlov and Tracey, 2012). However, given the link of a low BRS with vagal withdrawal and sympathetic activation (Cooke et al., 1999; Marchi et al., 2016b; De Maria et al., 2018), the association between a depressed BRS value and AKD could be the result of the abnormal reaction to inflammation and anomalous levels of oxidative stress favored by a limited vagal control and a high sympathetic drive (Pavlov and Tracey, 2012; Inoue et al., 2016a,b). Our interpretation of the findings privileges the causal pathway that an impaired BR causes AKD. This interpretation is supported by the lower BRS observed during POST well before the AKD development and by the observation that an impaired autonomic control is a risk factor for chronic kidney disease (Brotman et al., 2010). However, the reverse pathway, namely an incoming, or manifest, AKD could determine a BR impairment, cannot be dismissed. Indeed, previous studies have shown how the renal impairment can be an independent risk factor for cardiovascular events and heart failure (Omar and Zedan, 2013) and that an increased afferent renal sympathetic activity from impaired kidneys is critically involved in the pathogenesis of sympathetic hyperactivity (Blankestijn and Joles, 2012).

Remarkably, the association of BRS markers with the outcome was observed during POST, while it was not visible during PRE. This result might be at first sight quite surprising given the well-known depression of autonomic control and baroreflex regulation during propofol general anesthesia (Boer et al., 1990; Ebert et al., 1992; Sellgren et al., 1994; Hidaka et al., 2005; Sato et al., 2005; El Beheiry and Mak, 2013; Porta et al., 2013) confirmed even by the present study. However, on the one hand, baroreflex regulation is depressed but not absent (Porta et al., 2013) and, on the other hand, hemodynamic instability observed during CABG surgery, brief periods of inadequate delivery of oxygen to the tissues (Toner et al., 2016), and episodes of hypotension and hypoperfusion (Ranucci et al., 2017) might have stimulated more importantly the residual BR control during POST than PRE. Also mechanical ventilation, profoundly influencing venous return and stroke volume, might have contributed to solicit the residual BR at frequencies slower than the ventilatory one.

We point out that the cutoff values of BRS assessed according to the Youden's index varies with the strategy for BRS computation, being equal to 7.73, 3.17, 4.82, and −0.59 ms·mmHg^{-1} for BRS_{MAX}, BRS_{AVG}, BRS_{WCF}, and $BRS_{SAP\rightarrow HP}$ respectively. The results relevant to non-causal BRS estimates are in agreement with the different cutoff values of BRS utilized to predict adverse events present in literature (La Rovere et al., 1998; Gouveia et al., 2015; Toner et al., 2016; Ranucci et al., 2017; Pinna et al., 2017). Cutoff values depend on the method exploited for BRS estimation (Pinna et al., 2017), type of pathology (La Rovere et al., 1998; Gouveia et al., 2015) and endpoint of the analysis (Toner et al., 2016; Ranucci et al., 2017). This study suggests that even within the same class of methods for the BRS estimation (i.e., the non-causal class in the frequency domain) cutoff values might vary importantly according to the strategy followed to derive the final BRS values utilized to typify the patient. Since $BRS_{SAP\rightarrow HP}$ was computed according to a completely different method (i.e., the causal closed loop technique), it is not surprising that the cutoff value of $BRS_{SAP\rightarrow HP}$ was significantly different from those of the non-causal markers. Indeed, it was negative according to the possibility given by its definition computing the slope of the HP response to an artificial SAP rise (Baselli et al., 1994). A negative $BRS_{SAP\rightarrow HP}$ implies that, instead of having a bradycardic response to a SAP rise, a tachycardic reaction is observed. This result provides a new perspective on the BR control in CABG patients: indeed, the patients most at risk of developing AKD after CABG are not simply those who have the most depressed BR control but those who exhibit an antiparallel HP response to SAP variations. An additional factor that might increase the variability of the cutoff is the experimental condition during which the signals were recorded. For example, BRS estimates computed in this study were useless in separating AKD from noAKD individuals when evaluated during PRE. These considerations stress the need for a standardization of the BRS assessment to favor future clinical applications especially whether BRS methods based on spontaneous variability will be exploited. However, roughly speaking about non-causal frequency domain BRS markers, we confirmed that a cutoff value of about 3 ms·mmHg^{-1} can be utilized as a first attempt to make prediction of adverse outcomes in clinical context where BRS estimates are found to be significantly associated to the event (La Rovere et al., 1998). However, this value does not hold for causal closed loop BRS estimates.

Comparison of the Performances of Non-causal and Causal BRS Estimates in Stratifying the Risk of AKD in CABG Patients

The present study originally compares the performance of non-causal and causal BRS markers in stratifying the risk of AKD after CABG. Performances were similar regardless of the class of method (i.e., non-causal or causal class) and within the non-causal class irrespective of the strategy followed to derive a unique index from the transfer function gain in LF band. It can be observed that the BRS_{AVG} is slightly superior in terms of AUC at multivariate level (i.e., in combination with HTC) and the presumed superiority of $BRS_{SAP\rightarrow HP}$ compared to non-causal BRS indexes, resulting from its more complex model structure, was evident only at univariate level. The BRS_{AVG} should be preferred given the simplicity of its computation and remarkable performance. Indeed, the BRS_{AVG} does not require the presence of a spectral peak in the LF band in the SAP series like the BRS_{WCF}, the presence of a K^2 peak in the LF band like the BRS_{MAX}, and the identification of a complex model structure including RESP like the $BRS_{SAP\rightarrow HP}$. This study confirms the feeling pointed out in Pinna et al. (2017) that in practical applications the full adherence to the concept of the BR, undoubtedly provided by the causal closed loop strategy, does not assure a measurable advantage compared to simpler non-causal techniques likely due to the complexity of the physiological interactions and the effect of noise on the final estimate making alike the performance of all the considered methods.

Limitations of the Study and Future Developments

A limitation of this study is the impossibility of testing the ability of BRS in discriminating acute kidney injury (i.e., the increase of postoperative creatinine of more than 50% with respect to preoperative level), that is a more stringent and risky condition with respect to AKD. This limitation is due to the relatively small number of patients who developed acute kidney injury in our database that prevented any reliable association of BRS markers with this adverse event. The application of the same approach after the enlargement of the enrolled population would allow us in the future to test the association of BRS markers with acute kidney injury as well.

Moreover, in interpreting the results we privilege the possibility that a reduced BRS could play a role in the post-surgery development of AKD but the action of the reverse pathway, implying a potential influence of an incoming AKD on BR control, cannot be fully dismissed and calls for additional studies.

CONCLUSION

This work stresses the relevance of computing BRS markers from spontaneous variability of HP and SAP computed via causal and non-causal methods to stratify the risk of AKD after CABG and their complementary information compared to clinical and demographic factors. Remarkably, the present study provided cutoff values that are worth being exploited to identify subjects at risk of AKD after CABG. Moreover, we conclude that no evident clinical improvement can be derived from the application of causal BRS markers with respect to non-causal BRS ones. Future studies should verify the clinical impact of the application of the provided cutoff values and should test whether the use of premedications and/or countermeasures before CABG surgery aiming at increasing BRS might have a favorable impact on the incidence of postoperative AKD.

DATA AVAILABILITY STATEMENT

The datasets generated for this study are available on request to the corresponding author.

ETHICS STATEMENT

The study was performed in keeping with the Declaration of Helsinki for research studies involving humans and, before participating, subjects signed a written informed consent. The study was approved by the ethical committee in charge at the IRCCS Policlinico San Donato, San Donato Milanese, Milan, Italy.

AUTHOR CONTRIBUTIONS

VB and AP contributed to the conception and design of research. VB, EV, VP, AF, and MR performed the experiments. VB, EV, BC, and BD analyzed the data. VB and AP drafted the manuscript and prepared the figures. VB, EV, VP, AF, BC, BD, LD, MR, and AP interpreted the results, edited and revised critically the manuscript, and approved the final version of the manuscript.

FUNDING

This work was supported by Ricerca Finalizzata, Italian Ministry of Health, Grant GR-2013-02356272 to VB.

REFERENCES

Au, A. K., Steinberg, D., Thom, C., Shirazi, M., Papanagnou, D., Ku, B. S., et al. (2016). Ultrasound measurement of inferior vena cava collapse predicts propofol-induced hypotension. *Am. J. Emerg. Med.* 34, 1125–1128. doi: 10.1016/j.ajem.2016.03.058

Bari, V., Ranucci, M., De Maria, B., Cairo, B., Pistuddi, V., and Porta, A. (2018). Model-based directional analysis of cardiovascular variability identifies patients developing atrial fibrillation after coronary artery bypass grafting. *Int. J. Cardiol.* 258, 97–102. doi: 10.1016/j.ijcard.2018.01.071

Baselli, G., Cerutti, S., Badilini, F., Biancardi, L., Porta, A., Pagani, M., et al. (1994). Model for the assessment of heart period and arterial pressure variability

interactions and respiratory influences. *Med. Biol. Eng. Comput.* 32, 143–152. doi: 10.1007/bf02518911

Baselli, G., Porta, A., Rimoldi, O., Pagani, M., and Cerutti, S. (1997). Spectral decomposition in multichannel recordings based on multivariate parametric identification. *IEEE Trans. Biomed. Eng.* 44, 1092–1101. doi: 10.1109/10.641336

Bauer, A., Morley-Davies, A., Barthel, P., Muller, A., Ulm, K., Malik, M., et al. (2010). Bivariate phase-rectified signal averaging for assessment of spontaneous baroreflex sensitivity: pilot study of the technology. *J. Electrocardiol.* 43, 649–653. doi: 10.1016/j.jelectrocard.2010.05.012

Bertinieri, G., di Rienzo, M., Cavallazzi, A., Ferrari, A. U., Pedotti, A., and Mancia, G. (1985). A new approach to analysis of the arterial baroreflex. *J. Hypertens.* 33, S79–S81.

Blankestijn, P. J., and Joles, J. A. (2012). Hypertension: renal denervation in chronic kidney disease. *Nat. Rev. Nephrol.* 8, 439–440.

Boer, F., Ros, P., Bovill, J. G., van Brummelen, P., and van der Krogt, J. (1990). Effect of propofol on peripheral vascular resistance during cardiopulmonary bypass. *Br. J. Anaesth.* 65, 184–189. doi: 10.1093/bja/65.2.184

Brotman, D. J., Bash, L. D., Qayyum, R., Crews, D., Whitsel, E. A., Astor, B. C., et al. (2010). Heart rate variability predicts ESRD and CKD-related hospitalization. *J. Am. Soc. Nephrol.* 21, 1560–1570. doi: 10.1681/ASN.2009111112

Collier, D. J., Bernardi, L., Angell-James, J. E., Caulfield, M. J., and Sleight, P. (2001). Baroreflex sensitivity and heart rate variability as predictors of cardiovascular outcome in hypertensive patients with multiple risk factors for coronary disease. *J. Hum. Hypertens.* 15, S57–S60.

Cooke, W. H., Hoag, J. B., Crossman, A. A., Kuusela, T. A., Tahvanainen, K. U., and Eckberg, D. L. (1999). Human responses to upright tilt: a window on central autonomic integration. *J. Physiol.* 517, 617–628. doi: 10.1111/j.1469-7793.1999.0617t.x

de Boer, R. W., Karemaker, J. M., and Strackee, J. (1985). Relationships between short-term blood pressure fluctuations and heart rate variability in resting subjects I: a spectral analysis approach. *Med. Biol. Eng. Comput.* 23, 352–358. doi: 10.1007/bf02441589

De Boer, R. W., Karemaker, J. M., and Strackee, J. (1987). Hemodynamic fluctuations and baroreflex sensitivity in humans: a beat-to-beat model. *Am. J. Physiol.* 253, H680–H689.

De Ferrari, G. M., Sanzo, A., Bertoletti, A., Specchia, G., Vanoli, E., and Schwartz, P. J. (2007). Baroreflex sensitivity predicts long-term cardiovascular mortality after myocardial infarction even in patients with preserved left ventricular function. *J. Am. Coll. Cardiol.* 50, 2285–2290. doi: 10.1016/j.jacc.2007.08.043

De Maria, B., Bari, V., Ranucci, M., Pistuddi, V., Ranuzzi, G., Takahashi, A. C. M., et al. (2018). Separating arterial pressure increases and decreases in assessing cardiac baroreflex sensitivity via sequence and bivariate phase-rectified signal averaging techniques. *Med. Biol. Eng. Comput.* 56, 1241–1252. doi: 10.1007/s11517-017-1765-0

Ebert, T. J., Muzi, M., Berens, R., Goff, D., and Kampine, J. P. (1992). Sympathetic responses to induction of anesthesia in humans with propofol or etomidate. *Anesthesiology* 76, 725–733. doi: 10.1097/00000542-199205000-00010

El Beheiry, H., and Mak, P. (2013). Effects of aging and propofol on the cardiovascular component of the autonomic nervous system. *J. Clin. Anesth.* 25, 637–643. doi: 10.1016/j.jclinane.2013.07.004

Faes, L., Porta, A., Cucino, R., Cerutti, S., Antolini, R., and Nollo, G. (2004). Causal transfer function analysis to describe closed loop interactions between cardiovascular and cardiorespiratory variability signals. *Biol. Cybern.* 90, 390–399.

Gerritsen, J., Dekker, J. M., TenVoorde, B. J., Kostense, P. J., Heine, R. J., Bouter, L. M., et al. (2001). Impaired autonomic function is associated with increased mortality, especially in subjects with diabetes, hypertension, or a history of cardiovascular disease: the Hoorn Study. *Diabetes Care* 24, 1793–1798. doi: 10.2337/diacare.24.10.1793

Goldstein, D. S., Bentho, O., Park, M. Y., and Sharabi, Y. (2011). Low-frequency power of heart rate variability is not a measure of cardiac sympathetic tone but may be a measure of modulation of cardiac autonomic outflows by baroreflex. *Exp. Physiol.* 96, 1255–1261. doi: 10.1113/expphysiol.2010.056259

Gouveia, S., Scotto, M. G., Pinna, G. D., Maestri, R., La Rovere, M. T., and Ferreira, P. J. (2015). Spontaneous baroreceptor reflex sensitivity for risk stratification of heart failure patients: optimal cut-off and age effects. *Clin. Sci.* 129, 1163–1172. doi: 10.1042/CS20150341

Hidaka, S., Kawamoto, M., Kurita, S., and Yuge, O. (2005). Comparison of the effects of propofol and midazolam on the cardiovascular autonomic nervous system during combined spinal and epidural anesthesia. *J. Clin. Anesth.* 17, 36–43. doi: 10.1016/j.jclinane.2004.03.012

Holzmann, M. J., Gardell, C., Jeppsson, A., and Sartipy, U. (2013). Renal dysfunction and long-term risk of heart failure after coronary artery bypass grafting. *Am. Heart J.* 166, 142–149. doi: 10.1016/j.ahj.2013.03.005

Inoue, T., Abe, C., Sung, S. S., Moscalu, S., Jankowski, J., Huang, L., et al. (2016a). Vagus nerve stimulation mediates protection from kidney ischemia-reperfusion injury through α7nAChR+ splenocytes. *J. Clin. Invest.* 126, 1939–1952. doi: 10.1172/jci83658

Inoue, T., Rosin, D. L., and Okusa, M. D. (2016b). CAPing inflammation and acute kidney injury. *Kidney Int.* 90, 462–465. doi: 10.1016/j.kint.2016.07.009

La Rovere, M. T., Bigger, J. T. Jr., Marcus, F. I, Mortara, A., and Schwartz, P. J. (1998). Baroreflex sensitivity and heart-rate variability in prediction of total cardiac mortality after myocardial infarction. ATRAMI (Autonomic Tone and Reflexes After Myocardial Infarction) Investigators. *Lancet* 351, 478–484. doi: 10.1016/s0140-6736(97)11144-8

Landolina, M., Mantica, M., Pessano, P., Manfredini, R., Foresti, A., Schwartz, P. J., et al. (1997). Impaired baroreflex sensitivity is correlated with hemodynamic deterioration of sustained ventricular tachycardia. *J. Am. Coll. Cardiol.* 29, 568–575. doi: 10.1016/s0735-1097(96)00533-5

Laude, D., Elghozi, J. L., Girard, A., Bellard, E., Bouhaddi, M., Castiglioni, P., et al. (2004). Comparison of various techniques used to estimate spontaneous baroreflex sensitivity (the EuroBaVar study). *Am. J. Physiol.* 286, R226–R231.

Liotta, M., Olsson, D., Sartipy, U., and Holzmann, M. J. (2014). Minimal changes in postoperative creatinine values and early and late mortality and cardiovascular events after coronary artery bypass grafting. *Am. J. Cardiol.* 113, 70–75. doi: 10.1016/j.amjcard.2013.09.012

Mangano, C. M., Diamondstone, L. S., Ramsay, J. G., Aggarwal, A., Herskowitz, A., and Mangano, D. T. (1998). Renal dysfunction after myocardial revascularization: risk factors, adverse outcomes, and hospital resource utilization. The multicenter study of perioperative ischemia research group. *Ann. Intern. Med.* 128, 194–203.

Marchi, A., Bari, V., De Maria, B., Esler, M., Lambert, E., Baumert, M., et al. (2016a). Calibrated variability of muscle sympathetic nerve activity during graded head-up tilt in humans and its link with noradrenaline data and cardiovascular rhythms. *Am. J. Physiol.* 310, R1134–R1143. doi: 10.1152/ajpregu.00541.2015

Marchi, A., Bari, V., De Maria, B., Esler, M., Lambert, E., Baumert, M., et al. (2016b). Simultaneous characterization of sympathetic and cardiac arms of the baroreflex through sequence techniques during incremental head-up tilt. *Front. Physiol.* 7:438. doi: 10.3389/fphys.2016.00438

Montano, N., Gnecchi-Ruscone, T., Porta, A., Lombardi, F., Pagani, M., and Malliani, A. (1994). Power spectrum analysis of heart rate variability to assess the changes in sympatho-vagal balance during graded orthostatic tilt. *Circulation* 90, 1826–1831. doi: 10.1161/01.cir.90.4.1826

Muller, A., Morley-Davies, A., Barthel, P., Hnatkova, K., Bauer, A., Ulm, K., et al. (2012). Bivariate phase-rectified signal averaging for assessment of spontaneous baroreflex sensitivity: normalization of the results. *J. Electrocardiol.* 45, 77–81. doi: 10.1016/j.jelectrocard.2011.07.010

Nollo, G., Porta, A., Faes, L., Del Greco, M., Disertori, M., and Ravelli, F. (2001). Causal linear parametric model for baroreflex gain assessment in patients with recent myocardial infarction. *Am. J. Physiol.* 280, H1830–H1839.

Omar, S., and Zedan, A. (2013). Cardiorenal syndrome. *Southwest Respir.tory Crit. Care Chron.* 1, 11–19.

Pagani, M., Montano, N., Porta, A., Malliani, A., Abboud, F. M., Birkett, C., et al. (1997). Relationship between spectral components of cardiovascular variabilities and direct measures of muscle sympathetic nerve activity in humans. *Circulation* 95, 1441–1448. doi: 10.1161/01.cir.95.6.1441

Pagani, M., Somers, V., Furlan, R., Dell'Orto, S., Conway, J., Baselli, G., et al. (1988). Changes in autonomic regulation induced by physical training in mild hypertension. *Hypertension* 12, 600–610. doi: 10.1161/01.hyp.12.6.600

Patton, D. J., Triedman, J. K., Perrott, M. H., Vidian, A. A., and Saul, J. P. (1995). Baroreflex gain: characterization using autoregressive moving average analysis. *Am. J. Physiol.* 270, H1240–H1249.

Pavlov, V. A., and Tracey, K. J. (2012). The vagus nerve and the inflammatory reflex - linking immunity and metabolism. *Nat. Rev. Endocrinol.* 8, 743–754. doi: 10.1038/nrendo.2012.189

Pinna, G. D., Maestri, R., and La Rovere, M. T. (2015). Assessment of baroreflex sensitivity from spontaneous oscillations of blood pressure and heart rate: proven clinical value? *Physiol. Meas.* 36, 741–753. doi: 10.1088/0967-3334/36/4/741

Pinna, G. D., Maestri, R., Raczak, G., and La Rovere, M. T. (2002). Measuring baroreflex sensitivity from the gain function between arterial pressure and heart period. *Clin. Sci.* 103, 81–88. doi: 10.1042/cs1030081

Pinna, G. D., Porta, A., Maestri, R., De Maria, B., Dalla Vecchia, L. A., and La Rovere, M. T. (2017). Different estimation methods of spontaneous baroreflex sensitivity have different predictive value in heart failure patients. *J. Hypertens.* 35, 1666–1675. doi: 10.1097/HJH.0000000000001377

Pomeranz, B., Macaulay, R. J. B., Caudill, M. A., Kutz, I., Adam, D., Gordon, D., et al. (1985). Assessment of autonomic function in humans by heart-rate spectral-analysis. *Am. J. Physiol.* 248, H151–H153.

Porta, A., Bari, V., Bassani, T., Marchi, A., Pistuddi, V., and Ranucci, M. (2013). Model-based causal closed-loop approach to the estimate of baroreflex sensitivity during propofol anesthesia in patients undergoing coronary artery bypass graft. *J. Appl. Physiol.* 115, 1032–1042. doi: 10.1152/japplphysiol.00537.2013

Porta, A., Baselli, G., Lombardi, F., Cerutti, S., Antolini, R., Del Greco, M., et al. (1998). Performance assessment of standard algorithms for dynamic RT interval measurement: comparison between RTapex and RTend approach. *Med. Biol. Eng. Comput.* 36, 35–42. doi: 10.1007/bf02522855

Porta, A., Baselli, G., Rimoldi, O., Malliani, A., and Pagani, M. (2000). Assessing baroreflex gain from spontaneous variability in conscious dogs: role of causality and respiration. *Am. J. Physiol.* 279, H2558–H2567.

Porta, A., Bassani, T., Bari, V., Pinna, G. D., Maestri, R., and Guzzetti, S. (2012). Accounting for respiration is necessary to reliably infer Granger causality from cardiovascular variability series. *IEEE Trans. Biomed. Eng.* 59, 832–841. doi: 10.1109/TBME.2011.2180379

Porta, A., Colombo, R., Marchi, A., Bari, V., De Maria, B., Ranuzzi, G., et al. (2018). Association between autonomic control indexes and mortality in subjects admitted to intensive care unit. *Sci. Rep.* 8:3486. doi: 10.1038/s41598-018-21888-8

Porta, A., Furlan, R., Rimoldi, O., Pagani, M., Malliani, A., and van de Borne, P. (2002). Quantifying the strength of linear causal coupling in closed loop interacting cardiovascular variability series. *Biol. Cybern.* 86, 241–251. doi: 10.1007/s00422-001-0292-z

Preiss, G., and Polosa, C. (1974). Patterns of sympathetic neuron activity associated with Mayer waves. *Am. J. Physiol.* 226, 724–730. doi: 10.1152/ajplegacy.1974.226.3.724

Provenchere, S., Plantefeve, G., Hufnagel, G., Vicaut, E., De Vaumas, C., Lecharny, J. B., et al. (2003). Renal dysfunction after cardiac surgery with normothermic cardiopulmonary bypass: incidence, risk factors, and effect on clinical outcome. *Anesth. Analg.* 96, 1258–1264. doi: 10.1213/01.ane.0000055803.92191.69

Ranucci, M., Porta, A., Bari, V., Pistuddi, V., and La Rovere, M. T. (2017). Baroreflex sensitivity and outcomes following coronary surgery. *PLoS One* 12:e0175008. doi: 10.1371/journal.pone.0175008

Robbe, H. W., Mulder, L. J., Ruddel, H., Langewitz, W. A., Veldman, J. B., and Mulder, G. (1987). Assessment of baroreceptor reflex sensitivity by means of spectral analysis. *Hypertension* 10, 538–543. doi: 10.1161/01.hyp.10.5.538

Sato, M., Tanaka, M., Umehara, S., and Nishikawa, T. (2005). Baroreflex control of heart rate during and after propofol infusion in humans. *Br. J. Anaesth.* 94, 577–581. doi: 10.1093/bja/aei092

Saul, J. P., Berger, R. D., Albrecht, P., Stein, S. P., Chen, M. H., and Cohen, R. J. (1991). Transfer function analysis of the circulation: unique insights into cardiovascular regulation. *Am. J. Physiol.* 261, H1231–H1245.

Sellgren, J., Ejnell, H., Elam, M., Ponten, J., and Wallin, B. G. (1994). Sympathetic muscle nerve activity, peripheral blood flows, and baroreceptor reflexes in humans during propofol anesthesia and surgery. *Anesthesiology* 80, 534–544. doi: 10.1097/00000542-199403000-00009

Smyth, H. S., Sleight, P., and Pickering, G. W. (1969). Reflex regulation of arterial pressure during sleep in man. A quantitative method of assessing baroreflex sensitivity. *Circ. Res.* 24, 109–121. doi: 10.1161/01.res.24.1.109

Task Force of the European Society of Cardiology, and the North American Society of Pacing and Electrophysiology, (1996). Heart rate variability. Standards of measurement, physiological interpretation, and clinical use. *Eur. Heart J.* 17, 354–381. doi: 10.1093/oxfordjournals.eurheartj.a014868

Toner, A., Jenkins, N., Ackland, G. L., and Pom-O Study Investigators, (2016). Baroreflex impairment and morbidity after major surgery. *Br. J. Anaesth.* 117, 324–331. doi: 10.1093/bja/aew257

Tramer, M. R., Moore, R. A., and McQuay, H. J. (1997). Propofol and bradycardia: causation, frequency and severity. *Br. J. Anaesth.* 78, 642–651. doi: 10.1093/bja/78.6.642

Vanoli, E., and Adamson, P. B. (1994). Baroreflex sensitivity: methods, mechanisms, and prognostic value. *PACE-Pacing Clin. Electrophysiol.* 17, 434–445. doi: 10.1111/j.1540-8159.1994.tb01410.x

Westerhof, B. E., Gisolf, J., Stok, W. J., Wesseling, K. H., and Karemaker, J. M. (2004). Time-domain cross-correlation baroreflex sensitivity: performance on the EUROBAVAR data set. *J. Hypertens.* 22, 1371–1380. doi: 10.1097/01.hjh.0000125439.28861.ed

Xiao, X., Mullen, T. J., and Mukkamala, R. (2005). System identification: a multi-signal approach for probing neural cardiovascular regulation. *Physiol. Meas.* 26, R41–R71.

Conflict of Interest: The authors declare that the research was conducted in the absence of any commercial or financial relationships that could be construed as a potential conflict of interest.

The reviewer MJ declared a past co-authorship with one of the authors AP to the handling Editor.

Advantages of publishing in Frontiers

OPEN ACCESS
Articles are free to read for greatest visibility and readership

FAST PUBLICATION
Around 90 days from submission to decision

HIGH QUALITY PEER-REVIEW
Rigorous, collaborative, and constructive peer-review

TRANSPARENT PEER-REVIEW
Editors and reviewers acknowledged by name on published articles

Frontiers
Avenue du Tribunal-Fédéral 34
1005 Lausanne | Switzerland

Visit us: www.frontiersin.org
Contact us: info@frontiersin.org | +41 21 510 17 00

REPRODUCIBILITY OF RESEARCH
Support open data and methods to enhance research reproducibility

DIGITAL PUBLISHING
Articles designed for optimal readership across devices

FOLLOW US
@frontiersin

IMPACT METRICS
Advanced article metrics track visibility across digital media

EXTENSIVE PROMOTION
Marketing and promotion of impactful research

LOOP RESEARCH NETWORK
Our network increases your article's readership